Caractérisation des espèces métalliques présentes dans les asphaltènes. : Étude de leurs interactions dans les coupes pétrolières lourdes appliquée à l'hydrodémétallation

Rémi Moulian

Université de Pau et des Pays de l'Adour

Ecole doctorale des sciences exactes et de leurs applications (ED211)

Thèse de Doctorat

Pour l'obtention du grade de

DOCTEUR

Discipline : Chimie analytique

Par Rémi MOULIAN

Le lundi 21 septembre 2020

Caractérisation des espèces métalliques présentes dans les asphaltènes. Etude de leurs interactions dans les coupes pétrolières lourdes appliquée à l'hydrodémétallation

Characterization of metal species of asphaltenes and their interactions in heavy oil cuts applied to hydrodemetallation

Soutenance devant le jury composé de :

M. Jan H Christensen	Pr, Université de Copenhague	Rapporteur
Mme. Mariella Moldovan	Pr, Université d'Oviedo	Rapporteur
M. Hervé Carrier	Pr, UPPA	Examinateur
M. Sylvain Verdier	Dr, Aldor Topsoe	Examinateur
M. Ryan P Rodgers	Pr, FSU	Examinateur
Mme Caroline Mangote	Dr, Total	Examinateur
M. Brice Bouyssière	Pr, UPPA	Directeur

Remerciements

Premièrement je souhaiterais remercier mon directeur de thèse le Pr. Brice Bouyssiere et mon encadrante industriele la Dr.Caroline Mangote ainsi que le Dr Pierre Giusti sans qui la thèse n'aurait pas vu le jour.

J'ai eu la chance de pouvoir travailler dans plusieurs laboratoires, tout d'abord au TRTG ou je remercie Mathilde, Carole, Sabrina, Benoit, Johan, Anne-Sophie, Ahmad, Jérôme qui ont apporté une vision différente de l'université et qui sont avant tout des collègues très sympathiques.

Je remercie aussi le groupe de travail de Rouen, Carlos, Marie Hubert, Oscar qui m'ont accueilli à plusieurs reprises. En particulier je remercie Johann pour les bons moments partagées à Dunkerque et Asnières sur Oise.

Je remercie aussi le groupe de Tallahassee avec qui j'ai pu travailler, Ryan Rodgers, Martha, Chad, Greg. Mais surtout, je remercie Jonathan pour l'accueil, les discussions et les sorties.

Je remercie aussi toutes les personnes avec qui j'ai travaillé à l'IPREM, Sandra, Carine, Géraldine et Mickael. En particulier je remercie les différentes personnes du bureau, pour l'ambiance, les discussions les activités extras professionnelles, Victor, Maxime, Lucie, German, Genesis, Vicmary et Aurore.

Enfin je remercie aussi mes amis en particulier Valentin et ma famille qui ont réussi à me supporter que ça soit pendant les bons moments ainsi que pendant les moments parfois plus difficile.

Résumé

La présence d'hétéroatomes et de métaux dans les fractions lourdes du pétrole brut peut entraîner la désactivation des catalyseurs d'hydrotraitement et d'hydrocraquage. Les métaux les plus difficile à éliminer de leur matrice sont concentrés dans les asphaltènes. Ces travaux de thèse visent à obtenir une meilleure connaissance des métaux contenus dans les asphaltènes et de leur environnement chimique afin d'optimiser le processus de raffinage.

Des techniques de séparation telles que la *Gel Permeation Chromatography* (GPC), l'*High Performance Thin Layer Chromatography* (HPTLC) qui a été developpée et la séparation solide/liquide ont été combinées à des techniques d'analyse élémentaires telles que l'*Inductively Coupled Plasma High Resolution Mass Spectrometry* (ICP MS) ou la spectrométrie de masse moléculaire à résonance cyclotronique ionique pour la caractérisation des fractions lourdes du pétrole brut.

Dans une première partie, les profils de volume hydrodynamique des espèces qui contiennent du vanadium et du soufre, ont été déterminés par GPC précédés d'une extraction solide/liquide suivis d'une détection en ligne par ICP-MS et par *Fourier Transform Ion Cyclotron Resonance Mass Spectrometry* (FT-ICR MS). Il apparait que plus la taille des agrégats est importante, plus les composés sont aliphatiques. Cependant malgré le couplage de deux techniques de séparation, les porphyrines de vanadium contenues dans les agrégats de grandes tailles n'ont pas pu être caractérisées car inaccessibles lors de l'ionisation.

Ensuite, des analyses similaires ont été menées mais cette fois-ci par HPTLC qui permet une séparation des échantillons pétroliers par polarité. L'HPTLC a ainsi été couplée à une séparation solide liquide suivie d'une analyse élémentaire et moléculaire. Une méthode de séparation par HPTLC en une seule étape de migration a été développée. Cette méthode a permis d'isoler les porphyrines libres de celles agrégées. Cependant les molécules contenant le vanadium dans les fractions qui sont restées au point de dépôt n'ont pas pu être ionisées par *Matrix Assisted Laser Desorption Ionisation* (MALDI)-FT-ICR-MS.

Pour finir, une méthode a été développée à base de dopage avec de l'argent. Il apparait que doper un échantillon d'asphaltène avec de l'argent permet de désagréger une partie du vanadium contenu dans les agrégats de grandes tailles. Par la suite, cette méthode pourrait permettre une analyse beaucoup plus poussée des composés présents dans cette fraction.

Abstract

The presence of heteroatoms and metals in heavy fractions of crude oil can lead to the deactivation of hydrotreating and hydrocracking catalysts. The metals that are most difficult to remove from their matrix are concentrated in asphaltenes. The aim of this thesis work is to gain a better understanding of the metals contained in asphaltenes and their chemical environment in order to optimize the refining process.

Separation techniques such as Gel Permeation Chromatography (GPC), High Performance Thin Layer Chromatography (HPTLC) which has been developed and solid/liquid separation have been combined with elemental analysis techniques such as Inductively Coupled Plasma High Resolution Mass Spectrometry (ICP MS) or Ion Cyclotron Resonance Molecular Mass Spectrometry (ICR MS) for the characterization of heavy crude oil fractions.

In a first part, the hydrodynamic volume profiles of species containing vanadium and sulphur were determined by GPC preceded by solid/liquid extraction followed by on-line detection by ICP-MS and Fourier Transform Ion Cyclotron Resonance Mass Spectrometry (FT-ICR MS). It appears that the larger the size of the aggregates, the more aliphatic the compounds are. However, despite the coupling of two separation techniques, the vanadium porphyrins contained in the large aggregates could not be characterised because they were inaccessible during ionisation.

Similar analyses were then carried out but this time by HPTLC which allows separation of the oil samples by polarity. HPTLC was thus coupled to a solid-liquid separation followed by an elemental and molecular analysis. A method of separation by HPTLC in a single migration step has been developed. This method made it possible to isolate free porphyrins from aggregated porphyrins. However, the vanadium-containing molecules in the fractions that remained at the deposition point could not be ionised by Matrix Assisted Laser Desorption Ionisation (MALDI)-FT-ICR-MS.

Finally, a method was developed based on doping with silver. It appears that spiking a sample of asphaltene with silver can disaggregate some of the vanadium contained in the larger aggregates. Subsequently this method could allow much more detailed analysis of the compounds present in this fraction.

Plan

Liste des Figures

Liste des tableaux

Liste des abréviations

ABAN : Acide Base Amphotère Neutre

ACN : ACetoNitrile

ACS : American Chemical Society

AMD2 : Automated Multiple Development 2

APCI : Atmospheric Pressure Chemical Ionization

APPI : Atmospherique Pressure Photo Ionisation

ARDS : Atmospheric Residue Desulfurization

ATS4 : Automated TLC Sampler 4

BSS : Bright Stock Solve

C3 : Propane

C5 : Pentane

C6 : Hexane

C7 : Heptane

DAO : Desaphalted Oil

DAS : Desalphatage

DBE : Double Bond Equivalent

DCM : DiChloroMethane

DIHEN : Direct Injection High Efficiency Nebulizer

DIN : Direct Injecteur Nebulizer

DMF : DiMethyle Formamide

DPEP : Deoxophylloerythroetio

DSV : Distillat Sous Vide

ELSD : Evaporating Light Scattering Detector

ESI : ElectroSpray Ionisation

ETV : ElectroThermal Vaporization

FID : Free Induction Decay

FT-ICR MS : Fourier Transform Ion Cyclotron Resonance Mass Spectrometry

GPC : Gel Permeation Chromatography

HDM : HydroDeMetallation

HDN : HydroDeNitrification

HDO : HydroDesOxygénation

HDS : HydroDeSulfurization

HDT : Hydrotraitement

HPTLC : High Performance Thin Layer Chromatography

iC2MC : International Complex Matrices Molecular Characterization

ICP AES : Inductively Coupled Plasma Atomic Emission Spectrometry

ICP HR MS : Inductively Coupled Plasma High Resolution Mass Spectrometry

LA : Laser Ablation

MALDI : Matrix Assisted Laser Desorption Ionisation

PAH : Composés Aromatiques Polycycliques

PLS : Partial Least Square

PS : Polystyrene

QCR : Quartz Cristal Resonator

RSV : Résidu Sous Vide

SARA Saturé Aromatiques Résines Asphaltenes

SEC : Size Exclusion Chromatography

THF : Tetrahydrofurane

TISIS : Torch Integrated Sample Introduction System

Tol : Toluene

UV : Ultra-Violet

Introduction

Les produits pétroliers les plus utilisés proviennent des fractions légères telles que le gaz, l'essence ou le diesel. Par conséquent, les produits pétroliers lourds doivent être transformés en produits légers par craquage catalytique dans les raffineries. Or certains pétroles contiennent une grande quantité de ces fractions lourdes et nécessitent donc un traitement couteux avant utilisation. Ces fractions lourdes peuvent avoir une forte concentration d'hétéroatomes (S, N, O) et plusieurs centaines de ppm de métaux (V, Ni, Fe), qui sont des poisons pour les catalyseurs d'hydrocraquage. Ainsi, ils doivent d'abord être éliminés par l'*HydroDeMetallation* (HDM) suivi par de l'*HydroDeSulfurization* (HDS) pour produire des produits finis respectant les limites fixées par la réglementation européenne. Généralement, deux pétroles provenant d'endroits géographiques proches signifient deux pétroles avec une composition chimique proche. Or, ce n'est pas toujours vrai, citons le cas d'un incident industriel récent dans lequel deux pétroles d'origine géographique proche avaient été traités dans une unité de désulfuration de résidus atmosphériques, le premier n'ayant pas posé de problème mais le deuxième ayant sérieusement encrassé des unités de raffinages alors que les analyses standards indiquaient que ces pétroles étaient macroscopiquement semblables. Faisant passer la durée de vie du cycle catalytique de 18 à 11 mois et entrainant un sérieux surcout pour le raffinage.

Les hétéroatomes et les métaux dans les fractions lourdes du pétrole brut sont liés à la présence d'asphaltènes, les composants les plus problématiques des fractions lourdes. De plus, l'agrégation des composés contenant du S, du Ni et du V pourrait être impliquée dans divers problèmes liés à la précipitation des asphaltènes au cours de la récupération, du transport et du raffinage du pétrole. L'optimisation et la compréhension du traitement des fractions lourdes nécessitent une meilleure connaissance de la spéciation chimique des métaux présents et de la caractérisation au niveau moléculaire des constituants des produits pétroliers. La grande complexité de ces échantillons, avec des dizaines de milliers de composés et leurs isomères, rend nécessaire le développement de méthodes analytiques puissantes. Dans ce but, le laboratoire International commun de Cartographie Moléculaire des Matrices Complexes (iC2MC) a récemment été créé. Il se compose d'une structure de recherche commune entre les universités de Pau, Rouen, Tallahassee et une partie du département Analyse de la direction de Recherche et Développement de TOTAL Raffinage Chimie pour le partage des étudiants, des compétences et de l'instrumentation permettant une meilleure connaissance moléculaire et élémentaire des matrices complexes. Ces travaux de thèse ont été menés au sein du laboratoire commun international iC2MC.

Ce manuscrit se compose de quatre chapitres. Le premier est consacré à la description de la composition chimique de la matrice pétrolière et des procédés de raffinage. Les différentes techniques analytiques et méthodes utilisées au cours de cette thèse sont également présentées ici. Cela a permis d'identifier les trois techniques de séparation qui seront utilisées dans ces travaux. D'un côté la Chromatographie à Perméation de Gel (GPC). Il s'agit d'une technique qui sépare par volume hydrodynamique. Les molécules ayant un volume hydrodynamique élevé sont éluées avant celle ayant un volume hydrodynamique plus faible. La GPC peut être couplée avec un *Inductively Coupled Plasma High Resolution Mass Spectrometry* (ICP HR MS) et avec un *Fourier Transform Ion Cyclotron Resonance Mass Spectrometry* (FT-ICR MS) ce qui permet d'étudier simultanément la distribution en taille des molécules, les agrégats contenant S, V et Ni ainsi que la composition moléculaire des produits pétroliers. D'un autre côté la *High performance Thin Layer Chromatography* (HPTLC) permet de séparer la matrice pétrolière en fonction de l'affinité chimique des familles qui la composent. L'HPTLC peut aussi être couplée à une détection moléculaire et élémentaire. Enfin une méthode de séparation solide/liquide utilisant différents solvants a été utilisée. Le but de ces travaux a été d'associer une, deux ou trois de ces techniques de séparation pour simplifier toujours plus la matrice pétrolière afin de l'analyser plus finement.

Le deuxième chapitre se concentrera sur une séparation par taille d'échantillons pétroliers. Dans un premier temps un couplage GPC-ICP MS sera présenté. En effet il a été montré dans de précédents travaux que les métaux les plus difficiles à extraire se trouvent dans les fractions de plus haut poids moléculaire. La séparation en taille par GPC permet d'effectuer un premier fractionnement afin d'isoler cette partie problématique. Puis une séparation solide/liquide sera couplée à la GPC suivie d'une analyse élémentaire et moléculaire. Le couplage de deux méthodes de séparation a pour but de simplifier un maximum la matrice pétrolière qui est à la base très complexe.

Le troisième chapitre de cette thèse se concentrera sur la séparation par polarité grâce à l'utilisation de l'HPTLC. Dans un premier temps un développement de méthode introduisant un couplage HPTLC et *Laser Ablation* (LA)-ICP MS sera présenté. Ensuite l'HPTLC sera couplée à une séparation préalable solide/liquide suivie d'une analyse élémentaire et moléculaire.

Le quatrième et dernier chapitre du manuscrit est consacré à une nouvelle méthode de désagrégation consistant à doper des échantillons pétroliers avec de l'argent. L'ajout d'argent permet de désagréger une partie des porphyrines de vanadium présent dans les agrégats de grandes tailles. Le but de cette nouvelle méthode et de pouvoir analyser, pour la première fois, les parties les plus complexes des fractions lourdes désagrégées.

The most consumed petroleum products come from light fractions such as gas, petrol or diesel. Therefore, heavy petroleum products have to be transformed into light products by catalytic cracking in refineries. However, some oils contain a large amount of these heavy fractions and therefore require expensive treatment before use. These heavy fractions can have a high concentration of heteroatoms (S, N, O) and several hundred ppm of metals (V, Ni, Fe), which are poisons for hydrocracking catalysts. Thus, they must first be removed by HydroDeMetallation (HDM) followed by HydroDeSulfurization (HDS) to produce finished products that comply with the limits set by European regulations. Generally, two oils from close geographical locations means two oils with a close chemical composition. However, this is not always true, as in a recent industrial incident where two oils of close geographical origin were treated in an atmospheric residue desulphurisation unit. The first oil did not cause any problems, but the second seriously fouled refining units, even though standard analyses indicated that these oils were macroscopically similar. Extending the life of the catalytic cycle from 18 to 11 months and resulting in serious refining cost overruns.

Heteroatoms and metals in heavy crude oil fractions are related to the presence of asphaltenes, the most problematic components of heavy fractions. In addition, the aggregation of compounds containing S, Ni and V could be involved in various problems related to the precipitation of asphaltenes during oil recovery, transportation and refining. The optimization and understanding of the treatment of heavy fractions requires a better knowledge of the chemical speciation of the metals present and the characterization at the molecular level of the constituents of petroleum products. The great complexity of these samples, with tens of thousands of compounds and their isomers, makes it necessary to develop powerful analytical methods. To this end, the International Joint Laboratory for Complex Matrix Molecular Mapping (iC2MC) has recently been created. It consists of a joint research structure between the universities of Pau, Rouen, Tallahassee and part of the Analysis Department of the Research and Development Department of TOTAL Refining Chemistry for the sharing of students, skills and instrumentation for a better molecular and elementary knowledge of complex matrices. This thesis work was carried out within the iC2MC international joint laboratory.

This manuscript consists of four chapters. The first one is devoted to the description of the chemical composition of the petroleum matrix and refining processes. The different analytical techniques and methods used during this thesis are also presented here. This allowed the identification of the three separation techniques that will be used in this work. On the one hand, Gel Permeation Chromatography (GPC). This is a technique that separates by hydrodynamic volume. The molecules with a high hydrodynamic volume are eluted before those with a lower hydrodynamic volume. GPC can be coupled with Inductively Coupled Plasma High Resolution Mass Spectrometry (ICP HR MS) and Fourier Transform Ion Cyclotron Resonance Mass

Spectrometry (FT-ICR MS) which allows simultaneous study of the size distribution of molecules, aggregates containing S, V and Ni as well as the molecular composition of petroleum products. On the other hand, High Performance Thin Layer Chromatography (HPTLC) allows the separation of the petroleum matrix according to the chemical affinity of the families that make it up. HPTLC can also be coupled with molecular and elemental detection. Finally, a solid/liquid separation method using different solvents was used. The aim of this work was to combine one, two or three of these separation techniques to further simplify the petroleum matrix to analyse it more finely.

The second chapter will focus on separation by oil sample size. In a first step a GPC-ICP MS coupling will be presented. Indeed, it has been shown in previous work that the most difficult metals to extract are found in the higher molecular weight fractions. Size separation by GPC allows a first fractionation to isolate this problematic part. Then a solid/liquid separation will be coupled to the GPC followed by an elemental and molecular analysis. The coupling of two separation methods aims to simplify the matrix as much as possible.

Chapitre I : Contexte Scientifique

Ce premier chapitre a pour but de résumer une partie des connaissances sur l'analyse du pétrole. En effet le pétrole étant une matrice complexe, sa structure et sa composition exacte ne sont pas déterminées. De plus, par sa complexité, une simplification de la matrice pétrolière est souvent nécessaire avant analyse.

La première partie de ce chapitre présente la composition chimique de la matrice pétrolière. La connaissance des propriétés physico-chimiques du pétrole telles que la teneur en Soufre et en métaux ne suffit pas pour comprendre son comportement. De plus, les hypothèses actuelles sur les structures des asphaltènes seront données.

Puis une explication des différents processus de raffinage et d'extraction des hétéroéléments et des métaux a été donnée.

Enfin dans une troisième partie de ce chapitre a été présenté le principe des techniques et méthodes analytiques utilisées au durant cette thèse. Pour cela, une étape préliminaire de simplification de la matrice est recommandée. Ainsi la GPC est une technique de séparation chromatographique largement utilisée pour l'analyse des produits pétroliers. Une autre méthode décrite de séparation est le fractionnement par polarité par HPTLC. Enfin, une technique de séparation liquide/solide, appelée Extrographie a été présentée.

Ensuite, les techniques d'analyses seront présentées. Notamment l'ICP MS qui permet une analyse élémentaire des produits pétroliers. Enfin la technique de spectrométrie de masse à résonance cyclotronique ionique qui permet l'analyse moléculaire des produits pétroliers a aussi été présentée.

Part I: La matrice pétrolière

I.I.1 Le pétrole

I.I.1.1Définition

Le pétrole est une ressource non-renouvelable à notre échelle de temps qui provient de la décomposition de la matière végétale et animale durant des millions d'années à haute température et pression. La matière formée migre dans les sous-sols jusqu'à atteindre une couche imperméable et forme un réservoir [1] [2]. Le pétrole après un pic en 1973 à 42,6 %, a atteint en 2016 34,2% du mix énergétique mondial.

La composition du pétrole varie en fonction de la zone géographique d'où il vient. Ceci permet de connaître son origine [3] [4]. Cependant, la composition moyenne du pétrole se situe aux alentours de : 85% de carbone, 14% d'hydrogène. A ceci s'ajoute de faibles concentrations de nombreux éléments comme le soufre (0.04 à 8%), l'oxygène (0.1-5%), l'azote (0.1-1.5%) et des métaux comme le Nickel et le Vanadium avec une concentration allant jusqu'à plusieurs centaines de ppm [5], [6].

I.I.1.2 Les coupes pétrolières

Le pétrole brut peut être séparé par distillation selon le point d'ébullition pour fabriquer de nombreux produits utilisés dans tous les domaines.

- Gaz (de C1 à C4)

- Essence : distillée à 180°C (C4-C10)

- Kérosène : distillé entre 150 et 240°C (C10-C13)

- Gasoil : distillé entre 220 et 380°C (C13-C20/25)

- Résidu atmosphérique (RAT) : ce qui reste à 380°C à pression atmosphérique

- Distillat sous vide (DSV) : fraction distillée sous vide entre 360 et 550°C (C20-C50)

- Résidu sous vide (RSV) : ce qui reste sous vide après distillation à 550°C

I.I.1.3 Les fractions lourdes

Les réserves de pétrole conventionnel sont estimées à 1,64 trillion de barils (159 L). Le pétrole lourd, dont les réserves sont estimées à 8,90 trillion de barils, contenant un

pourcentage de coupes lourdes plus important que dans le pétrole conventionnel est alors utilisé et converti en fractions légères par craquage catalytique pour permettre la production d'essence, de gasoil et de kérosène nécessaires.[7]

Cependant les fractions lourdes contiennent plus d'hétéro éléments (N, O, S) et plus de métaux (V, Ni). Ces éléments posent des problèmes dans les unités de craquage et doivent donc être extraits en amont par de couteux traitements d'HDM et d'HDS, ce qui a pour conséquence d'augmenter le coût du processus de raffinage. De plus la présence de soufre et de métaux contribue à la pollution environnementale[8]–[13]. Pour les métaux, connaitre leur concentration totale n'est souvent pas suffisant pour prévoir leurs effets néfastes lors du raffinage du pétrole. En effet, il existe le cas où deux pétroles ont des concentrations en vanadium proches mais l'un des deux pétroles contient un vanadium beaucoup plus complexe à enlever Il faut pour cela connaitre les proportions des différents types de structures contenant des métaux.

I.I.1.3.1 Le Nickel et le Vanadium

I.I.1.3.1.1 Le Nickel et le Vanadium dans les porphyrines

Les deux principaux métaux contenus dans le pétrole sont le nickel et le vanadium. Leur concentration varie entre 10 ppm et 1000 ppm[3], [6], [14]–[18] en fonction des conditions de formation du pétrole et donc de son origine géographique. Une grande partie du nickel et du Vanadium a été identifiée comme appartenant de complexes porphyriniques [19]–[23].

Les porphyrines ont été décrites dès le début du XXème siècle comme ayant des structures similaires aux pigments de chlorophylle (plantes) et aux pigments de l'hème (animal). La chlorophylle étant présente en plus grande quantité, il est supposé qu'elle soit le précurseur le plus courant des porphyrines de nickel et de vanadium, l'ion Mg^{2+} étant remplacé par Ni^{2+} ou VO^{2+}. La constante chélatante de ce type de molécules étant élevée, cela conduit à une grande stabilité[5].

Six principaux types de porphyrines ont été identifiés [21], [24].

- Etio porphyrines (ETIO)

- Deoxophylloerythroetio porphyrins (DPEP)

- Dicyclic-deoxophylloerythroetio (di-DPEP)

- Rhodo-etio porphyrins (rhodo-ETIO)

- Rhodo-deoxophylloery-throetio porphyrins (rhodo DPEP)

- Rhodo-dicyclic-deox- ophylloerythroetio (rhodo-di-DPEP).

Les plus abondantes seraient les structures etio porphyrines (ETIO) et deoxophylloerythroetio porphyrins (DPEP) (voir Figure 1).

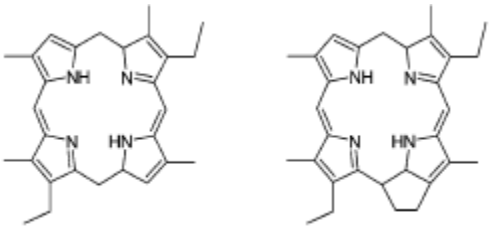

Figure 1: Structures ETIO (gauche) et DPEP (droite)

De plus d'autres espèces de porphyrines de vanadium (N_4VO_2, N_4VO_3, N_4VO_4) ont été identifiées dans le pétrole brut [24]. Il a aussi été montré que les porphyrines jouent un rôle dans l'agrégation des de la matrice pétrolière [20].

I.I.1.3.1.2 Le Nickel et le Vanadium hors porphyrines

Les métaux non-complexés par les porphyrines sont supposés être en minorité par rapport à la teneur totale en métaux. Cependant l'existence d'autres complexes métalliques n'a pas été prouvée car difficiles à identifier[16], [28], [29].

I.I.1.3.2 Le Fer

Le fer est aussi un métal présent dans le pétrole. Comme les autres métaux, il est nécessaire de l'extraire avant le raffinage car celui-ci désactive les catalyseurs d'hydrodemetallation ainsi que de Fluid Catalytic Craking. Comme les autres métaux, la connaissance de la teneur totale en fer n'est pas suffisante pour prévoir les problèmes que l'élément cause durant le raffinage. Le fer dans le pétrole existe principalement sous 4 formes [30], [31].

- Le fer sous forme de particules inorganiques.

- Les sels contenant du fer.

- Le fer dans un complexe porphyrinique.

- Le fer dans un complexe non porphyrinique.

I.I.1.3.3 Le Soufre

Les composés soufrés sont très problématiques dans l'industrie pétrolière notamment pour des raisons de fiabilité des installations puisque le S est principalement éliminé sous forme d'H2S, un gaz corrosif et toxique, ainsi que pour des raisons environnementales. En effet, depuis le 1er janvier 2009, la concentration totale en soufre dans les essences et les gazoles doit être inférieure à 10 ppm pour les véhicules routiers. Ces teneurs sont issues de la transposition en droit français de la directive européenne 2009/30/CE. Cela impose à l'industrie pétrolière de lourds traitements de désulfuration. En effet le soufre est présent dans le pétrole jusqu'à 7 à 8% en masse, ce qui en fait l'hétéro-élément le plus présent.

Bien avant la mise en place de ces législations de plus en plus drastiques, l'industrie pétrolière utilisait déjà l'HDS pour augmenter la stabilité de l'essence et diminuer la formation de fumée dans le kérosène [10] mais ces traitements s'appliquaient principalement à des pétroles légers. Les composés soufrés peuvent de plus être à l'origine de problèmes de corrosion [12] et vont produire des effets indésirables sur les catalyseurs et les filtres. Ils sont notamment des poisons des différents catalyseurs utilisés lors du raffinage (reformage, isomérisation, craquage catalytique, …). Il faut donc d'étudier les composés soufrés et leur spéciation dans les pétroles lourds [32], [33] afin d'adapter les procédés déjà existant. La présence de soufre est aussi responsable d'émissions de SO2 et SO3 lors de la combustion.

Le Soufre est souvent trouvé sous forme de thiols, sulfides, disulfides, tiophènes et benzothiophènes (voir figure 2). On peut aussi trouver de l'H_2S dans le pétrole en fonction de son origine. Ce risque est la plupart du temps maitrisé par l'ajout d'additifs de type « scavenger H_2S » permettant de réagir avec l'H_2S pour le piéger en phase organique.

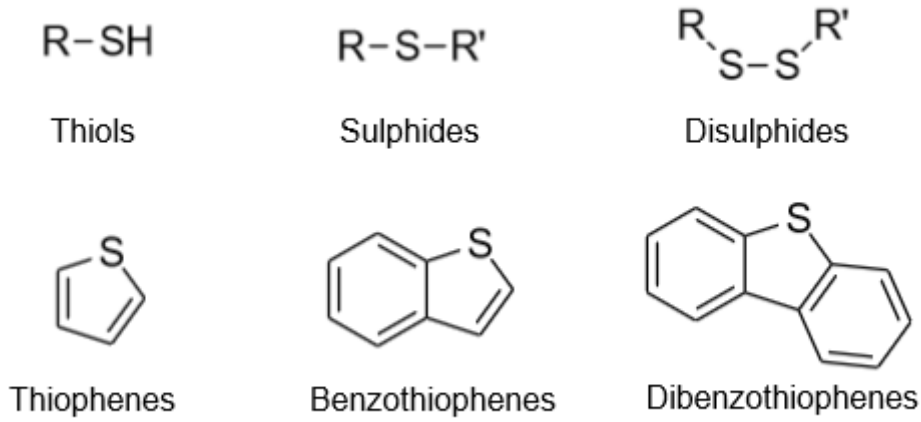

Figure 2: Schéma de six composés contenant du soufre présent dans le pétrole

I.I.1.3.4 Autres hétéro éléments

En plus du soufre, le pétrole brut contient deux autres hétéroatomes dans des quantités importantes, l'oxygène (jusqu'à 5 %) et l'azote (jusqu'à 1,5 %). Les espèces hétéroatomiques comportent souvent des cycles aromatiques et naphténiques et se retrouvent typiquement dans les fractions lourdes, les asphaltènes et les fractions aromatiques et résines lors d'une séparation SARA. Tout comme les composés soufrés, les composés oxygénés et azotés vont être problématiques pour des problèmes de corrosion et de désactivation de catalyseurs.

Les composés oxygénés, qui sont présents sous forme de phénols et d'acides carboxyliques [32]–[35], sont connus pour être parmi les responsables principaux de la corrosion des infrastructures durant l'extraction et le raffinage des produits pétroliers. Leur concentration est de moins de 2 % dans le pétrole brut mais leur teneur augmente fortement avec la température d'ébullition pour atteindre des valeurs de 8 % dans les coupes lourdes. Ces composés ont été et sont toujours largement étudiés dans le milieu pétrolier. L'oxygène sous forme d'ester, de cétones, d'aldéhyde et d'amides, sont eux moins abondants.

La teneur totale d'un brut en azote est généralement comprise entre 0,1 et 0,9 %. Les composés azotés peuvent être de deux types, soit basiques sous forme de composés de type pyridinique, soit neutres sous forme de composés de type pyrrole, indole ou carbazole (voir Figure 3). Les composés azotés (basiques et neutres) sont présents à toutes les températures d'ébullition mais leurs teneurs augmentent dans les coupes lourdes et les résidus. Les espèces azotées vont être à l'origine de problèmes tels que la formation de NOx lors de la combustion

ainsi que l'empoisonnement des catalyseurs d'hydrocraquage et d'hydrodésulfurisation d'où l'intérêt d'étudier ces composés [32], [33], [36]–[39].

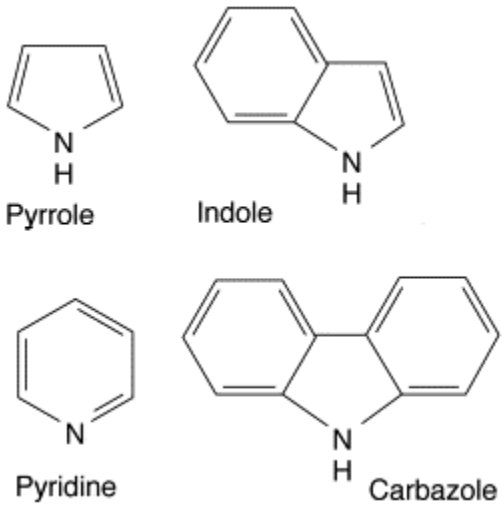

Figure 3: Schéma de quatre composés azotés présent dans le pétrole

Déterminer l'environnement chimique de ces éléments est important pour optimiser les processus d'extraction[40]. Cependant le pétrole étant une matrice complexe, il faut dans un premier temps la simplifier avant de l'analyser. Plusieurs processus de séparation peuvent alors être utilisés.

I.I.1.4 Fractionnement

I.I.1.4.1 Fractionnement ABAN

Une deuxième séparation du pétrole (voir Figure 4) utilisée est la séparation ABAN (acide, base, amphotère, neutre)[13], [41].

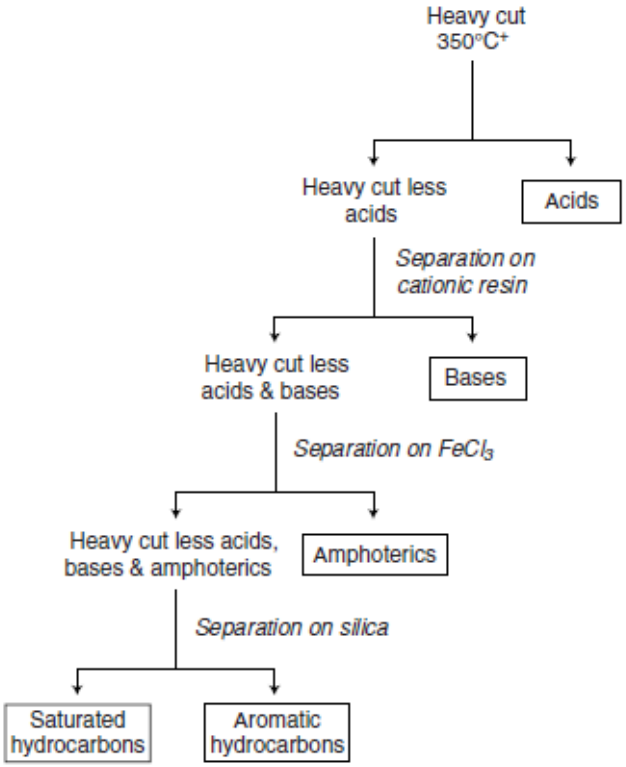

Figure 4 : Schéma du fractionnement ABAN[13]

- Acide : fraction contenant beaucoup de phénols et groupe carbonyles
- Base : principalement composés azotés
- Amphotère : polys aromatiques contenant des hétéro atomes
- Neutre : saturés et aromatiques

I.I.1.4.2 Fractionnement SARA

Une autre séparation très utilisée est la séparation du pétrole lourd par chromatographie dite SARA (Saturés, Aromatiques, Résines et Asphaltènes)[2], [42] (voir Figure 5).

- Saturés : alcanes et cyclo alcanes

- Aromatiques : molécules avec un ou plusieurs cycles benzéniques

- Résines : molécules aromatiques contenant des hétéro atomes

- Asphaltènes : mélanges complexe de molécule de grande taille et de polarités extrêmes, contenant une part importante des métaux et des hétéroatomes.

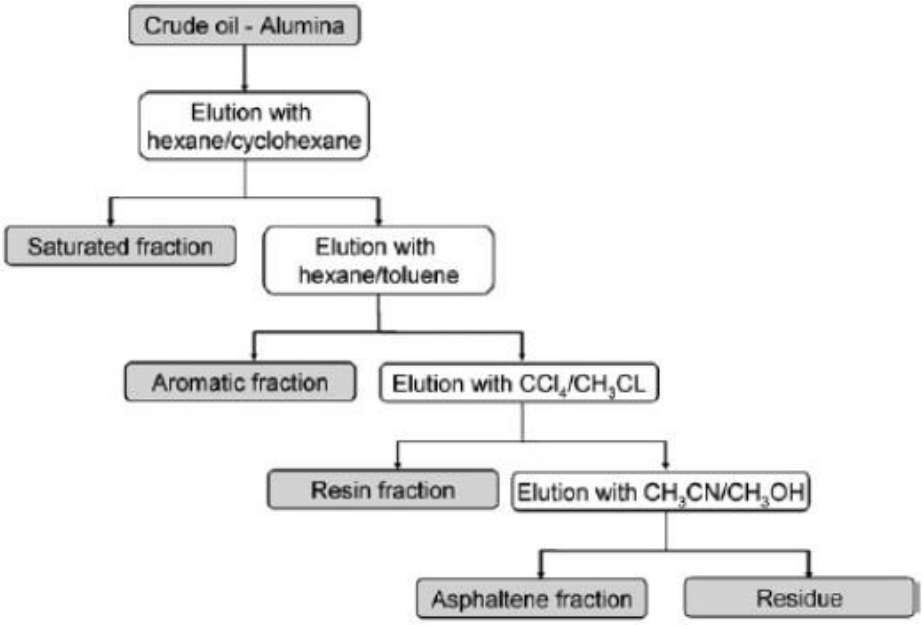

Figure 5 : Schéma du fractionnement SARA[2]

La quantité d'hétéro éléments est directement reliée à la quantité de composés très polaires qui sont contenus dans les résines et les asphaltènes. L'étude des asphaltènes est essentielle pour connaître l'environnement chimique des métaux et des hétéro-éléments contenus dans le pétrole [13].

I.I.1.4.3 Précipitation des asphaltènes

Enfin, il est possible de séparer le pétrole en deux fractions qui sont les « maltènes » et les « asphaltènes ». Dans un premier temps le pétrole brut est dissout dans du toluène, puis un excès d'alcanes (C3, C5, C6 ou C7) est ajouté. La partie qui précipite est appelée « asphaltène ».

I.I.1.5Les asphaltènes

Les asphaltènes contiennent les composés du pétrole les plus lourds, de nombreux groupes fonctionnels ainsi que beaucoup d'hétéro-éléments et des métaux (V, Ni) [43]–[45]. Les propriétés des asphaltènes varient en fonction du solvant utilisé pour leur précipitation. De plus, les asphaltènes peuvent s'auto-agréger en solution lorsque les conditions opératoires changent et précipiter [46]–[49]. La structure des asphaltènes varie en fonction de la composition du pétrole et des solvants utilisés pour les précipiter. Cependant il est estimé que leur masse molaire moyenne se situe aux alentours de 750 $g.mol^{-1}$ [48]. De plus, plusieurs travaux proposent de possibles structures générales.

I.I.1.5.1 Supramolecular Assembly Model

Un des modèles pour la représentation des asphaltènes (voir Figure 6) est proposé par Gray *et al* [50] en 2011. L'asphaltène aurait une composition chimique complexe comprenant, des chaines alkyles, des cycles naphténiques, des aromatiques, des hétéro éléments (O, N, S), des métaux (V, Ni) notamment contenue dans des structures de type porphyrines, liés par différents types de forces (liaison hydrogène, complexation, interaction π-π). Cette structure permet d'expliquer la tendance des asphaltènes à l'auto agrégation, et d'envisager l'inclusion de petites molécules au sein des agrégats [51], [52] [53].

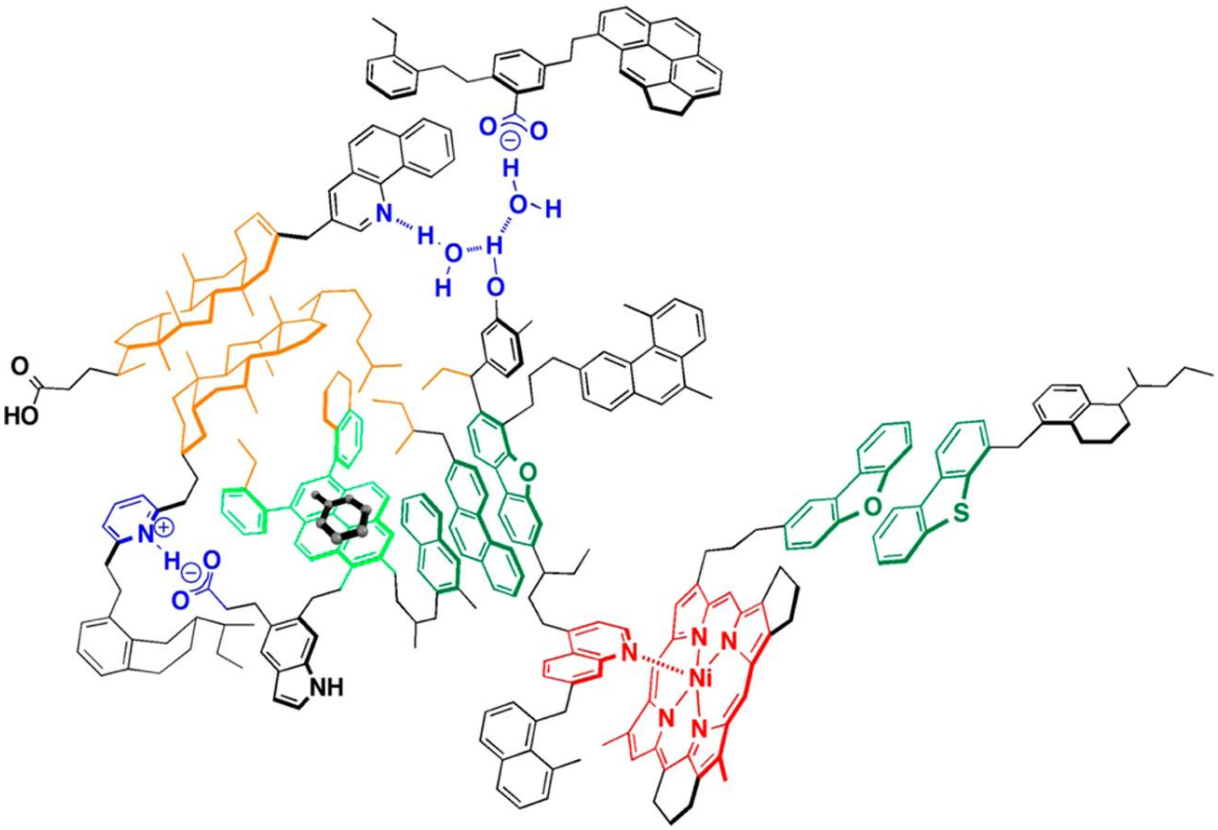

Figure 6: modèle "supramolecular assembly"[50]

I.I.1.5.2 Yen-Mullins model (island)

Le modèle de Yen-Mullins ([40], [53]–[57]) propose qu'une molécule d'asphaltène mesure en moyenne 1.5 nm de diamètre et est composé d'un cœur aromatique avec des chaines alkyles (Figure 7, gauche). Puis ces molécules peuvent s'associer par liaisons π-π pour former des nano-agrégats (centre) de 2 nm. Enfin quand la concentration est supérieure à plusieurs grammes par litre, la concentration micellaire critique est atteinte et les nano-agrégats peuvent former des complexes de plus grande taille (droite) de 5 nm qui peuvent précipiter. D'autres travaux, comme ceux de Sabbah *et al* [40], [58] mettent en évidence des pertes correspondant à des chaines alkyl lors de l'utilisation de laser. Ce qui correspondrait au modèle « island ».

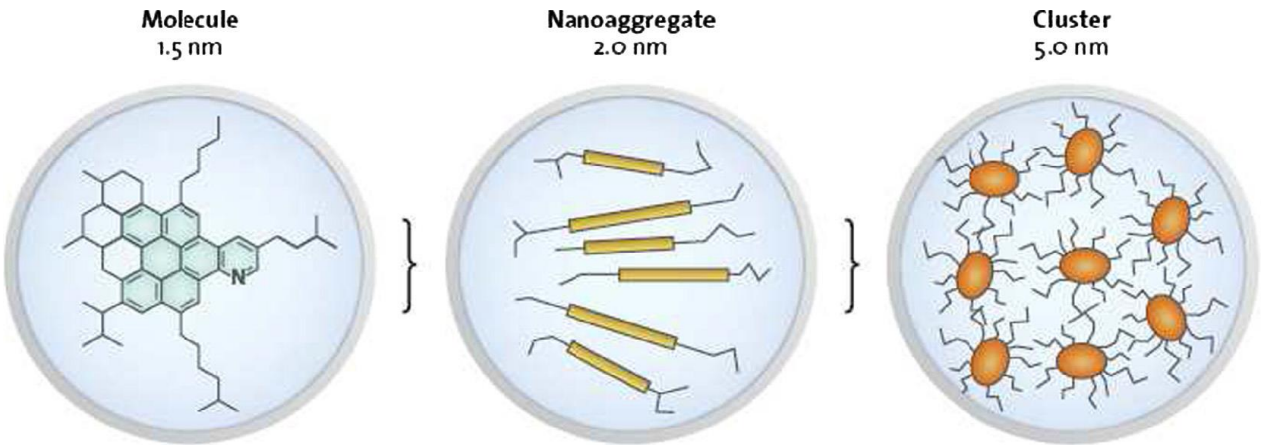

Figure 7: Le modèle de Yen-mullins (island)[59]

Cependant ce modèle est critiqué car il n'explique pas plusieurs propriétés physiques des asphaltènes[25], [60] comme l'occlusion de composés saturés et aromatiques et des produits issus du craquage thermique[61]–[64].

I.I.1.5.3 Le modèle "archipel"

Ce modèle propose que les molécules d'asphaltènes ne sont pas constituées d'un cœur mais de plusieurs reliés entre eux par des ponts alkyles [65]. D'après les récents travaux de Chacón-Patiño *et al* [66]–[68], les asphaltènes sont composés à la fois des structures de type island dans les fractions les plus accessibles et de poids moléculaire faible ainsi que de structure de type archipel formant des agrégats de plus grandes tailles et difficilement ionisables en *Atmospherique Pressure Photo Ionisation* (APPI)-FT-ICR MS. Ce qui expliquerait que les précédents travaux utilisant principalement cette technique n'aient pas détecté de telles structure Toujours selon ces mêmes auteurs, la quantité « d'island » et « d'archipelago » varie de façon significative en fonction des échantillons.

Part II: Le raffinage du pétrole

Le raffinage du pétrole correspond à l'ensemble des procédés de traitement et de transformation que le pétrole va subir dans la raffinerie afin de produire une quantité maximale de produits à haute valeur commerciale, comme les différents carburants utilisés dans les moteurs à combustion et les monomères qui serviront à alimenter l'industrie pétrochimique. Le design d'une raffinerie va tenir compte des propriétés physico-chimiques du ou des bruts qu'elle servira à traiter. Il peut arriver pour des gisements importants qu'une raffinerie ne soit utilisée que pour le traitement de ce seul brut, mais en général, les raffineries européennes sont construites afin de traiter une gamme de bruts assez large. De manière générale, la structure des raffineries va être plus simple dans les pays en développement que dans les pays développés et aussi dans les régions où les besoins en carburants sont élevés. Dans le dernier cas, le nombre d'unités de traitement sera plus important. Seules les étapes de séparation et une partie des étapes de conversion en rapport avec le sujet seront décrites dans cette partie de la thèse.

Le raffinage s'opère en plusieurs étapes :

- Dessalage
- Distillation atmosphérique et sous vide
- La chaine de fabrication des huiles (si production d'huile)
- Conversion des fractions lourdes

I.II.1 Dessalage

Des sels inorganiques peuvent être présent dissout dans l'eau contenue dans le pétrole. Comme les autres éléments, la quantité de sels présent dans le pétrole dépend de son origine et peut varier de façon significative. Si ces sels ne sont pas enlevés, ils peuvent dans la colonne de distillation former entre autres du HCl qui posera des problèmes de corrosion.

De l'eau est injectée et mélangée au pétrole dans le but de créer une émulsion. La création de l'émulsion est importante pour maximiser le contact eau/pétrole. Dans un second temps, la partie contenant la majorité des sels inorganiques est extraite. Une fois le pétrole dessalé il est envoyé dans la colonne de distillation pour fractionnement.

I.II.2 La distillation atmosphérique et sous vide

La distillation s'effectue en deux étapes : d'abord la distillation atmosphérique, puis la distillation sous vide.

Durant la distillation atmosphérique, le pétrole brut est chauffé et introduit dans une colonne à distillation. Les différentes coupes pétrolières sont ainsi extraites et envoyées vers d'autres unités de la raffinerie afin de poursuivre leurs traitements plus ou moins lourds selon la coupe considérée ainsi que la qualité du pétrole brut introduit initialement. Les coupes extraites du pétrole brut vont être détaillées ci dessous :

- Les gaz
- Les essences légères
- Les essences lourdes
- Le kérosène
- Les diesels légers
- Les diesels lourds
- Le distillat atmosphérique
- Le résidu atmosphérique

Les gaz et les essences sont extraits sous forme gazeuse en tête de colonne et sont ensuite traités dans des colonnes de distillation à deux produits. Les coupes kérosène, diesel et distillat sont soutirés latéralement et le résidu atmosphérique est soutiré par le fond.

Durant la distillation sous vide, on utilise comme charge le résidu atmosphérique issu de la première étape de distillation afin de la séparer en plusieurs coupes pétrolières. Le découpage réalisé va dépendre à la fois de la composition du résidu atmosphérique servant de charge, mais aussi des utilisations souhaitées pour les coupes obtenues.

Les coupes formées sont alors :

- Les distillats sous vide (DSV).

- Le résidu sous vide (RSV).

Le gazole et les distillats sous vide sont soutirés latéralement tandis que le résidu sous vide est soutiré par le fond de la colonne.

I.II.3 La chaine de fabrication des huiles

La chaine de fabrication des huiles de base commence à partir du RSV et opère un fractionnement chimique suivant 3 unités. L'unité de désaphaltage (DAS), l'unité d'extraction au Furfural et l'unité d'extraction MEK/toluène.

I.II.3.1 Unité DAS

Dans un premier temps, une extraction est effectuée sur le RSV avec du propane. Le but de l'opération est d'enlever tous les asphaltènes présents. On récupère ainsi deux fractions, le Brai et l'huile désaphaltée (DAO). La DAO contient des paraffines, des iso-paraffines, des cycles et des aromatiques de petites tailles (1,2 ou 3 cycles). Il est ensuite envoyé dans la deuxième unité de fractionnement chimique.

I.II.3.2 Unité Furfural

La charge du furfural est la DAO. Une extraction au solvant furfural est effectuée. L'extrait obtenu est principalement constitués d'aromatiques. Le raffinat lui est constitué de paraffines, d'iso paraffines, de naphtènes ainsi que de molécules contenant un cycle aromatique ou deux.

I.II.3.3 Unité méthyléthylcétone (Mec)/Toluène

La charge de cette unité est le raffinat obtenu précédemment. Un mélange de toluène et MEC est utilisé. La paraffine brute, nommée cire, cristallise et est récupérée. La partie huileuses (BSS) contient des iso-paraffines, des naphtènes et quelques molécules aromatiques.

I.II.4 Conversion pour les fractions lourdes

La conversion est nécessaire afin d'adapter la composition du pétrole extrait à la demande du marché. Les produits lourds doivent être valorisés sous forme de produits légers pour la fabrication des carburants. Les unités de conversion mises en place à cet effet vont utiliser comme charges les coupes lourdes. La conversion est basée sur des réactions chimiques de craquage des molécules d'hydrocarbure lourd par rupture de liaisons carbone-carbone. Ces ruptures vont donner des molécules de taille plus faible. Cependant avant ces unités de craquage, il faut dans un premier temps enlever les différents hétéro-éléments car ces derniers sont des poisons pour les lits catalytiques.

I.II.4.1 Pretraitement : Généralités

Le terme hydrotraitement (HDT) va rassembler l'ensemble des procédés visant à éliminer des composés indésirables présents dans les coupes pétrolières. Ces procédés utilisent un traitement catalytique en présence d'hydrogène afin d'éliminer des composés soufrés, oxygénés, azotés et des métaux. Tous ces composés sont considérés comme des impuretés dans les coupes pétrolières car ils sont indésirables dans les produits finis et/ou sont néfastes pour le bon déroulement des procédés de conversion des coupes pétrolières en étant par exemple des poisons pour les catalyseurs du procédé de craquage catalytique.

Les catalyseurs d'hydrotraitement ont dû évoluer et continueront d'évoluer du fait des changements de législation et des différents types de pétroles. Les catalyseurs utilisés pour l'HDT des charges lourdes soient différents de ceux utilisés pour les charges légères du fait de la présence de molécules asphalténiques de hauts poids moléculaires et de composés organométalliques [69], [70]. La taille et la forme des particules du catalyseur vont jouer sur sa surface spécifique qui doit être adéquate à la charge.

Les principaux groupes de catalyseurs sont les oxydes de molybdène ou de tungstène activés soit par le nickel soit par le cobalt. En fonction de la combinaison utilisée ils seront

appelés catalyseur NiMo, CoMo, NiW ou CoW. Ces catalyseurs sont déposés sur un support qui peut être une alumine, des zéolithes, de la silice ou un mélange silice-alumine.

Dans le cas de ces charges qui contiennent des métaux et des asphaltènes, les propriétés physiques des catalyseurs doivent être bien choisis. Les charges utilisées ici sont plus visqueuses et plus aromatiques que les charges légères et la composition chimique du catalyseur doit également être modifiée afin d'obtenir une activité d'HDM correcte. En effet Oelderick *et al* [71] a montré comment le choix du catalyseur avait un impact sur l'activité d'HDS sur deux charges lourdes. Sur l'une des charges, l'HDS était constante sur toute la durée du traitement sans ajustement de la température ou de la pression d'hydrogène tandis l'efficacité de l'HDS diminuait de façon continue ce qui nécessitait une modification de la température et de la pression afin de prévenir cette désactivation.

De plus, d'après Maity *et al* [72], [73], l'ajout d'additif permet d'améliorer l'efficacité des catalyseurs. Des adjonctions de phosphore, fluor ou de bore ont par exemple été étudiées. Il est aussi possible de trouver des catalyseurs constitués de multiples oxydes métalliques [74], [75] ou encore des catalyseurs où le volume et le diamètre moyen des pores vont pouvoir être contrôlés par un ajout de TiO_2 (jusqu'à 5 %) au support alumine classique [76].

Pour ce qui est des propriétés physiques, les paramètres importants vont être le volume des pores, la distribution en taille des pores, la taille et la forme des particules du catalyseur. Une grande surface spécifique alliée à une taille de pore moyenne va présenter une activité catalytique importante du fait de la dispersion des métaux actifs dans les pores. Cependant des pores de petites tailles se boucheront plus régulièrement que des pores de grandes tailles mais qui seront moins efficace. Rana *et al* ont montré que les réactions d'HDS et d'HDM ont des rendements différents en fonction de la taille des pores, celle de l'HDM étant favorisé par des macro-pores tandis que celle de l'HDS est plutôt favorisé avec des micro- ou méso-pores[77]. De ce fait, des catalyseurs bimodaux ou même polymodaux possédant des distributions de volume de pores micro, méso et macro sont développés et commercialisés [78].

En fonction de l'impureté qui est ciblée le procédé s'appellera l'HDS, *hydrodesoxygenation* (HDO), *hydrodenitrification* (HDN) ou HDM dans le cas du soufre, de l'oxygène, de l'azote et des métaux respectivement. La différence entre ces procédés va provenir du type de catalyseur employé. De manière générale un catalyseur va permettre d'éliminer plusieurs types de composés hétéroatomiques ou contenant des métaux et sa sélectivité plus grande pour l'un d'eux donnera son nom au procédé[69], [70].

I.II.4.2 Prétraitement ARDS

I.II.4.2.1 Les composés soufrés

Les premiers composés concernés par les procédés d'hydrotraitement sont ceux contenant du soufre comme les mercaptans, les sulfures et les composés thiophéniques et benzothiophéniques. Les produits de combustion de ces composés que sont SO_2 et SO_3 sont une source de pollution atmosphérique ou de corrosion comme le H_2S et le SO_3. Enfin, ces composés soufrés sont de manière générale des poisons pour de nombreux catalyseurs utilisés dans les procédés de raffinage et notamment dans ceux de reformage et d'isomérisation. Leur élimination est donc primordiale afin de pouvoir réaliser des traitements poussés et nécessite un ajout d'hydrogène en présence d'un catalyseur adapté.

I.II.4.2.2 Les métaux

Les coupes lourdes contiennent une multitude de métaux dans des concentrations allant de quelques ppb à plusieurs centaines de ppm. Deux métaux sont principalement visés lors des procédés d'hydrodémétallation, le vanadium et le nickel qui, en plus d'être parmi les métaux les plus abondants dans les produits pétroliers (jusqu'à 1000 ppm), sont de très puissants poisons des catalyseurs utilisés dans les traitements de conversion. Les procédés d'HDM vont permettre, en présence d'hydrogène et d'un catalyseur adapté, d'éliminer les composés contenant ces métaux.

I.II.4.2.3 Les composés azotés

Les composés azotés sont nuisibles de par le caractère basique de certains d'entre eux dans les coupes lourdes. Cette basicité va provoquer l'empoisonnement des catalyseurs de conversion ayant un caractère acide dans les procédés de craquage catalytique et d'hydrocraquage par exemple. Les réactions d'HDN (hydrodenitrification) ont des caractéristiques voisines de celles d'HDS à savoir la consommation d'hydrogène et l'exothermicité. Elles sont cependant plus difficiles pour l'élimination de l'azote que pour celle du soufre.

I.II.4.2.4 Les composés oxygénés

L'oxygène peut être présent dans les produits pétroliers en quantités notables sous forme par exemple d'acides naphténiques à l'origine de problèmes de corrosion ou encore

sous forme de phénols. L'élimination de ces composés se fait de manière relativement aisée en présence d'hydrogène et d'un catalyseur adapté et conduit à la formation d'eau qui va pouvoir être séparée à l'état liquide par décantation.

Une fois les différents hétéro-élément enlevés, il est possible de craquer les différentes charges lourdes pour obtenir des fractions plus légères et valorisables. Il existe différents types de procédés de craquage en fonction de la façon dont les ruptures vont être provoquées. Les unités de craquage thermique vont utiliser la température, celles de craquage catalytique utilisent une combinaison de température élevée et d'un catalyseur et enfin, les unités d'hydrocraquage combinent les actions de la température et d'un catalyseur en présence d'hydrogène. Chacun de ces procédés a ses atouts et ses faiblesses.

I.II.4.3 Craquage catalytique sur lit fluidisé (FCC)

Le FFC permet de traiter des charges lourdes comme des RAT et des RSV pour les transformer en coupes d'essence.

Ici, on utilise et la température (entre 500 et 530°C) et un catalyseur dans le but de craquer les molécules. Cela permet également de modifier les rendements en produisant moins de gaz et de coke et plus d'essence. Contrairement au craquage thermique, l'utilisation dans ces procédés d'un catalyseur va interdire le traitement des charges riches en métaux[79].]

Les catalyseurs de craquage sont constitués de silice et d'alumine ou d'un mélange entre silice-alumine amorphe et silice-alumine cristallisée est utilisé. Le catalyseur silice-alumine cristalliser est aussi appelé zéolithe ou tamis moléculaire. Ils possèdent une grande acidité, ce qui a permis d'accroitre de manière significative l'activité des catalyseurs. La sélectivité des réactions de craquage est grandement améliorée par rapport au craquage thermique.

Part III: Techniques utilisées pour l'analyse du pétrole

I.III.1 Méthode de séparation des échantillons pétroliers

La méthode de préparation de l'échantillon par dilution dans un solvant organique est largement répandue et mise en œuvre pour les analyses par ICP *Atomic Emission Spectroscopy* (AES) et ICP MS car elle est rapide et simple. Le point le plus important dans le cas de la dilution est le choix du solvant. En effet, ce choix doit tenir compte de la quantité des éléments étudiés, de la nature même de l'échantillon (matrice, solubilité) et la toxicité du solvant si de grandes quantités sont nécessaires. Enfin il faut s'assurer que ce solvant ne sera pas à l'origine d'interférences lors des analyses. Les solvants les plus employés pour l'analyse des produits pétroliers lourds sont le toluène, le xylène, le tétrahydrofurane (THF) ou encore le chloroforme.

Ce type de préparation va permettre de conserver l'échantillon dans un état proche de celui initial en conservant la spéciation des éléments et donnera de ce fait une analyse représentative du produit pétrolier analysé.

Cependant dans le cas de l'analyse d'échantillons pétroliers, l'analyse totale ne suffit pas pour révéler toutes les informations pertinentes. Il est donc important de développer des techniques de séparation enfin de fractionner les échantillons puis de les analyser. Les différences existantes entre les différentes fractions d'un échantillon pétrolier peuvent expliquer les différences de réaction lors des étapes de raffinages.

I.III.1.1 Séparation liquide/solide

Chacón-Patiño *et al*[66]–[68] ont procédé à une série d'extraction, nommée extrographie, grâce à un soxlhet en utilisant successivement les solvants suivant : acétone, ACetoNitrile (ACN), C7, C7/Tol, Tol, Tol/THF, THF et THF/MeOH. Les asphaltènes sont dans un premier temps dissout puis déposés sur de la silice ou de l'oxyde d'aluminium afin d'augmenter sa surface réactive ce qui permet une meilleure extraction. Ensuite avec un solvant choisit on procède à l'extraction pendant 24h. Ce système permet de fractionner efficacement par solubilité les asphaltènes. Ensuite la partie soluble est récupérée puis séchée sous flux d'azote. Grâce à ce système il est possible de fractionner une quantité d'échantillons suffisante pour permettre d'autres analyses sur chacune des fractions obtenues.

Puis ils ont analysé l'échantillon pétrolier complet et les fractions par APPI-FT-ICR MS. Ils en ont déduit que la fraction extraite à l'acétone était principalement composée de structure moléculaire de type Island et que l'analyse des fractions séparées donnait des signaux plus

nombreux que l'analyse de l'asphaltène complet grâce à une meilleure ionisation elle-même dû à une simplification de la matrice. Au contraire l'extraction faite avec du Tol/THF/MeOH donne une fraction enrichie en archipelago, plus difficile à analyser par spectrométrie de masse. Cette fraction contient aussi le vanadium le plus difficile à extraire en raffinerie.

Un autre type d'extraction solide liquide a été développé par Gascon *et al*[80], [81]. Ils ont utilisé de l'ACN, de l'acétone et du *DiMethyle Formamide* (DMF) afin de séparer ces échantillons en fonction de leurs tailles d'agrégats.

I.III.1.2 Chromatographie liquide

La chromatographie liquide est utilisée pour la séparation de matrices en fonction de leurs propriétés physiques et/ou chimique. En fonction de son affinité chimique avec les différentes phases ou en fonction de ses propriétés physiques, les différentes molécules contenues dans l'échantillons seront éluées à des vitesses différentes. Les molécules qui auront le plus d'affinité avec la phase stationnaire ou qui seront le plus retenues par leur taille ou formes seront élué plus lentement. On peut ainsi séparer notre échantillon afin d'obtenir plus d'information lors de l'analyse

Plusieurs facteurs sont utilisés pour évaluer la séparation en chromatographie liquide. Par exemple, k' est utilisé pour exprimer le facteur de rétention, il peut se calculer grâce à la formule suivante :

$$k' = \frac{Vr - Vm}{Vm}$$

Vr est le volume de rétention d'un compose et Vm est le volume mort. De même il est possible de l'exprimer en temps de rétention (Tr et Tm) avec l'ajout d'un facteur représentant le débit de la phase mobile.

On peut calculer la résolution (Rs) qui représente la qualité de la séparation entre deux pics chromatographiques.

$$Rs = \frac{(\alpha - 1)\sqrt{N} \times k'}{4(1 + k')}$$

Avec N qui est le nombre de plateau et α la sélectivité de séparation. Si Rs est supérieur ou égal à 1 alors la séparation est suffisante, si Rs est inférieur à 1 alors la séparation n'est pas suffisante.

Dans le cas d'une chromatographie sur plaque, le facteur de rétention s'exprime de la façon suivante

$$Rf = \frac{distance\ parcourue\ par\ le\ soluté}{distance\ du\ front\ de\ solvant}$$

Le facteur de capacité, k', est le ratio de la quantité d'échantillons présent dans la phase mobile et la phase stationnaire. Autrement dit, la capacité de l'échantillon à migrer avec un solvant et une phase stationnaire donnée.

$$k' = \frac{Temps\ de\ rétention\ dans\ la\ phase\ stationnaire}{Temps\ de\ rétention\ dans\ la\ phase\ mobile} = \frac{1 - Rf}{Rf}$$

I.III.1.2.1 High Performance Thin Layer Chromatography

L'HPTLC peut être utilisée pour la séparation de la matrice pétrolière. L'utilisation de la HPTLC avec des plaques à usage unique pour la caractérisation de la matrice pétrolière peut éviter les dommages aux colonnes de chromatographie causés par l'adsorption irréversible des composés polaires présents sur la phase stationnaire et la précipitation des asphaltènes.

I.III.1.2.1.1 Mécanisme

L'HPTLC est une chromatographie planaire ou une petite quantité d'échantillon (quelques microgrammes) est déposé près d'un bord de la phase stationnaire. Puis comme indiqué sur la figure 9, un bord de la plaque est immergé dans un fond de solvant à l'intérieur d'une enceinte fermée sans que les échantillons ne soient en contact direct avec le solvant. Le solvant imprègne toute la plaque par capillarité et élue l'échantillon[82]. Le procédé repose

sur un non-équilibre entre la phase stationnaire, la phase mobile et la phase gazeuse La séparation est due à des différences d'affinité entre les molécules présentes dans l'échantillon et la phase stationnaire/phase mobile qui font que la hauteur de migration sera différente en fonction des différentes molécules.

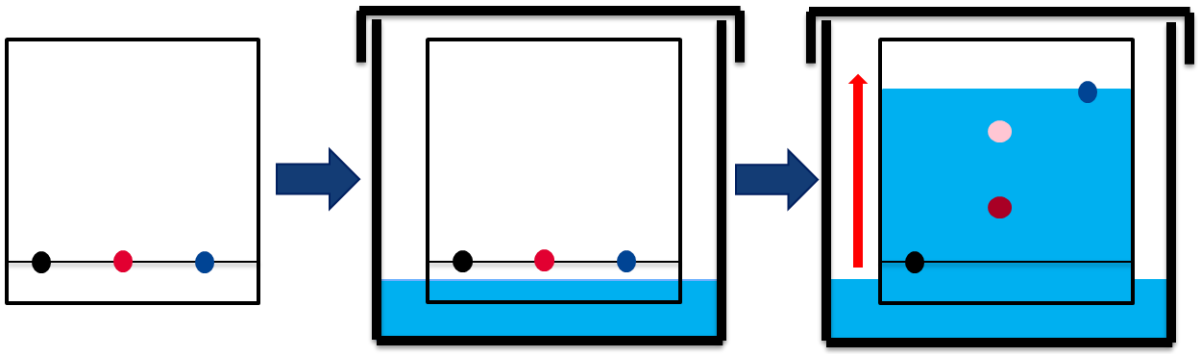

Figure 8:Schéma du principe de l'HPTLC

I.III.1.2.1.2 Phases stationnaires

La phase stationnaire est déposée sur une plaque de verre ou d'aluminium en fine couche entre 60 µm et 250 µm en fonction des phases stationnaires et la qualité de la plaque. Cette phase stationnaire est faite d'un matériau adsorbant comme la silice, l'oxyde d'aluminium, la cellulose… Ensuite les phases stationnaires peuvent être modifiées pour améliorer la séparation de composés spécifiques. De plus il est possible de rajouter sur certaines phases un indicateur fluorescent pour améliorer la détection. Le tableau 1 liste les phases stationnaires les plus utilisées.[82]

Tableau 1: listes des phases stationnaire couramment utilisées en TLC [82]

Phase stationnaire	Modification	Applications
Silice	-	Polyvalent
	Caffeine	Composé aromatique polycyclique (PAH)
	Cyano-modified layer	Pesticides, phenol
	Diol-modified layer	Hormones, stéroides
	Amino modified layer	Acides carboxyliques, Acide sulphoniques
Cellulose	-	Substance hydrophile (acide aminés, acide carboxyliques, ion inorganiques)
Polyamide	-	Phenol
Oxyde d'aluminium	-	Aliphatiques, aromatiques, composés basiques

Plusieurs qualités de plaques existent comme (HPTLC, TLC…). L'HPTLC possède une phase stationnaire faite de particules de taille plus réduite (6 µm en HPTLC pour 12 µm en TLC) et plus uniforme (voir figure 10). L'uniformisation des particules améliore la qualité de la migration lors de la séparation et une meilleure détection. Réduire la taille des particules apporte une plus grande surface pouvant interagir et diminue la distance de migration nécessaire pour la séparation des composés.[82]

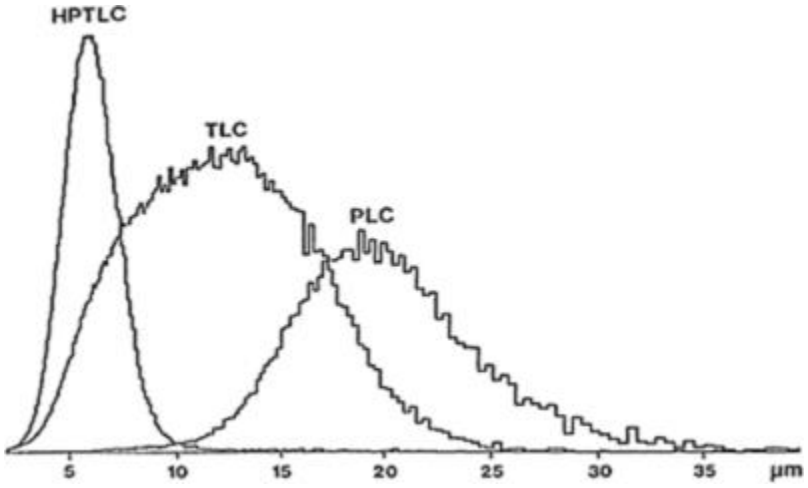

Figure 9: Taille des particules (ici silice) en fonction de la qualité de la phase stationnaire[82]

Pour terminer, il est nécessaire d'effectuer un prétraitement des plaques avant utilisation. Un chauffage de quelques minutes à 110°C ou un chauffage de plusieurs heures à 40°C permettra d'enlever l'humidité présente sur les plaques et un lavage au solvant permettra d'enlever les différentes impuretés.

I.III.1.2.1.2.a Silice

Le gel de silice est la phase stationnaire la plus utilisée. Il est composé de groupe Si-OH et Si-O-Si (voir figure 11). Les échantillons sont séparés en fonction de leur polarité par des interactions avec le support (liaison hydrogène et dipôle/dipôle. [82]

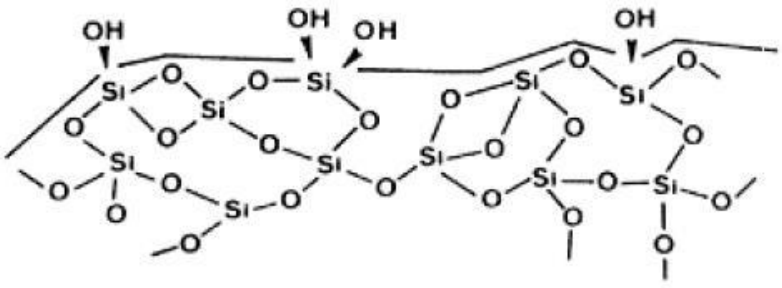

Figure 10: Structure chimique du gel de silice[82]

I.III.1.2.1.2.b Cellulose :

En général, la cellulose utilisée est composée de longues chaines composées d'unité de B-glucopyranose connectés entre eux par des liaisons hydrogène. En raison de leur nombreux groupe hydroxyle (voir figure 12), la cellulose est plus utilisée pour la séparation de composés polaires.

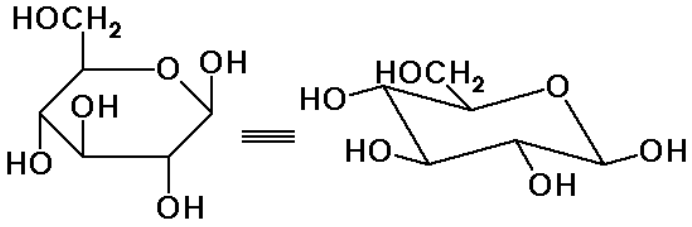

Figure 11: Structure chimique de la cellulose

I.III.1.2.1.2.c Polyamide:

Une autre composition de phase stationnaire est le polyamide. Comme la cellulose, le polyamide peut être utilisée pour la séparation de composés polaires qui pourront interagir avec le groupe amide par les liaisons hydrogène. Deux types de polyamides sont utilisés, le polyamide 6 (Figure 13 gauche) et le polyamide 10 (Figure 13 droite).

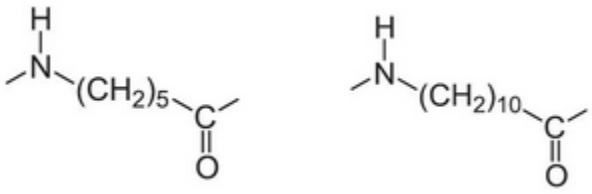

Figure 12: Structure chimique du polyamide

I.III.1.2.1.3 Phases mobiles

La phase mobile permet le transport des échantillons et doit être capable de les dissoudre. En variant la force du solvant et en créant des mélanges, il est possible de faire varier la distance de migration des composés contenus dans les échantillons pour obtenir une séparation efficace. Snyder à étudier plus de 80 solvants et les a classés par groupes en fonction de leurs propriétés présentés Figure 14 et Tableau 2.

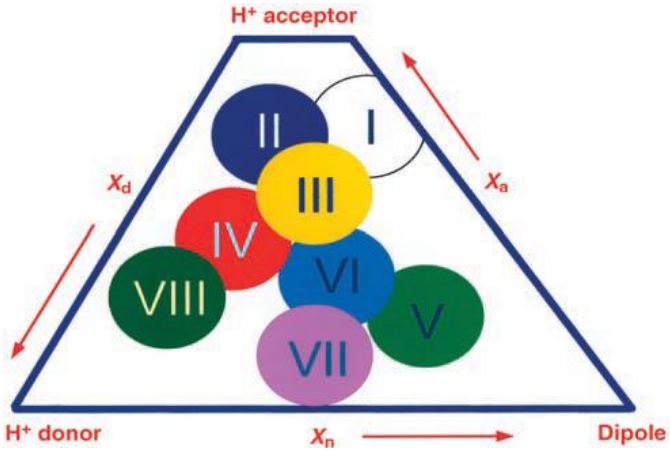

Figure 13: Triangle de sélectivité de Snyder[83]

Tableau 2: Exemples de solvants pour chacune des 8 groupes présentés figure 14

Groupe	Solvant
I	Ethers aliphatique
II	Alcool aliphatique
III	THF
IV	Acide acétique, Formamide
V	Dichlorométhane
VI	Cétones, Acetone, Acetonitrile
VII	Hydrocarbones aromatiques
VIII	Chloroforme, Eau

Il existe des méthodes systématiques pour optimiser la phase mobile en HPTLC pour permettre d'obtenir la séparation la plus efficace. C'est le cas de la méthode « PRISMA » , développé par CAMAG, fournisseur d'instrumentation HPTLC [84]. Dans un premier temps, plusieurs solvants des différents groupes (tableau 2) sont testés. Ensuite on mélange les

solvants qui ont une force éluante importante avec ceux qui en ont une plus faible afin de trouver un bon compromis. Pour finir on ajuste les proportions des différents solvants afin d'obtenir la séparation la plus efficace (voir figure 15).

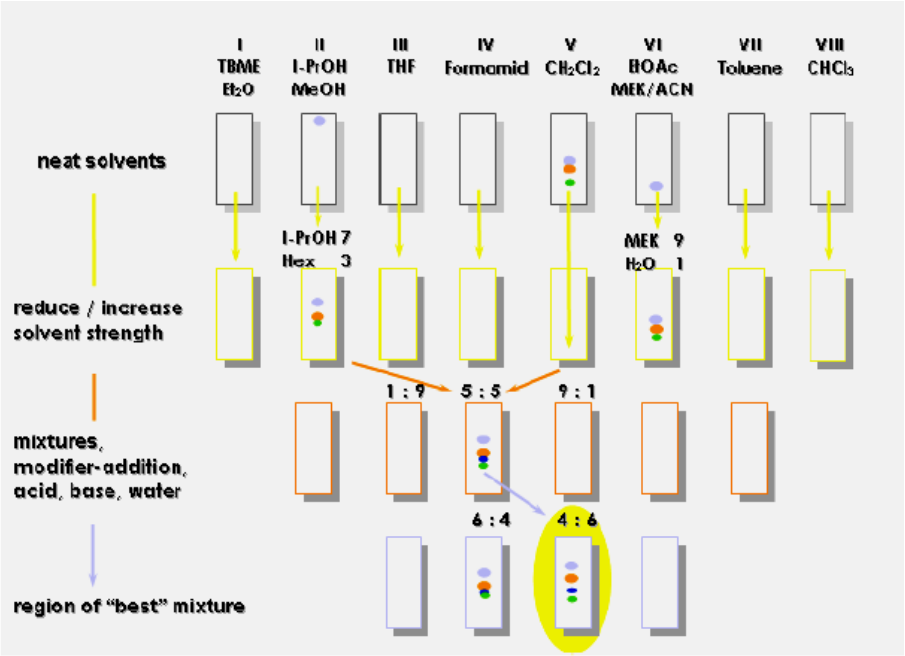

Figure 14: Schéma d'optimisation des solvants d'élution

I.III.1.2.1.4 Instrumentation

Durant cette thèse, quatre appareils de chez CAMAG ont été utilisés pour effectuer la dépose, la migration et l'analyse par Ultra-Violet (UV). L'utilisation de ces appareils permet d'automatiser la dépose et la migration ce qui améliore la reproductibilité des analyses.

I.III.1.2.1.4.a Dépose des échantillons

L'*Automated TLC Sampler 4* (ATS4) permet de déposer jusqu'à 1 µL d'échantillon de façon plus reproductible qu'une dépose manuelle. De plus la dépose est effectuée sur une bande fine d'épaisseur réglable ce qui permet d'obtenir une meilleure résolution du fait d'une moindre dispersion de l'échantillons suivant l'axe d'élution.

I.III.1.2.1.4.b Migrations

L'*Automated Multiple Development 2* (AMD2) permet les migrations avec un ou plusieurs solvants purs de force éluante différente et permet aussi une migration en plusieurs étapes. Entre les essais, le solvant est complètement évaporé de la chambre de développement et la couche est séchée sous vide. Les développements successifs sont réalisés dans le même sens. Ceci est utile pour séparer dans la même analyse des échantillons contenant des composés polaires et non polaires.

I.III.1.2.1.4.c Analyses

Les chromatogrammes des plaques HPTLC seront obtenus par analyse densitométrique UV à balayage[82] à partir d'un TLC Scanner 4. Un faisceau de lumière à une ou plusieurs longueurs d'onde sélectionnées est dirigé sur la plaque après migration, qui est déplacée pour analyser chacun des échantillons.

Le TLC Scanner 4 est un instrument à faisceau unique et à longueur d'onde unique. Il est possible d'utiliser trois lampes différentes : lampe au deutérium, halogène-tungstène et au mercure à haute pression. Le faisceau lumineux frappe la plaque verticalement et le détecteur est aligné à un angle de 30 °.

Le détecteur mesure la lumière réfléchie de manière diffuse en mode absorbance ou fluorescence. La majorité des mesures densitométriques des chromatogrammes en couche mince sont effectuées en mode absorbance dans la plage UV inférieure (de 300 nm à 190 nm). Le spectre est automatiquement corrigé en mesurant les spectres de la lampe ou de la lumière, ainsi que de la plaque et du blanc de solvant, et cela dépend de la quantité de substance.

Les composés aromatiques et conjugués absorbent naturellement les rayons ultraviolets. En revanche, les composés saturés, tels que les hydrocarbures saturés dans les produits dérivés du pétrole, ne donnent ni spectres UV ni de fluorescence et ne peuvent être détectés directement. Des plaques de gel de silice imprégnées de berbérine ou de coralyne peuvent être utilisées dans ce cas avec une densitométrie à balayage de fluorescence à 365 nm pour la berbérine et à 410 nm pour des longueurs d'onde d'excitation de Coralyne[85].

Il a été rapporté depuis longtemps que la révélation des plaques avec des composés paraffiniques augmentait la fluorescence d'une grande variété de solutés adsorbés sur des plaques HPTLC. Par exemple, Cebolla *et al* [86] ont utilisés des plaques de gel de silice imprégnées de berbérine pour séparer les composants SARA (saturés, asphaltènes, résines, aromatiques) des échantillons de pétrole. La berbérine était nécessaire pour détecter les

composés saturés. Mateos *et al*[87] ont utilisé des plaques de gel de silice imprégnées d'une solution de cation coraline, qui est plus sensible que la berbérine pour de nombreux composés.

L'HPTLC est généralement effectué sur plaques de silice, a été largement utilisée pour la caractérisation d'échantillons de pétrole. Jarne *et al*[88] ont utilisé des plaques de gel de silice modifiée imprégnées de caféine pour séparer les produits pétroliers en fonction du nombre de cycles.

Bien que les plaques à base de silice soient généralement utilisées pour les analyses HPTLC, notamment pour les analyses de type hydrocarbure, elles peuvent être affectées par une adsorption irréversible [22] au point d'application en raison de la forte polarité des groupes silanol présents, et cet effet est particulièrement important dans l'analyse des asphaltènes. L'utilisation d'absorbants moins polaires, tels que la cellulose, pourrait permettre une spéciation plus robuste de l'asphaltène. En effet la phase stationnaire de la cellulose contient des particules plus fines et plus uniformes que la silice. Cela donne une meilleure séparation et une meilleure détection.

I.III.1.2.1.5 Couplage HTPLC et détecteurs

Enfin, l'HPTLC peux servir à préparer les échantillons dans le but d'analyser les plaques par d'autres techniques comme des techniques de LA-ICP MS ou seulement pour récupérer les fractions éluées et les utiliser comme échantillons.

Récemment Chacón-Patiño *et al*[89] et Giraldo-Davila *et a*l[90] ont utilisé des plaques de gel de silice pour séparer des échantillons d'asphaltènes. Ils ont utilisé un mélange de DiChloroMethane (DCM) / MeOH et ensuite du toluène pour séparer les asphaltènes en trois fractions. Cette technique peut également être utilisée à l'échelle préparative pour séparer des fractions qui peuvent ensuite être grattées, extraites au moyen de solvants et ensuite analysées par d'autres techniques (Li et al[51]). Vorapalawut *et al*[15] ont utilisé la chromatographie en couche mince conjointement avec LA-ICP MS pour la séparation SARA avec des plaques à base de silice pour la spéciation du soufre, du vanadium et du nickel à partir des fractions SARA d'échantillons de pétrole. Chirinos *et al*[92] ont également utilisé cette technique pour la détermination rapide du rapport vanadium/nickel dans différents échantillons d'asphaltènes.

Plusieurs auteurs ont utilisé la chromatographie en couche mince pour la séparation des porphyrines et des métalloporphyrines. En 1978, Hajibrahim *et al* [93] ont utilisé la TLC

préparative pour séparer des porphyrines pour de futures analyses. En 1989, Van Berkel *et al* [94] ont eu recours à la chromatographie en phase liquide pour obtenir des fractions enrichies en porphyrine de vanadium et en nickel porphyrine à partir d'échantillons de bitume. Ensuite, ils ont utilisé la chromatographie en couche mince avec des plaques à base de silice pour séparer les différentes porphyrines dans chacune des fractions précédentes. Toutes les porphyrines de Nickel sont éluées avec de l'heptane/DCM à 3/2% v/v, alors que les porphyrines de vanadium ont besoin d'un solvant plus polaire, tel que 100% de DCM.

I.III.1.2.2 Chromatographie à perméation de gel

I.III.1.2.2.1 Principe

La GPC est utilisée pour séparer les molécules en fonction de leur volume hydrodynamique. Lors de la séparation, les molécules de poids moléculaire élevé sont éluées en premier car exclues des pores de la colonne alors que les molécules de poids moléculaire plus faibles explorent plus de pores de la colonne et sont éluées après. Toutes les molécules dépassant la taille des pores de la colonne seront rapidement éluées et au même moment, il s'agit du volume mort de la colonne. De même, toutes les molécules plus petites que le plus petit des pores, comme le solvant la plupart du temps, seront éluées au même moment avec un volume d'élution élevé, il s'agit du volume de perméation de la colonne (voir figure 16). Contrairement aux autres types de chromatographie, la GPC ne se base pas sur des interactions chimiques à l'intérieur de la colonne mais uniquement sur la forme et le volume hydrodynamique des composés.

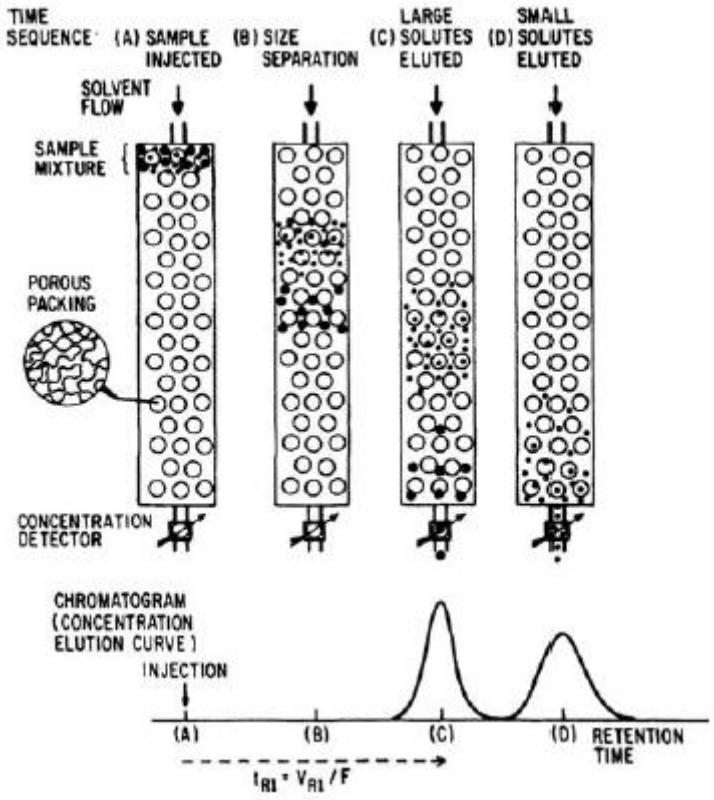

Figure 15: Schéma du principe de fonctionnement de la GPC [95]

De plus la GPC peut aussi être utilisée pour la préparation d'échantillons. En effet des colonnes de plus grande taille appelé GPC préparative peuvent être utilisée. Le volume des colonnes étant plus élevé, il est possible d'injecter une plus grande quantité d'échantillon et de collecter des fractions contenant des molécules de tailles différentes dans le but de les analyser plus tard avec une autre technique.

I.III.1.2.2.2 Etalonnage de la GPC

La GPC est très utilisée pour l'étude des polymères. Les chaines de polymères sont composées de nombreuses unités (monomères). Un échantillon de polymère contiendra une distribution de molécules de différentes longueurs ou poids. Dans un solvant, le polymère se dissout, la longue chaine se rétracte et forme une pelote. Plus la longueur des chaines est élevée, plus la sphère sera grande et donc plus le temps d'élution sera faible.

L'étalonnage des colonnes GPC permet d'obtenir la relation entre le volume de rétention et les poids moléculaires. L'étalonnage des colonnes se fait habituellement avec des solutions de polystyrènes (PS) de masses connues et différentes, ce qui permet d'évaluer la masse des composés de nos échantillons en fonction du temps de rétention. Idéalement l'étalonnage est effectuée avec des composés chimiques connues proches des échantillons

utilisés. Dans le cas du pétrole et des asphaltènes, la structure et la masse des composés étant peu ou pas connues, l'étalonnage est effectué avec des étalons de PS de masses connues. Cependant ce type d'étalonnage induit des erreurs d'estimations des masses des composés pétroliers.

De nombreux travaux sur la GPC ont été effectués. Par exemple Pohl *et al* ont développé la *Micro Size Exclusion Chromatography* (µSEC)-HR-ICP MS avec un débit de 15 $\mu L.min^{-1}$, ce qui permet de réduire significativement la consommation de solvant [96]. La GPC a aussi été utilisée par Gutierrez Sama *et al* [46] pour étudier le phénomène d'agrégation en fonction du temps et montre qu'un asphaltene mis en solution se réagrège au fil du temps et ce principalement sur la première semaine. Rietjens *et al* [97] montrent l'évolution de l'état d'agrégation lorsque le pétrole est mis en contact avec de l'acide. Parks *et al* [98] effectuent dans un premier temps une séparation SARA puis analysent chaque fraction par GPC-ICP MS et HT-GC-AED et montrent que les porphyrines présentes dans les asphaltènes sont dans un état d'agrégation supérieure à celle présentes dans les résines. Gascon *et al* [99] obtiennent des résultats similaires.

I.III.1.2.2.3 Limitations de la GPC

Plusieurs limitations à la GPC sont connues. Par exemple, le fait que la phase stationnaire polaire est supposée inerte, il est possible d'avoir des interaction soluté/phase stationnaire. En effet la matrice pétrolière est très complexe et est composées de nombreuses molécules polaires. Ces molécules peuvent être, à cause des interactions, plus retenues qu'elles ne le devraient ce qui entraine une sous-estimation des masses moléculaires. Dans le cas des échantillons pétroliers séparés par GPC, il y a toujours une partie de l'échantillon qui est élué après le volume d'exclusion totale de la colonne, ce qui veut dire que certaines molécules ont une interaction avec la phase stationnaire. L'ajout d'un additif ou le changement de solvant peut réduire voire empêcher le problème des interactions phase stationnaire/soluté. Cependant l'état d'agrégation des composés pétroliers dépend de leur concentration en solution mais aussi du solvant utilisé, cette solution n'a donc pas été retenue.[95]

Un autre exemple de limitations de la GPC, la dégradation par cisaillement. Ce type de dégradation a lieu pour les polymères de masse très élevé. La séparation est considérée comme étant indépendante du débit du solvant [95], [100]. Cependant, certains travaux ont montré que le débit pouvait modifier le temps de rétention des composés. Cela peut avoir plusieurs raisons. L'augmentation du débit peut amener à un changement du volume d'élution

de la colonne dû à l'augmentation de pression ou peut dégrader les polymères ou les agrégats[46], [101]–[103].

I.III.1.2.2.4 Couplage de la GPC

La GPC est très utilisée pour la séparation et la simplification de la matrice pétrolière, notamment pour l'étude du soufre et des métaux ou l'étude moléculaire lorsque celle-ci est couplée à des techniques de détection, comme de l'UV ou de la spectrométrie de masse [2], [46], [104], [104]–[108]. Non seulement cela permet de simplifier la matrice pétrolière avant analyse mais en plus l'état d'agrégation impacte directement leur réactivité durant les processus de démétallation[109]. En effet les métaux contenus dans les fractions les plus légères sont plus faciles à extraire que les métaux contenus dans des molécules très agrégées [51], [110]–[112].

Desprez *et al* [113] ont étudié la distribution en taille des molécules contenant du soufre par GPC-ICP MS en fonction des différentes coupes de distillation et montrent que plus le point d'ébullition est élevé, plus l'état d'agrégation est important. Ligiero *et al* [114] utilisent la GPC-ICP MS pour analyser des échantillons pétroliers et montrent qu'il y a une corrélation directe entre l'état d'agrégations du soufre et la stabilité de l'émulsion du pétrole. Vargas *et al* [115] couplent une séparation par polarité avec une séparation par GPC pour étudier l'agrégation en fonction de la nature des composant présents dans le pétrole. Plus le poids moléculaire est faible, moins il y a de composés polaires[116], [117].

I.III.1.2.2.4.a Analyse moléculaire

La séparation par GPC facilite aussi une future analyse moléculaire. Guricza et Schrader [118] ont utilisé la GPC en utilisant du THF, toluène ou chloroforme et ont montré que le THF était le solvant le plus efficace pour la séparation. De plus, dans le cadre d'analyse de produit pétroliers, d'après Panda *et al*[119], la GPC permet la séparation des composés en fonction de leur aromaticité.

I.III.1.2.2.4.b GPC Preparative

Il est aussi possible d'utiliser de la GPC dans le but de collecter des fractions pour de futures analyses [120]–[123]. La GPC préparative est conçue pour la collecte. En effet, la GPC

préparative utilise le même principe que la GPC classique mais le volume intérieur des colonnes est environ six fois plus élevé. Cela permet d'appliquer un débit de solvant plus élevé et d'injecter des quantités d'échantillon plus grandes pour permettre une collecte d'échantillon suffisante. Putman *et al* [124] ont fractionné l'asphaltène par GPC. Puis ils ont analysé ces fractions séparément par APPI (+) FT-ICR MS. Plus la fraction était légère, plus l'ionisation était élevée. L'analyse de chacune des fractions a permis de mettre en évidence que l'agrégation est corrélée avec la présence plus importante de grand composés aliphatiques.

I.III.2 Techniques de détection

I.III.2.1 UV

La détection UV-Visible permet d'étudier les métallo porphyrines qui présentent unsignal d'absorption UV caractéristique proche de 400/420 nm.. Freeman *et al* [23] ont montré que la longueur d'onde de cette bande dite « de Soret » variait en fonction du type de porphyrines et des chaînes alkyl, ou des groupes fonctionnels présents sur le tour des porphyrines (voir Figure 17).

	Wavelength (nm)		
Vanadyl porphyrins	Soret band	β band	α band
No substitution	399.4	523.8	559.4
ETIO	406.6	532.8	570.7
Octaethyl	407.3	533.2	570.9
DPEP	410.5	533.3	573.0
Benzo	414.0	544.7	578.7

Figure 16: Longueur d'onde d'absorption des différents types de porphyrines selon Freeman et al[23]

Castillo et Vargas[22] ont mélangé porphyrines et solution d'asphaltène et ont montré une diminution importante de la bande de Soret typique des porphyrines. Ils en ont déduit que les asphaltènes piégeaient lors de l'agrégation les porphyrines et de ce fait masquaient le signal UV. Evdokimov *et al* [176], [177] ont étudié l'asphaltènes par UV-Visible et ont montré que l'intensité de la bande de Soret augmente lorsque que certains taux de dilution sont

atteints et ont mis cela en parallèle avec l'état d'agrégation des asphaltènes. Yokota *et al* [178] suggèrent d'après les spectre UV de ses échantillons que l'agrégation des asphaltènes commence à des concentrations supérieures à 5 $mg.L^{-1}$.

De plus l'UV-visible est souvent complémentaire d'autres technique d'analyse élémentaire ou moléculaires comme l'ICP-MS ou le FT-ICR MS.

I.III.2.2 ICP

I.III.2.2.1 Principe ICP MS et ICP AES :

I.III.2.2.1.1 ICP MS

L'ICP permet l'atomisation et l'ionisation des échantillons grâce à sa torche à plasma pouvant aller à plus de 7000 K. Cette source d'ion est suivie d'un analyseur de masse et d'un détecteur qui permettent respectivement de séparer et suivre le signal des ions.

La première utilisation de l'ICP MS a été faite dans les années 80 [125]. Sa grande sensibilité ainsi que sa capacité d'analyse multi élémentaire en font un instrument très utilisé pour les analyses inorganiques comme organiques. Sa grande sensibilité a permis l'analyse de certains éléments à l'état d'ultra-traces, ce qui n'était pas possible auparavant.

Cependant cette technique a plusieurs certaines limitations. La préparation d'échantillons avant introduction est souvent faite grâce à une minéralisation ou à une dilution. La dilution est plus simple mais due à la présence de produit volatils elle risque de causer une déstabilisation du plasma. De plus les matrices organiques lors de la combustion risquent de déposer du carbone, notamment sur les cônes de l'appareil. Pour pallier ce problème, de l'oxygène est ajouté au flux d'argon enfin de transformer ce carbone en CO_2.

Une autre limitation de l'ICP MS est la formation d'ions poly atomiques comme O_2, ArO qui risque d'interférer avec des éléments intéressant comme le soufre ou le fer. Pour éviter ces problèmes, il est possible d'utiliser un ICP MS à haute résolution ($300<R<10\ 000$), qui permet de distinguer les différents ions. Plus on augmente la résolution, plus la gamme de masse acceptée pour analyse diminue, cela a pour effet de diminuer la sensibilité mais permet de séparer des interférences et des ions proches en masse.

Cependant les produits pétroliers étant trop visqueux pour être analysés directement, des méthodes de préparation ou de séparation d'échantillons sont nécessaires.

I.III.2.2.1.2 ICP AES

L'ICP AES est un instrument très utilisé pour l'analyse multi-élémentaire. En effet celui-ci permet dans le cadre des analyses de produits pétroliers d'atteindre une limite de détection de l'ordre de la dizaine de ppb. [3], [126]

Les échantillons sont introduits après dilution dans un solvant ce qui comme dans le cas de l'ICP-MS peux entrainer une déstabilisation du plasma dû à la quantité de solvant organique entrant dans la torche. L'ICP AES à deux avantages comparés à l'ICP MS. D'abord il ne nécessite pas d'ajout d'oxygène dans le gaz de nébulisation. Ensuite l'ICP AES est moins couteux que l'ICP MS. Cependant le fait que l'ICP MS est une technique plus sensible, il est souvent préféré par rapport à l'ICP AES.

I.III.2.2.2 Techniques d'introduction pour ICP

L'analyse directe par ICP MS [4], [108] nécessite dans un premier temps soit de dissoudre l'échantillon dans un solvant (Toluène, THF ou Xylène) soit d'effectuer une minéralisation, le plus souvent par digestion acide par micro-ondes avec HNO_3 ou H_2O_2.

De plus, plusieurs développements ont été proposés pour l'analyse pétrolière en ce qui concerne l'introduction d'échantillons car le plasma ne peut supporter qu'une quantité limitée de matrice organique. Pour ce faire, différents nébuliseurs ont été développés. De plus l'introduction peut être effectuée par LA, ce qui évite l'utilisation d'une chambre et permet l'analyse d'échantillons solides. De même l'*ElectroThermal Vaporization* (ETV) peut être utilisée.

I.III.2.2.2.1 Nébuliseurs

L'introduction d'échantillons liquides est effectuée grâce à un nébuliseur ayant pour rôle de créer un aérosol à partir de la solution liquide introduite. L'aérosol ou spray est produit et transporté, au moyen d'un gaz vecteur généralement composé d'argon, à travers la chambre de nébulisation et ce jusqu'au plasma via un injecteur. Il existe différents types de nébuliseurs et différentes chambres de nébulisation. Les classiques comme les nébuliseurs concentriques, cross-flow, les chambres de nébulisation cycloniques et les chambres de Scott. Ils fonctionnent à des débits de solvants de l'ordre du millilitre par minute. Cependant, seule la partie la plus homogène de l'aérosol crée par le nébuliseur (environ 5 %) va être introduite dans le plasma afin que le débit soit compatible avec les capacités d'ionisation de ce dernier. Le reste de l'aérosol formé sera évacué par un drain. Le rôle de la chambre de nébulisation

est de délivrer un échantillon le plus homogène possible à partir de l'aérosol produit par le nébuliseur.

I.III.2.2.2.1.a Nébuliseur à ultrasons (USN)

L'USN comporte un système de désolvatation par ultrason permet un gain d'un facteur 5 par rapport au nébuliseur classique.

Le principal inconvénient de ce système est dû aux effets mémoire. Ces effets mémoire sont dû au volume mort à l'intérieur du nébuliseur et des étapes de chauffage/refroidissement qui peuvent favoriser le dépôts d'espèces organiques.[127]

I.III.2.2.2.1.b Micro-nébuliseur à consommation totale

Ces nébuliseurs sont largement utilisés pour l'analyse de matrices organiques car ils offrent des avantages par rapport aux systèmes de nébulisation conventionnels. Cette fois ci, la totalité de l'échantillons est envoyé dans le plasma. Du coup les débits de travail sont faibles afin de ne pas déstabiliser voire souffler le plasma.

Ces nébuliseurs ayant une grande capacité de transport, ne consomment que peu d'échantillons ce qui permet de réduire la charge organique entrant dans la torche à plasma ainsi que la consommation de solvant. le volume de déchets générés et les effets mémoires [128], [129]. Les *Direct Injection Nebulizer* (DIN) [130] et direct injection high efficiency nebulizer (DIHEN) sont des exemples de ce type de systèmes [130], [131]. Le DIHEN est moins cher et plus facile d'utilisation que le DIN car il ne nécessite pas une haute pression afin d'obtenir un débit convenable. La quantité d'échantillon qui atteint le plasma dans le cas du DIN et du DIHEN est jusqu'à quatre fois supérieure aux systèmes d'introduction conventionnels.

Un micro nébuliseur DS-5 modifié[133] (voir Figure 18) a été utilisé avec succès par Giusti *et al* pour l'analyse de la matrice pétrolière. Ce type de nébuliseurs utilise un débit entre 10 et 50 $\mu L.min^{-1}$ en entrée et en sortie sans circuit d'évacuation. Cela permet une faible consommation de solvant et d'échantillon étant donné que tout le débit entre dans l'ICP MS.

Ce type de chambre doit permettre un passage de l'échantillon linéaire entre la formation de l'aérosol et la torche à plasma. L'aérosols crée doit être assez fin afin que celui-ci s'évapore avant l'entrée dans la torche à plasma car comme vu précédemment, la totalité de l'échantillon est envoyé dans la torche.

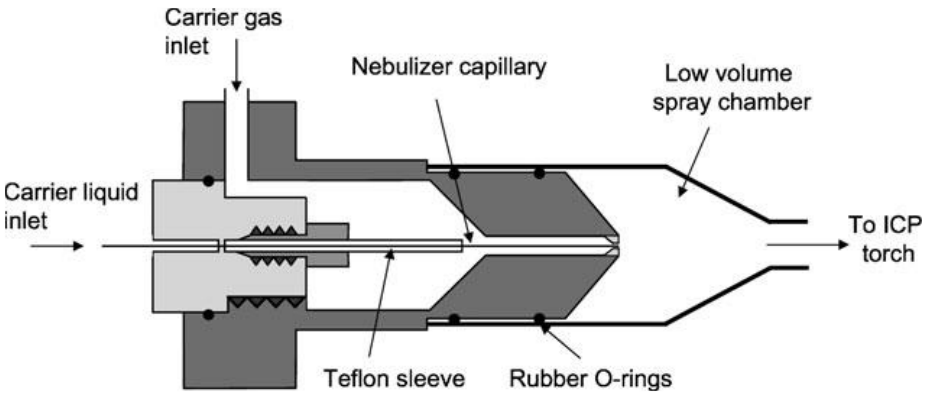

Figure 17: Schéma du nébuliseur DS-5 utilisé par Giusti et al[133]

I.III.2.2.2.2 Introduction par chambre de nébulisation chauffée

De plus, plusieurs auteurs [133]–[138] ont travaillé sur une chambre de nébulisation chauffée qui permet une meilleur évaporation du solvant dans la chambre de nébulisation et donc d'augmenter la sensibilité par rapports aux autres systèmes d'introduction.

Par exemple, Grotti *et al* [134] ont utilisé une chambre de nébulisation chauffée (voir Figure 19) appelé *Torch integrated sample introduction system* (TISIS). Avec cette chambre chauffée, l'utilisation d'un débit de solvant de 20 µL.min^{-1}, un débit de gaz Ar (sheating gas port) de 0,35 L.min^{-1} et un débit de gaz de nébulisation Ar de 0,7 L.min^{-1}. Ils ont obtenu une sensibilité entre 2 et 8 fois supérieurs comparé aux nébuliseurs classiques.

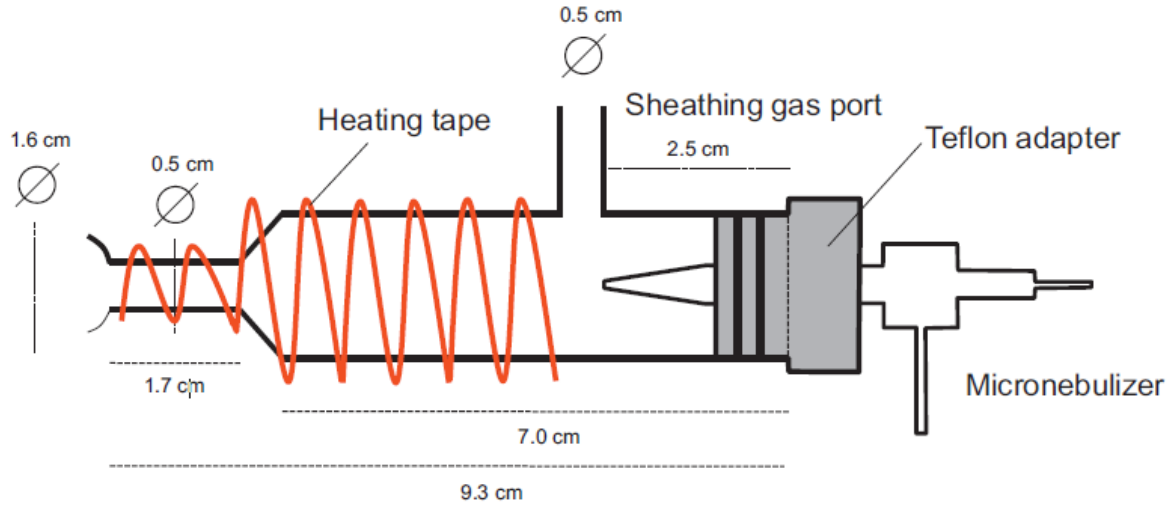

Figure 18: Chambre de nébulisation chauffée TISIS[134]

I.III.2.2.2.3 Ablation Laser

Le système d'ablation laser est un système qui est capable d'ablater un échantillon suivant une trajectoire linéaire. La zone ablatée peut chauffer jusqu'à 10 000K ce qui va permettre de vaporiser, atomiser et ioniser l'échantillons. L'aérosol produit est ensuite transporté par un flux d'hélium et est mélangé à de l'argon afin de régler le débit. Le mélange aérosol, Ar, He est directement envoyé dans la torche à plasma sans utilisation de chambre de nébulisation (voir Figure 20).

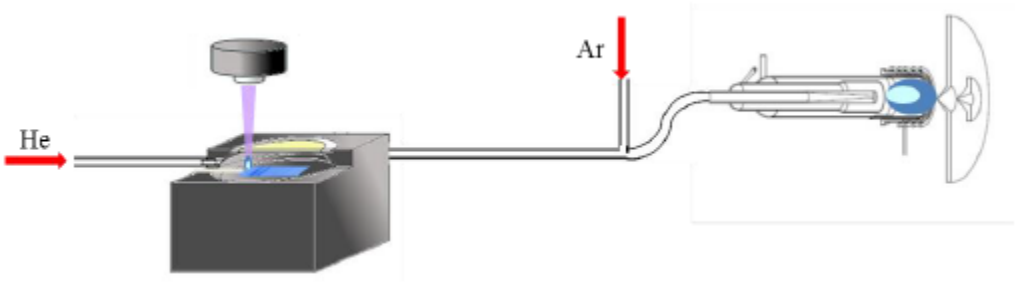

Figure 19: Schéma d'un système d'ablation laser couplé à une torche à plasma

L'ablation laser est une technique d'introduction qui peut être couplée à un ICP MS ou ICP AES [139], [140]. L'ablation Laser va permettre d'analyser un échantillon sans passer par une étape de préparation d'échantillon qui peuvent être longues et apporter des contaminants. Cependant l'ablation laser peut apporter des interférences spectrales [139]–[141]. Mais ce type d'interférences peut être évitées si on utilise un spectromètre de masse de haute résolution [142]. L'étalonnage en ablation laser est important étant donné que l'ablation de l'échantillon en question va dépendre de la matrice dans laquelle il se trouve, il est impératif de réaliser un étalonnage avec la même matrice ou alors de faire des ajouts dosés ou une dilution isotopique (dans le cas de l'ICP MS) [141], [143], [144].

L'ablation laser peut-être utilisée pour analyser des échantillons déjà séparés sur plaques HPTLC et couplé à un ICP MS.

Il est possible d'analyser des échantillons liquides par ablation laser, dans ce cas il est important d'utiliser une méthode de piégeage afin d'éviter les projections lors de l'ablation. Par exemple, Heilmann *et al* [145] ont travaillé avec de la cellulose imprégnée.

Un autre développement est l'utilisation de xerogel pour la préparation d'échantillons [146], [147]. Grâce à cette méthode de piégeage, l'analyse de liquide est possible et les limites de détection obtenues sont plus basses que lors de la dilution.

I.III.2.2.2.4 Electrothermal Vaporization

I.III.2.2.2.4.a Principe de l'ETV :

Le principe de l'ETV (Figure 21) est de déposer une quantité d'échantillon solide ou liquide dans une nacelle que l'on place dans un four en graphite. Le four peut chauffer de 20 à 3000°C en quelques seconde, et vaporise complètement l'échantillon. De l'argon est utilisé comme gaz porteur afin de transporter l'échantillon. Il est souvent rajouté un gaz de réaction qui facilite la pyrolyse de l'échantillon. Une deuxième arrivée d'argon (gaz by-pass) vient ensuite former un aérosol pour le transport jusqu'au détecteur.

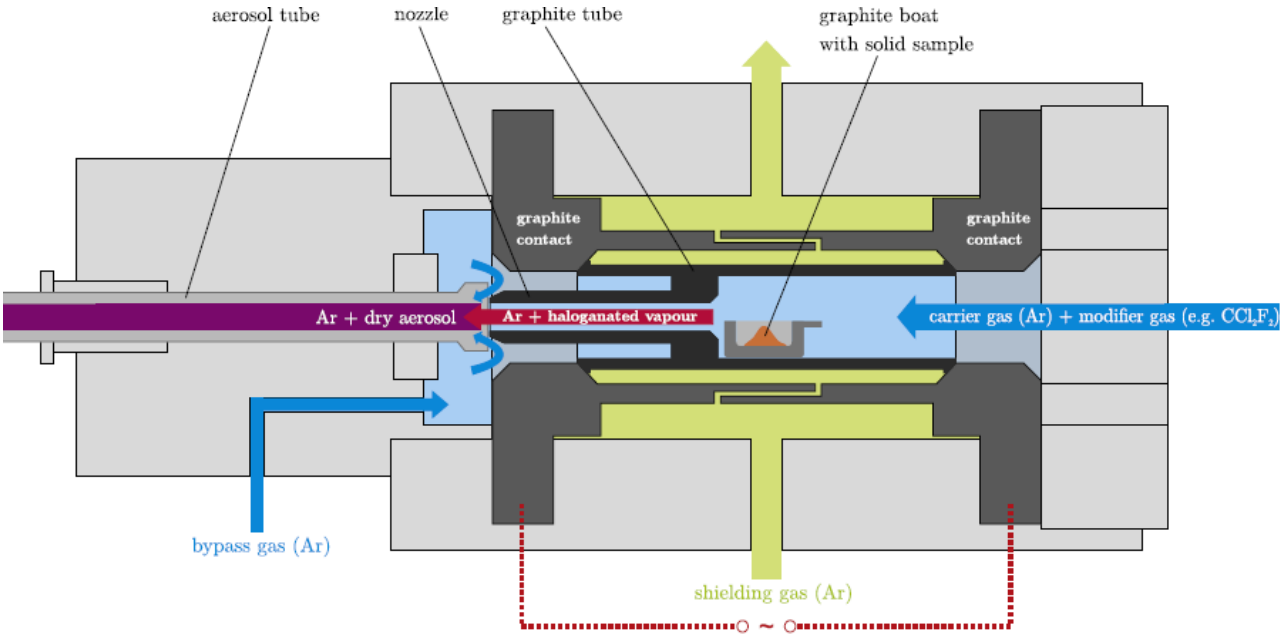

Figure 20: Schéma de principe de l'ETV[148]

L'ETV permet l'introduction d'échantillons avec peu de préparation, réduisant la consommation de réactif et de solvant. De plus, la consommation d'échantillon étant totale et l'ETV ne consommant pas de solvant, il n'y a pas de résidu [149]–[152]. La consommation

totale de l'échantillon à chaque analyse permet aussi d'obtenir une bonne sensibilité là ou l'utilisation d'une chambre de nébulisation classique rejette 95% de l'échantillon [151]–[154].

Certains travaux pointent les limitations de l'ETV. En effet, l'utilisation de masses faibles (0,1 à 5 mg) pose la question de la représentativité de l'échantillon. De plus les effets de matrice sont particulièrement importants et peuvent gêner l'étape d'étalonnage.[152], [155]. Cependant ces limitations peuvent être surmontées en optimisant les conditions de fonctionnement du système comme le programme de chauffe, les débits de gaz, l'utilisation d'un gaz de réaction[156], et la quantité d'échantillons[149], [154], [155], [157], [158].

I.III.2.2.2.4.b Utilisation de l'ETV :

Seuls quelques travaux font état de l'utilisation de l'ETV généralement couplé à un ICP MS ou AES pour l'analyse du pétrole. Chaves *et al* [159] ont déterminé la concentration du Co, Cu, Fe, Mn, Ni et V dans des biodiesels par ETV-ICP MS. Ils ont utilisé le standard NIST 1634C afin de vérifier leur méthode. Ils ont optimisé les débits de gaz (0.95 $L.min^{-1}$ pour le gaz porteur et 0.15 $L.min^{-1}$ pour le gaz by-pass). Enfin, ils ont obtenu 20% de déviation sur leurs résultats.

Saint'Pierre *et al*[160] ont analysé le Cu, Mn, Ni et Sn dans le gasoil par ETV-ICP MS. Ils ont obtenu des limites de détection de 0,22, 0,02, 0,38 et 0,03 $\mu g.L^{-1}$ respectivement. Récemment Silva *et al* [161] ont utilisé un couplage ETV-ICP MS pour analyser du pétrole brut. Après optimisation de leurs paramètres, ils ont utilisé du Fréon (CCl_2F_2) comme gaz de réaction à un débit de 3 $mL.min^{-1}$ et 0,4 L $.min^{-1}$ pour le gaz porteur et le gaz by-pass. Ils ont analysé plusieurs éléments (La, Ce, Pr, Nd, Sm, Eu, Gd, Tb, Dy, Ho, Er, Tm, Yb, Lu et Y) et ont obtenu des limites de quantification entre 0,02 et 0,8 $ng.g^{-1}$.

Malgré la grande sensibilité et la bonne résolution que peut avoir un ICP MS, il ne s'agit la que d'une analyse élémentaire. Pour certain domaine d'étude l'analyse moléculaire apporte aussi son lot d'information. Pour cela un FT-ICR MS peut être utilisé.

I.III.2.3 FT-ICR MS

I.III.2.3.1 Principe

Le FT-ICR MS, est un instrument qui associe une très grande précision de mesure de masse à une très haute résolution[162]. Ses caractéristiques en font une technique de choix

pour l'analyse de matrices complexes. En effet, la précision de mesure et la très haute résolution permettent d'attribuer une formule brute aux ions detectés.

Le FT-ICR MS est basé sur le mouvement cyclotronique des ions piégés dans un champ magnétique. Les ions à une vitesse donnée v soumis à un champ magnétique vont adopter un mouvement circulaire uniforme perpendiculaire au champ magnétique. La vitesse angulaire de rotation des ions W_c dépend du champ magnétique B, de la charge q de l'ion mais aussi de sa masse m.

$$Wc = \frac{qB}{m}$$

La fréquence cyclotronique $F_{c,}$ est directement proportionnelle au champ magnétique, inversement proportionnelle au rapport masse sur charge.

$$Fc = \frac{Wc}{2\pi} = \frac{qB}{2\pi m}$$

Donc, la mesure de la fréquence Fc permet de retrouver le rapport *m/z* des ions. Pour cela, les ions sont piégés dans une cellule ICR. L'excitation est effectuée par un champ électrique radiofréquence qui augmente l'énergie cinétique des ions et le rayon de leur oscillation à leur fréquence cyclotronique. Cela permet d'obtenir un mouvement des ions cohérent et détectable.

Le courant induit par le mouvement cyclotronique des ions dans la cellule ICR sur les plaques de détections conduit à un signal analogique sinusoïdal amorti dans le temps appelé Free Induction Decay (FID). Il s'agit d'un signal sinusoïdal. La résolution d'un spectromètre de masse est définie par l'équation suivante :

$$R = \frac{m}{\Delta m 50\%}$$

Avec R la résolution et $\Delta m_{50\%}$ la largeur du pic à mi-hauteur.

La résolution qui peut être obtenue sur un FT-ICR MS est donnée par la relation suivante :

$$R = \frac{0.132qBTa}{m}$$

Avec T_a la durée d'acquisition du signal FID.

La transformée de Fourrier est appliquée au signal FID et permet de convertir l'échelle de temps en échelle de fréquence et ainsi obtenir le rapport *m/z* des ions[163].

I.III.2.3.2 Source d'ionisation

I.III.2.3.2.1 Electrospray Ionization (ESI) :

Cette source d'ionisation aujourd'hui très largement répandue a été développée en 1984 par John B. Fenn [164], [165]. La source ESI permet de former un aérosol chargé à partir d'un échantillon en solution à l'aide d'une différence de potentiel élevée.

La formation des ions s'effectue majoritaire en solution et a lieu en plusieurs étapes. L'échantillon en solution est introduit à un débit faible (5 – 20 µL min^{-1}) puis est transformé en gouttelettes chargées par le champ électrique intense appliqué entre le capillaire d'introduction et l'orifice d'entrée du spectromètre de masse. Le flux de solution est étiré en un cone de Taylor par champs électrique intense appliqué au capillaire. Les gouttelettes chargées sont formés par rupture du cône de Taylor. La taille de ces gouttelettes va alors diminuer par évaporation partielle du solvant conduisant à l'augmentation de la densité de charge. Ce processus va se produire jusqu'à formation d'ions en phase gazeuse.

L'ionisation ayant lieu en solution, ce sont les propriétés des molécules en solution et du solvant qui vont influencer l'ionisation. Cette source peut conduire à la formation d'ions multichargés notamment dans le cas d'espèces de haute masse. Cette source permet ainsi l'analyse de molécules de hautes masses même avec des analyseurs de gamme de masse relativement faible par la diminution du rapport *m/z*.

I.III.2.3.2.2 Atmospheric Pressure Photo Ionization:

Cette source a été introduite en 2000 par Bruins et permet de vaporiser un échantillon liquide à l'aide d'un gaz de désolvatation chauffé (azote entre 200°C et 400°C) et de l'ioniser par bombardement de photons produits par une lampe au krypton [166]. L'échantillon liquide est introduit à un débit entre 200 et 1000 µL min^{-1}.

Les photons produits par la lampe au krypton sont très énergétiques (10.6 eV) et vont exciter la molécule en phase gazeuse. L'énergie de ce photon étant supérieure à l'énergie d'ionisation de la plupart des molécules organiques, celles-ci vont perdre un électron. Ce processus d'ionisation induit la formation d'ions moléculaires ($M^{+\bullet}$). Suivant le mode d'ionisation positif ou négatif, on obtiendra des anions ou des cations radicalaires. En présence de solvants protiques, des processus plus complexes peuvent se produire conduisant notamment à la formation de molécules protonés $[M+H]^+$.

Putman *et al* [124] ont fractionné un échantillon d'asphaltène par GPC, en ont récolté les fractions puis ont analysé les ont par APPI-FT-ICR MS. Il a été mis en évidence que la fraction contenant les agrégats de plus grande taille est la plus difficile à ioniser. De plus c'est la fraction ou les composés ont une valeur de *Double Bond Equivalent* (DBE) la plus faible et le nombre de carbone le plus élevé. Une faible valeur de DBE et un nombre élevé de carbone par molécules ne correspond pas à des espèces poly aromatiques. Il semblerait aussi que c'est la fraction contenant le moins d'hétéro-élément. Contrairement à ce qui était attendu, il semblerait que l'agrégation ne soient pas liés à des composés polaires et aromatiques. Dans cette thèse un couplage GPC et APPI-FT-ICR MS sera utilisé. Non seulement il sera faible en ligne mais aussi couplage a une séparation préalable liquide/solide dans le but de simplifier la matrice pétrolière.

I.III.2.3.2.3 Laser désorption ionisation (LDI)

Pour cette technique d'ionisation, le zone d'irradiation du laser va servir à la fois pour la volatilisation de l'échantillon solide et pour l'ionisation des molécules désorbées. De manière générale cette technique va être appliquée aux composés piégés dans une matrice solide.

Cette technique repose sur l'interaction entre un faisceau laser et une cible qui va être le point de départ d'une suite de processus complexes menant à la formation d'un nuage gazeux plus ou moins ionisé. Les phénomènes mis en jeu ici sont l'ablation et/ou la désorption. La répartition des espèces au sein du nuage gazeux formé va dépendre à la fois des caractéristiques optiques (coefficient de réflexion R, coefficient d'absorption α, …) et thermiques (diffusivité thermique K, …) de l'échantillon et des caractéristiques du faisceau laser (longueur d'onde λ, durée d'impulsion, densité d'énergie aussi appelée fluence F).

Deux paramètres importants sont la longueur d'onde du laser utilisé et l'irradiance (en $W.cm^{-2}$) définie comme la puissance par unité de surface. L'interaction du faisceau laser avec le solide va induire différents processus conduisant à l'expulsion d'espèces neutres et ionisées

dans la phase gazeuse. Parks et Haglund [167] ont proposé une description qualitative de ces processus. Selon lui, la pulvérisation par le laser peut se décomposer en quatre phases :

- Absorption de l'énergie laser par un processus simple ou multi photonique (importance de ce fait des propriétés d'absorption de l'échantillon étudié en phase solide),

- Conversion de l'énergie en chaleur.

- Ejection d'espèces de la surface irradiée. Ces espèces peuvent être des atomes, des molécules, ioniques ou neutres, des électrons et des espèces excitées,

- Formation et expansion d'une plume plus ou moins dense de neutres et d'ions. Les mécanismes de formation des neutres et des ions peuvent être variés.

Les molécules organiques passant en phase gazeuse vont être susceptibles soit de perdre un électron par des processus de photo-ionisation, soit d'en capter, menant ainsi à la formation d'espèces radicalaires positives ou négatives respectivement.

Si l'énergie absorbée est suffisante, la rupture de la liaison d'un proton labile peut être envisagée menant à la formation d'ions $[M-H]^-$. Une espèce à caractère basique peut alors capter ce proton et former ainsi des ions $[M+H]^+$. Si l'énergie fournie par les photons du faisceau laser est suffisante, cet excès d'énergie interne au sein des ions moléculaires radicalaires ou protonés peut conduire à une fragmentation.

La seule différence entre le LDI et le *Matrix Assisted Laser Desorption Ionisation* (MALDI) est l'ajout d'une matrice (MA pour matrix assisted) qui va favoriser ou non l'ionisation de certains composés par différents mécanismes (transfert de proton ou d'électron). Durant ces travaux de thèse la source la source d'ionisation LDI/MALDI va être utilisé dans le but d'analyser des échantillons d'asphaltène déjà déposés et séparés sur des plaques HPTLC.

Giraldo-davila *et al*[168] ont analysé les porphyrines par LDI/MALDI FT-ICR MS après extraction à l'acétonitrile avec un soxlhet. L'analyse MALDI de cette fraction a été faite avec une nouvelle matrice : CNPV-CH3 ((2Z,2′Z)-2,2′- (1,4-phenylene)bis(3-(p-tolyl)acrylonitrile)). Cette matrice permet une meilleure ionisation des porphyrines présent dans les échantillons. Cela a permis de détecter plus de 100 signaux pouvant être attribués aux porphyrines.

Ramirez-pradilla et *al* [169] ont travaillé de la même façons par FT-ICR MS avec une source d'ionisation MALDI. Pour la préparation d'échantillons, ils ont procédé à une extraction liquide-liquide avec de l'ACN dans le but d'extraire une fraction enrichie en porphyrines. Puis sur plaques HPTLC, ils ont fait migrer un échantillon pétrolier avec de l'acétonitrile. Ensuite ils

ont analysé l'extrait et la partie élué sur la plaque HPTLC. Ils ont pu identifier 350 signaux attribués aux porphyrines de vanadium et de nickel. Sur plaques HPTLC ils ont pu en identifier 518, un nombre encore jamais atteint jusqu'à présent.

I.III.2.3.3 Représentation

Dans le cadres d'analyses de composés pétroliers, le spectre obtenu peut contenir plusieurs dizaines de milliers de pics peuvent être identifiés sur les spectres de masse. Il est plus facile alors pour avoir une meilleure vue d'ensemble de les représenter sous forme de carte afin de les trier par groupement chimique ou par DBE.

I.III.2.3.3.1 Diagramme de Kendrick

Le diagramme de Kendrick est basé sur une échelle de masse de M (CH2) = 14,0000 Da proposée par Kendrick [170] en 1963. Ce diagramme peut être utilisé alors que la formule moléculaire du composé est inconnue. La masse expérimentale IUPAC, correspondant à M (C) = 12,0000 Da, est facilement convertie en masse de Kendrick. Le calcul de la masse de Kendrick est donné par la formule suivante :

Kendrick's mass = experimental IUPAC

mass X (14.00000/14.01565)

Le défaut de masse de Kendrick est donné par la différence entre la masse nominale de Kendrick et la masse de Kendrick.

Comme présenté dans les travaux de Hughey *et al* [171], les données sur le pétrole peuvent être représentées en utilisant le défaut de masse de Kendrick en fonction de la masse nominale de Kendrick (voir Figure 22).

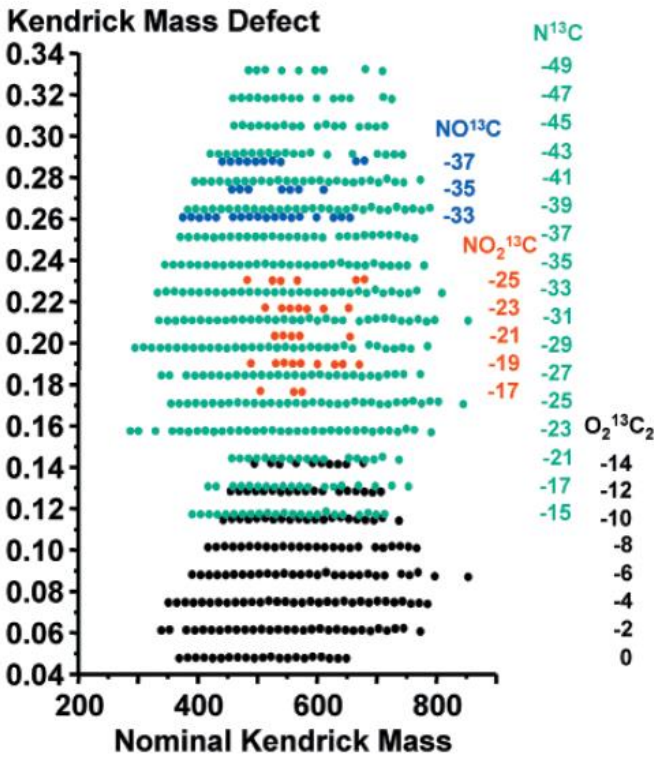

Figure 21: Exemple de diagramme de Kendrick[171]

Le principal avantage de ce graphique est qu'il met clairement en évidence les composés avec la même unité de répétition, généralement CH_2, ce qui correspond aux composés avec le même contenu en hétéroatomes et DBE. Ainsi, la technique permet de comparer facilement des échantillons complexes afin d'identifier les différences de composition.

I.III.2.3.3.2 Diagramme de Van Krevelen

Une autre méthode de représentation des données est appelée diagramme de Van Krevelen. La composition élémentaire CvHwNxOySz est nécessaire pour cette représentation, qui trace le rapport atomique H/C en fonction du rapport atomique O/C ou N/C (voir Figure 23)

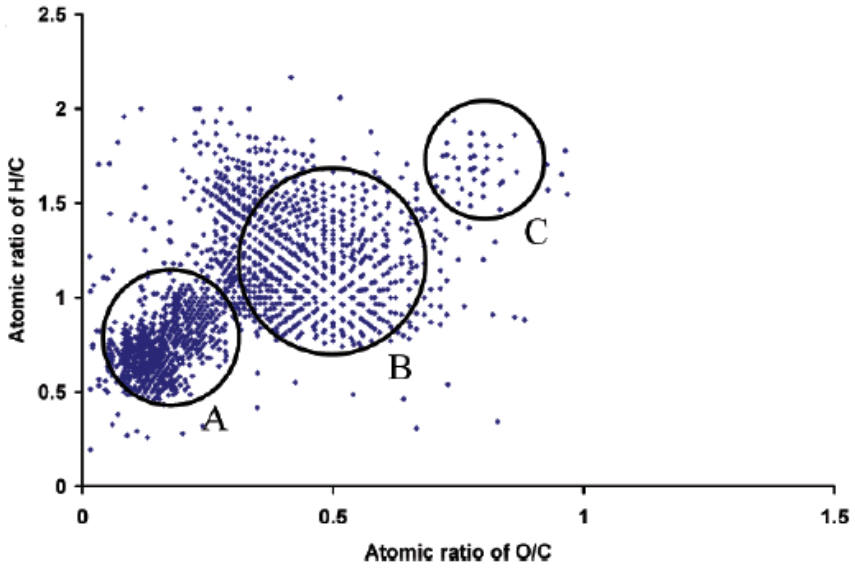

Figure 22: Exemple de diagramme de Van Krevelen[172]

La première utilisation de ce diagramme dans le domaine du pétrole a été rapportée par Kim *et al* [172]. Ce diagramme permet de comparer facilement deux échantillons, mais son principal inconvénient est que la masse moléculaire n'est pas prise en compte dans cette représentation.

I.III.2.3.3.3 Composition Spatiale (DBE/C)

Dans ce diagramme, le rapport H/C est directement lié à la valeur DBE (voir Figure 24). La valeur DBE peut être facilement calculée à partir de la formule moléculaire d'un composé via l'équation :

$$DBE = C - \frac{H}{2} + \frac{N}{2} + 1$$

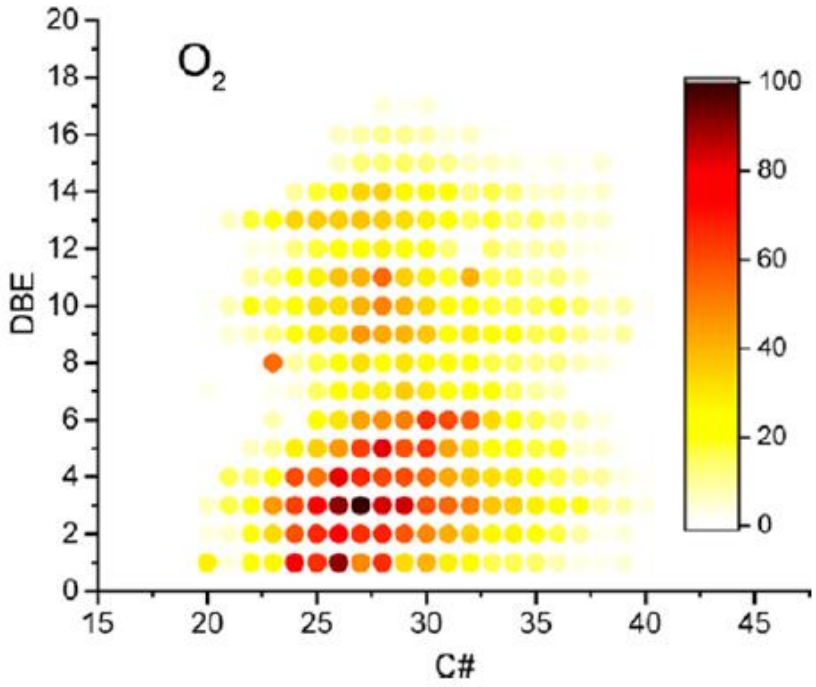

Figure 23: Exemple de représentation par composition spatiale[108]

La valeur DBE est un indicateur de la structure moléculaire. Une valeur DBE de 4 pour un composé d'hydrocarbure de pétrole est caractéristique d'un cycle aromatique ou de quatre cycles parafiniques [173]. La DBE en fonction du nombre de carbones pour des classes spécifiques de composés s'est révélé être un bon indicateur de la structure moléculaire, car il fournit une représentation graphique de l'échantillon à partir duquel des informations chimiques peuvent être obtenues [174].

Ce graphique permet de visualiser la distribution continue de la composition du pétrole obtenue à partir de données de spectrométrie de masse à haute résolution pour une classe d'hétéroatomes donnée [175]. Ce graphique fournis aussi des informations sur l'aromaticité et la masse des composés. L'abondance relative des différents composés est souvent montrée à l'aide d'un code de couleur. Cette représentation permet de comparer rapidement différents échantillons. Toutefois, cette représentation ne peut être appliquée qu'à une seule classe et la représentation de toutes les classes d'un échantillon nécessite plusieurs graphes.

Chapitre II : Etude de la répartition en taille des produits pétroliers par chromatographie à perméation de gel

Comme présenté dans le chapitre I, la GPC permet la séparation des échantillons pétroliers en fonction de la taille des agrégats qui les composent. De précédent travaux ont montré l'utilité de la GPC couplée à un ICP MS dans le domaine de l'analyse du soufre et des métaux dans les matrices pétrolières en fonction de leur volume hydrodynamique [46]. Ces informations peuvent être d'une grande importance dans les activités de raffinage, notamment pour aider à choisir la porosité des catalyseurs utilisés dans les différents procédés.

Dans une première partie de ce chapitre, la GPC a été couplée à un ICP MS pour analyser des échantillons de la chaine de raffinage des huiles (produits décrits chapitre I) dans le cadre d'une analyse en collaboration avec les laboratoires composant le laboratoire iC2MC. Dans ces travaux, la GPC-ICP MS permet une analyse du vanadium et du soufre en fonction de la taille des nano agrégats qui le contiennent. Ces résultats ont été mis en commun avec une analyse moléculaire par HPLC3 et par FT-ICR MS, mettant en évidence la complémentarité des approches.

Dans une seconde partie sera présenté un deuxième type de séparation liquide/solide qui sera couplé à la séparation par GPC. Le couplage de deux techniques de séparations permettra d'obtenir plus d'information notamment sur les parties les plus agrégés de l'échantillon, là où se situe le vanadium le plus difficile à extraire. L'analyse se fera par ICP MS. Enfin ces résultats ont été corrélés avec de résultats d'analyses par Quartz Cristal Resonator (QCR) et par FT-ICR MS.

Enfin, dans une troisième partie à la suite des travaux de Putman *et al* [124] sur un couplage hors ligne d'une GPC avec un FT-ICR MS, ici une séparation par GPC a été couplée à la séparation par extrographie. Ensuite deux couplages en ligne avec un ICP MS pour la partie élémentaire et avec un FT-ICR MS pour la partie moléculaire ont été effectués. Ces travaux se concentrerons sur la spéciation des porphyrines de vanadium dans les asphaltenes.

As presented in Chapter I, the GPC allows the separation of petroleum samples according to the size of the aggregates that make up the sample. Previous work has shown the usefulness of GPC coupled with an ICP MSI for the analysis of sulphur and metals in petroleum matrices as a function of their hydrodynamic volume [46]. This information can be of great importance in refining activities, particularly to help select the porosity of the catalysts used in the various processes.

In the first part of this chapter, the GPC was coupled with an ICP MS to analyse samples of the oil refining chain (products described in chapter I) in the framework of an analysis in collaboration with the laboratories composing the iC2MC laboratory. In this work, the GPC-ICP MS allows analysis of vanadium and sulphur as a function of the size of the nano aggregates containing it. These results were pooled with molecular analysis by HPLC3 and FT-ICR MS, highlighting the complementarity of the approaches.

In a second part, a second type of liquid/solid separation will be presented, which will be coupled with GPC separation. The coupling of two separation techniques will provide more information especially on the more aggregated parts of the sample where the vanadium is most difficult to extract. The analysis will be carried out by ICP MS. Finally, these results were correlated with the results of analysis by Quartz Cristal Resonator (QCR) and FT-ICR MS.

Finally, in a third part following the work of Putman et al [124] on an off-line coupling of a GPC with an FT-ICR MS, here a separation by GPC was coupled to the separation by extrography. Then two in-line couplings with an ICP MS for the elementary part and with an FT-ICR MS for the molecular part were performed. This work will focus on the speciation of vanadium porphyrins in asphaltenes.

Partie I : Apport de la GPC-ICP MS dans le cadre de l'analyse d'échantillons de la chaine de raffinage des huiles.

Cette partie a fait l'objet d'un article publié dans le journal Processes. Cet article a été laissé tel qu'il a été publié.

Dans la partie 1 de ce chapitre II, le but est de montrer la complémentarité de techniques de séparation suivis d'analyse UV, élémentaire et moléculaire appliqué à des échantillons de la chaine de fabrication des huiles de base. Comme vu dans le chapitre I, les huiles de base sont des produits pétroliers raffinés devant respecter certaines caractéristiques. Ici, la viscosité des échantillons est un paramètre important.

Dans le but d'aider à la compréhension des phénomènes chimiques se produisant lors des étapes de raffinage, les échantillons ont d'abord été analysés avec un système de chromatographie liquide avec un *Evaporating Light Scattering Detector* (ELSD) qui apporte des informations sur la teneur en saturés et en aromatiques[179]. En effet, d'après les travaux de Mehrkesh *et al*[180] la viscosité est liée à la teneur en composés présent dans l'échantillons. Puis l'analyse a été effectuée par le système GPC-ICP MS afin de connaitre l'état d'agrégation de du soufre et du vanadium. Puis enfin les huiles de base ont été analysées en APPI-FT-ICR MS afin de connaitre l'aromaticité des familles chimiques S_1 et CH. Pour finir les différents paramètres obtenus par les trois techniques seront mis en commun en utilisant un traitement statistique utilisant la méthode *Partial Least Square* (PLS) dans le but de déterminer quelles sont les paramètres qui influent sur la viscosité. Ces informations permettront d'aider à l'optimisation de la viscosité dans les unités de traitement de la raffinerie.

This part was the subject of an article published to Processes journal. This article has been left as published.

In part 1 of this chapter II, the aim is to show the complementarity of separation techniques followed by UV, elemental and molecular analysis applied to samples of the base oil production chain. As seen in Chapter I, base oils are refined petroleum products that must meet certain characteristics. Here, the viscosity of the samples is an important parameter.

In order to help understand the chemical phenomena occurring during the refining stages, the samples were first analysed using a liquid chromatography system with an Evaporating Light Scattering Detector (ELSD) which provides information on the content of saturates and aromatics [179]. Indeed, according to the work of Mehrkesh et al [180] the viscosity is related to the content of compounds present in the sample. The analysis was then carried out by the GPC-ICP MS system to determine the state of aggregation of sulphur and vanadium. Finally, the base oils were analysed in APPI-FT-ICR MS to determine the aromaticity of the chemical families S1 and CH. Finally, the different parameters obtained by the three techniques were pooled using a statistical treatment using the Partial Least Square (PLS) method to determine which parameters influence viscosity. This information will be used to help optimize the viscosity in the refinery's process units.

processes

MDPI

Article

Chemical Characterization Using Different Analytical Techniques to Understand Processes: The Case of the Paraffinic Base Oil Production Line

Rémi Moulian [1,2,3], Johann Le Maître [2,3,4], Hélène Leroy [2], Ryan Rodgers [1,2,5,6,7], Brice Bouyssiere [1,2,*], Carlos Afonso [2,4], Pierre Giusti [2,3] and Caroline Barrère-Mangote [2,3,*]

1 E2S UPPA, CNRS, IPREM, Institut des Sciences Analytiques et de Physico-chimie pour l'Environnement et les Materiaux, Universite de Pau et des Pays de l'Adour, UMR5254, Hélioparc, 64053 Pau, France; remi.moulian@gmail.com (R.M.); rrodgers@fsu.edu (R.R.)

2 International Joint Laboratory—iC2MC: Complex Matrices Molecular Characterization, TRTG, BP 27, 76700 Harfleur, France; johann.lemaitre@yahoo.com (J.L.M.); helene.leroy@total.com (H.L.); carlos.afonso@univ-rouen.fr (C.A.); pierre.giusti@total.com (P.G.)

3 TOTAL Refining and Chemicals, Normandy Platform, 76700 Harfleur, France

4 COBRA, UMR 6014 et FR 3038, INSA de Rouen, CNRS, IRCOF, Normandie Université, Université de Rouen, 76130 Mont Saint Aignan CEDEX, France

5 National High Magnetic Field Laboratory, Florida State University, 1800 East Paul Dirac Drive, Tallahassee, FL 32310, USA

6 Department of Chemistry and Biochemistry, 95 Chieftain Way, Florida State University, Tallahassee, FL 32306, USA

7 Future Fuels Institute, 1800 Paul Dirac Drive, Tallahassee, FL 32310–4005, USA

* Correspondence: brice.bouyssiere@univ-pau.fr (B.B.); caroline.mangote@total.com (C.B.-M.); Tel.: +33-0-559-407-752 (B.B.); +33-0-235 551-102 (C.B.-M.)

Received: 11 October 2020; Accepted: 12 November 2020; Published: 18 November 2020

Abstract: Mineral base oils are used to produce commercial lubricants and are obtained from refining vacuum residue. Lubricants are used to reduce friction in industry devices, so their viscosity is a key characteristic that needs to be optimized throughout the process. The purpose of this study is to show how global chemical characterization of samples from the base oil production chain can facilitate a better understanding of the molecular impacts of processing and their effect on macroscopic properties like viscosity. Eight different samples were characterized by different analytical techniques, including liquid chromatography and mass spectrometry techniques, to understand their chemical evolution through the different process units at the molecular level. Furthermore, a statistical treatment allowed for the identification of parameters that influence viscosity, mainly sulfur and polyaromatics content. This study demonstrates the importance and effectiveness of cross-checking results from different complementary analytical techniques to acquire valuable data on lubricating oil base samples.

Keywords: lubricant base oil; GPC ICP HRMS; APPI FT ICR MS; HPLC3; aromatics; viscosity

1. Introduction

High viscosity grade lubricants are used as marine lubricants to reduce friction in slow-speed engine cylinder oils. As for other lubricants, they are composed of a base oil and additives packages that aimed to neutralize acidic combustion by-products, providing detergency or cleaning effect, preventing deposit formation by keeping deposit precursors soluble in the oil (dispersant) and reducing friction and wear. For these high viscosity grade lubricants, base oil or solvent-extracted bright stock, is most commonly obtained by solvent refining. The viscosity (between 30.0 and 35.0 mm^2/s (cSt) at 100 °C), the viscosity index, and pour point are key characteristics of these samples that need to be optimized

throughout the refining process. The viscosity index (VI) is the rate of change in viscosity with changes in temperature while pour point is the temperature below which the liquid loses its flow characteristics.

The solvent extracted bright stock (BSS) is produced from crude oil vacuum residue (VR) by precipitating asphaltenes with liquid propane; this step allows for the optimization of the oil viscosity [1]. The Common "contaminants" in the deasphalted oil (DAO) are aromatic and naphthenic hydrocarbon species, which must be removed to increase the viscosity index [2]. The extraction process consists of treating the DAO with a solvent (furfural (FF) [3] or n-methyl-pyrrolidone), which yields an extract rich in aromatic molecules and a raffinate fraction rich in paraffin [2]. Finally, during the dewaxing process, the raffinate is treated with methyl ethyl ketone (MEK) and toluene to selectively precipitate the n-paraffin from the oils and to optimize the pour point. These different refining steps are aimed at optimizing the viscosity properties (viscosity, viscosity index, pour point, etc.) of the lubricant [2]. Also, commercial specifications, like the aniline point for the lube extract and viscosity for the wax, have to be reached for the co-products of the solvent refining. For this purpose, the different process units are tuned to optimize the different properties of the products.

To obtain a better understanding of the refining processes, it is important to have good chemical characterization of the samples at each step. For base oils, some studies have been published. For example, Mehrkesh et al. [2] found a correlation between the aromatics content of six raffinate samples and their viscosity, regardless of temperature. Varotsis and Pasadakis [4] developed a method to determine the percentage of monoaromatics, diaromatics, and triaromatics using a gel permeation chromatography (GPC)-UV-RI system. They used the differences in the absorption wavelengths of each compound to calculate the amount of each compound in the sample. In this work, Pasadakis showed that aromatics can be determined by a simple technique, such as GPC-UV, in these types of samples. Alawani et al. [5] suggested that the aromaticity of compounds found in crude oil samples increases with increasing elution time in GPC when using toluene as the mobile phase.

Mass spectrometry techniques are also useful for the characterization of base oil samples. Wang and Zhang [6] used GC-MS and found a correlation between the isoparaffins index and viscosity after the dewaxing process. Manheim et al. and Liang et al. [7,8] used a gas chromatography 2D (GC × GC)/EI TOF mass spectrometer to identify and quantitate linear alkanes. Linear alkanes negatively affect the performance of lubricant base oils. Desprez et al. [9] used GPC with inductively coupled plasma mass spectrometry (GPC-ICP HR MS) to correlate the viscosity and sulfur aggregation behavior in crude oil, atmospheric residue (AR), vacuum gas oil (VGO) and VR samples. Panda et al. [10] fractionated crude oil by preparative GPC and analyzed it using atmospheric pressure photo ionization (APPI) and Fourier transformation ion cyclotron resonance mass spectrometry (FT-ICR MS). They found that the more the retention time increased, the more the aromaticity of the samples increased. Putman et al. [11] obtained similar results; they observed that more aliphatic compounds have a greater tendency to aggregate, leading to a reduced retention time. Duan et al. [12] and Nyadong et al. [13] each used laser-induced acoustic desorption with different chemical ionization (LIAD-CI) methods, atmospheric pressure chemical ionization (APCI) [13] and with the aqua chloromanganese II cation [12], to determine the molecular mass of the compounds present as well as the percentage of saturate, monoaromatics, and diaromatics in lubricant oils. Hourani et al. [14] used high performance liquid chromatography (HPLC), gas chromatography 2D (GC × GC) and FT-ICR MS to identify mono-, di-, and triaromatic compounds in lubricant base oil. For FT-ICR MS, they used two different ionization techniques, APPI and APCI, which allowed them to determine the molecular structure of the base oils. Furthermore, they found that APCI was more effective for studying saturated compounds. These works showed the importance of mass spectrometry for acquiring molecular information about paraffinic and polyaromatic species, which are key parameters in lubricant base oil samples.

According to the literature [2,4,5], the content of aromatics and sulfur in base oils had an impact on their viscosity as well as on the aniline point for lube extract. In this work, samples from all phases of the lubricant oil production line, from vacuum residue to bright stock solvent and wax, were characterized and compared. Three main techniques were used to provide different information.

First, HPLC with an evaporative light scattering detector (ELSD) was used to obtain information about the quantity of saturate, mono-, and polyaromatic compounds. This method, referred to as HPLC3, was previously described by Putman et al. [15]. HPLC3 provides information on the percentage of saturates and aromatics. Then, GPC with inductively coupled plasma mass spectrometry (ICP HR MS) was used to analyze the sulfur and vanadium containing compounds in each sample. This technique can be used to quantify the sulfur and vanadium present in the sample, but more importantly, it provides information on the aggregation state of vanadium- and sulfur-containing molecules. Then, APPI [14–17]/APCI [18–22]-FT-ICR MS [23–26] was used to obtain molecular data of the different samples. In particular, information was obtained on the degree of aromaticity of sulfur [27,28] and hydrocarbon molecules. In the present study, 8 samples were analyzed, and all the data collected were correlated with the viscosity [29] of each sample. Statistical treatment using partial least square (PLS) regression was performed to determine which parameters affect viscosity [30].

2. Materials and Methods

2.1. Samples, Materials, and Reagents

The three units of the production line, solvent de-asphalter (SDA), furfural, and dewaxing, were studied separately to examine potential "tank" effects as described in Figure 1. Eight industrial samples were available.

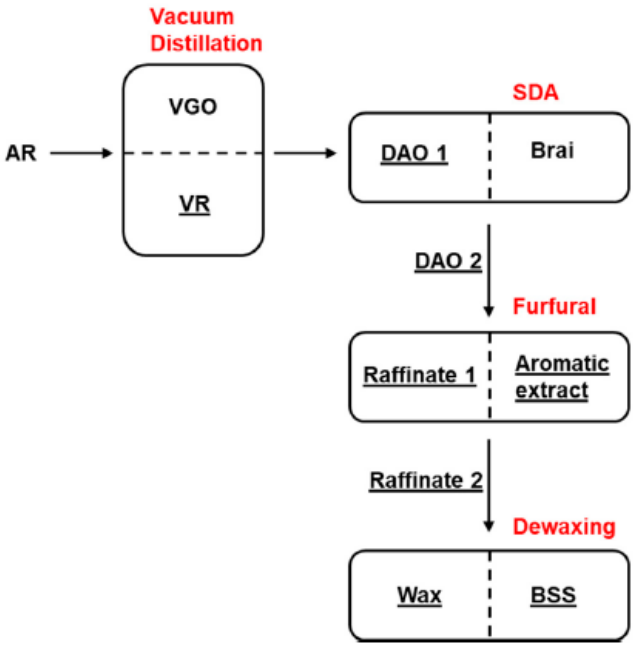

Figure 1. Lubricant oil production scheme.

Vacuum residue (VR) and the corresponding desulphated oil (DAO 1) were obtained with propane in the SDA unit. The other effluent of the SDA unit, which contains the asphaltene fraction and is referred to as brai, was not available for study. Thus, a similar DAO feed of furfural (FF), referred to as DAO 2, with the corresponding effluents raffinate 1 and aromatic extract, was studied. Finally, a similar raffinate sample, the feed of the dewaxing unit, referred to as raffinate 2 with corresponding wax and BSS, was available. This sample was obtained with methyl ether ketone and toluene as the dewaxing solvent.

2.2. Analytical Techniques

2.2.1. HPLC3

As in previous works, the HPLC3 system came from commercially available components [15]. A Waters HPLC system composed of an Alliance e2695 Separation Module, of a WAT 005.319 2 µM as precolumn inline filter, of a 2998 photodiode array and of a 2424 evaporative light scattering detector (ELSD) operated with EMPOWER3 software (Waters, Milford, MA, USA) were used. Two columns were used, the first column was a Chromegabond Dinitroanilinopropyl (DNAP, 4.6 × 250 mm, 5 µM) with a 3.2 × 10 mm Chromegabond DNAP as guard cartridge (ES Industries, West Berlin, NJ, USA). The other column was a Spherisorb strong cation exchange (SCX, 4.6 × 250 mm, 5 µM) (Waters, Milford, MA). To ensure metal saturation of the SCX column to yield the desired Ag-SCX column, a solution of 30 mg/mL silver nitrate in acetonitrile was sent through the column before analysis. A postcolumn dilution using cyclohexane was utilized to facilitate a uniform ELSD response throughout the gradient. The analyses were made with an injection of 40 µL of sample at a concentration of 40 mg/mL during 140 min for each run. The temperature of the columns was not controlled. Only the sample wax was not analyzed with this technique because of its insolubility with the solvent. For data treatment, an external calibration curve was used to determine the percentage in mass for each peak. All the samples were analyzed in triplicate and standard deviations were below 2%.

2.2.2. GPC ICP HR MS

The carrier solution was delivered by a Dionex High-Performance Liquid Chromatography (HPLC) system with an UltiMate 3000 microflow pump and an UltiMate 3000 autosampler. THF and Multisolvent® GPC-grade ACS stabilized with 250 ppm of BHT (Scharlau) were used as solvents for the dilution of samples and as mobile phases. Chromatographic separation was performed by three GPC columns (from 1000 to 600,000 Dalton) connected in series. A Styragel guard column (4.6 mm inner diameter, 30 mm length, 10,000 Da exclusion limit) was used as the guard column. Twenty microliters of solution were injected and eluted at 1 mL min^{-1} of THF for 90 min. A postcolumn splitter was used to send 40 µL min^{-1} in the ICP HR MS, sending the other part to the waste. Samples were analyzed a maximum of a few hours after preparation.

As in our previous works [9,11,31], the introduction system of the mass spectrometer used in this work is a modified DS-5 microflow total consumption nebulizer (CETAC, Omaha, NE, USA) mounted with a laboratory-made glass spray chamber already used during prior study [31–33]. The temperature was maintained at 60 °C using a temperature-controlled bath with water (Neslab RTE-111, Thermo Fisher Scientific, Waltham, MA, USA). An argon gas flow was used at 16 L min^{-1} as plasma, an argon auxiliary gas was used at 0.9 L min^{-1} and an argon nebulizer gaz was used at 0.6 L min^{-1}. An O_2 gas flow was added to avoid carbon deposition at 0.08 L min^{-1}. The mass spectrometer was equipped with a quartz injector (inner diameter 1.0 mm), a Pt sampler (orifice diameter 1.1 mm) and skimmer (orifice diameter 0.8 mm) cones. With a double-focusing sector field inductively coupled plasma mass spectrometer (Element XR, Thermo Fisher Scientific, Bremen, Germany), enough resolution was obtained to avoid the spectrally interfered isotopes of ^{32}S, ^{51}V.

2.2.3. APPI/APCI FTICR-MS

Toluene was used to dissolve the samples; the samples were then diluted in methanol/toluene (50/50 v/v) until a concentration of 0.5 mg mL^{-1} was reached, for APPI analysis. The BSS and wax samples were dissolved and diluted in heptane at a concentration of 0.5 mg mL^{-1} for APCI analysis.

A hybrid quadrupole FT-ICR instrument (SolariXR, Bruker Daltonics, Bremen, Germany) equipped with a 12 T superconducting magnet was operated using APPI (10/10.6 eV, Kr-lamp) and the APCI source [19]. Mass spectra were acquired with a mass range of m/z 147–1300 for 128 scans from broadband experiments. The signal was digitalized with 8 M points, giving a transient length of 3.4 s. The accumulation time was set to 0.025 s at a flow rate of 600 µL h^{-1}. The experimental conditions

were: desolvation gas flow of 3 L min^{-1}, vaporizer temperature of 300 °C, source temperature of 220 °C, capillary voltage of −900 V in APPI and −4000 V in APCI, corona needle of 9000 nA in APCI, nebulizer pressure of 2.5 bar, octopole energy of 350 Vpp, quadrupole lower cut-off *m*/*z* 200, quadrupole collision energy 1 of 200 Vpp, and TOF duration of 0.8 ms. A blank was recorded during 8 min prior to the introduction of each sample.

Mass spectrometers were externally calibrated using a sodium trifluoroacetate solution before sample analyses. Data Analysis (version 4.4) was used for instrument control and data acquisition. PetroOrg (version 9.4.1), CERES (self-developed Matlab-based interface) and OriginPro (version 2016) were used to process the data [34].The molecular formulas were determined from the accurate mass measurements (typically <0.2 ppm). The number of double bond equivalents (DBEs) were calculated from Equation (1) (*c*: carbon number; *h*: hydrogen number; *n*: nitrogen number) for a molecule of the crude formula $C_cH_hN_nO_oS_s$ [35]. Given a resolving power of 0.9×10^6 at *m*/*z* 400, it is possible to separate class C_xH_y ions from class S_1 (mass split: 3.4 mDa) compounds.

$$DBE = c - \frac{h}{2} + \frac{n}{2} + 1 \quad (1)$$

2.2.4. Statistical Treatment Using Partial Least Square (PLS) Regression

All the data acquired using the three different techniques, as well as the easily acquired refinery data given in Table 1, were used for the statistical treatment. The crystallizable fraction (CF) parameter represents the percentage of normal paraffin in wax obtained by differential scanning calorimetry (DSC). DSC measured the temperature of the transition between solid and liquid of one sample. This temperature made it possible to determine the quantity crystallizable paraffin in the sample. Conradson carbon residue (CCR) then represents the quantity of matter remaining after evaporation and pyrolysis of the sample.

Table 1. Measurable data of different samples.

		Sulfur Content (%w)	Vanadium Content (ppm)	Carbon Content (%w)	Hydrogen Content (%w)	Viscosity at 100 °C (cSt)	Crystallizable Fraction (FC, %w)	Carbon Conradson (CCR, %w)
SDA	VR	2.95	150	85.6	10.9	353.8	5.7	15.36
	DAO 1	1.67	1.6	85.9	12.5	33.83	12.7	1.65
FF	DAO 2	1.70	2.2	85.3	12.5	34.52	12.2	2.01
	Raffinate 1	0.83	<0.1	85.9	13.4	26.72	19.6	0
	Aromatic Extract	2.80	4.8	84.5	11.1	61.39	3.2	0
Dewaxing	Raffinate 2	0.77	<0.1	85.7	13.5	29.79	21.4	0.34
	BSS	0.94	<0.1	86.2	13.3	31.87	6.3	0.53
	Wax	0.38	<0.1	85.2	14.2	17.31	72.7	0

Statistical treatment by partial least square (PLS) analysis was used to determine which parameters affected viscosity: % carbon, % hydrogen, % sulfur, % saturate, % one ring, % 2−5 rings, crystallizable fraction (FC), CCR, retention time at maximum intensity for ^{32}S (GPC-ICP HR MS), ratio x_2/x_1 (GPC-ICP HR MS), and all the parameters given by FT-ICR MS for the CH and S_1 maps: nC/DBE minimum, nC/DBE maximum, and plot size nC/DBE.

3. Results

This section is divided by subheadings. It provides a concise and precise description of the experimental results, their interpretation, as well as the experimental conclusions that can be drawn.

3.1. HPLC3 Results

HPLC3 makes it possible to fractionate and quantify the saturate (Sat), 1−ring aromatic, 2−ring aromatic, 3−ring aromatic, 4−ring aromatic, and 5+ aromatic and polar compounds present in the samples. All the samples were analyzed, with the exception of wax, for solubility reasons. The results are shown for each process unit in Figure 2.

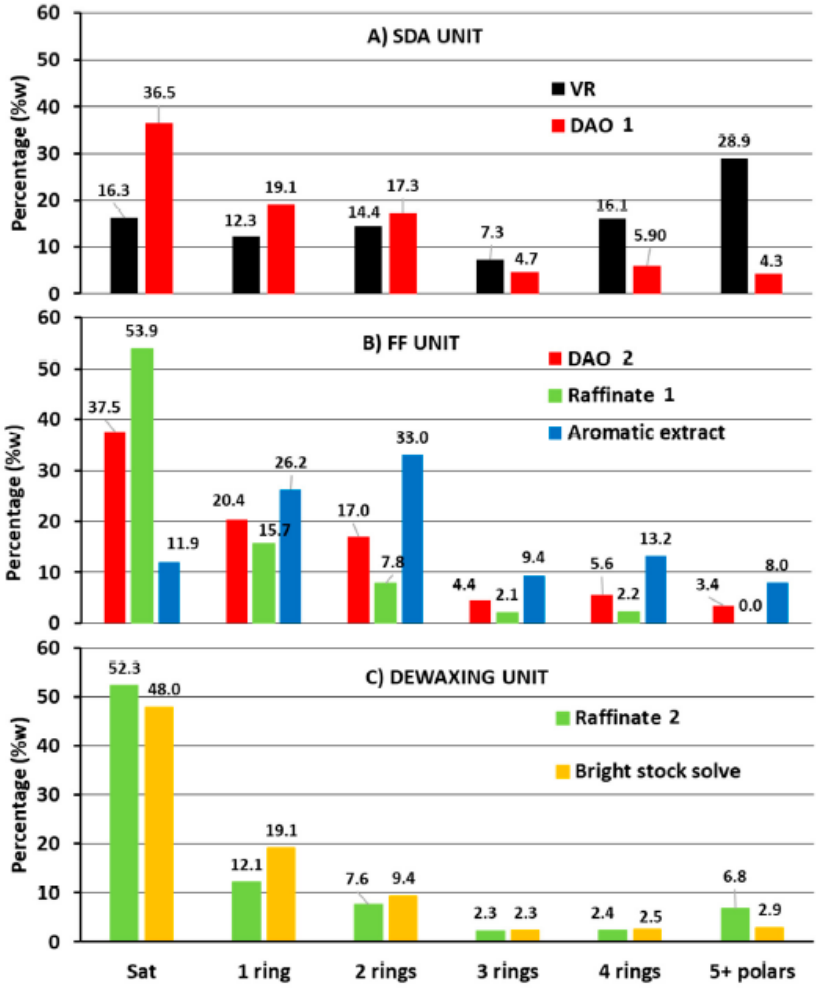

Figure 2. Percentage (%w) of saturate and aromatics by high performance liquid chromatography (HPLC) with an evaporative light scattering detector (ELSD) (HPLC3) for solvent de-asphalter (SDA) (**A**), furfural (FF) (**B**) and (**C**) DEWAXING units.

Figure 2A presents the percentage of different fractions for the SDA UNIT samples, VR and DAO 1. As expected, in Figure 2A, when comparing DAO 1 with VR, note the significant decreases of polyaromatics and polars (5+ polar, 4 rings, and 3 rings). This result means that the highly aromatic and polar components, which are not soluble in propane, enter the brai fraction. Moreover, note that, for DAO 1, the saturated and weakly aromatic compounds (1 ring and 2 rings) increased in proportion.

Figure 2B presents the percentage of different fractions of the FF unit samples. As expected, in Figure 2B, the aromatic extract contains a higher content of aromatics and polar compounds (3, 4, and 5+ polars rings) than DAO 2 and raffinate 1. The aromatic extract also exhibits an important decrease in the proportion of saturate compounds compared to DAO 2. In contrast, raffinate 1 has a similar composition to DAO 2, but with a higher content of saturate compounds.

Figure 2C presents the percentage of different fractions for the dewaxing unit, the samples raffinate 2 and BSS. In Figure 2C, both samples have the same pattern. As expected, a decrease in Sat compounds can be observed due to the dewaxing process. Mono- and diaromatic compounds, which are known for their lubrication properties, increase in BSS.

As viscosity is an important specification for lubricants, all the units were tuned to obtain the targeted viscosity value. Thus, it is particularly interesting to correlate viscosity to other chemical parameters to improve the understanding of the processes taking place in the different production units. As proposed by Mehrkesh et al. [2], the log of viscosity has been compared with the % of polyaromatics, calculated here as the sum of 2 rings, 3 rings, 4 rings, 5+ rings and polar compounds obtained by HPLC3. Table 2 presents the obtained percentage of aromatics for each sample.

Table 2. Percentage of monoaromatics and multiple aromatics in each sample.

Samples	Saturates (%w)	Percentage Mono Aromatic (%w)	Percentage Multiple Aromatics 2R-5R (%w)
VR	16.3	12.3	66.7
DAO 1	36.5	19.1	32.1
DAO 2	37.5	20.4	30.4
Raffinate 2	53.9	15.7	12.2
Aromatic Extract	11.9	26.2	63.6
Raffinate 3	52.3	12.1	15.7
BSS	48.0	19.1	17.1

Figure 3A presents the percentage of monoaromatics as a function of the logarithm of the viscosity for the seven samples, except for the VR. VR is the only sample of the series that contains asphaltene. It can be supposed that, due to its aggregation tendency [28], asphaltene has a large impact on viscosity. Thus, this sample has not been considered for the correlation. Figure 3B presents the correlation with the sum of all the polyaromatics (2/3/4/5 cores). The percentage of monoaromatics was less correlated with the log of viscosity with an $r^2 = 0.75$. In contrast, Figure 3B shows a linear trend between the aromatic content and viscosity, with $r^2 = 0.96$.

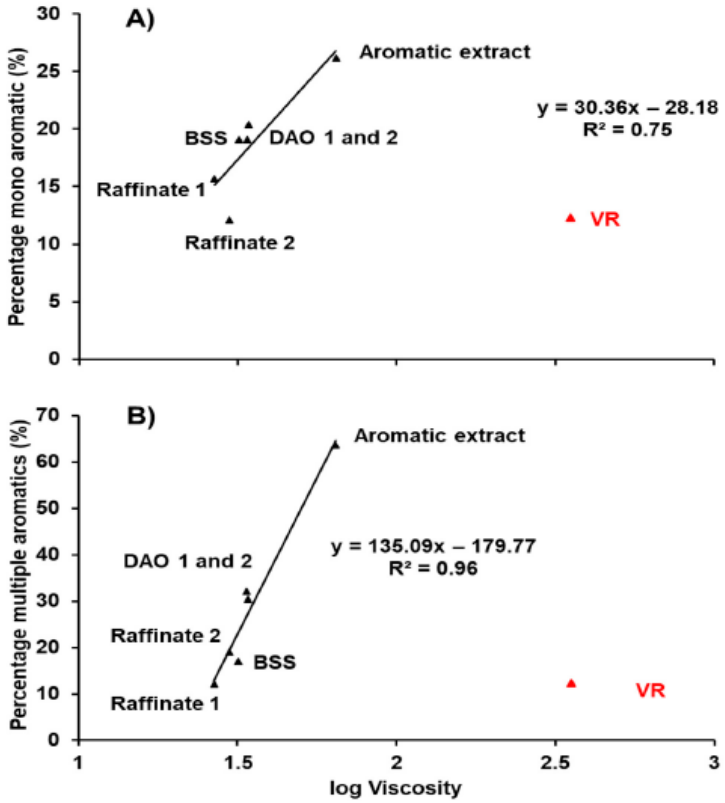

Figure 3. Correlation between the percentage of monoaromatic (**A**) and multiple aromatic (**B**) compounds and the log of viscosity for all the samples except vacuum residue (VR) (in red) and wax.

3.2. GPC-ICP HR MS Results

GPC is a chromatographic technique used to separate molecules or aggregates according to their hydrodynamic volume. Coupling GPC with an elemental detector such as ICP HR MS helps to determine the speciation of the different elements contained in petroleum samples, such as sulfur and metals. In previous works, the aggregation state of ^{32}S- and ^{51}V-containing molecule/aggregates [9,31,36] in different types of samples was studied. In particular, in the study by Desprez et al. [9], GPC-ICP HR MS was used to demonstrate a correlation between viscosity and specific, highly aggregated sulfur compounds in crude Oil, AR, VGO, and VR samples. To further understand the chemical parameters that impact viscosity, all the samples were analyzed by GPC-ICP HR MS to measure ^{32}S- and ^{51}V-containing molecules/aggregates. The results obtained for ^{32}S by GPC-ICP HR MS for all eight samples are presented in Figure 4 and Table 3.

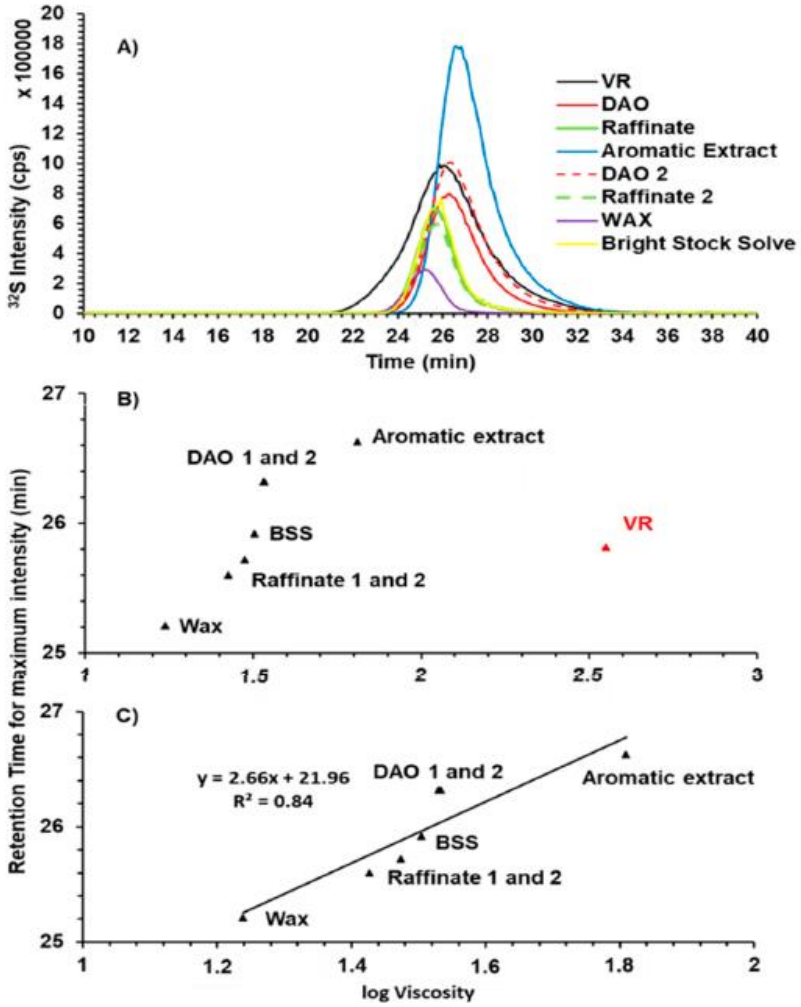

Figure 4. Chromatogram of sulfur containing molecules by GPC with inductively coupled plasma mass spectrometry (GPC-ICP HR MS) for all the samples (**A**). Retention time at the maximum intensity as a function of the log of viscosity for all the samples (**B**) and without VR (**C**). Abbreviations: GPC: gel permeation chromatography; ICP: inductively coupled plasma; MS: mass spectrometry

Table 3. Retention time at maximum intensity and at 10% maximum intensity for ^{32}S obtained by GPC-ICP HR MS for each sample.

Sample Name	Area for ^{32}S	Retention Time at Intensity Max (min)	x_1 at 10% Intensity Max (min)	x_2 at 10% Intensity Max (min)	Ratio x_2/x_1
VR	4114574	25.82	22.49	30.57	1.42
DAO 1	2302789	26.33	24.31	29.66	1.65
DAO 2	3094691	26.33	24.31	30.06	1.85
Raffinate 2	1477765	25.62	24.01	27.84	1.37
Aromatic Extract	5092305	26.63	24.92	30.46	2.24
Raffinate 3	1263077	25.72	24.01	27.84	1.24
BSS	1534473	25.92	24.11	27.84	1.06
Wax	550407	25.22	23.60	26.83	1.00

Table 3 presents the retention time at maximum intensity for all samples. Figure 4A presents the intensity of ^{32}S for the eight samples as a function of the retention time of the aggregates containing sulfur in GPC. All the samples were eluted between 22 min (higher molecular weight) and 32 min

(lower molecular weight). The chromatogram is separated into three different fractions: high molecular weight (20/24 min), medium molecular weight (24/28 min) and low molecular weight (28/32 min) [31]. Figure 4B presents the retention time for the maximum intensity as a function of the log of viscosity. In Figure 4C, as for the HPLC3 results, VR was removed because it contains many asphaltenes not present in the other samples, which are refining products. Figure 4C shows the relationship between retention time and viscosity. According to the HPLC3 results, this relationship is correlated with the percentage of aromatics in the sample.

As can be observed in Figure 4, none of the peaks in the chromatogram are Gaussian; they present one main peak and a tail (a fraction of the lower molecular weight) eluted after the main peak. Desprez et al. [9] correlated the log of viscosity with the percentage of trapped compounds (compounds eluted after the main peaks, as can be seen in Figure 3), but only for crude oil samples. In the work of Desprez, the chromatogram was composed of two visible peaks. Here, it can only be observed that the peaks are not Gaussian towards the lower molecular weights. Here, x_1 and x_2 were used to study these trapped compounds (the asymmetry aspect of the curve). In Table 3, x_1 and x_2 represent the two retention times at 10% of the maximum intensity compared with the retention time at the maximum intensity. The higher the ratio x_2/x_1, the higher the quantity of compounds eluted after the main peak. Figure 5 presents the percentage of x_2 compared to x_1 as a function of the log of viscosity for the 7 samples after removal of the VR sample.

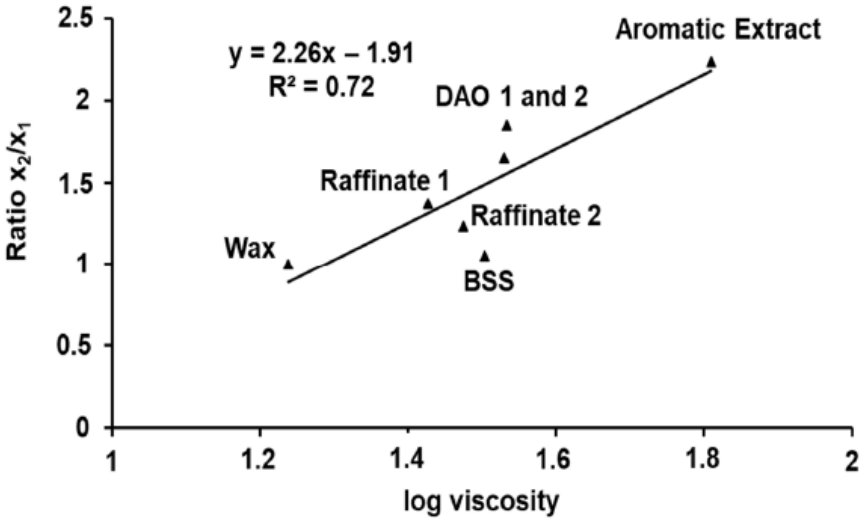

Figure 5. Ratio of x_2/x_1 as a function of the log of viscosity.

As can be seen in Figure 5, there is a relationship between the quantity of tailing after the main peak and the log of viscosity. These results, coupled with the amount of polyaromatics given by HPLC3, suggest that the aromatic compounds have a later elution time, as was already suggested by Panda et al. [10] and by Alawani et al. [5]. This result means that retention time, asymmetry of the curve, the percentage of aromatics, and viscosity are linked.

During this study, the signal of vanadium was also measured. Figure 6 presents the different chromatograms obtained.

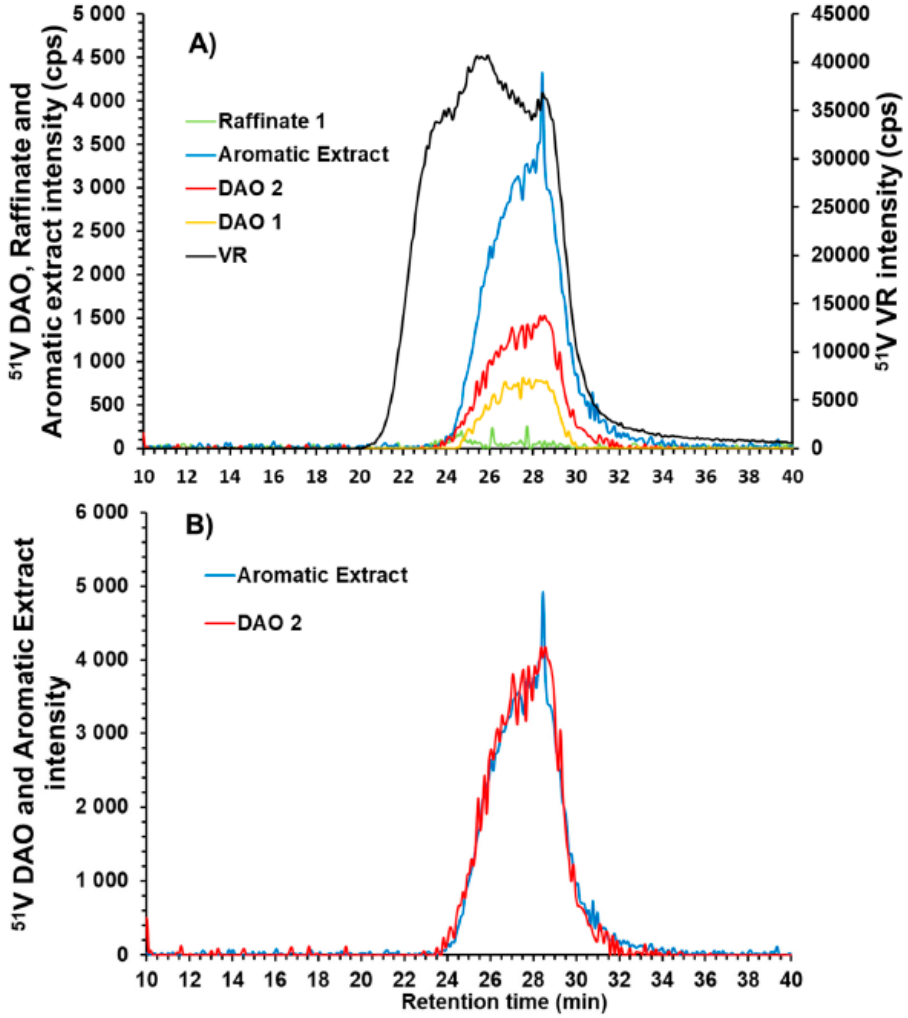

Figure 6. Chromatogram of vanadium-containing molecules by GPC-ICP HR MS for aromatic extract, de-asphalted oil (DAO 1), DAO feed of furfural (DAO 2), raffinate 1, and VR (**A**) and normalized chromatograms for aromatic extract and DAO 2 (**B**).

Figure 6A presents the intensity of ^{51}V as a function of the retention time in the GPC for VR, DAO 2, raffinate 1 and aromatic extract. The profile of vanadium-containing aggregates is trimodal for VR, as already observed for this kind of petroleum product [11,31]. As expected, HMW compounds containing ^{51}V were present in the VR sample (black line). Considered to be soluble nanoaggregates, these compounds were eliminated by the SDA unit. In contrast, a part of the low and medium molecular weights for ^{51}V remain in the DAO sample. The intensity of vanadium for DAO 1 and 2 are different. According to Table 1, the concentration of vanadium for these two samples was 1.6 and 2.2 ppm, respectively, which could be due to the tank effect, as the two samples come from different tanks - after the SDA unit (DAO 1) and before the FF unit (DAO 2). It is worth noting that all the remaining ^{51}V from the DAO was concentrated in the aromatic extract sample. This result is consistent with the high aromaticity of the supposed porphyrinic structure of ^{51}V-containing molecules. it should also be noted that furfural, used to produce the aromatic extract in the FF unit, is also used to extract porphyrins in residual oil [37]. In Figure 6B, it can been seen the profile of ^{51}V for DAO (red line)

and aromatic extract (blue line) normalized to the same area. Note that both profiles are identical, indicating that the FF unit induces no chemical change for vanadium-containing molecules.

3.3. APPI/APCI FT ICR Results

To determine the molecular composition of these samples, they were analyzed by FT-ICR MS. The APPI source promotes the ionization of the protonated molecules $[M + H]^+$ and/or cation radicals $M^{+\bullet}$ [16,17]. Paraffinic species, on the other hand, are not detectable in APPI+ but could be ionized in positive mode APCI using small alkanes, such as heptane as the solvent, yielding [M − H]+ ions through a hydride abstraction reaction [14]. These paraffinic species were mainly found in the wax and raffinate samples.

In the recorded APPI mass spectra, mostly $M^{+\bullet}$ radical cations were observed. Thus, in the following discussion, only these radical cations are considered. Figure 7 shows the DBE vs. C# plot for the HC and S_1 chemical classes of the radical species detected by APPI+ in the VR and DAO 1 samples.

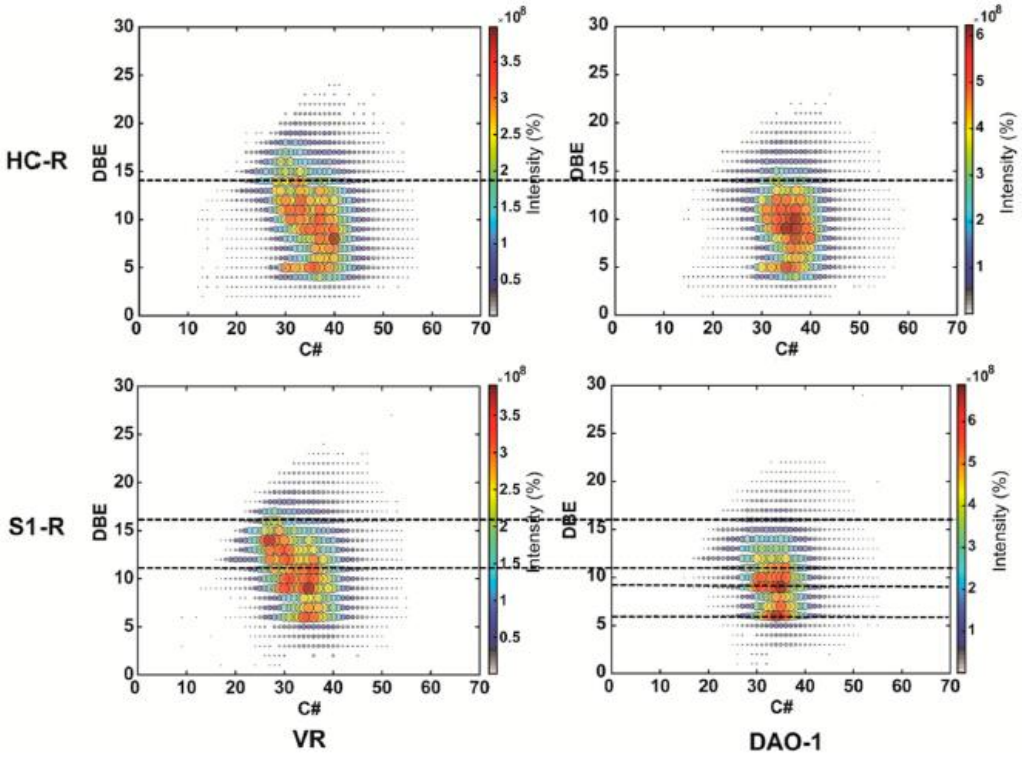

Figure 7. Double bond equivalent (DBE)/C# maps of the HC and S_1 chemical classes showing the cation radical species detected by the atmospheric pressure photo ionization (APPI) ± Fourier transformation ion cyclotron resonance (FT-ICR) mass spectra of VR (feed) and deasphalted oil (DAO) obtained from the SDA unit.

It can be observed that for both the S_1 and HC classes, the DAO 1 compound loses more aromatic (high DBE) compounds than the VR feed. In the HC class, a strong decrease of molecules with DBE higher than 14 is found. In the same way for the S_1 class, a strong decrease of molecules with DBE higher than 11 is found. This situation is consistent with the propane deasphalting process, which is expected to precipitate asphaltenes that contain the most aromatic species. Note that for sulfur-containing compounds, most species are between DBE 9 and 16 in the VR sample and between DBE 9 and 11 in the DAO 1 sample. Two series emerge for the S_1 class the in DAO 1 sample, at DBE 6 and 9. These series most certainly represent alkyl-benzothiophene (BT) and alkyl-dibenzothiophene (DBT) molecules,

respectively, which correspond to the one- and two-ring class species in HPLC3. For the HC class, two ion series are detected. The first series corresponds to the DBE 5 species, most likely naphthenic molecules. The other series, centered at DBE 10, involves mainly aromatic species.

Figure 8 shows the DBE vs. C# plot of the HC and S_1 chemical classes of the radical species detected by APPI+ in the DAO 2, raffinate 1, and aromatic extract samples.

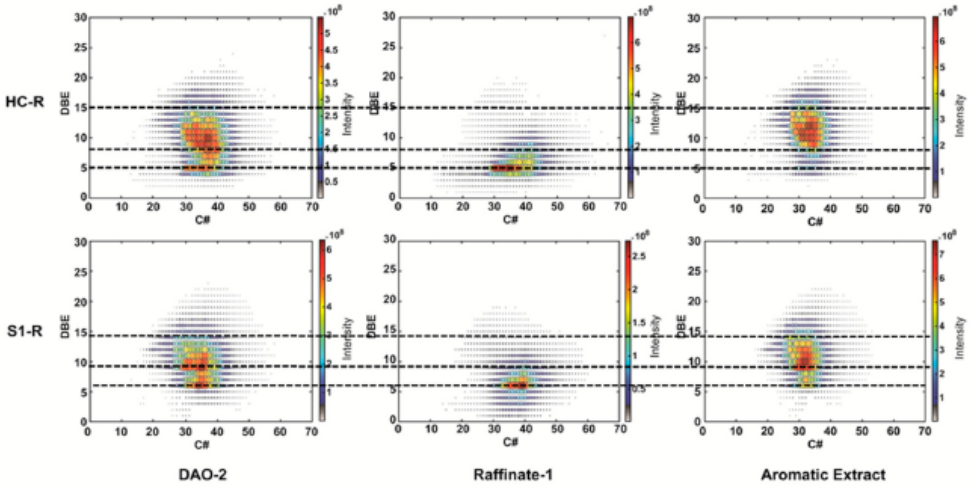

Figure 8. DBE/C# maps of the HC and S_1 chemical classes of the radical species detected by APPI+ in DAO 2, raffinate 1, and aromatic extract for the FF unit.

In Figure 8, the comparison of the three samples shows that the molecules have been selectively fractionated in the raffinate and aromatic extract using the furfural extraction process. In particular, for the S_1 family, it can be seen that the alkyl-BT species (DBE 6) are in raffinate, whereas the alkyl-DBT species are in the aromatic extract [28]. Furthermore, for the HC class, the naphthenic compounds (DBE 5) are in raffinate, whereas the more aromatic species are in the aromatic extract. This finding is consistent with the result of the HPLC3 analysis, which showed that most of the aliphatic species were mainly present in raffinate 1 as paraffinic (linear and/or branched) and naphthenic compounds. As the APPI source does not allow the detection of paraffins, they do not appear on the molecular maps shown in Figure 8. As expected, most of the aromatic species in the aromatic extract sample are found between DBE 8 and 15 for the HC family and between 9 and 14 for the S_1 class.

For the Dewaxing unit, as paraffins are not detectable in APPI+, the raffinate 2, BSS, and wax samples were analyzed using APCI+ [38], which allows the ionization of alkanes through the hydride abstraction processes with heptane as the solvent [21,39]. Figure 9 shows the DBE vs. C# plot of the HC and S_1 chemical classes according to the $[M - H]^+$ and/or $[M + H]^+$ electron ions in the samples.

The comparison of the raffinate fractions in Figures 8 and 9 highlights the use of APCI to effectively ionize the saturated compounds. In Figure 9, for HC and S_1, the aromatic compounds present in raffinate 2 are found in BSS, and paraffin is found in wax. As in the HPLC3 and GPC-ICP HR MS results, raffinate 2 and BSS are similar. For BSS, the same important series as are found in raffinate 2 are found in DBE from 4–7 for the HC family and in DBE 5–6 for the S_1 family. A significant decrease in paraffinic compounds at DBE 0 is observed in BSS.

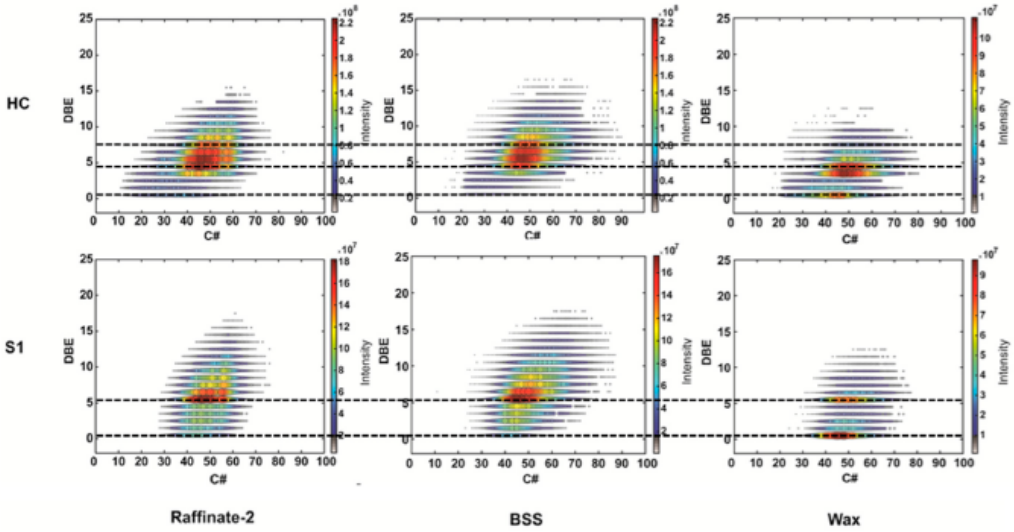

Figure 9. DBE/C# maps of the HC and S_1 chemical classes of proton species detected in atmospheric pressure chemical ionization (APCI)+ in raffinate 1, solvent extracted bright stock (BSS), and wax for the DEWAXING unit.

These paraffinic species are extracted in wax; in wax samples the maps show a series with high intensity at DBE 0 for HC and S_1, representing alkanes of the *n*-paraffin or isoparaffinic type. The main families in the HC series at DBE 3 and 4 represent cycloparaffins, polynaphthenic or monoaromatic species. For the S_1 family, the series with DBE 0 is also very much in the majority, representing structures of the thiol and/or thioether type. A second series at DBE 5 is clearly represented in the wax samples. As shown in Figure 9, compounds in the S_1 family of DBE 6, including benzothiophene sulfur compounds, are disappearing. However, this DBE 5 series is either residual aromatic compounds or naphthenic compounds. These may be cyclopentathiophene-type structures or thioethers/thiols with naphthenic rings. Looking at the intensity ratios, there is a 50% decrease in the intensity of the DBE 5 series for wax compared to the intensities in raffinate and BSS, showing that a small amount of DBE 5 sulfur compounds are present in wax.

In regards to the HPLC3 and GPC-ICP HR MS results, correlations between the FT-ICR MS results and the log of viscosity were made (Figure 10). Table 4 shows all the results that could be extracted from the S1 and HC plot. nC min represents the minimum carbon number, where peaks were found for each sample for the plot of HC and S_1. In the same way, nC max represents the maximum carbon number. DBE min and max represent the same for DBE. The HC and DBE size map represents the difference between the minimum and the maximum. A high DBE, or at least a high ratio of nC/DBE, suggests the presence of aromatics compounds. The HPLC3 and GPC-ICP-MS results suggest that aromatics compounds were correlated with the log of viscosity.

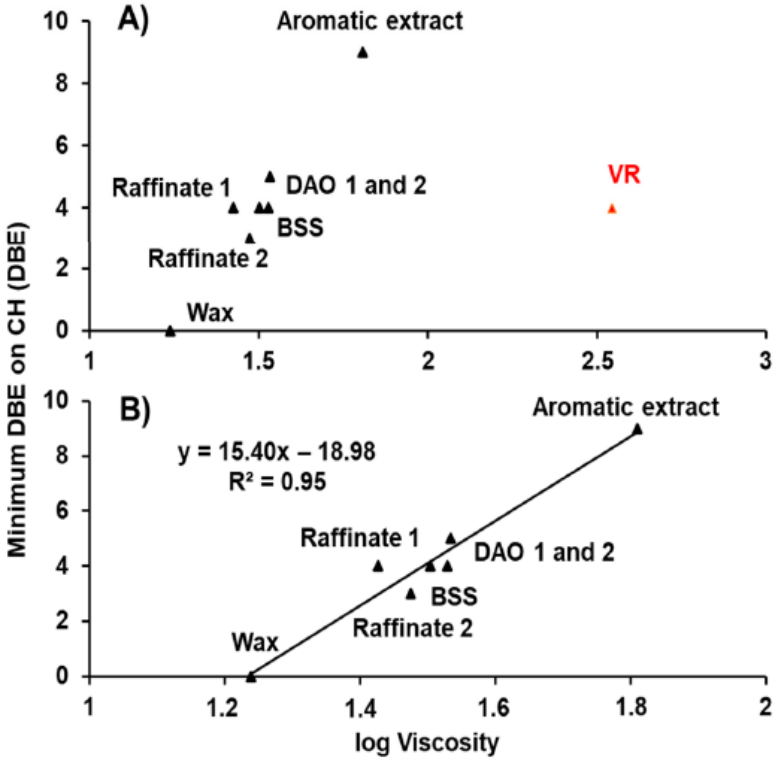

Figure 10. Minimum of DBE as a function of the log of viscosity for all the samples (**A**) except VR (**B**).

Table 4. Carbon number and DBE min and max data extracted from HC and S_1 (Figures 7–9).

		CH						S_1					
		nC min	nC max	nC Size Map	DBE min	DBE max	DBE Size Map	C min	C max	nC Size Map	DBE min	DBE max	DBE Size Map
SDA	VR	29	41	12	4	14	10	26	39	13	6	16	10
	DAO 1	29	39	10	4	14	10	28	39	11	6	13	7
FF	DAO 2	29	39	10	5	14	9	28	39	11	6	14	8
	Raffinate 1	30	43	13	4	8	4	30	43	13	6	9	3
	Aromatic Extract	28	39	11	9	15	6	26	38	12	6	14	8
Dewaxing	Raffinate 2	40	60	20	3	8	5	40	58	18	0	9	9
	BSS	38	58	20	4	8	4	38	60	22	0	9	9
	Wax	40	60	20	0	6	6	40	56	16	0	5	5

Figure 10 shows the minimum of DBE found in the HC maps for all the samples (Figure 10A), except VR (Figure 10B), as a function of the log of viscosity. As expected, VR was not correlated with the other samples. A linear correlation was found between the minimum DBE and the log of viscosity for all the other samples. Other correlations with nC max and min, as well as DBE max, did not show good correlation and are not shown here.

3.4. Statistic Treatment Using PLS Regression

By using three different advanced analytical techniques, it appears that, as suggested by several works [2,6,9], several parameters influence the viscosity of the sample. The HPLC3 data confirmed that the log of viscosity was correlated with the percentage of aromatics. The GPC-ICP HR MS data confirmed that the log of viscosity was correlated with the retention time of the maximum ^{32}S intensity.

Finally, the FT-ICR MS results suggested that the log of viscosity was correlated with the minimum of DBE for the HC map.

Statistical techniques were used to determine which variables affected viscosity. For this determination, all of the variables given by the three techniques (Tables 2–4), plus the variables given in Table 1, were correlated with the logarithm of viscosity. As before, VR was removed for the statistical treatment because this sample did not correlate with viscosity, probably due to its non-negligible asphaltene content. The results are given in Figure 11.

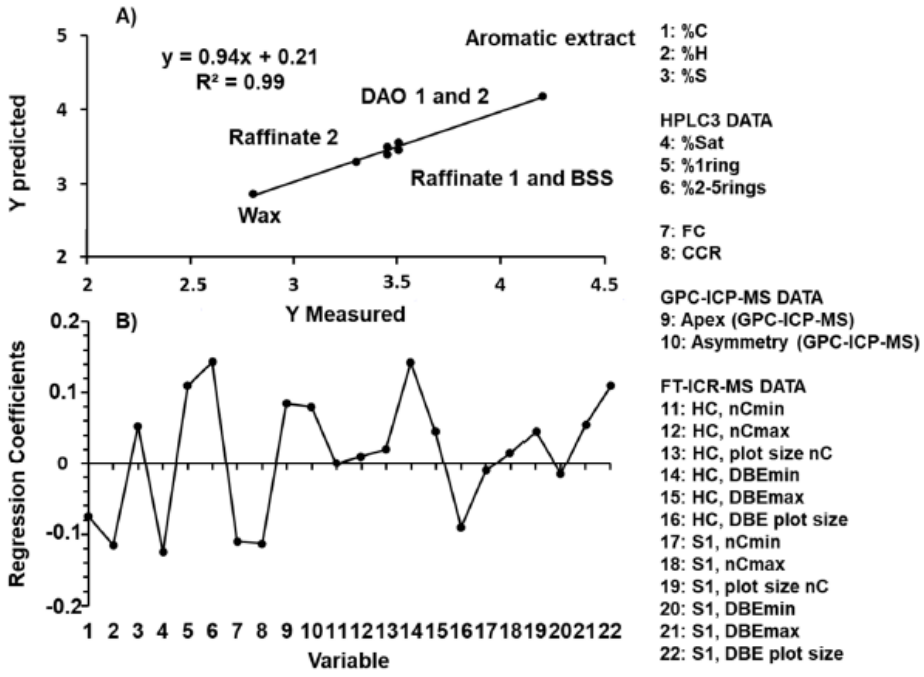

Figure 11. Calibration curves between the viscosity predicted by partial least square (PLS) and measured (**A**) except for the VR sample. Influence of 22 different variables on viscosity (**B**).

It can be seen in Figure 11A that the use of all these parameters provides a good correlation (R^2 = 0.97) between the log of the measured viscosity (Y measured) and the viscosity predicted by PLS (Y predicted). Figure 11B shows which parameters have a large influence on viscosity. It appears that viscosity increases when the percentage of sulfur, the percentage of one ring and polyaromatics (2R−5R), the retention time at maximum intensity, and the asymmetry ratio x_2/x_1 increases. These results confirm those presented in Figures 4 and 5, which showed that viscosity increased with the maximum intensity of the ^{32}S peak and asymmetry. The PLS results also suggest that the more sulfur there is in the samples, the more the viscosity increases, which could be explained by the possibility that sulfur is mainly present in aromatic compounds, such as BT and DBT, as suggested by the FT-ICR MS results in Figures 7–9, as well as the HPLC3 results in Figure 2. In contrast, the logarithm of viscosity decreased when the quantity of hydrogen, the percentage of Sat, the FC, and the CCR increased. FC represents the quantity of paraffin. Paraffin did not contain aromatic compounds and, as has already been stated, the log of viscosity increased with the quantity of aromatics. For hydrogen, meanwhile, a greater quantity of hydrogen suggested the presence of fewer aromatics compounds (and lower DBE), which is in agreement with the FT-ICR MS results.

To help daily optimization of the unit, it is necessary to develop a model using accessible data, such as elemental content. The advanced analytical techniques used in this article confirmed that viscosity is mainly linked to the aromatic and sulfur contents. Considering these results, it has been

tried to construct another PLS model with data available daily in a refinery. The aromatic content is linked to the C and H contents, while the S content is linked to CCR. The results are presented in supplemental information (Figure S1). It should be noted that the trends for the new model are the same as in the previous, more complex model. Viscosity increased when the % H decreased and when the % C and the % S increased.

Obviously, a model with seven points is not directly useful in a refinery. It should be noted that only one feedstock was used for this study, and the conclusions cannot be applied to all the samples used in a refinery. However, these results can predict tendencies and assist with the daily optimization of the unit. The development of a refining model would certainly require the use of molecular data, such as those acquired during this study. Such a model would allow us to describe more accurately the differences between two different feedstocks.

4. Conclusions

The aim of this study was to better understand the refining process of lubricants from a molecular point of view. The analytical techniques used in this study allowed us to identify and characterize the hydrocarbon-, sulfur-, and vanadium-containing compounds present in the different samples. The combination of three advanced analytical techniques (HPLC3, GPC-ICP HR MS and FT-ICR MS), all usually measurable in refinery data on lubricating oil base samples and statistic treatment, allowed the viscosity of a lubricating oil base sample to be predicted. Viscosity increases when the percentage of sulfur, the percentage of mono- and polyaromatics (2R−5R), the apex, and the asymmetry increase. In contrast, the logarithm of the viscosity decreases when the hydrogen content, the percentage of Sat, and the FC increase. This study showed the importance and effectiveness of cross-checking results with different complementary analytical techniques to acquire valuable data on lubricating oil base samples. This kind of methodology can be used for other types of samples or matrices. Furthermore, the relation between viscosity and different parameters of the lubricants can help for the daily optimization of the refinery unit.

Supplementary Materials: The following are available online at http://www.mdpi.com/2227-9717/8/11/1472/s1, Figure S1: Calibration curves between viscosity predicted by the second PLS model and measured (**A**) except for the VR sample. Influence of four different variables on the viscosity (**B**).

Author Contributions: Conceptualization and resources, C.B.-M. and P.G.; methodology, R.M., R.R., B.B., C.A., P.G. and C.B.-M.; formal analysis and data curation R.M. and J.L.M.; supervision, R.R., B.B., C.A., P.G. and C.B.-M.; writing—original draft preparation, R.M., J.L.M. and C.B.-M.; writing—review and editing, R.M., H.L., R.R., B.B., C.A., P.G. and C.B.-M. All authors have read and agreed to the published version of the manuscript.

Funding: The authors thank TOTAL for supplying the oil samples and Jonathan Putman for HPLC3 experiments. Work was performed at the National High Magnetic Field Laboratory ICR User Facility, which is supported by the National Science Foundation Division of Chemistry through Cooperative Agreements DMR-1157490 and DMR-1644779 and the state of Florida. This work was also supported by Conseil Régional d'Aquitaine (20071303002PFM) and FEDER (31486/08011464). The authors thank the EU for funding via the ERC PRIMCHEMproject (No. 636829). This work was supported at the Chimie Organique Bioorganique Réactivité Analyse (COBRA) laboratory by the European Regional Development Fund (ERDF) No. HN0001343, the European Union's Horizon 2020 Research Infrastructures program (grant agreement 731077), the national FT-ICR network (FR 3624 CNRS), the Région Normandie, and the Laboratoire LabEx SynOrg (ANR-11-LABX-0029).

Conflicts of Interest: The authors declare no conflict of interest.

References

1. Wilson, R.E.; Keith, P.C.; Haylett, R.E. LIQUID PROPANE Use in Dewaxing, Deasphalting, and Refining Heavy Oils. *Ind. Eng. Chem.* **1936**, *28*, 1065–1078. [CrossRef]
2. Mehrkesh, A.H.; Hajimirzaee, S.; Hatamipour, M.S. A Generalized Correlation for Characterization of Lubricating Base-oils from Their Viscosities. *Chin. J. Chem. Eng.* **2010**, *18*, 642–647. [CrossRef]
3. Kemp, L.C., Jr.; Hamilton, G.B.; Gross, H.H. Furfural as a Selective Solvent in Petroleum Refining. *Ind. Eng. Chem.* **1948**, *40*, 220–227. [CrossRef]

4. Varotsis, N.; Pasadakis, N. Rapid Quantitative Determination of Aromatic Groups in Lubricant Oils Using Gel Permeation Chromatography. *Ind. Eng. Chem. Res.* **1997**, *36*, 5516–5519. [CrossRef]
5. Alawani, N.A.; Panda, S.K.; Lajami, A.R.; Al-Qunaysi, T.A.; Muller, H. Characterization of Crude Oils through Alkyl Chain-Based Separation by Gel Permeation Chromatography and Mass Spectrometry. *Energy Fuels* **2020**, *34*, 5414–5425. [CrossRef]
6. Wang, F.C.-Y.; Zhang, L. Chemical Composition of Group II Lubricant Oil Studied by High-Resolution Gas Chromatography and Comprehensive Two-Dimensional Gas Chromatography. *Energy Fuels* **2007**, *21*, 3477–3483. [CrossRef]
7. Manheim, J.; Wehde, K.; Zhang, W.T.J.; Vozka, P.; Romanczyk, M.; Kilaz, G.; Kenttämaa, H.I. Identification and Quantitation of Linear Alkanes in Lubricant Base Oils by Using GC × GC/EI TOF Mass Spectrometry. *J. Am. Soc. Mass Spectrom.* **2019**, *30*, 2670–2677. [CrossRef]
8. Liang, Z.; Chen, L.; Alam, M.S.; Rezaei, S.Z.; Stark, C.; Xu, H.; Harrison, R.M. Comprehensive chemical characterization of lubricating oils used in modern vehicular engines utilizing GC × GC-TOFMS. *Fuel* **2018**, *220*, 792–799. [CrossRef]
9. Desprez, A.; Bouyssiere, B.; Arnaudguilhem, C.; Krier, G.; Vernex-Loset, L.; Giusti, P. Study of the Size Distribution of Sulfur, Vanadium, and Nickel Compounds in Four Crude Oils and Their Distillation Cuts by Gel Permeation Chromatography Inductively Coupled Plasma High-Resolution Mass Spectrometry. *Energy Fuels* **2014**, *28*, 3730–3737. [CrossRef]
10. Panda, S.K.; Alawani, N.A.; Lajami, A.R.; Al-Qunaysi, T.A.; Muller, H. Characterization of aromatic hydrocarbons and sulfur heterocycles in Saudi Arabian heavy crude oil by gel permeation chromatography and ultrahigh resolution mass spectrometry. *Fuel* **2019**, *235*, 1420–1426. [CrossRef]
11. Putman, J.C.; Sama, S.G.; Barrère-Mangote, C.; Rodgers, R.P.; Lobinski, R.; Marshall, A.G.; Bouyssiere, B.; Giusti, P. Analysis of Petroleum Products by Gel Permeation Chromatography Coupled Online with Inductively Coupled Plasma Mass Spectrometry and Offline with Fourier Transform Ion Cyclotron Resonance Mass Spectrometry. *Energy Fuels* **2018**, *32*, 12198–12204. [CrossRef]
12. Duan, P.; Qian, K.; Habicht, S.C.; Pinkston, D.S.; Fu, M.; Kenttämaa, H.I. Analysis of Base Oil Fractions by $ClMn(H_2O)^+$ Chemical Ionization Combined with Laser-Induced Acoustic Desorption/Fourier Transform Ion Cyclotron Resonance Mass Spectrometry. *Anal. Chem.* **2008**, *80*, 1847–1853. [CrossRef] [PubMed]
13. Nyadong, L.; Quinn, J.P.; Hsu, C.S.; Hendrickson, C.L.; Rodgers, R.P.; Marshall, A.G. Atmospheric Pressure Laser-Induced Acoustic Desorption Chemical Ionization Mass Spectrometry for Analysis of Saturated Hydrocarbons. *Anal. Chem.* **2012**, *84*, 7131–7137. [CrossRef]
14. Hourani, N.; Muller, H.; Adam, F.M.; Panda, S.K.; Witt, M.; Al-Hajji, A.A.; Sarathy, S.M. Structural Level Characterization of Base Oils Using Advanced Analytical Techniques. *Energy Fuels* **2015**, *29*, 2962–2970. [CrossRef]
15. Putman, J.C.; Rowland, S.M.; Podgorski, D.C.; Robbins, W.K.; Rodgers, R.P. Dual-Column Aromatic Ring Class Separation with Improved Universal Detection across Mobile-Phase Gradients via Eluate Dilution. *Energy Fuels* **2017**, *31*, 12064–12071. [CrossRef]
16. Bae, E.; Na, J.-G.; Chung, S.H.; Kim, H.S.; Kim, S. Identification of about 30,000 Chemical Components in Shale Oils by Electrospray Ionization (ESI) and Atmospheric Pressure Photoionization (APPI) Coupled with 15 T Fourier Transform Ion Cyclotron Resonance Mass Spectrometry (FT-ICR MS) and a Comparison to Conventional Oil. *Energy Fuels* **2010**, *24*, 2563–2569. [CrossRef]
17. Purcell, J.M.; Hendrickson, C.L.; Rodgers, R.P.; Marshall, A.G. Atmospheric Pressure Photoionization Fourier Transform Ion Cyclotron Resonance Mass Spectrometry for Complex Mixture Analysis. *Anal. Chem.* **2006**, *78*, 5906–5912. [CrossRef]
18. Jin, C.; Viidanoja, J.; Li, M.; Zhang, Y.; Ikonen, E.; Root, A.; Romanczyk, M.; Manheim, J.; Dziekonski, E.; Kenttämaa, H.I. Comparison of Atmospheric Pressure Chemical Ionization and Field Ionization Mass Spectrometry for the Analysis of Large Saturated Hydrocarbons. *Anal. Chem.* **2016**, *88*, 10592–10598. [CrossRef]
19. Tose, L.V.; Cardoso, F.M.; Fleming, F.P.; Vicente, M.A.; Silva, S.R.; Aquije, G.M.; Vaz, B.G.; Romão, W. Analyzes of hydrocarbons by atmosphere pressure chemical ionization FT-ICR mass spectrometry using isooctane as ionizing reagent. *Fuel* **2015**, *153*, 346–354. [CrossRef]

20. Mead, W.L. Field ionization mass spectrometry of heavy petroleum fractions. Waxes. *Anal. Chem.* **1968**, *40*, 743–747. [CrossRef]
21. Souza, L.M.; Tose, L.V.; Cardoso, F.M.R.; Fleming, F.P.; Pinto, F.E.; Kuster, R.M.; Filgueiras, P.R.; Vaz, B.G.; Romão, W. Evaluating the effect of ion source gas (N_2, He, and synthetic air) on the ionization of hydrocarbon, condensed aromatic standards, and paraffin fractions by APCI(+)FT-ICR MS. *Fuel* **2018**, *225*, 632–645. [CrossRef]
22. Manheim, J.; Zhang, Y.; Viidanoja, J.; Kenttämaa, H.I. An Automated Method for Chemical Composition Analysis of Lubricant Base Oils by Using Atmospheric Pressure Chemical Ionization Mass Spectrometry. *J. Am. Soc. Mass Spectrom.* **2019**, *30*, 2014–2021. [CrossRef] [PubMed]
23. Marshall, A.G.; Hendrickson, C.L.; Jackson, G.S. Fourier transform ion cyclotron resonance mass spectrometry. *Mass Spectrom. Rev.* **1998**, *17*, 1–35. [CrossRef]
24. Boldin, I.A.; Nikolaev, E.N. Fourier transform ion cyclotron resonance cell with dynamic harmonization of the electric field in the whole volume by shaping of the excitation and detection electrode assembly. *Rapid Commun. Mass Spectrom.* **2011**, *25*, 122–126. [CrossRef]
25. Chen, H.; Hou, A.; Corilo, Y.E.; Lin, Q.; Lu, J.; Mendelssohn, I.A.; Zhang, R.; Rodgers, R.P.; McKenna, A.M. 4 Years after the *Deepwater Horizon* Spill: Molecular Transformation of Macondo Well Oil in Louisiana Salt Marsh Sediments Revealed by FT-ICR Mass Spectrometry. *Environ. Sci. Technol.* **2016**, *50*, 9061–9069. [CrossRef]
26. Marshall, A.G.; Chen, T. 40 years of Fourier transform ion cyclotron resonance mass spectrometry. *Int. J. Mass Spectrom.* **2015**, *377*, 410–420. [CrossRef]
27. Hourani, N.; Andersson, J.T.; Möller, I.; Amad, M.; Witt, M.; Sarathy, S.M. Atmospheric pressure chemical ionization Fourier transform ion cyclotron resonance mass spectrometry for complex thiophenic mixture analysis. *Rapid Commun. Mass Spectrom.* **2013**, *27*, 2432–2438. [CrossRef]
28. Muller, H.; Adam, F.M.; Panda, S.K.; Al-Jawad, H.H.; Al-Hajji, A.A. Evaluation of Quantitative Sulfur Speciation in Gas Oils by Fourier Transform Ion Cyclotron Resonance Mass Spectrometry: Validation by Comprehensive Two-Dimensional Gas Chromatography. *J. Am. Soc. Mass Spectrom.* **2012**, *23*, 806–815. [CrossRef]
29. Loh, G.C.; Lee, H.-C.; Tee, X.Y.; Chow, P.S.; Zheng, J.W. Viscosity Prediction of Lubricants by a General Feed-Forward Neural Network. *J. Chem. Inf. Model.* **2020**, *60*, 1224–1234. [CrossRef]
30. Braga, J.W.B.; Junior, A.A.D.S.; Martins, I.S. Determination of viscosity index in lubricant oils by infrared spectroscopy and PLSR. *Fuel* **2014**, *120*, 171–178. [CrossRef]
31. Sama, S.G.; Desprez, A.; Krier, G.; Lienemann, C.-P.; Barbier, J.; Lobinski, R.; Barrere-Mangote, C.; Giusti, P.; Bouyssiere, B. Study of the Aggregation of Metal Complexes with Asphaltenes Using Gel Permeation Chromatography Inductively Coupled Plasma High-Resolution Mass Spectrometry. *Energy Fuels* **2016**, *30*, 6907–6912. [CrossRef]
32. Caumette, G.; Lienemann, C.-P.; Merdrignac, I.; Bouyssiere, B.; Lobinski, R. Element speciation analysis of petroleum and related materials. *J. Anal. At. Spectrom.* **2009**, *24*, 263–276. [CrossRef]
33. Giusti, P.; Ordóñez, Y.N.; Lienemann, C.-P.; Schaumlöffel, D.; Bouyssiere, B.; Łobiński, R. µFlow-injection–ICP collision cell MS determination of molybdenum, nickel and vanadium in petroleum samples using a modified total consumption micronebulizer. *J. Anal. At. Spectrom.* **2007**, *22*, 88–92. [CrossRef]
34. Zhang, L.; Hou, Z.; Horton, S.R.; Klein, M.T.; Shi, Q.; Zhao, S.; Xu, C. Molecular Representation of Petroleum Vacuum Resid. *Energy Fuels* **2014**, *28*, 1736–1749. [CrossRef]
35. Kim, S.; Kramer, R.W.; Hatcher, P.G. Graphical Method for Analysis of Ultrahigh-Resolution Broadband Mass Spectra of Natural Organic Matter, the Van Krevelen Diagram. *Anal. Chem.* **2003**, *75*, 5336–5344. [CrossRef] [PubMed]
36. Caumette, G.; Lienemann, C.-P.; Merdrignac, I.; Bouyssiere, B.; Lobinski, R. Fractionation and speciation of nickel and vanadium in crude oils by size exclusion chromatography-ICP MS and normal phase HPLC-ICP MS. *J. Anal. At. Spectrom.* **2010**, *25*, 1123–1129. [CrossRef]
37. Ali, M.F.; Abbas, S. A review of methods for the demetallization of residual fuel oils. *Fuel Process. Technol.* **2006**, *87*, 573–584. [CrossRef]

38. Řezanka, T.; Sigler, K. Identification of very long chain fatty acids from sugar cane wax by atmospheric pressure chemical ionization liquid chromatography–mass spectroscopy. *Phytochemistry* **2006**, *67*, 916–923. [CrossRef]
39. Aasen, A.J.; Hofstetter, H.H.; Iyengar, B.T.R.; Holman, R.T. Identification and analysis of wax esters by mass spectrometry. *Lipids* **1971**, *6*, 502–507. [CrossRef]

Trois techniques d’analyses avancées suivis d’un traitement statistique ont permis de mettre en corrélation la viscosité des échantillons en fonction de plusieurs paramètres donnés par les analyses élémentaires et moléculaires. Avec notamment du côté GPC-ICP MS une tendance entre la viscosité d’un échantillon d’huile de base et le temps de rétention de l’intensité maximum du pic de Soufre dans les colonnes GPC.

De plus différents types d'agrégats de tailles différentes ont été observés de façon nette pour les composés contenant du vanadium et du soufre en fonction des unités de traitement des huiles de base. Ces informations permettent de mieux comprendre les paramètres influençant la viscosité des échantillons. En obtenant de meilleures connaissances sur l’évolution de la viscosité, les informations apportées par cet article permettent d’aider à l’optimisation des unités de la chaine de raffinage des huiles.

De plus, le couplage de technique de séparation, d’analyse élémentaire et moléculaire a permis d’obtenir des informations complémentaires sur les échantillons de la chaine de raffinage des huiles. Maintenant l’association de plusieurs techniques d’analyses sera systématiquement utilisée dans le cadre de l’analyse d’échantillons d’asphaltènes qui est la partie du pétrole la plus complexe.

Three advanced analysis techniques followed by statistical processing allowed the viscosity of the samples to be correlated according to several parameters given by the elementary and molecular analyses. In particular, the GPC-ICP MS side shows a trend between the viscosity of a base oil sample and the retention time of the maximum intensity of the Sulphur peak in the GPC columns.

In addition, different types of aggregates of different sizes were clearly observed for vanadium and sulphur containing compounds depending on the base oil processing units. This information allows a better understanding of the parameters influencing the viscosity of the samples. By gaining a better understanding of the evolution of viscosity, the information provided by this paper can help in the optimisation of the units in the oil refining chain.

In addition, the coupling of separation techniques, elemental and molecular analysis has made it possible to obtain additional information on the samples of the oil refining chain. Now the combination of several analytical techniques will be systematically used in the analysis of asphaltene samples, which is the most complex part of the oil.

Partie II : Apport de la GPC-ICP MS couplée à une séparation solide/liquide dans le cadre de l'analyse d'asphaltènes

Cette partie a fait l'objet d'un article publié dans le journal *Energy and Fuels* de l'*American Chemical Society* (ACS). Cet article a été laissé tel qu'il a été publié.

Une étude a été menée sur deux asphaltènes différents provenant de pétroles aux caractéristiques différentes mais provenant tout deux du Moyen Orient. Cette proximité géographique fait que les deux pétroles ont des caractéristiques (teneur en métaux, teneur en asphaltènes) proches selon les techniques d'analyses habituellement utilisées. Cependant lors des étapes de d'hydrodésulfurisation et d'hydrodémetalaltion, les deux pétroles ont des comportements très différents, l'un est plus facile à traiter alors que l'autre présente de nombreux problèmes de désactivation de catalyseurs, dépôt de coke. En effet l'un des deux pétroles a déjà causé un incident réduisant la durant de vie du catalyseur d'une unité d'ARDS de 18 à 11 mois, ce qui entraine un fort surcout pour la démétallation. Afin de déterminer quelles sont les différences entre ces deux pétroles et quelles sont les paramètres qui peuvent être liés à aux problèmes de précipitation, les asphaltènes de ces pétroles qui en sont la partie la plus complexe seront étudiées par plusieurs techniques de séparation et de détection.

Dans un premier temps, les deux échantillons d'asphaltènes ont été fractionnés par extrographie en trois fractions : fraction acétone composée d'Island, la fraction Heptane/ Toluène composée d'Island polaire et enfin la fraction Toluène/THF/MeOH composée d'archipelago. Déjà, il est remarqué que le pétrole ayant posé le plus de problème en raffinerie contient une fraction Tol/THF/MeOH significativement plus importante (50% en masse contre 25%). Puis, comme dans la partie I de ce chapitre, toutes les fractions ont été analysées par GPC-ICP MS afin de suivre l'état d'agrégation du vanadium et du soufre en fonction du volume hydrodynamique ainsi que par FT-ICR MS afin d'obtenir des informations sur leur composition moléculaires. Enfin, toutes les fractions ont aussi été analysées QCR. Le QCR permet de savoir quand est-ce qu'une fraction préalablement dissoute dans du toluène précipite lorsque l'on ajoute de l'heptane. Cette technique donne des informations sur la stabilité de l'échantillon.

This section was the subject of an article published to the American Chemical Society (ACS) journal Energy and Fuels. This article has been left as published.

A study was conducted on two different asphaltenes from oils with different characteristics but both from the Middle East. This geographical proximity means that the two oils have similar characteristics (metal content, asphaltene content) according to the analytical techniques usually used. However, during the hydrodesulphurisation and hydrodemetalation stages, the two oils have very different behaviour, one is easier to treat while the other has many problems with catalyst deactivation and coke deposition. Indeed, one of the two oils has already caused an incident reducing the catalyst lifetime of an ARDS unit from 18 to 11 months, which leads to a strong overcost for demetallation. In order to determine what the differences between these two oils are and what parameters can be linked to precipitation problems, the asphaltenes of these oils, which are the most complex part, will be studied using several separation and detection techniques.

First, the two asphaltene samples were fractionated by extrography into three fractions: the Island acetone fraction, the polar Island Heptane/Toluene fraction and finally the archipelago Toluene/THF/MeOH fraction. It has already been noted that the oil that has caused the most problems in refineries contains a significantly higher Tol/THF/MeOH fraction (50% by mass against 25%). Then, as in Part I of this chapter, all fractions were analysed by GPC-ICP MS to monitor the state of aggregation of vanadium and sulphur as a function of hydrodynamic volume and by FT-ICR MS to obtain information on their molecular composition. Finally, all fractions were also analysed QCR. QCR allows to know when a fraction previously dissolved in toluene precipitates when heptane is added. This technique gives information on the stability of the sample.

energy&fuels

pubs.acs.org/EF Article

Understanding Asphaltene Fraction Behavior through Combined Quartz Crystal Resonator Sensor, FT-ICR MS, GPC ICP HR-MS, and AFM Characterization. Part I: Extrography Fractionations

Nelson Acevedo, Remi Moulian, Martha L. Chacon Patiño, Aurora Mejia, Sadia Radji, Jean-Luc Daridon, Caroline Barrère-Mangote, Pierre Giusti, Ryan P. Rodgers, Vincent Piscitelli, Jimmy Castillo, Hervé Carrier, and Brice Bouyssiere*

Cite This: https://dx.doi.org/10.1021/acs.energyfuels.0c02687 Read Online

ACCESS | Metrics & More | Article Recommendations | Supporting Information

ABSTRACT: Multiscale characterization of asphaltenes and their extrography fractions titrated with *n*-heptane was performed. Chemical characterization via FT-ICR MS and GPC ICP HR-MS, stability monitoring via QCR, and AFM images of deposits indicate that "island"-enriched samples tend to form fewer, well-organized deposit aggregates, whereas samples with abundant "archipelago"-like molecules form larger aggregates and less well-organized deposits. The combination of QCR and AFM leads to the conclusion that "island"-enriched samples lead to a smaller deposit compared to "archipelago"-like molecules.

INTRODUCTION

General View of Asphaltene Chemistry. For more than five decades, the definition of asphaltenes has remained unaltered and constrained to the solubility of nanoaggregates in toluene and their insolubility in aliphatic solvents, such as pentane or heptane.[1] Asphaltenes are ultracomplex mixtures that include a polydispersed collection of nanoaggregates, with a high diversity of size, shape, and chemical properties such as solubility.[2−4] Historically, asphaltene structure has been described as a single aromatic core with alkyl side chains, known as the island or continental structural model, which was introduced by Yen[5] in 1961 and then more precisely by Dickie and Yen[6] in 1967. The second and less accepted proposed structure is known as the archipelago model, which includes several (more than one) aromatic cores (multicore) linked by covalent bonds, and was proposed by Strausz et al.[7,8] in 1992. The original Dickie and Yen[6] model and the modified Yen model proposed by Mullins[9,10] have ruled the understanding of asphaltenes for many decades and have perpetuated the idea that asphaltene aggregation is exclusively driven by aromatic stacking or $\pi-\pi$ interactions between the aromatic cores of single-core molecules.[11] Heteroatom-based intermolecular forces, such as hydrogen bonding, are not considered to be of main importance to asphaltene properties, according to the Yen−Mullins theory.[11,12]

Conversely, the supramolecular assembly model for asphaltene aggregation, first proposed by Agrawala et al.[13] and later refined by Gray et al.,[14] suggests a more complex structure for asphaltene nanoaggregates, with the presence of different structural motifs (single-core and multicore), diverse intermolecular forces (e.g., $\pi-\pi$, hydrogen bonding, acid−base conjugation), and the occlusion of alkane-soluble compounds (or maltenes) inside asphaltene nanoaggregates.[15] This theory is more consistent with several asphaltene properties, including behavior in mild pyrolysis, gas-phase fragmentation (tandem mass spectrometry), adsorption on polar surfaces, occlusion of maltenes, and adsorption at the oil/water interface. Regardless of the inherent difficulties in understanding mild pyrolysis data, any asphaltene model should be suitable to the production of 1−5-ring alkyl-aromatics upon thermal stress.

These nanoaggregates are then producing macro-aggregation and precipitation. Their solubility behavior is strongly linked to the polarity and the presence of possible hydrogen bonding.[16,17] The presence of Archipelago/Island-type asphaltene monomers can also influence precipitation.[18,19] Modelization of the asphaltene precipitation needs to divide the samples into different components/families such as saturate, aromatics, resins, and subdivision of asphaltenes into different families.[20]

Asphaltene Fractionation Strategies. Recently, separation methods such as extrography coupled to molecular-level characterization by Fourier transform ion cyclotron resonance mass spectrometry (FT-ICR MS) have allowed the detection of both island and archipelago structural motifs in asphaltene samples when applied to asphaltene investigation.[21−23] Extrography involves the adsorption of petroleum samples on a polar adsorbent, such as silica gel, alumina, or cellulose. The subsequent fractionation is achieved by Soxhlet extraction with specific solvents. Chacon-Patiño et al.[21] used acetone followed by an elutropic gradient composed of heptane, toluene, and tetrahydrofuran/methanol. The initial extraction with acetone, in which the predominant intermolecular forces consist of

Received: August 12, 2020
Revised: October 7, 2020

dipolar interactions, facilitates the selective separation of highly aromatic/condensed structures. The subsequent extraction with mixtures of heptane/toluene allows the isolation of alkyl-aromatic compounds. Finally, the use of tetrahydrofuran/methanol produces asphaltene compounds with abundant polarizable functionalities that interact strongly, via hydrogen bonding, with the active silanol groups on the SiO_2 surface.

Molecular-Level Characterization by FT-ICR MS. Recent reports from FT-ICR MS and gas-phase fragmentation via infrared multiphoton dissociation (IRMPD) indicate that the acetone extrography fraction has a high concentration of single-core or island structural motifs.[21,24] Moreover, the acetone fraction exhibits a high ionization efficiency in atmospheric pressure photoionization (APPI).[25] Conversely, the toluene/tetrahydrofuran/methanol fractions are more difficult to ionize, presumably because of their stronger aggregation tendency, and reveal abundant multicore or archipelago motifs. The authors concluded that single- and multicore motifs coexist in petroleum asphaltenes and the dominance of a particular structure depends on the sample.[21,26] For instance, Wyoming deposit asphaltenes, known to be consistent with the modified Yen model because they produce high amounts of coke in thermal cracking, revealed abundant single-core motifs. In contrast, Athabasca bitumen asphaltenes, known to produce a high yield of distillable products in the thermal cracking, were shown to be enriched in multicore species. Therefore, the extrography methodology confirmed that asphaltenes are composed of different structural motifs. Importantly, because of the lesser aromaticity of multicore-type compounds, $\pi-\pi$ interactions are not the dominant force that drives nanoaggregation, as also recently shown by theoretical calculations.[27,28]

Among all of the available analytical techniques, high-field FT-ICR MS offers the most comprehensive molecular analyses because it can reveal tens of thousands of elemental compositions present in petroleum-derived samples.[29,30] The high mass accuracy and resolution exclusively offered by FT-ICR MS allows the assignment of a unique elemental formula to each detected peak. Commonly, the assigned formulas are sorted by heteroatom content (e.g., all of the compounds with C, H, and one S atom belong to the class S_1), carbon number, and double bond equivalent (DBE = number of rings plus double bonds to carbon), and the information is represented by contoured plots of DBE versus carbon number with the relative abundance shown by a color scale. Although FT-ICR MS only reveals molecular formulas, when coupled to gas-phase fragmentation such as IRMPD and collision-induced dissociation, it can supply useful structural information. However, all MS-based techniques are limited because of selective ionization, ion suppression, and matrix effects.[31−36] Currently, there is no "universal" ion source that allows for ionization of complex mixtures without any discrimination toward specific compound classes and structures. Therefore, prior sample fractionation is critical to achieving more complete molecular characterization of complex samples such as asphaltenes.[37−39]

Gel Permeation Chromatography Hyphenated with Inductively Coupled Plasma Mass Spectrometry. Gel permeation chromatography combined with inductively coupled plasma mass spectrometry (ICP-MS) has been recently used to understand metal (V and Ni) and heteroatom (S) content as a function of nanoaggregate size distribution in asphaltene samples.[40−43] The results reveal that asphaltenes exist as a trimodal distribution of nanoaggregates. GPC chromatograms for geologically diverse samples suggest that asphaltenes can be separated into high molecular weight (HMW), medium molecular weight (MMW), and low molecular weight (LMW) aggregates and nonaggregated species (called "tailing" fraction).[38,43,44] Fraction collection and their reinjection into the GPC system yields a chromatogram in which the compounds are mostly eluted at the same retention time as in the initial sample, which demonstrates the stability of the collected nanoaggregate and the reproducibility of the technique.[38] Thus, GPC/ICP-MS allows comparison of nanoaggregates because it reveals differences in hydrodynamic volume as a function of metal/heteroatom content.

Atomic Force Microscopy for Asphaltene Characterization. At the nanoscale level, atomic force microscopy (AFM) is an interesting technique that offers access to three-dimensional information. For asphaltene characterization, AFM has been applied from single asphaltene molecule imaging (Schuler et al.)[45,46] to observation of asphaltene aggregates in different media/support.[47−50] Therefore, AFM is a technique of choice for observation and comparison of the type and form of macroaggregates deposited on metal surfaces or sensors.

Quartz Crystal Resonator for Trace Asphaltenes Flocculation. Due to the simplicity and versatility of this technique, quartz crystal resonator sensors (QCR or QCM) are increasingly used to understand asphaltene destabilization, aggregation, and deposition. In recent years, many studies have been published on this aspect.[51−56] The QCR sensor consists of a quartz disc with electrodes deposited on both faces and oscillated by applying an AC current between them. The oscillation is achieved due to the piezoelectric properties of the quartz. The resonance frequency at which the oscillation occurs depends on the characteristics of the crystal and can vary due to changes on its surface (mass adsorption, roughness) and in the surrounding media (viscosity, temperature, pressure, etc.).[57−60] A simplified model can be used to correlate changes in the frequency (eq 1) and dissipation (eq 2) with the properties of the system, such as mass absorbed on the quartz surface and viscosity, when the QCR is immersed in a liquid:[54]

$$\Delta f_n = -n(2C_m\Delta m) - \sqrt{n}\frac{C_m}{\sqrt{\pi f_0}}\sqrt{\rho\eta} \quad (1)$$

$$\Delta\Gamma_n = \sqrt{n}\frac{C_m}{\sqrt{\pi f_0}}\sqrt{\rho\eta}(1+R) \quad (2)$$

where C_m is a constant that depends on the crystal characteristics, Δm is the theoretical mass deposited on the quartz surface, $\rho\eta$ is the density-viscosity product of the medium, f_0 is the fundamental resonance frequency of the crystal, and R is an empirical correction term that accounts for viscous friction on rough surfaces.

This work focuses on the study of asphaltene extrography fractions by QCR, AFM, GPC, and FT-ICR MS to establish correlations between molecular composition, nanoaggregate size and shape, and asphaltene precipitation trends.

EXPERIMENTAL SECTION

Asphaltene Fractionation by Extrography. Asphaltene samples were adsorbed on silica gel with a mass loading of 1%. The mixture was dried under nitrogen, the temperature in the Soxhlet

https://dx.doi.org/10.1021/acs.energyfuels.0c02687
Energy Fuels XXXX, XXX, XXX−XXX

reservoir was below 50 °C, and it was protected from light. The dried material was extracted in a Soxhlet apparatus using three different solvents: acetone (100%), Hep/Tol (1:1), and Tol/THF/MeOH (10:10:1). Fractions were dried under nitrogen and stored in the dark for subsequent analyses. Gravimetric mass yields for the fractions and vanadium content are included in Table 1.

Table 1. Extrography Fractionation: Gravimetric Yields for Asp-1 and Asp-2 with V and S Content

sample	extract	extracted mass (% of the initial asphaltene)	V content in ppm	S content in ppm
Asp-1	Asphaltene	-	338	34 140
	Acetone	15	909	68 700
	Hep-Tol	46	275	29 110
	Tol-THF-MeOH	25	275	30 037
	Mass Balance (%)	86.0 ± 2.5	98	92
Asp-2	Asphaltene	-	588	43 300
	Acetone	19	1397	66 779
	Hep-Tol	29	340	29 450
	Tol-THF-MeOH	48	468	43 220
	Mass Balance (%)	96.1 ± 3.7	97	100

Materials. High-performance liquid chromatography (HPLC) grade heptane (Hep or C_7), toluene (Tol), tetrahydrofuran (THF), methanol (MeOH), and acetone from J.T. Baker (Phillipsburg, NJ) were used as received. Silica gel (100−200 mesh, type 60 Å, Fisher Scientific) was used in extrography. High-purity glass microfiber thimbles were used in Soxhlet extraction.

Samples. Two asphaltene samples were obtained by the standard method ASTM D6560-12 for precipitation of C_7 insolubles applied to Middle East atmospheric residues. Table 2 includes elemental analysis and weight content for both atmospheric residues.

GPC-ICP HR MS. After dilution in THF by a factor of 100, all samples were analyzed by the GPC-HR-MS method, as published elsewhere.[42−44,61] In short, the liquid chromatographic system was set up with three Styragel gel permeation chromatographic columns in series (HR 4, HR2, HR 0.5 (7.8 × 300 mm) from Waters (Saint Quentin en Yvelines, France) and combined with a high-resolution ICP mass spectrometer (Thermo, City) with a custom-built interface. The isocratic THF (with 250 ppm of butylated hydroxytoluene (BHT) as a stabilizer) flow rate was 1 mL/min, and the injection volume was 40 μL. Three isotopes were followed: ^{51}V, ^{60}Ni, and ^{32}S.

FT-ICR MS. Asphaltene samples were diluted in toluene to a final concentration of 50 μg/mL. The solutions were directly infused at 50 μL/min into an atmospheric-pressure photoionization (APPI) Ion Max source (Thermo Scientific) operated with a vaporizer temperature of 350 °C. Gas-phase neutrals were ionized with 10.2 eV photons, and positive ions were transferred to the mass spectrometer through a heated metal capillary operated at ∼350 °C. Ions were analyzed with a dynamically harmonized FT-ICR cell.[62] For each sample, 200 time-domain transients were summed and Fourier transformed. Data collection and mass spectra calibration were assisted by Predator custom software. PetroOrg software facilitated molecular formula assignment and data visualization.

Quartz Crystal Resonator (QCR). Stock solutions (1000 ppm) were prepared by dissolving the dried asphaltenes and fractions in toluene and placing them in a temperature-controlled oven at 30 °C for 72 h. A dilution with toluene was performed, resulting in 200 ppm solutions. Amounts of 17.5 g were used in titration with *n*-heptane. The experimental setup of the titration is shown in Figure 1. The quartz sensor (4) was placed inside the custom double-wall vessel (3), and the isothermal bath was set at 25 °C. Transmission of electrical signals and monitoring of the QCR sensor response were conducted through a network analyzer (Agilent E5071C) (2) connected by coaxial cables to a computer (1) with an internally automated LabVIEW program. The sensor was allowed to stabilize (frequency changes of <0.5 Hz), and the frequencies in air (background) were recorded. The sample solution was placed in the cell, and the system was held for approximately 30 min to reach a stable signal. The titration was performed with *n*-heptane (8) supplied at a constant speed of 0.25 g/min, and the mixture in the vessel was stirred at a constant rate using a magnetic stirrer and a stir bar (6) rotating below the quartz. The titration was stopped once a concentration of 80 wt % of *n*-heptane was reached. Gold coupons (5) immersed in the same container in the immediate vicinity of the resonator were used in the AFM images.

Estimation of the destabilization onset was obtained using a simple approach based on the model used. When a titration is performed in a system without any mass load on the quartz, the first term in eq 1 becomes 0, and all frequency shifts are due to liquid loading, and thus the following equality can be obtained:

$$\Delta f_{n,m} = \frac{-\Delta\Gamma_{n,\eta}}{(1+R)} \quad (3)$$

A plot of Δf as a function of $\Delta\Gamma$ (Figure 2, left) presents a linear behavior with a slope equal to $-1/(1+R)$. Deviations from this linearity must be linked with mass loading effects and thus can be used to detect asphaltene destabilization.

The amount of deposit on the sensor surface was estimated by analyzing the behavior of Δf for the different overtones (third, fifth, seventh, and ninth) and plotting the linear relation of $\Delta f/n$ vs $1/\sqrt{n}$.

$$\frac{\Delta f_n}{n} = -2C_m\Delta m - \frac{1}{\sqrt{n}}\frac{C_m}{\sqrt{\pi f_0}}\sqrt{\rho\eta_l} \quad (4)$$

AFM Images of Coupons after Deposition. After titration, the gold coupons were rinsed in *n*-heptane and dried in air. Atomic force microscopy (AFM) images of the surface were collected with a Multi-Mode VIII (BRUKER) instrument using Nanoscope ver. 8.15 software. To image these samples, the peak force quantitative nanomechanical mapping (QNM) mode was selected. Silicon nitride cantilevers with a calibrated spring constant of 0.36 $N.m^{-1}$ and a typical tip radius of approximately 10 nm were used.

RESULTS

Molecular Characterization by FT-ICR MS. Figures 3 and 4 (upper panel) present the isoabundance contoured plots of DBE versus carbon number for HC-, N-, and O-containing compounds (upper row); all species with at least one S atom (S-containing, middle row); and vanadyl porphyrins or class $N_4O_1V_1$ (lower row). The lower panels of Figures 3 and 4 present the gravimetric yields for extrography separation. The major difference is that Asp-2 contains a higher concentration of the most polarizable extrography fraction, Tol/THF/MeOH

Table 2. Elemental Composition and Asphaltene Content for Middle East Atmospheric Residues[a]

sample	N (%)	Ni (ppm)	V (ppm)	Fe (ppm)	S (%)	Na (ppm)	Asphaltene (wt %)	CCR (%)
AR-1	0.32	23	60	12	4.16	4.1	4.9	11.5
AR-2	0.47	60	82	13	4.33	5.8	8.0	13.6

[a]CCR Corresponds to Conradson Carbon Residue.

https://dx.doi.org/10.1021/acs.energyfuels.0c02687
Energy Fuels XXXX, XXX, XXX−XXX

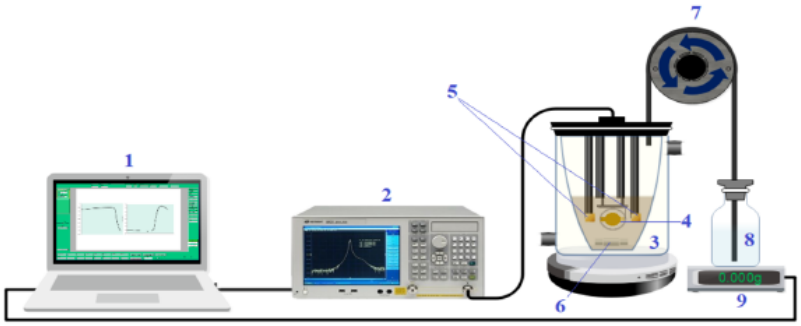

Figure 1. Experimental Setup. (1) Computer, (2) Network analyzer, (3) Double-walled glass vessel, (4) QCR sensor, (5) Gold coupons, (6) Magnetic stir bar, (7) Peristaltic pump, (8) *n*-Heptane, and (9) Balance.

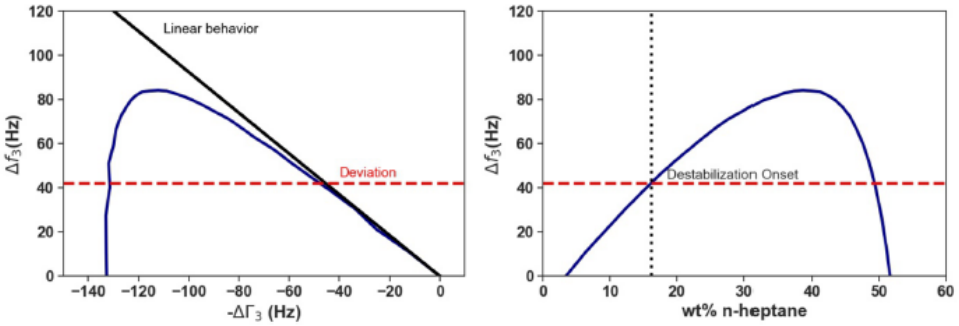

Figure 2. Destabilization onset determination. Left panel - Frequency shift (Δf) as a function of dissipation shift ($\Delta\Gamma$). Right panel - Frequency shift (Δf) as a function of *n*-heptane composition.

(~48 wt %). According to Table 1, Tol/THF/MeOH and Hep-Tol from Asp-2 have lowest concentrations of vanadium compared to the acetone fraction that reveal vanadyl porphyrins ($N_4O_1V_1$ class). The lower panels of Figures 3 and 4 also present the ionization efficiency, or monomer ion yield (MIY), as determined by APPI FT-ICR MS. MIY is inversely proportional to the accumulation period required to hit a target signal magnitude optimal for data collection in FT-ICR MS. Samples that ionize efficiently in APPI, such as PAHs and aromatic fractions from light crude oils, require a short accumulation period in an external ion trap before transferring to the ICR cell (~5−50 ms). Conversely, difficult-to-ionize samples, such as asphaltenes, polar petroleum fractions, and vacuum residues, require a longer accumulation, up to ~5000 ms. Thus, poor ion production translates into a longer accumulation period and thus lower MIY. The results indicate that the acetone fractions from both asphaltenes samples ionize ~25−90-fold more efficiently than the Tol/THF/MeOH fractions. Thus, analysis of whole asphaltene samples (without prior fractionation) preferentially reveals the acetone species. From Figures 3 and 4, it is clear that the acetone fractions closely resemble the compositional range of the whole samples (upper panels). However, the Hep/Tol and Tol/THF/MeOH fractions, with a lower monomer ion yield, present a completely different compositional range. The results highlight that the most strongly adsorbed compounds on the silica gel (Tol/THF/MeOH) have lower DBE values than the acetone and Hep/Tol fractions. The major difference is shown again by the Tol/THF/MeOH species, which for the S-containing compounds of the sample Asp-2 extend to carbon numbers beyond 40, suggesting a higher content of carbon atoms in the alkyl side chains.

All samples (and fractions) contain vanadium, but porphyrins were detected only in the whole samples and the acetone fractions. For instance, the Tol/THF/MeOH Asp-2 fraction, with similar concentration of vanadium than whole asphaltene, displayed no porphyrin mass spectral peaks compared to asphaltene that reveal some. Previous reports demonstrate that the Tol/THF/MeOH fractions from several asphaltene samples have a stronger precipitation tendency when titrated with heptane.[22] We hypothesize that the stronger aggregation tendency of the Tol/THF/MeOH fractions is responsible for the lack of MS detection of vanadyl porphyrins. It is likely that porphyrin species are locked into asphaltene nanoaggregates and thus are not detected in the mass range to which the ICR cell is tuned ("monomeric"/nonaggregated ions, m/z ~ 100−1200 g/mol).

Gas-phase fragmentation studies conducted for the extrography fractions indicate that the acetone and Hep/Tol fractions for both samples contain abundant single-core motifs (or island), whereas the Tol/THF/MeOH fractions reveal a significant amount of multicore (or archipelago) compounds. The results are summarized in Figures S1−3 of the Supporting Information.[63]

The compositional range of S-containing compounds reveals abundant low-DBE species with higher content of CH_2 groups (longer homologous series), in particular, for the most polar extrography fraction (Tol/THF/MeOH). Previous reports by

https://dx.doi.org/10.1021/acs.energyfuels.0c02687
Energy Fuels XXXX, XXX, XXX−XXX

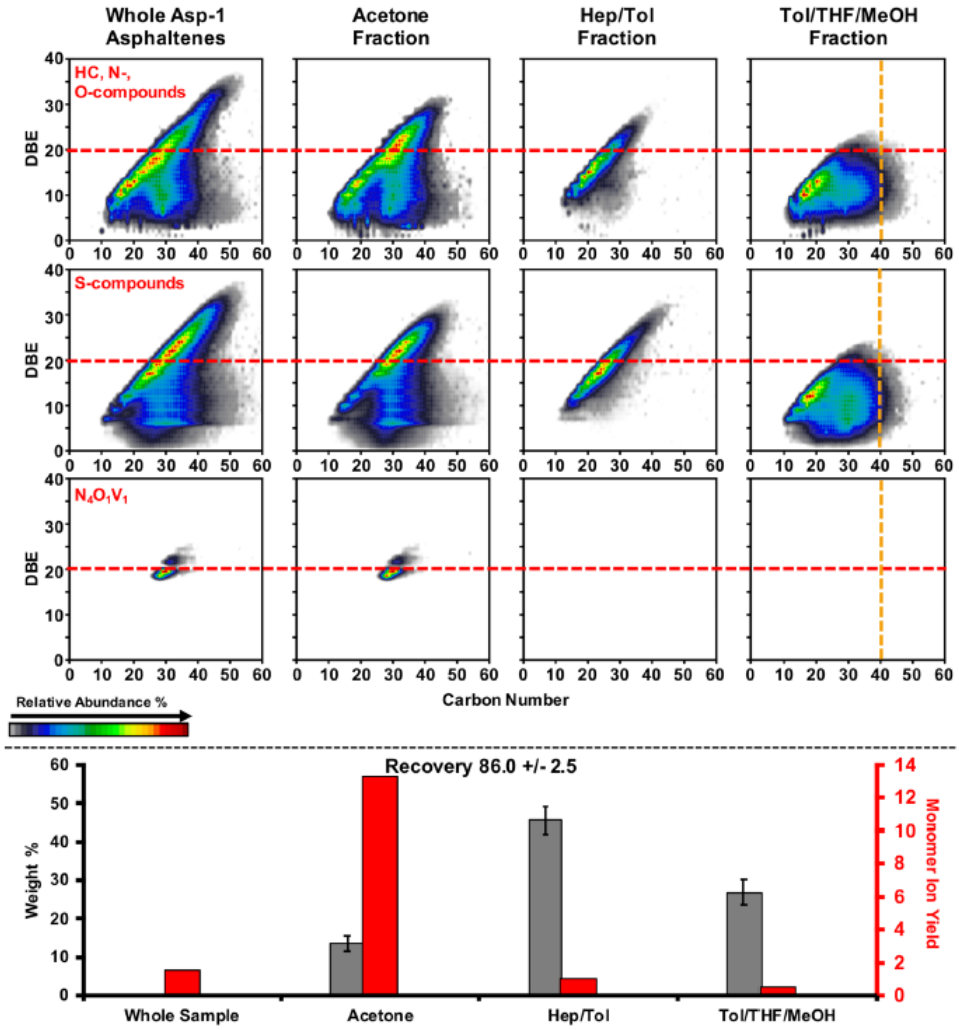

Figure 3. Upper panel: Combined isoabundance contoured plots of DBE vs carbon number for HC-, N-/O-containing compounds (upper row), S-containing species (middle row), and vanadyl porphyrins (lower row) for whole Asp-1 asphaltenes and extrography fractions. Lower panel: Gravimetric yields for extrography separation (gray bars) and monomer ion yield (red bars) or ionization efficiency as determined by APPI-MS.

Chacon-Patiño,[22] Xu,[49,64] Kilpatrick,[65,66] and Stanford[67,68] suggest the existence of asphaltene molecules with low aromaticity or low DBE but high heteroatom content. In particular, Xu et al. highlighted that "atypical" S-containing species with low aromaticity could be sulfoxides (R—S═O), which can participate in hydrogen bonding.[63] Therefore, heteroatom-based intermolecular forces, such as hydrogen bonding and acid/base interactions, likely dominate the aggregation/solubility behavior of atypical low-DBE compounds that are abundant in the Tol/THF/MeOH extrography fraction, which exhibits, as discussed below, the strongest deposition trends and the most irregular aggregate microstructure. This hypothesis seems to be consistent with the aggregation model proposed by Gray[14] and Yarranton et al.[13]

GPC ICP HR MS Analysis of Both Samples and Extrography Subfractions. Figure 5 (sample Asp-1) and Figure 6 (sample Asp-2) show the S and V chromatograms of the whole asphaltene samples and their extrography fractions. The chromatograms of the extrography fractions clearly show that the acetone fraction has a completely different hydrodynamic volume than the two other fractions. The acetone fraction elutes primarily in the MMW and LMW region of the chromatogram. Conversely, the Hep/Tol and Tol/THF/MeOH fractions are both eluted in the HMW region. The results indicate that the reconstructed chromatogram based on the summed chromatograms of each fraction for both elements (S and V) is different than the one for the whole sample, suggesting that the extrography separation partially disrupts the nanoaggregation behavior of the original asphaltene solution, as previous softer fractionation, by liquid−liquid extraction, has shown that the reconstructed chromatogram was similar to the original asphaltene.[69]

https://dx.doi.org/10.1021/acs.energyfuels.0c02687
Energy Fuels XXXX, XXX, XXX−XXX

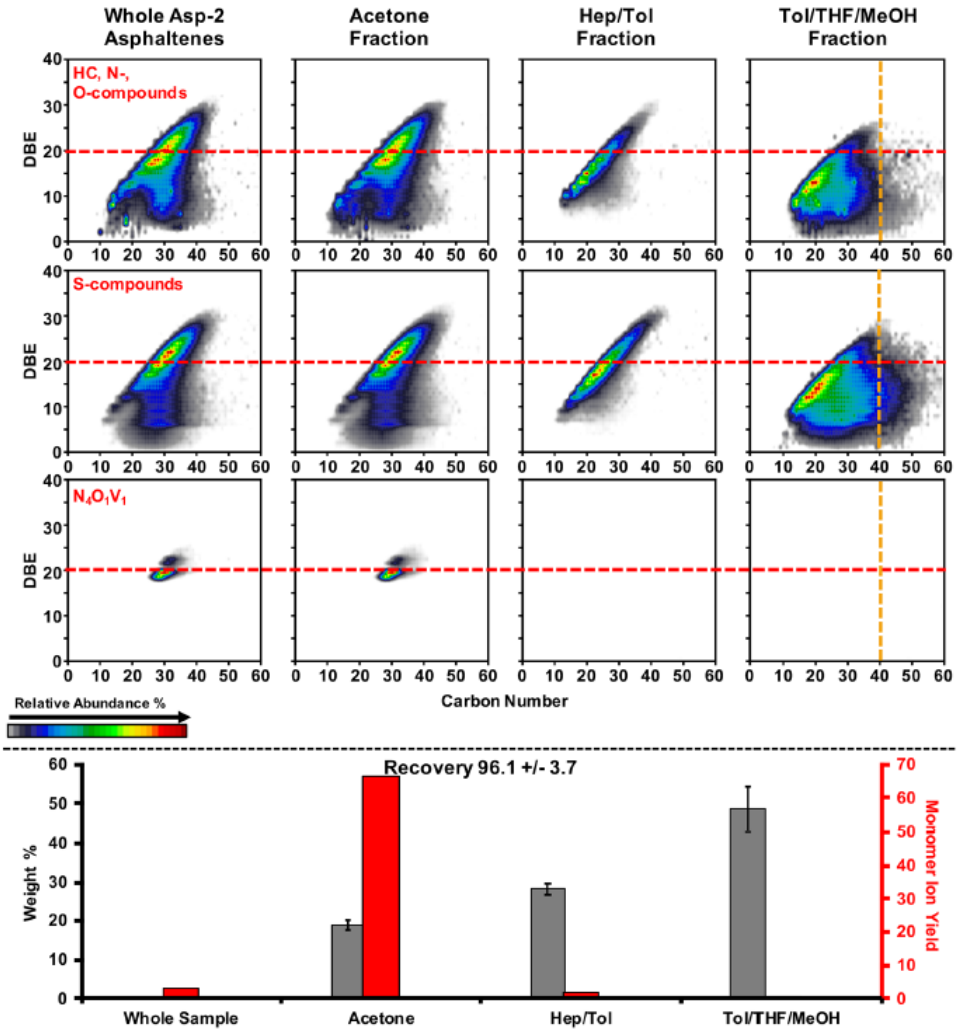

Figure 4. Upper panel: Combined isoabundance contoured plots of DBE vs carbon number for HC-, N-/O-containing compounds (upper row), S-containing species (middle row), and vanadyl porphyrins (lower row) for whole Asp-2 asphaltenes and extrography fractions. Lower panel: Gravimetric yields for extrography separation (gray bars) and monomer ion yield (red bars) or ionization efficiency as determined by APPI-MS.

Figure 7 shows a comparison of the S and V chromatograms obtained for each sample and subfraction. Both whole asphaltene samples have a similar S chromatogram, but analyses of the extrography fractions suggest that there are more S-containing compounds in the Asp-2 Tol/THF/MeOH fraction than in the Asp-1 fraction. The behavior is the opposite for the Hep/Tol and acetone fractions. For the GPC profile, all members of the families of both samples have the same S chromatographic profile. The V chromatograms show behavior similar to that of S, except for the acetone fraction, where the MMW V nanoaggregate appears in Asp-1 and more LMW compounds appear in Asp-2.

Quartz Crystal Resonator (QCR) Sensor Analysis of Both Samples and Extrography Fractions. Destabilization of whole asphaltenes and their extrography fractions in toluene was achieved using *n*-heptane as a destabilizing agent (titrant). The flocculation and deposition processes were followed using a QCR sensor. The frequency shift (Δf) signals shown in Figures 8 and 9a exhibit a smooth increase during the entire titration for a nonflocculating system (pure toluene) due to reduction of the viscosity−density product ($\eta\rho$) by the addition of *n*-heptane. This behavior is also observed for the whole asphaltene and fraction samples at a low weight% of *n*-heptane (wt %) in which the flocculation process has not yet begun. A progressive reduction of the signal is observed as the unstable compounds in solution are destabilized and flocculation begins, followed by an abrupt change in the slope (negative) due to the aggregation process. Ultimately, the changes in slope become less negative, indicating the end of the aggregation process (clear for Tol/THF/MeOH fraction).

https://dx.doi.org/10.1021/acs.energyfuels.0c02687
Energy Fuels XXXX, XXX, XXX−XXX

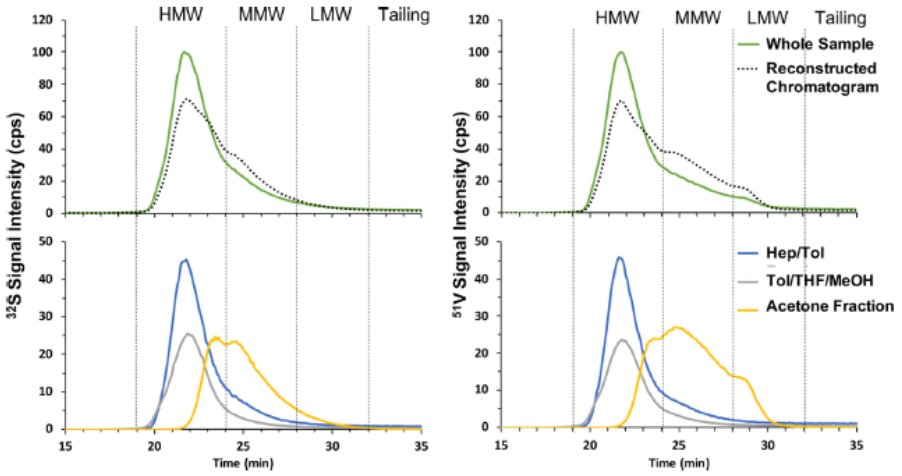

Figure 5. Sample Asp-1 and its extrography fractions—GPC ICP MS of ^{32}S and ^{51}V and reconstructed chromatogram.

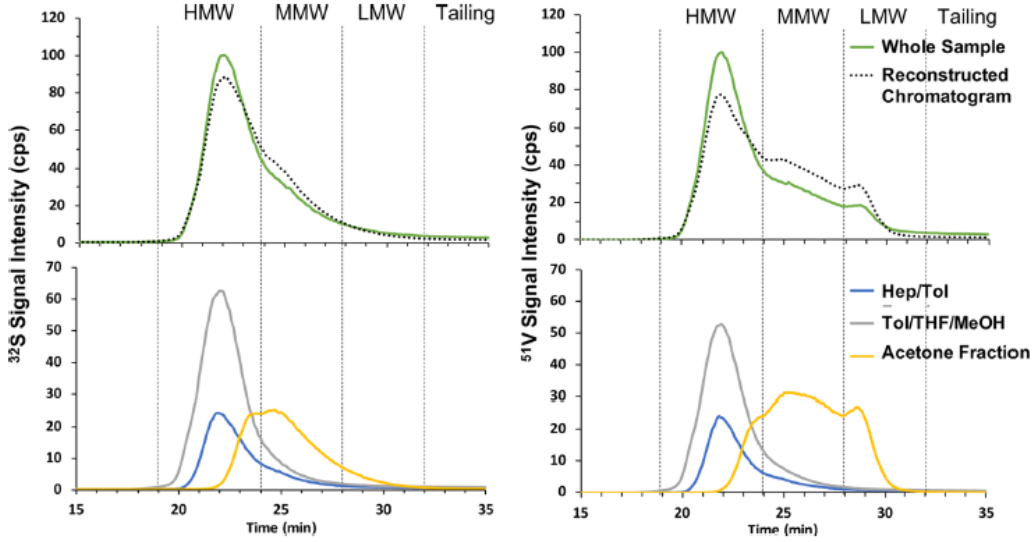

Figure 6. Sample Asp-2 and its extrography fractions—GPC ICP MS of ^{32}S and ^{51}V and reconstructed chromatogram.

Once the destabilization begins, the aggregation process occurs more rapidly for the whole asphaltenes, Tol/THF/MeOH and Hep/Tol fractions (from both samples), than it does for the acetone fraction. The Tol/THF/MeOH fraction is the one that destabilizes more rapidly, as expected and as previously discussed, and the Hep/Tol fraction is the one that destabilizes last. In Figures 8 and 9b, deposition onto quartz is shown as Δm. Both figures highlight that the acetone fraction tends to adsorb less on the quartz surface compared with the other fractions. Interestingly, the Asp-2 Tol/THF/MeOH fraction presents a maximum near 68 wt % of composition, and then a "decrease" of the deposit is observed. Rather than a desorption process, this diminution could be attributed to a slippage effect of the deposit on the quartz surface. This slippage causes a positive frequency shift, which represents a "negative mass" loading, causing an underestimation of the Δm value.[54,70−72]

Figure 10 shows the destabilization onset and mass deposit values for all samples, when the system reaches a mass composition of 80% heptane added. If we compare the behavior between samples with similar chemistries, (i.e., whole/whole; acetone/acetone, etc.) the phenomenon observed in the solution is contrary to the one observed in the quartz surface: the sample that requires greater volume for destabilization generates less deposit. This occurs for both asphaltenes and their corresponding fractions. It is also clear that the difference in stability between both whole asphaltene samples can be related with the difference in content of both less stable (Tol/THF/MeOH) and most stable (HepTol) fractions. In other words, Asp-2 which destabilizes first contains a higher amount of Tol/THF/MeOH (46 wt %)

https://dx.doi.org/10.1021/acs.energyfuels.0c02687
Energy Fuels XXXX, XXX, XXX−XXX

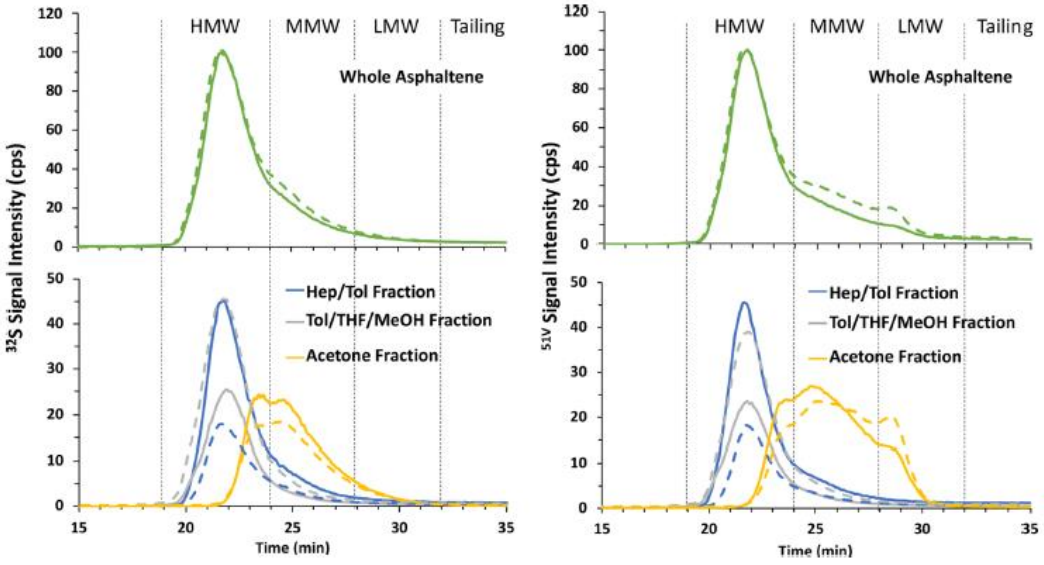

Figure 7. Sample Asp-1 (solid line) and Asp-2 (dotted line) and their extrography fraction—GPC ICP MS of ^{32}S and ^{51}V.

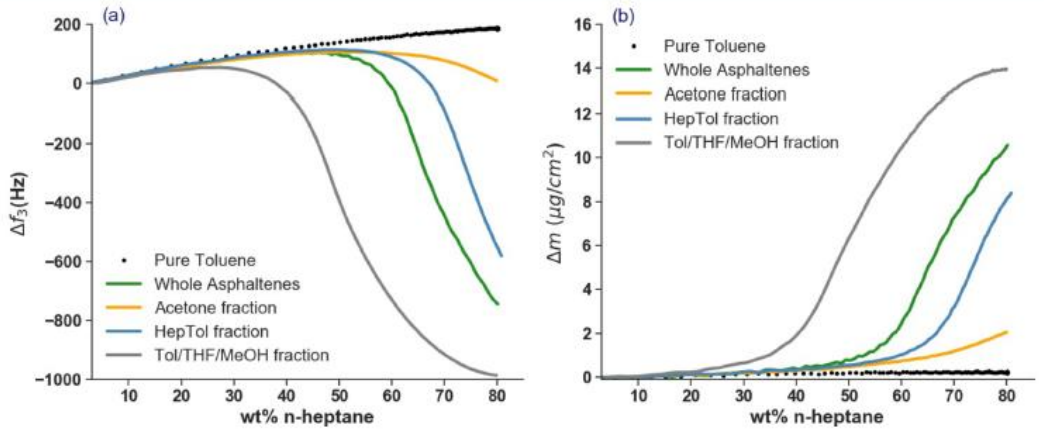

Figure 8. QCR titration curves for Asp-1 samples. (a) Frequency shifts (Δf) of the third harmonic and (b) deposited mass (Δm) on the quartz surface vs composition of *n*-heptane.

than Asp-1 (25 wt %) and a lesser amount of HepTol (29 wt % vs 46 wt %).

AFM Images of QCR Coupon after Asphaltene Deposit. Representative height images (1×1 μm^2) of the deposit formed on the coupon gold surface at the end of QCR titration experiments are presented in Figure 11. These images visualize the "macrostructural" differences between deposits formed for each fraction. The whole asphaltene, Tol/THF/MeOH, and Hep/Tol fractions of both samples displayed a layer of aggregates of irregular shapes, whereas both acetone fractions presented an organized structure of aggregates. The size of the aggregates varied in accordance with the amount of deposit estimated by the QCR experiments. The Asp-1 Tol/THF/MeOH fraction presented the largest aggregates (ø ~ 120 nm), and both acetone fractions presented the smallest aggregates (ø ~ 50 nm). A difference was observed between the distribution of the aggregates for the Hep/Tol fraction; Hep/Tol fraction from Asp-1 is distributed in an irregular way, while the Asp-2 Hep/Tol fraction is distributed in a more homogeneous way.

DISCUSSION

Fractionation by Extrography. All of the analytical techniques used (AFM, FT ICR MS, GPC ICP MS) show that extrography fractionation allows asphaltene separation into fractions with similar behavior (e.g., both acetone fractions have similar composition, GPC elution); thus, they likely comprise nanoaggregates with similar size and chemistry. For QCR, although the destabilization onsets for the two whole asphaltene samples are different, after extrography, the flocculation behaviors of Asp-1/Asp-2 extrography fractions are similar. For the deposited mass, the acetone fraction

https://dx.doi.org/10.1021/acs.energyfuels.0c02687
Energy Fuels XXXX, XXX, XXX−XXX

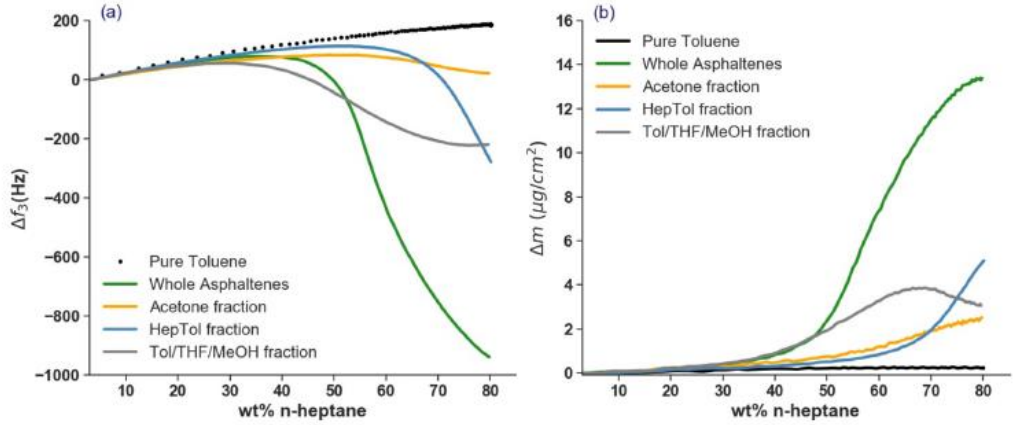

Figure 9. QCR titration curves for Asp-2 samples. (a) Frequency shifts (Δf) of the third harmonic and (b) deposited mass (Δm) on the quartz surface vs composition of *n*-heptane.

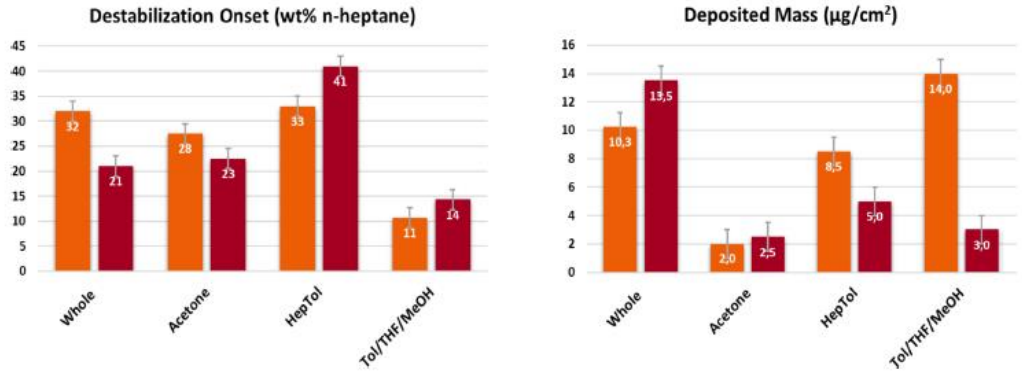

Figure 10. Destabilization onset (left) and deposited mass on the quartz surface at 80 wt % of *n*-heptane (right) comparison between Asp-1 (orange bars) and Asp-2 (red bars) whole asphaltenes and corresponding fractions.

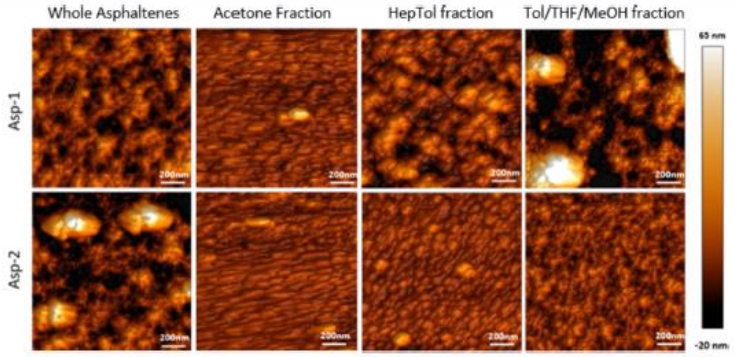

Figure 11. AFM micrographs ($1 \times 1\ \mu m^2$) of the deposit formed on the gold surface at 80 wt % of *n*-heptane.

revealed the same trend for both samples, whereas Tol/THF/MeOH and HepTol fractions exhibited different deposited masses. Collectively, the results show that the acetone fraction from both samples, enriched with island-type structural motifs (FT ICR MS characterization), feature the same behavior for nanoaggregation (GPC) and macroaggregation (QCR). The macroaggregation is spatially well-organized (AFM), and this well-organized molecular layer emphasizes that the main interaction between each molecule might be π stacking between the aromatic cores. The size of these macroaggregates

https://dx.doi.org/10.1021/acs.energyfuels.0c02687
Energy Fuels XXXX, XXX, XXX−XXX

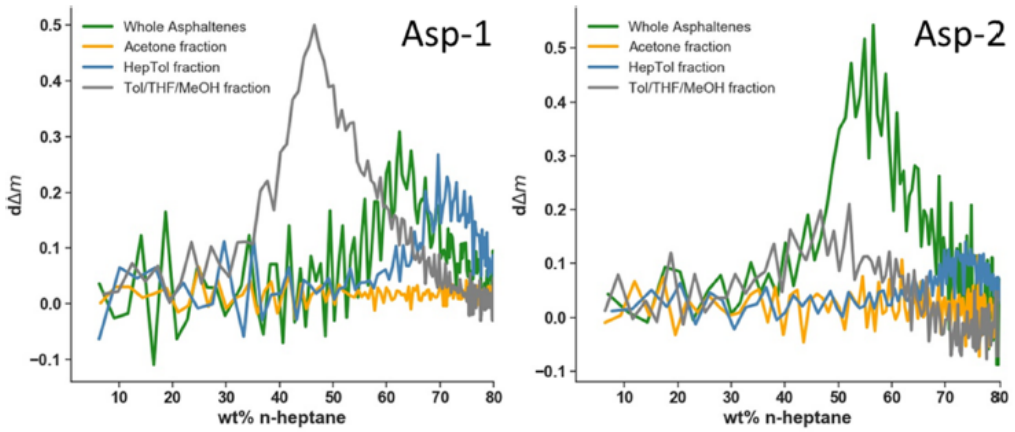

Figure 12. Derivation of the deposited mass ($d\Delta m$) on the quartz surface vs composition for Asp-1 (left) and Asp-2 (right) whole asphaltenes and fractions.

is the smallest (near 50 nm) of all fractions, consistent with the elution behavior of the acetone fractions in GPC. Conversely, the Hep/Tol and Tol/THF/MeOH fractions have larger nanoaggregates (GPC) and macroaggregates (AFM). As expected for the Hep/Tol fraction of Asp-2, the macroaggregates are less spatially organized, suggesting that aggregation is less driven by $\pi-\pi$ interaction, and it is more consistent with a supramolecular network similar to the structures hypothesized by Gray et al.[14]

In Figure 12, the plot (derivation of the deposited mass ($d\Delta m$) on the quartz surface vs composition in heptane) discriminates clearly between the aggregate growing in size versus the aggregate growing in number in the solution. The acetone and Hep/Tol fractions, which contain abundant island molecules (FT-ICR MS characterization), tend to deposit less material than Tol/THF/MeOH (with more archipelago content) in both samples. In this fraction, heptane titration induces larger aggregates that progressively increase in size. The acetone fractions produce highly organized/regular macroaggregates with similar and smaller sizes than the other extrography fractions.

Thus, it appears that asphaltene precipitation is strongly linked to the chemical composition of the molecules contained in the sample/fractions.

Properties of the Fraction-Link to the Crude Oil. The GPC results show that during the extrography process, a portion of the HMW compounds move to MMW and LMW. Because most of the MMW and LMW molecules are contained in the acetone fraction, we can assume that a subset of "island"-type molecules are contained in the HMW nanoaggregates in the bulk samples and are found in the acetone fraction after extrography extraction. Thus, these results support the idea that asphaltene aggregation is highly heterogeneous and there may be cooperative effects between asphaltene fractions.[14] The HMW portion of the GPC chromatogram is strongly linked to the deposited mass in the QCR sensor. For both asphaltenes, the AFM images of the deposit of the bulk asphaltenes are not as well structured as the image of the TOL/THF/MeOH fraction. It appears that macroaggregation (asphaltene destabilization) might be driven by the HMW nanoaggregate and the presence of "archipelago"-type molecules in the samples.

Porphyrins in Fractions and Samples. Petroporphyrins that belong to the $N_4O_1V_1$ class were identified only in bulk samples and acetone fractions. As the GPC reconstructed chromatogram of V shows, a shift from HMW to MMW and LMW occurs during extrography; thus, we hypothesize that the $N_4O_1V_1$ porphyrins detected in the bulk sample are likely the ones identified in the acetone fraction. This result might indicate that porphyrins surround the nanoaggregate in the HMW portion of the chromatogram in bulk/whole samples. GPC ICP-MS analysis can detect a large amount of vanadium in the HMW region, but FT-ICR MS fails to detect any vanadyl porphyrins. This result might occur because of poor ionization efficiency for these HMW compounds and thus a notably low sensitivity for this trace compound.

CONCLUSION

A combination of chemical and physical characterization was applied to whole/unfractionated asphaltene samples and their extrography fractions to better understand the aggregation process. The results showed that the extrography extraction, which is linked to the polarity of the molecule/nanoaggregate adsorbed on silica, produces families with different behaviors in the aggregation process. The aggregation and deposition (QCR and AFM) of the samples during *n*-heptane titration are related to the structure (FT ICR MS) and size of the aggregates (GPC ICP HR-MS). The smallest and "island"-type fraction (acetone) is the one that forms lesser deposit amounts with more organized structures, whereas the larger and "archipelago"-type fraction (Tol/THF/MeOH) is the one that produces a greater deposit amount with a less organized macrostructure. This multiscale characterization technique can be useful in understanding asphaltene behavior during precipitation processes on production facilities and catalysts.

ASSOCIATED CONTENT

Supporting Information

The Supporting Information is available free of charge at https://pubs.acs.org/doi/10.1021/acs.energyfuels.0c02687.

https://dx.doi.org/10.1021/acs.energyfuels.0c02687
Energy Fuels XXXX, XXX, XXX−XXX

Infrared Multiphoton Dissociation of the Acetone, Hep/Tol, and Tol/THF/MeOH fractions of Asp-1 and Asp-2 (PDF)

AUTHOR INFORMATION

Corresponding Author

Brice Bouyssiere − *Université de Pau et des Pays de l'Adour, E2S UPPA, CNRS, IPREM, Institut des Sciences Analytiques et de Physico-chimie pour l'Environnement et les Materiaux, UMR5254, Hélioparc, 64053 Pau, France; International Joint Laboratory C2MC: Complex Matrices Molecular Characterization, Total Research & Technology, Gonfreville, BP 27, 76700 Harfleur, France;* orcid.org/0000-0001-5878-6067; Phone: +33 (0) 559 407 752; Email: brice.bouyssiere@univ-pau.fr

Authors

Nelson Acevedo − *Universite de Pau et des Pays de l'Adour, E2S UPPA, CNRS, TOTAL, LFCR, UMR 5150, 64012 Pau, France; Facultad de Ciencias, Escuela de Química, Universidad Central de Venezuela, 1050 Caracas, Venezuela*

Remi Moulian − *Université de Pau et des Pays de l'Adour, E2S UPPA, CNRS, IPREM, Institut des Sciences Analytiques et de Physico-chimie pour l'Environnement et les Materiaux, UMR5254, Hélioparc, 64053 Pau, France; International Joint Laboratory C2MC: Complex Matrices Molecular Characterization, Total Research & Technology, Gonfreville, BP 27, 76700 Harfleur, France; TOTAL Raffinage Chimie, TRTG, BP 27, 76700 Harfleur, France*

Martha L. Chacon Patiño − *International Joint Laboratory C2MC: Complex Matrices Molecular Characterization, Total Research & Technology, Gonfreville, BP 27, 76700 Harfleur, France; National High Magnetic Field Laboratory and Future Fuels Institute, Florida State University, Tallahassee, Florida 32310, United States;* orcid.org/0000-0002-7273-5343

Aurora Mejia − *Universite de Pau et des Pays de l'Adour, E2S UPPA, CNRS, TOTAL, LFCR, UMR 5150, 64012 Pau, France*

Sadia Radji − *Université de Pau et des Pays de l'Adour, E2S UPPA, CNRS, IPREM, Institut des Sciences Analytiques et de Physico-chimie pour l'Environnement et les Materiaux, UMR5254, Hélioparc, 64053 Pau, France*

Jean-Luc Daridon − *Universite de Pau et des Pays de l'Adour, E2S UPPA, CNRS, TOTAL, LFCR, UMR 5150, 64012 Pau, France;* orcid.org/0000-0002-0522-0075

Caroline Barrère-Mangote − *International Joint Laboratory C2MC: Complex Matrices Molecular Characterization, Total Research & Technology, Gonfreville, BP 27, 76700 Harfleur, France; TOTAL Raffinage Chimie, TRTG, BP 27, 76700 Harfleur, France*

Pierre Giusti − *International Joint Laboratory C2MC: Complex Matrices Molecular Characterization, Total Research & Technology, Gonfreville, BP 27, 76700 Harfleur, France; TOTAL Raffinage Chimie, TRTG, BP 27, 76700 Harfleur, France;* orcid.org/0000-0002-9569-3158

Ryan P. Rodgers − *Université de Pau et des Pays de l'Adour, E2S UPPA, CNRS, IPREM, Institut des Sciences Analytiques et de Physico-chimie pour l'Environnement et les Materiaux, UMR5254, Hélioparc, 64053 Pau, France; International Joint Laboratory C2MC: Complex Matrices Molecular Characterization, Total Research & Technology, Gonfreville, BP 27, 76700 Harfleur, France; National High Magnetic Field Laboratory and Future Fuels Institute, Florida State University, Tallahassee, Florida 32310, United States;* orcid.org/0000-0003-1302-2850

Vincent Piscitelli − *Facultad de Ciencias, Escuela de Química, Universidad Central de Venezuela, 1050 Caracas, Venezuela*

Jimmy Castillo − *Facultad de Ciencias, Escuela de Química, Universidad Central de Venezuela, 1050 Caracas, Venezuela*

Hervé Carrier − *Universite de Pau et des Pays de l'Adour, E2S UPPA, CNRS, TOTAL, LFCR, UMR 5150, 64012 Pau, France; International Joint Laboratory C2MC: Complex Matrices Molecular Characterization, Total Research & Technology, Gonfreville, BP 27, 76700 Harfleur, France*

Complete contact information is available at: https://pubs.acs.org/10.1021/acs.energyfuels.0c02687

Notes

The authors declare no competing financial interest.

ACKNOWLEDGMENTS

The authors would like to thank TOTAL for supplying the oil samples. Work performed at the National High Magnetic Field Laboratory ICR User Facility was supported by the National Science Foundation Division of Chemistry through Cooperative Agreements DMR-1157490 and DMR-1644779 and the state of Florida. This work was also supported by Conseil Régional d'Aquitaine (20071303002PFM) and FEDER (31486/08011464). The financial support provided by the Franco-Venezuelan Project RMR (Réseau Marcel Roche) is gratefully acknowledged.

REFERENCES

(1) Boussingault, J. B. Memoire sur la Composition des Bitumes. *Ann. Chim. Phys.* **1837**, *LXIV*, 141−151.

(2) McKenna, A.; Rodgers, R. P.; Robbins, W. K.; Marshall, A. G. In Molecular characterization of asphaltenes and maltenes by FT-ICR mass spectrometry and implications to island and archipelago structural models; *ACS National Meeting Book of Abstracts*, Vol. *2011*; American Chemical Society: Washington, DC, 2011.

(3) McKenna, A. M.; Donald, L. J.; Fitzsimmons, J. E.; Juyal, P.; Spicer, V.; Standing, K. G.; Marshall, A. G.; Rodgers, R. P. Heavy Petroleum Composition. 3. Asphaltene Aggregation. *Energy Fuels* **2013**, *27* (3), 1246−1256.

(4) McKenna, A. M.; Marshall, A. G.; Rodgers, R. P. Heavy Petroleum Composition. 4. Asphaltene Compositional Space. *Energy Fuels* **2013**, *27* (3), 1257−1267.

(5) Yen, T. F.; Erdman, J. G.; Pollack, S. S. Investigation of the Structure of Petroleum Asphaltenes by X-Ray Diffraction. *Anal. Chem.* **1961**, *33* (11), 1587−1594.

(6) Dickie, J. P.; Yen, T. F. Macrostructures of the Asphaltic Fractions by Various Instrumental Methods. *Anal. Chem.* **1967**, *39* (14), 1847−1852.

(7) Mojelsky, T. W.; Lown, E. M.; Montgomery, D. S.; Ignasiak, T. M.; Frakman, Z.; Strausz, O. P. Structural Features of Alberta Oil Sand Bitumen and Heavy Oil Asphaltenes. *Energy Fuels* **1992**, *6* (1), 83−96.

(8) Strausz, O. P.; Mojelsky, T. W.; Lown, E. M. The Molecular Structure of Asphaltene: An Unfolding Story. *Fuel* **1992**, *71* (12), 1355−1363.

(9) Mullins, O. C. The Modified Yen Model. *Energy Fuels* **2010**, *24* (4), 2179−2207.

(10) Mullins, O. C.; Sabbah, H.; Eyssautier, J.; Pomerantz, A. E.; Barré, L.; Andrews, A. B.; Ruiz-Morales, Y.; Mostowfi, F.; McFarlane, R.; Goual, L.; et al. Advances in Asphaltene Science and the Yen-Mullins Model. *Energy Fuels* **2012**, *26* (7), 3986−4003.

(11) Eyssautier, J.; Levitz, P.; Espinat, D.; Jestin, J.; Gummel, J.; Grillo, I.; Barré, L. Insight into Asphaltene Nanoaggregate Structure

https://dx.doi.org/10.1021/acs.energyfuels.0c02687
Energy Fuels XXXX, XXX, XXX−XXX

Inferred by Small Angle Neutron and X-ray Scattering. *J. Phys. Chem. B* **2011**, *115* (21), 6827−6837.
(12) Wang, W.; Taylor, C.; Hu, H.; Humphries, K. L.; Jaini, A.; Kitimet, M.; Scott, T.; Stewart, Z.; Ulep, K. J.; Houck, S.; et al. Nanoaggregates of Diverse Asphaltenes by Mass Spectrometry and Molecular Dynamics. *Energy Fuels* **2017**, *31* (9), 9140−9151.
(13) Agrawala, M.; Yarranton, H. W. An Asphaltene Association Model Analogous to Linear Polymerization. *Ind. Eng. Chem. Res.* **2001**, *40* (21), 4664−4672.
(14) Gray, M. R.; Tykwinski, R. R.; Stryker, J. M.; Tan, X. Supramolecular Assembly Model for Aggregation of Petroleum Asphaltenes. *Energy Fuels* **2011**, *25* (7), 3125−3134.
(15) Derakhshesh, M.; Bergmann, A.; Gray, M. R. Occlusion of Polyaromatic Compounds in Asphaltene Precipitates Suggests Porous Nanoaggregates. *Energy Fuels* **2013**, *27* (4), 1748−1751.
(16) Spiecker, P. M.; Gawrys, K. L.; Kilpatrick, P. K. Aggregation and solubility behavior of asphaltenes and their subfractions. *J. Colloid Interface Sci.* **2003**, *267* (1), 178−193.
(17) Gawrys, K. L.; Matthew Spiecker, P.; Kilpatrick, P. K. The Role of Asphaltene Solubility and Chemical Composition on Asphaltene Aggregation. *Pet. Sci. Technol.* **2003**, *21* (3−4), 461−489.
(18) Lin, Y.-J.; Cao, T.; Chacón-Patiño, M. L.; Rowland, S. M.; Rodgers, R. P.; Yen, A.; Biswal, S. L. Microfluidic Study of the Deposition Dynamics of Asphaltene Subfractions Enriched with Island and Archipelago Motifs. *Energy Fuels* **2019**, *33* (3), 1882−1891.
(19) Giraldo-Dávila, D.; Chacón-Patiño, M. L.; McKenna, A. M.; Blanco-Tirado, C.; Combariza, M. Y. Correlations between Molecular Composition and Adsorption, Aggregation, and Emulsifying Behaviors of PetroPhase 2017 Asphaltenes and Their Thin-Layer Chromatography Fractions. *Energy Fuels* **2018**, *32* (3), 2769−2780.
(20) Alboudwarej, H.; Akbarzadeh, K.; Beck, J.; Svrcek, W. Y.; Yarranton, H. W. Regular solution model for asphaltene precipitation from bitumens and solvents. *AIChE J.* **2003**, *49* (11), 2948−2956.
(21) Chacón-Patiño, M. L.; Rowland, S. M.; Rodgers, R. P. Advances in Asphaltene Petroleomics. Part 3. Dominance of Island or Archipelago Structural Motif Is Sample Dependent. *Energy Fuels* **2018**, *32* (9), 9106−9120.
(22) Chacón-Patiño, M. L.; Rowland, S. M.; Rodgers, R. P. Advances in Asphaltene Petroleomics. Part 2: Selective Separation Method That Reveals Fractions Enriched in Island and Archipelago Structural Motifs by Mass Spectrometry. *Energy Fuels* **2018**, *32* (1), 314−328.
(23) Chacón-Patiño, M. L.; Rowland, S. M.; Rodgers, R. P. Advances in Asphaltene Petroleomics. Part 1: Asphaltenes Are Composed of Abundant Island and Archipelago Structural Motifs. *Energy Fuels* **2017**, *31* (12), 13509−13518.
(24) Chacón-Patiño, M. L.; Rowland, S. M.; Rodgers, R. P. The Compositional and Structural Continuum of Petroleum from Light Distillates to Asphaltenes: The Boduszynski Continuum Theory As Revealedby FT-ICR Mass Spectrometry. In *The Boduszynski Continuum: Contributions to the Understanding of the Molecular Composition of Petroleum*; American Chemical Society: 2018; pp 113−171.
(25) Rodgers, R. P.; Mapolelo, M. M.; Robbins, W. K.; Chacón-Patiño, M. L.; Putman, J. C.; Niles, S. F.; Rowland, S. M.; Marshall, A. G. Combating selective ionization in the high resolution mass spectral characterization of complex mixtures. *Faraday Discuss.* **2019**, *218* (0), 29−51.
(26) Chacón-Patiño, M. L.; Smith, D. F.; Hendrickson, C. L.; Marshall, A. G.; Rodgers, R. P. Advances in Asphaltene Petroleomics. Part 4. Compositional Trends of Solubility Subfractions Reveal that Polyfunctional Oxygen-Containing Compounds Drive Asphaltene Chemistry. *Energy Fuels* **2020**, *34* (3), 3013−3030.
(27) Santos Silva, H.; Alfarra, A.; Vallverdu, G.; Begue, D.; Bouyssiere, B.; Baraille, I. Asphaltene Aggregation Studied by Molecular Dynamics Simulations: Role of the Molecular Architecture and Solvents on the Supramolecular or Colloidal Behavior. *Pet. Sci.* **2019**, *16* (3), 669−684.
(28) Santos Silva, H.; Alfarra, A.; Vallverdu, G.; Begue, D.; Bouyssiere, B.; Baraille, I. Impact of H-Bonds and Porphyrins on Asphaltene Aggregation As Revealed by Molecular Dynamics Simulations. *Energy Fuels* **2018**, *32* (11), 11153−11164.
(29) Marshall, A. G.; Rodgers, R. P. Petroleomics: Chemistry of the Underworld. *Proc. Natl. Acad. Sci. U. S. A.* **2008**, *105* (47), 18090−18095.
(30) Marshall, A. G.; Rodgers, R. P. Petroleomics: The Next Grand Challenge for Chemical Analysis. *Acc. Chem. Res.* **2004**, *37* (1), 53−59.
(31) Chacón-Patiño, M. L.; Blanco-Tirado, C.; Orrego-Ruiz, J. A.; Gómez-Escudero, A.; Combariza, M. Y. High Resolution Mass Spectrometric View of Asphaltene−SiO2 Interactions. *Energy Fuels* **2015**, *29* (3), 1323−1331.
(32) Klein, G. C.; Angström, A.; Rodgers, R. P.; Marshall, A. G. Use of Saturates/Aromatics/Resins/Asphaltenes (SARA) fractionation to determine matrix effects in crude oil analysis by electrospray ionization fourier transform ion cyclotron resonance mass spectrometry. *Energy Fuels* **2006**, *20* (2), 668−672.
(33) Gaspar, A.; Zellermann, E.; Lababidi, S.; Reece, J.; Schrader, W. Characterization of Saturates, Aromatics, Resins, and Asphaltenes Heavy Crude Oil Fractions by Atmospheric Pressure Laser Ionization Fourier Transform Ion Cyclotron Resonance Mass Spectrometry. *Energy Fuels* **2012**, *26* (6), 3481−3487.
(34) Palacio Lozano, D. C.; Orrego-Ruiz, J. A.; Barrow, M. P.; Cabanzo Hernandez, R.; Mejía-Ospino, E. Analysis of the molecular weight distribution of vacuum residues and their molecular distillation fractions by laser desorption ionization mass spectrometry. *Fuel* **2016**, *171*, 247−252.
(35) Putman, J. C.; Gutiérrez Sama, S.; Barrère-Mangote, C.; Rodgers, R. P.; Lobinski, R.; Marshall, A. G.; Bouyssière, B.; Giusti, P. Analysis of Petroleum Products by Gel Permeation Chromatography Coupled Online with Inductively Coupled Plasma Mass Spectrometry and Offline with Fourier Transform Ion Cyclotron Resonance Mass Spectrometry. *Energy Fuels* **2018**, *32* (12), 12198−12204.
(36) Putman, J. C.; Moulian, R.; Smith, D. F.; Weisbrod, C. R.; Chacón-Patiño, M. L.; Corilo, Y. E.; Blakney, G. T.; Rumancik, L. E.; Barrère-Mangote, C.; Rodgers, R. P.; et al. Probing Aggregation Tendencies in Asphaltenes by Gel Permeation Chromatography. Part 2: Online Detection by Fourier Transform Ion Cyclotron Resonance Mass Spectrometry and Inductively Coupled Plasma Mass Spectrometry. *Energy Fuels* **2020**, *34* (9), 10915−10925.
(37) Gutierrez Sama, S.; Farenc, M.; Barrere-Mangote, C.; Lobinski, R.; Afonso, C.; Bouyssiere, B.; Giusti, P. Molecular Fingerprints and Speciation of Crude Oils and Heavy Fractions Revealed by Molecular and Elemental Mass Spectrometry: Keystone between Petroleomics, Metallopetroleomics, and Petrointeractomics. *Energy Fuels* **2018**, *32* (4), 4593−4605.
(38) Putman, J. C.; Sama, S. G.; Barrère-Mangote, C.; Rodgers, R. P.; Lobinski, R.; Marshall, A. G.; Bouyssière, B.; Giusti, P. Analysis of Petroleum Products by Gel Permeation Chromatography Coupled Online with Inductively Coupled Plasma Mass Spectrometry and Offline with Fourier Transform Ion Cyclotron Resonance Mass Spectrometry. *Energy Fuels* **2018**, *32* (12), 12198−12204.
(39) Putman, J. C.; Moulian, R.; Barrère-Mangote, C.; Rodgers, R. P.; Bouyssiere, B.; Giusti, P.; Marshall, A. G. Probing Aggregation Tendencies in Asphaltenes by Gel Permeation Chromatography. Part 1: Online Inductively Coupled Plasma Mass Spectrometry and Offline Fourier Transform Ion Cyclotron Resonance Mass Spectrometry. *Energy Fuels* **2020**, *34* (7), 8308−8315.
(40) Acevedo, S.; Guzmán, K.; Labrador, H.; Carrier, H.; Bouyssiere, B.; Lobinski, R. Trapping of Metallic Porphyrins by Asphaltene Aggregates: A Size Exclusion Microchromatography with High-Resolution Inductively Coupled Plasma Mass Spectrometric Detection Study. *Energy Fuels* **2012**, *26* (8), 4968−4977.
(41) Gascon, G.; Negrin, J.; Garcia-Montoto, V.; Acevedo, S.; Lienemann, C. P.; Bouyssiere, B. Simplification of Heavy Matrices by Liquid-Liquid Extraction: Part I - How to Separate LMW, MMW, and

https://dx.doi.org/10.1021/acs.energyfuels.0c02687
Energy Fuels XXXX, XXX, XXX−XXX

HMW Compounds in Maltene Fractions of V, Ni, and S Compounds. *Energy Fuels* **2019**, *33* (3), 1922−1927.
(42) Gascon, G.; Vargas, V.; Feo, L.; Castellano, O.; Castillo, J.; Giusti, P.; Acavedo, S.; Lienemann, C. P.; Bouyssiere, B. Size Distributions of Sulfur, Vanadium, and Nickel Compounds in Crude Oils, Residues, and Their Saturate, Aromatic, Resin, and Asphaltene Fractions Determined by Gel Permeation Chromatography Inductively Coupled Plasma High-Resolution Mass Spectrometry. *Energy Fuels* **2017**, *31* (8), 7783−7788.
(43) Gutierrez Sama, S.; Desprez, A.; Krier, G.; Lienemann, C.-P.; Barbier, J.; Lobinski, R.; Barrere-Mangote, C.; Giusti, P.; Bouyssiere, B. Study of the Aggregation of Metal Complexes with Asphaltenes Using Gel Permeation Chromatography Inductively Coupled Plasma High-Resolution Mass Spectrometry. *Energy Fuels* **2016**, *30* (9), 6907−6912.
(44) Caumette, G.; Lienemann, C. P.; Merdrignac, I.; Bouyssiere, B.; Lobinski, R. Fractionation and Speciation of Nickel and Vanadium in Crude Oils by Size Exclusion Chromatography-ICP MS and Normal Phase HPLC-ICP MS. *J. Anal. At. Spectrom.* **2010**, *25* (7), 1123−1129.
(45) Schuler, B.; Meyer, G.; Peña, D.; Mullins, O. C.; Gross, L. Unraveling the Molecular Structures of Asphaltenes by Atomic Force Microscopy. *J. Am. Chem. Soc.* **2015**, *137* (31), 9870−9876.
(46) Schuler, B.; Fatayer, S.; Meyer, G.; Rogel, E.; Moir, M.; Zhang, Y.; Harper, M. R.; Pomerantz, A. E.; Bake, K. D.; Witt, M.; et al. Heavy Oil Based Mixtures of Different Origins and Treatments Studied by Atomic Force Microscopy. *Energy Fuels* **2017**, *31* (7), 6856−6861.
(47) Gonzalez, V.; Taylor, S. E. Asphaltene adsorption on quartz sand in the presence of pre-adsorbed water. *J. Colloid Interface Sci.* **2016**, *480*, 137−145.
(48) Raj, G.; Lesimple, A.; Whelan, J.; Naumov, P. Direct Observation of Asphaltene Nanoparticles on Model Mineral Substrates. *Langmuir* **2017**, *33* (25), 6248−6257.
(49) Qiao, P.; Harbottle, D.; Li, Z.; Tang, Y.; Xu, Z. Interactions of Asphaltene Subfractions in Organic Media of Varying Aromaticity. *Energy Fuels* **2018**, *32* (10), 10478−10485.
(50) Balestrin, L. B. d. S.; Cardoso, M. B.; Loh, W. Using Atomic Force Microscopy To Detect Asphaltene Colloidal Particles in Crude Oils. *Energy Fuels* **2017**, *31* (4), 3738−3746.
(51) Tavakkoli, M.; Panuganti, S. R.; Vargas, F. M.; Taghikhani, V.; Pishvaie, M. R.; Chapman, W. G. Asphaltene Deposition in Different Depositing Environments: Part 1. Model Oil. *Energy Fuels* **2014**, *28* (3), 1617−1628.
(52) Campen, S.; Di Mare, L.; Smith, B.; Wong, J. S. S. Determining the Kinetics of Asphaltene Adsorption from Toluene: A New Reaction-Diffusion Model. *Energy Fuels* **2017**, *31* (9), 9101−9116.
(53) Campen, S. M.; Moorhouse, S. J.; Wong, J. S. S. Effect of Aging on the Removal of Asphaltene Deposits with Aromatic Solvent. *Langmuir* **2019**, *35* (37), 11995−12008.
(54) Daridon, J. L.; Carrier, H. Measurement of Phase Changes in Live Crude Oil Using an Acoustic Wave Sensor: Asphaltene Instability Envelope. *Energy Fuels* **2017**, *31* (9), 9255−9267.
(55) Daridon, J. L.; Cassiède, M.; Nasri, D.; Pauly, J.; Carrier, H. Probing Asphaltene Flocculation by a Quartz Crystal Resonator. *Energy Fuels* **2013**, *27* (8), 4639−4647.
(56) Rudrake, A.; Karan, K.; Horton, J. H. A Combined QCM and XPS Investigation of Asphaltene Adsorption on Metal Surfaces. *J. Colloid Interface Sci.* **2009**, *332* (1), 22−31.
(57) Sauerbrey, G. Verwendung von Schwingquarzen zur Wägung Dünner Schichten und zur Mikrowägung. *Eur. Phys. J. A* **1959**, *155* (2), 206−222.
(58) Keiji Kanazawa, K; Gordon, J. G The Oscillation Frequency of a Quartz Resonator in Contact with Liquid. *Anal. Chim. Acta* **1985**, *175* (C), 99−105.
(59) Johannsmann, D. *The Quartz Crystal Microbalance in Soft Matter Research*; Springer: Cham, 2015.
(60) Ferreira, G. N. M.; da-Silva, A. C.; Tomé, B. Acoustic Wave Biosensors: Physical Models and Biological Applications of Quartz Crystal Microbalance. *Trends Biotechnol.* **2009**, *27* (12), 689−697.
(61) Desprez, A.; Bouyssiere, B.; Arnaudguilhem, C.; Krier, G.; Vernex-Loset, L.; Giusti, P. Study of the Size Distribution of Sulfur, Vanadium, and Nickel Compounds in Four Crude Oils and Their Distillation Cuts by Gel Permeation Chromatography Inductively Coupled Plasma High-Resolution Mass Spectrometry. *Energy Fuels* **2014**, *28* (6), 3730−3737.
(62) Niles, S. F.; Chacón-Patiño, M. L.; Smith, D. F.; Rodgers, R. P.; Marshall, A. G. Comprehensive Compositional and Structural Comparison of Coal and Petroleum Asphaltenes Based on Extrography Fractionation Coupled with Fourier Transform Ion Cyclotron Resonance MS and MS/MS Analysis. *Energy Fuels* **2020**, *34* (2), 1492−1505.
(63) Ren, L.; Wu, J.; Qian, Q.; Liu, X.; Meng, X.; Zhang, Y.; Shi, Q. Separation and Characterization of Sulfoxides in Crude Oils. *Energy Fuels* **2019**, *33* (2), 796−804.
(64) Qiao, P.; Harbottle, D.; Tchoukov, P.; Masliyah, J.; Sjoblom, J.; Liu, Q.; Xu, Z. Fractionation of Asphaltenes in Understanding Their Role in Petroleum Emulsion Stability and Fouling. *Energy Fuels* **2017**, *31* (4), 3330−3337.
(65) Kilpatrick, P. K. Water-in-Crude Oil Emulsion Stabilization: Review and Unanswered Questions. *Energy Fuels* **2012**, *26* (7), 4017−4026.
(66) Spiecker, P. M.; Kilpatrick, P. K. Interfacial Rheology of Petroleum Asphaltenes at the Oil-Water Interface. *Langmuir* **2004**, *20* (10), 4022−4032.
(67) Stanford, L. A.; Rodgers, R. P.; Marshall, A. G.; Czamecki, J.; Wu, X. A. Compositional characterization of bitumen/water emulsion films by negative- and positive-ion electrospray ionization and field desorption/ionization fourier transform ion cyclotron resonance mass spectrometry. *Energy Fuels* **2007**, *21* (2), 963−972.
(68) Stanford, L. A.; Rodgers, R. P.; Marshall, A. G.; Czamecki, J.; Wu, X. A.; Taylor, S. Detailed elemental compositions of emulsion interfacial material versus parent oil for nine geographically distinct light, medium, and heavy crude oils, detected by negative- and positive-ion electrospray ionization fourier transform ion cyclotron resonance mass spectrometry. *Energy Fuels* **2007**, *21* (2), 973−981.
(69) Gascon, G.; Negrín, J.; Montoto, V. G.; Acevedo, S.; Lienemann, C. P.; Bouyssiere, B. Simplification of Heavy Matrices by Liquid-Solid Extraction: Part II-How to Separate the LMW, MMW, and HMW Compounds in Asphaltene Fractions for V, Ni, and S Compounds. *Energy Fuels* **2019**, *33* (9), 8110−8117.
(70) Huang, K.; Szlufarska, I. Friction and Slip at the Solid/Liquid Interface in Vibrational Systems. *Langmuir* **2012**, *28* (50), 17302−17312.
(71) McHale, G.; Newton, M. I. Surface roughness and interfacial slip boundary condition for quartz crystal microbalances. *J. Appl. Phys.* **2004**, *95* (1), 373−380.
(72) Johannsmann, D. Viscoelastic, mechanical, and dielectric measurements on complex samples with the quartz crystal microbalance. *Phys. Chem. Chem. Phys.* **2008**, *10* (31), 4516−4534.

https://dx.doi.org/10.1021/acs.energyfuels.0c02687
Energy Fuels XXXX, XXX, XXX−XXX

Le vanadium présent dans l'asphaltène est réparti sur une large plage de taille d'agrégats allants d'un million de dalton à quelques centaines de dalton selon un étalonnage utilisant des standards de polystyrène. En ce qui concerne le vanadium des fractions extrographie analysées par GPC-ICP MS, le vanadium est contenu pour les fractions Heptane/Toluène et Toluène/THF/MeOH dans les hauts poids moléculaires. Alors que pour la fraction acétone le vanadium est contenu dans les poids moléculaire moyen et faible. Du côté de l'analyse FT-ICR MS, Les familles CH, O, N, S de la fraction Tol/THF/MeOH sont plus aliphatiques que le reste de l'échantillon. D'après les analyses par QCR il s'agit aussi de la fraction la moins stable dans l'heptane et donc la plus prompte à précipiter. Cette étude a permis de montrer que l'extrographie permettait d'obtenir des « familles » de molécule qui avait la même taille d'agrégat en GPC ICP MS pour les fractions Tol/THF/MeOH et Heptane/Tol) mais qui ont des propriétés différentes en termes de précipitation ou analyse moléculaire.

Ce sont dans les hauts poids moléculaire où se concentre le vanadium le plus difficile à extraire lors des étapes de raffinage et notamment dans la fraction Tol/THF/MeOH. Or un des deux asphaltènes contient, en pourcentage de masse, une part plus élevée de fraction Tol/THF/MeOH (50% contre 25%) et il s'agit de l'échantillon le plus complexe à raffiner. Il serait intéressant par la suite de se concentrer sur l'étude de la fraction Tol/THF/MeOH de différent échantillons afin de déterminer quel paramètre impacte la démétallation.

Pour cela un couplage GPC-FT-ICR MS pour analyser les asphaltènes préalablement séparés par extrographie a été développé. La partie III de ce chapitre se concentrera sur l'analyse MS hors ligne puis en ligne par GPC-FT-ICR MS des échantillons d'asphaltènes.

The vanadium present in asphaltene is distributed over a wide range of aggregate sizes ranging from a million dalton to a few hundred dalton according to a calibration using polystyrene standards. As regards vanadium in the extrographic fractions analysed by GPC-ICP MS, vanadium is contained in the Heptane/Toluene and Toluene/THF/MeOH fractions in the high molecular weight range. Whereas for the acetone fraction vanadium is contained in the medium and low molecular weights. In the FT-ICR MS analysis, the CH, O, N, S families of the Tol/THF/MeOH fraction are more aliphatic than the rest of the sample. According to the QCR analyses, it is also the least stable fraction in heptane and therefore the most readily precipitated. This study showed that extrography was able to obtain "families" of molecules that had the same aggregate size in GPC ICP MS for the Tol/THF/MeOH and Heptane/Tol fractions) but had different properties in terms of precipitation or molecular analysis.

It is in the high molecular weight range where vanadium is most difficult to extract in the refining stages and particularly in the Tol/THF/MeOH fraction. However, one of the two asphaltenes contains a higher percentage by mass of the Tol/THF/MeOH fraction (50% versus 25%) and is the most complex sample to refine. It would be interesting thereafter to focus on studying the Tol/THF/MeOH fraction of different samples in order to determine which parameter impacts demetallation.

For this purpose, a GPC-FT-ICR MS coupling to analyze asphaltenes previously separated by extrography has been developed. Part III of this chapter will focus on the off-line and then on-line GPC-FT-ICR MS analysis of asphaltene samples.

Partie III : Couplage de la GPC avec un ICP HR MS et un FT-ICR MS dans le cadre d'analyses d'asphaltènes

Cette partie a fait l'objet d'une série de trois articles publiés dans le journal *Energy and Fuels* de ACS. Ces articles ont été laissés tels qu'ils ont été publiés.

Putman *et al* [124] ont montré en utilisant un couplage hors ligne d'une GPC avec un FT-ICR MS que la partie la plus agrégée est la plus difficile à ioniser et donc à analyser. Or il s'agit de la partie où se concentre le vanadium le plus difficile à extraire et donc la plus intéressante à étudier.

Dans cette troisième partie, le but a été de simplifier la matrice pétrolière avec une première séparation par extrographie suivis d'un couplage en ligne GPC-FT-ICR MS. Le couplage en ligne permet de scanner toutes les 6 secondes les éléments qui sont élués de la colonne et non de récolter une fraction toutes les 4 minutes comme cela a été précédemment effectué ce qui a pour effet de simplifier considérablement la matrice.

Les articles présentés ci-dessous se concentrerons sur l'analyse d'asphaltènes par GPC-FT-ICR MS hors ligne puis en ligne. Le troisième article ajoutera une seconde séparation par extrographie et se concentrera sur l'analyse du vanadium. De plus dans le troisième article, l'asphaltene 2017 sera utilisé comme échantillon. Il s'agit d'un asphaltène provenant du même pétrole brut que celui ayant posé un problème et qui a été étudié chapitre II partie 2. L'objectif est de réussir à analyser les éléments contenus dans les agrégats de hauts poids moléculaire et notamment ceux de la fraction Tol/THF/MeOH de l'asphaltène.

This part was the subject of a series of three articles published to ACS's Energy and Fuels journal. These articles have been left as published.

Putman et al [124] showed using off-line coupling of a GPC with an FT-ICR MS that the most aggregated part is the most difficult to ionize and thus to analyze. This is the most difficult part of the vanadium to extract and therefore the most interesting to study.

In this third part the aim has been to simplify the petroleum matrix with a first separation by extrography followed by in-line coupling GPC-FT-ICR MS. The in-line coupling makes it possible to scan every 6 seconds the elements that are eluted from the column and not to collect a fraction every 4 minutes as was previously done, which has the effect of considerably simplifying the matrix.

The papers presented below will focus on the analysis of asphaltenes by GPC-FT-ICR MS off-line and then on-line. The third paper will add a second extrographic separation and will concentrate on the analysis of vanadium. In addition in the third paper, asphaltene 2017 will be used as a sample. This is an asphaltene derived from the same crude oil as the one which posed a problem and which has been discussed in Chapter II Part 2. The objective is to successfully analyze the elements contained in the high molecular weight aggregates and in particular those in the Tol/THF/MeOH fraction of the asphaltene.

energy&fuels

pubs.acs.org/EF Article

Probing Aggregation Tendencies in Asphaltenes by Gel Permeation Chromatography. Part 1: Online Inductively Coupled Plasma Mass Spectrometry and Offline Fourier Transform Ion Cyclotron Resonance Mass Spectrometry

Jonathan C. Putman, Rémi Moulian, Caroline Barrère-Mangote, Ryan P. Rodgers, Brice Bouyssiere,* Pierre Giusti, and Alan G. Marshall*

Cite This: https://dx.doi.org/10.1021/acs.energyfuels.0c01522 Read Online

ACCESS | Metrics & More | Article Recommendations | Supporting Information

ABSTRACT: This study probes the nanoaggregation behavior of asphaltenes by gel permeation chromatography (GPC). Compounds containing sulfur, vanadium, and nickel were monitored online with elemental detection by inductively coupled plasma mass spectrometry (ICP-MS), and four fractions that vary in nanoaggregation state were analyzed by positive atmospheric pressure photoionization 9.4 T Fourier transform ion cyclotron resonance mass spectrometry ((+)APPI FT-ICR MS). We also highlight some of the challenges associated with the analysis of asphaltene fractions by direct infusion. Nanoaggregate size and monomer ion yield were inversely correlated. The extremely low ionization efficiency for the largest aggregate GPC fractions collected from the asphaltenes limited their characterization to only a few of the most abundant heteroatom classes. However, for all of the characterizable heteroatom classes, aggregation closely correlated with increased relative abundance of larger, more aliphatic compounds. These observations agree with results from the parent whole crude oil, suggesting that the interactions among the more alkylated compounds in asphaltenes may be a major contributor to asphaltene nanoaggregation.

INTRODUCTION

Asphaltenes are one of the most complex and problematic components of petroleum crude oils. Across[1] the entire production chain, asphaltenes pose potential complications.[2] Upstream, on the oil recovery side, asphaltene deposits can block pipelines, often requiring production shutdowns to remedy, resulting in massive losses. Downstream, on the upgrading and refining side, crude oils with high asphaltene concentrations typically have lower yields and higher maintenance costs. Defined purely on the basis of insolubility in an *n*-alkane solution (typically *n*-pentane or *n*-heptane), asphaltenes are not a well-defined (or well-understood) chemical compound class.[3] Compared to their parent crude oils, asphaltenes are typically more aromatic with greater heteroatom content.[4−6] Thus, historically it has long been hypothesized that $\pi-\pi$ stacking and hydrogen bonding between polar compounds drive asphaltene nanoaggregation, which leads to precipitation and eventual deposition. However, asphaltenes are extremely difficult to analyze due to their tendency to aggregate, resulting in very poor ionization efficiency in mass spectrometry analysis.

Linking molecular structure to aggregation potential requires detailed molecular level information. On a bulk scale, asphaltenes are more aromatic and contain more polar compounds than their parent crude oils. However, recent works have started to illuminate the importance of wax-like interactions between more aliphatic compounds that may contribute to asphaltene aggregation. Unstable asphaltenes have also been shown to have higher binding capacities for alkanes and waxes.[7] Berrueco et al. observed a correlation between decreases in fluorescence intensity and UV absorbance in the largest, excluded molecular weight regime of GPC fractions from asphaltenes, petroleum pitch, and coal-derived materials.[8−10] They hypothesized that compounds in the largest, excluded GPC peak may be larger and more aliphatic.[10] Characterization by Fourier transform ion cyclotron resonance mass spectrometry (FT-ICR-MS) for GPC aggregate fractions collected from a typical atmospheric residue revealed a surprisingly strong correlation between nanoaggregation potential and decreased aromaticity.[11] Large, very aliphatic compounds with extremely low ionization efficiencies comprised the largest, most aggregated fractions. Similar observations have been made in several recent works that have reinforced the correlation between alkylation and decreased GPC elution times.[12−15] Interfacially active asphaltenes (IAA) refer to the subfraction (~2%) of the whole asphaltenes that adsorbs at the surface of water droplets. Characterization of the IAA by electrospray ionization mass spectrometry (ESI-MS) and ^{1}H and ^{13}C nuclear magnetic resonance (NMR) spectroscopy revealed that the interfacially active species have a higher molecular weight distribution. The

Received: May 13, 2020
Revised: June 8, 2020
Published: June 8, 2020

https://dx.doi.org/10.1021/acs.energyfuels.0c01522
Energy Fuels XXXX, XXX, XXX−XXX

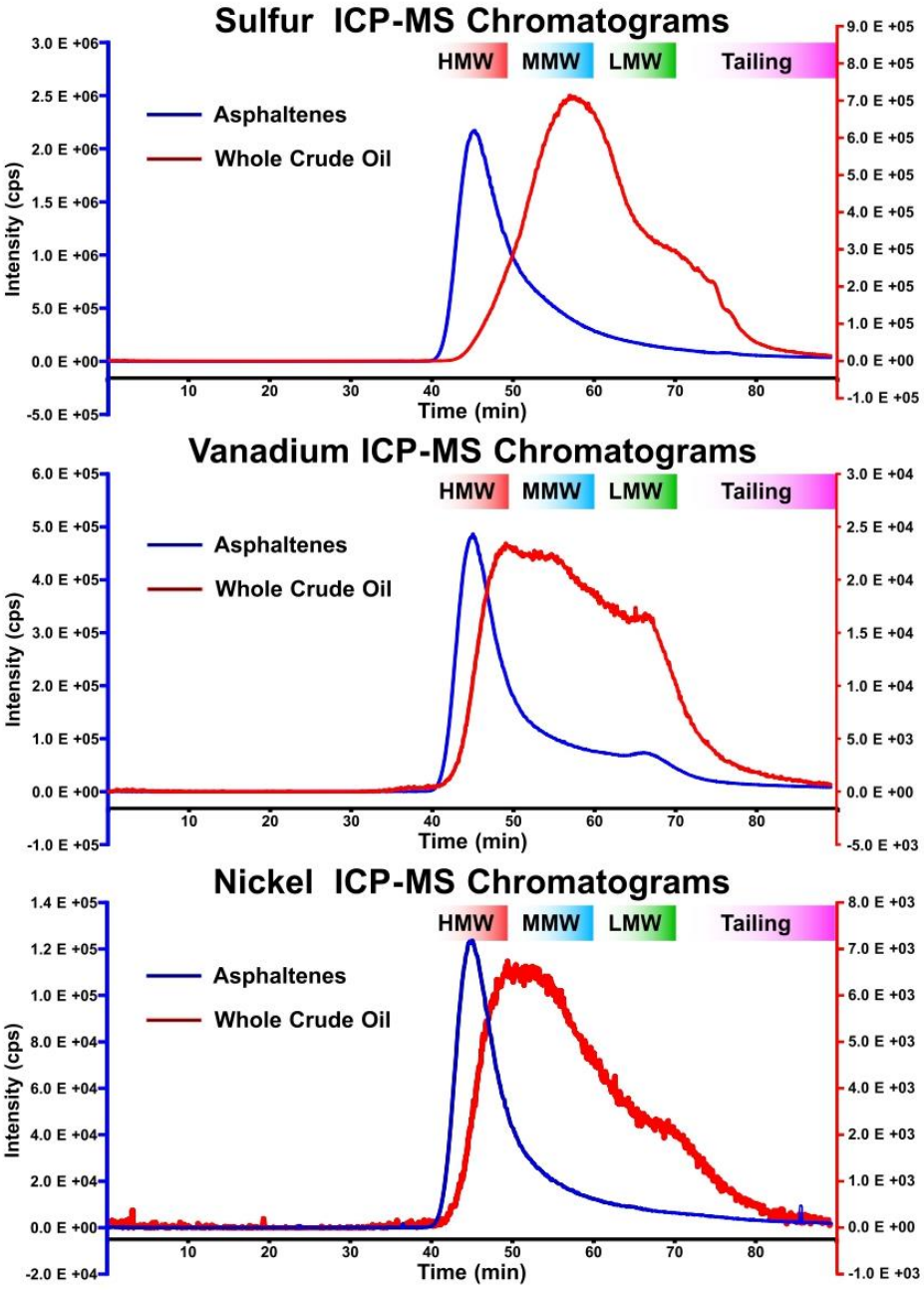

Figure 1. Sulfur (top), vanadium (middle), and nickel (bottom) GPC ICP mass chromatograms. Intensities for the Petrophase 2017 purified asphaltenes are plotted in blue, and parent whole crude oil's intensities are in red. High, medium, and low molecular weight (HMW, MMW, and LMW) and tailing fraction elution ranges are indicated at the top.

IAA was also less aromatic (more aliphatic) on average and was enriched in sulfoxides relative to the whole asphaltenes.[12] Guricza and Schrader also observed similar trends and reported a GPC separation based on both mass and H/C ratio. Compounds with long aliphatic side chains on an aromatic core eluted first, and later-eluting species were primarily condensed polyaromatics with shorter side chains.[16] Works by Panda et al.[14] and Alawani et al.[15] also reported GPC elution based primarily on the degree of alkylation (i.e., more alkylated compounds eluted earliest).

Trace metals present in crude oils also complicate refinery processes by potentially deactivating hydrotreatment and hydrocracking catalysts. Vanadium, nickel, and iron are typically the most abundant metals found in petroleum

https://dx.doi.org/10.1021/acs.energyfuels.0c01522
Energy Fuels XXXX, XXX, XXX−XXX

products. Structurally, these metals are incorporated into heterocyclic macrocycles with four modified pyrrole subunits, known as porphyrins.[17,18] The forces driving asphaltene aggregation are not well understood: although metal-containing petroporphyrins are greatly enriched in precipitated asphaltenes, the nature of their involvement is unknown.[19] To probe the forces driving asphaltene aggregation in a laboratory, gel permeation chromatography (GPC) acts as a proxy for real-world aggregation. However, it is not entirely clear how well on-column nanoaggregation mimics that of asphaltene aggregation in the field.

Inductively coupled plasma mass spectrometry (ICP-MS) coupled with GPC yields quantitative chromatograms, commonly called size distributions or size profiles, for individual elements. For porphyrinic metals like vanadium and nickel, GPC chromatograms generally yield trimodal/multimodal aggregate size profiles sufficiently unique to act as "fingerprints" for petroleum samples.[20,21] The aggregate size profiles also help determine the cut points between GPC aggregate fractions. Significant effort in recent years has been made to understand the importance of GPC aggregate size distributions regarding specific refinery problems. GPC size profiles have been determined for saturates, aromatics, resins, and asphaltenes fractions,[21,22] distillation cuts,[20] and isolated interfacial material.[23] Ideally, analytes should not interact with the GPC stationary phase at all, and elution should be dictated entirely by hydrodynamic volume.[24] Completely eliminating potential surface effects during GPC separations is difficult, if not impossible,[25,26] and mobile phase and column conditions should be chosen to ensure that hydrodynamic volume is the dominant retention mechanism.[10] Even so, caution should be taken not to infer too much from GPC results on their own. For that reason, results presented here will discuss aggregation tendencies observed during GPC separations. In this way, we hope to probe the relationship between the forces driving on-column aggregation and asphaltene nanoaggregation.

Four GPC fractions corresponding to various aggregate sizes were collected from an Arabian heavy crude oil and its corresponding purified asphaltenes for further analysis by 9.4 T Fourier transform ion cyclotron resonance mass spectrometry (FT-ICR-MS). For petroleum product and complex mixtures, differences in ionization efficiency and aggregation tendency between compounds result in the preferential detection of the most easily ionized species. Although ionization bias can be partially overcome by chromatographic separations,[27,28] the choice of ionization method is still critical. Here, we chose positive-ion atmospheric pressure photoionization ((+)APPI), which is believed to be the most suitable method for characterization of asphaltenes.[29−31] Although APPI is well known to preferentially ionize aromatic compounds, ionization is more uniform than electrospray.[29,32] This work is the first part of a two-part study investigating the molecular composition of the PetroPhase 2017 asphaltene sample across a GPC elution profile. Here, we focus on the results from offline fraction collection and direct infusion and highlight some of the challenges we faced with that approach. In part 2, we shall examine the benefits of coupling the GPC method with online detection by 21T FT-ICR-MS, which reveals a more comprehensive molecular characterization.

■ EXPERIMENTAL METHODS

Instrumentation and Materials. An AKTA*purifier* liquid chromatography system equipped with a UV-900 multiwavelength UV absorbance detector and a Frac-950 fraction collector (GE Healthcare Bio-Sciences, Pittsburgh, PA, USA) was used to perform the GPC separation. As previously described, three Shodex preparative GPC columns were connected in series (KF-2004, KF-2002.5, and KF-2001) (Showa Denko America, Inc., New York, NY, USA).[11] The flow rate was set to 3 mL/min with 100% ACS reagent-grade xylene (Scharlab, S.L., Gato Pérez, Barcelona, Spain). Most of the eluent was directed to a fraction collector by a postcolumn split, and the low-flow outlet from the splitter (~40 μL/min) was diverted to an ICP-MW instrument for elemental detection (Thermo Scientific Element XRsector field ICP-HRMS). ICP experimental conditions have been described extensively in previous works.[11,20,21,33,34]

A custom-built adapter was used to interface the APPI source (ThermoFisher Scientific, San Jose, CA, USA) with the front stage of a custom-built 9.4 T FT-ICR mass spectrometer.[29,35−37] Samples were analyzed by positive APPI with the source set to a vaporization temperature of 350 °C. To avoid sample oxidation, N_2 was used for the sheath gas (50 psi) and the auxiliary gas (32 mL/min). Direct infusion experiments of the samples and fractions were performed at a concentration of 100 μg/mL toluene and a flow rate of 50 μL/min. Analysis of each sample consisted of the coaddition of 100 time-domain transients (each with a 6 s acquisition period) followed by Hanning apodization, Fourier transformation with one zero fill, and broad-band phase correction.[38] The resulting absorption-mode FT-ICR mass spectra had a resolving power greater than 1 100 000 at m/z 500. Predator Analysis and PetroOrg were used to perform calibration and data processing.[36,39]

Purified Asphaltenes. Asphaltenes were isolated from an Arabian heavy crude oil provided by Total according to the standard ASTM D6560-12 method.[40] Once isolated, the asphaltenes were further purified to remove occluded material. Depending on the sample, occluded material can account for as much as 50 wt % of asphaltenes.[41,42] Purification to remove occluded material was performed by four iterations of maceration followed by Soxhlet extraction with clean n-C_7 for 5 h (20 h total) as previously reported.[43] The purified asphaltenes are also referred to as the PetroPhase 2017 asphaltene sample, as they were obtained as part of an international collaborative effort to study asphaltenes (Asphaltene 2017; Asphaltene Characterization Interlaboratory Study for PetroPhase 2017. In *Proceedings of the 18th International Conference on Petroleum Phase Behavior and Fouling*, Le Havre, France, June 11−15, 2017).[44]

■ RESULTS AND DISCUSSION

Aggregate Size Distributions for Sulfur, Vanadium, and Nickel. Online detection by ICP-MS was utilized during the GPC fractionation to monitor ^{32}S, ^{51}V, and ^{58}Ni isotopes. The mass chromatograms in Figure 1 show that compared to the starting whole crude oil, in red, the mass distributions of the asphaltenes, in blue, shift dramatically to a more aggregated (earlier eluting) state. For the asphaltenes more than one-half of the ICP-MS chromatogram area and more than one-half of the total mass recovered elute in the most-aggregated, highest MW GPC fraction. The mass profiles for sulfur (Figure 1a) exhibit pseudo-monomodal distributions, but the whole crude oil profile centers around the medium and low-MW fractions, whereas the mass profile of the asphaltenes is centered in the high-MW aggregate fraction, in accord with the area distributions and mass recoveries shown in Tables 1 and 2. For the asphaltenes, ~70% of the recovered mass eluted in the largest aggregate high-MW fraction, compared to ~7% for the parent crude oil. The poor recovery of ~75% with xylene as the mobile phase prompted a change in mobile phase to tetrahydrofuran (THF). The eluent was visibly yellowish during the first blank THF injection, likely indicating adsorption of asphaltenic material to the stationary phase. As shown in Table S1, the total mass recovery improved to ~93%

https://dx.doi.org/10.1021/acs.energyfuels.0c01522
Energy Fuels XXXX, XXX, XXX−XXX

Table 1. Average and % RSD for the Mass Recovery and Area Distributions from the Arabian Heavy Crude Parent Oil Sample (n = 3)

fraction	mass recovery (%)	^{32}S area (%)	^{51}V area (%)	^{58}Ni area (%)
high MW	7.4 ± 3.1	3.5 ± 0.3	14.2 ± 0.6	15.3 ± 0.6
medium MW	54.3 ± 5.4	43.3 ± 1.2	37.5 ± 0.9	40.4 ± 0.4
low MW	26.1 ± 6.7	30.0 ± 0.7	27.6 ± 0.4	21.1 ± 0.2
tailing	12.3 ± 0.9	15.7 ± 1.1	10.0 ± 1.4	11.9 ± 0.5
total	93.4 ± 5.6	100	100	100

Table 2. Average and % RSD for the Normalized Mass Recovery and Area Distributions from the Purified Asphaltene Sample (Asphaltene 2017) (n = 3)

fraction	mass recovery (%)	^{32}S area (%)	^{51}V area (%)	^{58}Ni area (%)
high MW	69.4 ± 3.2	51.4 ± 3.2	49.8 ± 3.1	56.8 ± 3.2
medium MW	20.0 ± 1.3	24.0 ± 1.5	21.0 ± 1.1	19.4 ± 1.4
low MW	7.6 ± 2.6	7.9 ± 0.5	13.2 ± 0.8	7.5 ± 0.6
tailing	3.0 ± 1.4	5.8 ± 1.0	6.6 ± 0.9	6.6 ± 1.0
total	74.9 ± 5.2	100	100	100

with THF, with the high-MW fraction still accounting for ~70% of that. Unfortunately, multiple attempts to collect and characterize these fractions by direct infusion were unsuccessful for reasons which will be discussed below. The difficulties associated with fraction collection and analysis by direct infusion will also be addressed in a follow-up study that utilizes online detection by 21T FT-ICR-MS to help overcome the limitations faced during this study. The present results focus on characterization of the GPC aggregate fractions collected with xylene as the mobile phase.

Characterization of Aggregate Fractions by FT-ICR-MS. Further characterization of the asphaltene and its GPC aggregate fractions was performed by positive APPI 9.4 T FT-ICR-MS, and Figure 2 shows the heteroatom class distribution for the whole asphaltene and its GPC aggregate fractions. The most abundant heteroatom classes in the whole asphaltene sample were S_x. When measured quantitatively by ICP-MS, more than one-half of the sulfur elutes in the largest aggregate, high-MW fraction. However, the distribution of S_x and O_xS_y heteroatom classes exhibits similar monomodal distributions, with the relative abundance focused around the medium- and low-MW aggregate fractions. The heteroatom class distributions for the parent crude oil and its GPC fractions are provided in the Supporting Information: whereas some of the heteroatom classes shift slightly toward the higher MW aggregate size in the asphaltenes, none of the sulfur-containing heteroatom classes shifted nearly enough to account for the quantitative shift measured by ICP-MS. The relative abundance for heteroatom classes that contain nitrogen increases as aggregation lessens and is most abundant in the smallest aggregate fractions of the asphaltenes.

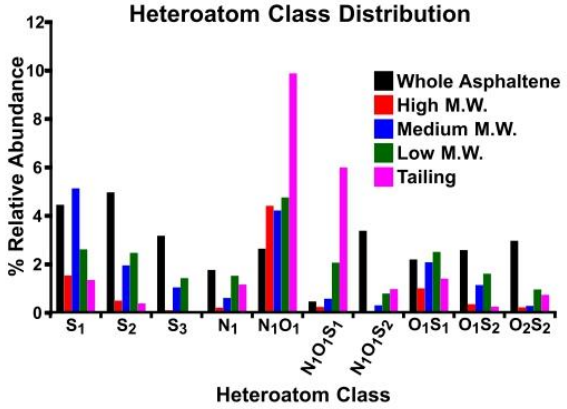

Figure 2. Heteroatom class distributions from (+) APPI 9.4 T FT-ICR mass spectral analysis for the PetroPhase 2017 purified asphaltenes and its corresponding GPC fractions. Heteroatom classes represent the most abundant heteroatom classes for the purified asphaltenes prior to fractionation.

Figure 3 shows the abundance-weighted average H/C ratios for heteroatom class groups and provides a measure of aromaticity of the asphaltenes and its GPC aggregate fractions. Asphaltenes typically have lower H/C ratios (more aromatic) than their parent crude oils. Because more than 50% of the total mass elutes in the most aggregated high-MW fraction, it would be reasonable to expect the high MW fraction to have the lowest H/C ratios. In fact, we see the opposite trend in the GPC aggregate fractions. For almost all of the heteroatom groups, the high-MW aggregate fraction has the highest H/C ratio, indicating that aggregate size is inversely related to aromaticity. That result is consistent with our previous work on an atmospheric residual sample.[11] Stated concisely, as aggregation increases, there is a general trend toward more aliphatic species. The only two exceptions likely result from our inability to satisfactorily characterize the HC and O_x heteroatom groups. As shown in Figure S1, which is a continuation of Figure 2, the most abundant classes in the GPC aggregate fractions were hydrocarbon (HC) and O_x (O_{1-4}). Together, these classes all sum to less than 5% of the relative abundance in the starting whole asphaltene, but they make up well over one-half of the total signal for all of the GPC aggregate fractions except the tailing fractions. This anomaly, combined with the composition of these heteroatom classes (discussed below and shown in Figure S2), likely indicates contamination in the HC and O_x heteroatom classes. However,

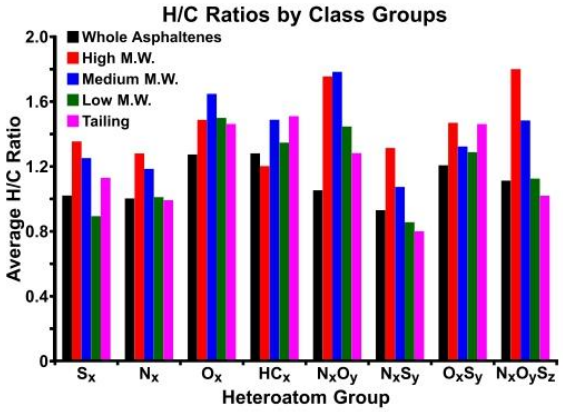

Figure 3. Average H/C ratios for the heteroatom class groups from the purified asphaltenes and its corresponding GPC aggregate fractions.

https://dx.doi.org/10.1021/acs.energyfuels.0c01522
Energy Fuels XXXX, XXX, XXX−XXX

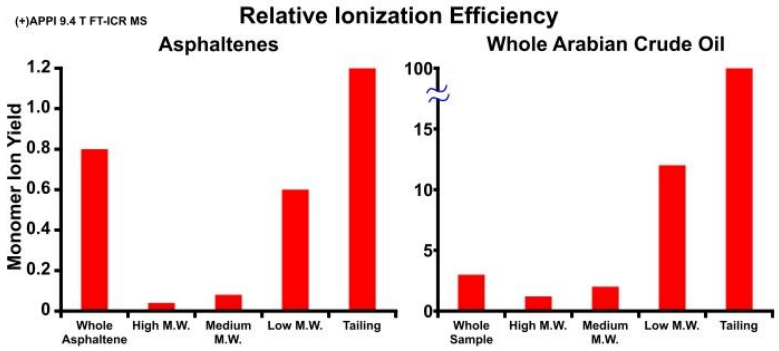

Figure 4. (Right) Monomer ion yields for the Arabian whole crude oil and its fractions. (Left) Monomer ion yields for the purified asphaltenes and its fractions. Ionization efficiencies were calculated from the inverse of the ion accumulation periods used to collect the FT-ICR mass spectra (see text). Those values were then normalized to the tailing fraction from the whole crude oil. Both the whole crude oil and the purified asphaltenes show an inverse relationship between ionization efficiency and aggregate size.

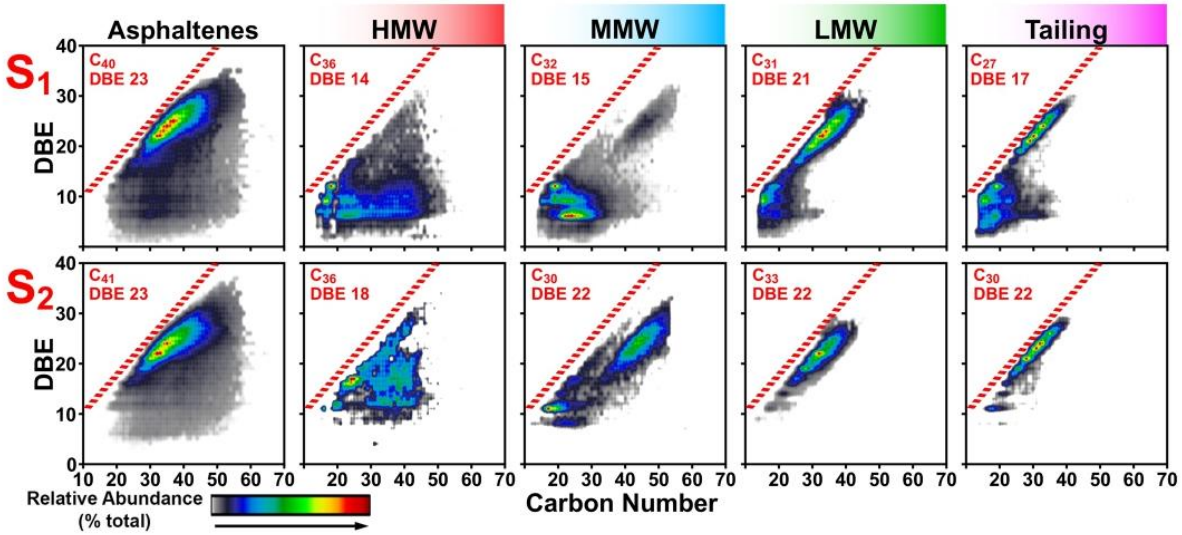

Figure 5. Positive-ion APPI-derived isoabundance-contoured plots of double-bond equivalents vs carbon number for the S_1 class (top) and S_2 class (bottom) for the asphaltenes and its corresponding GPC fractions. Red dashed lines represent the polycyclic aromatic hydrocarbon planar limit.[47,48]

they are included in the Supporting Information in the interest of full transparency.

No apparent trends in the heteroatoms classes or groups explain why the ICP-MS mass profiles (and the mass recovery) shifted to >50% in the largest aggregate GPC fraction of the asphaltenes. However, low ionization efficiencies limited the amount of molecular characterization possible for the GPC aggregate fractions. Asphaltenes are already notoriously difficult to ionize, but the large aggregate GPC fractions were even more challenging. Figure 4 shows the monomer ion yields for the parent crude oil, the asphaltenes, and their GPC aggregate fractions. Calculated from the inverse of the accumulation period required to reach a target number of ions, monomer ion yield provides a qualitative comparison of ionization efficiencies.[27,45] For both the crude oil and the asphaltenes, aggregate size is correlated inversely with monomer ion yield: the largest aggregate fractions ionize least efficiently. The high- and medium-MW aggregate fractions from the asphaltenes required 20−30 s accumulation periods, compared to just a few milliseconds to accumulate the same number of ions in the tailing fraction of the parent crude oil. Such long accumulation periods mean that any chemical contaminants introduced from blowing down large volumes of solvents can completely swamp the sample signal. It took several attempts to sufficiently minimize sources of chemical contamination to obtain useful data. However, there were still chemical contaminant peaks ~1000× greater in magnitude than the signal from the sample. The high-magnitude contaminant peaks resulted in large fluctuations in the mass error, which made it difficult to identify a Kendrick series[46] to enable calibration. Ultimately, each spectrum had to be broken up into 50−100 Da segments and calibrated separately before the resultant peak lists were recombined and molecular formulas could be assigned reliably. Also, due to the dynamic range limitation of our instrument (~50 000), characterization was limited to only the most abundant heteroatom classes.

Molecular Composition of GPC Nanoaggregate Fractions from Asphaltenes. Figure 5 shows isoabun-

https://dx.doi.org/10.1021/acs.energyfuels.0c01522
Energy Fuels XXXX, XXX, XXX−XXX

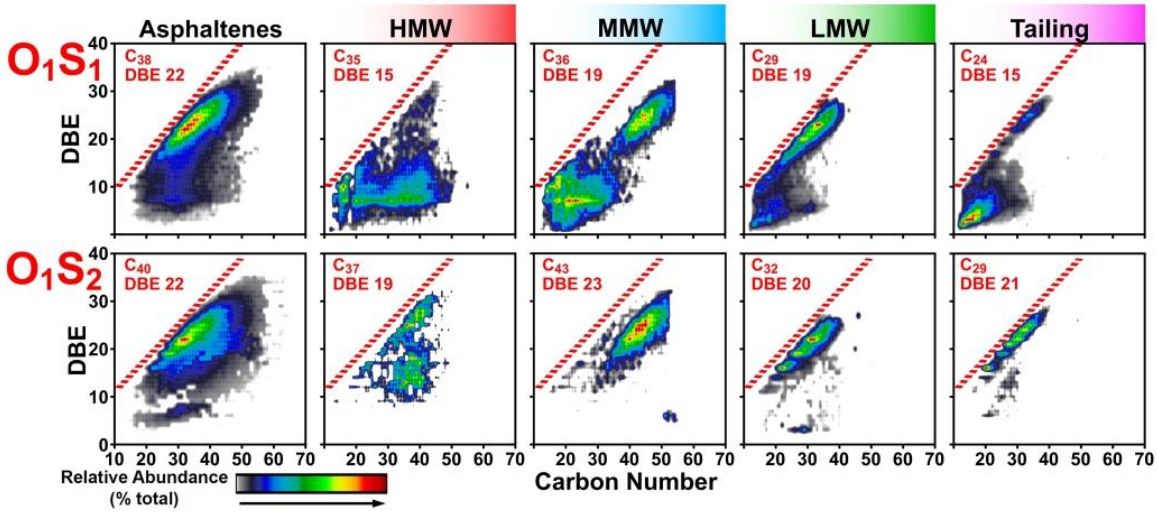

Figure 6. Positive ion APPI-derived isoabundance-contoured plots of double-bond equivalents vs carbon number for the O_1S_1 class (top) and O_1S_2 class (bottom) for the asphaltenes and its corresponding GPC fractions. Red dashed lines represent the polycyclic aromatic hydrocarbon planar limit.

dance-contoured plots of double-bond equivalents (DBE = number of rings plus double bonds to carbon) vs carbon number for the S_1 (top) and S_2 (bottom) heteroatom classes, which had the greatest relative abundance in the asphaltenes prior to fractionation. The abundance-weighted average carbon number and average DBE are displayed in the corner of each plot. On the far left, plots for the whole asphaltenes exhibit a fairly typical compositional range for asphaltenes with distributions out to ~60 carbons, average carbon numbers of ~40−41, and average DBE values of ~23. The red dashed lines represent the polycyclic aromatic hydrocarbon (PAH) planar limit and provide a comparison of aromaticity for the aggregate fractions.[47,48] On the far right, the tailing fraction has a lower average number of carbons than the whole sample and does not contain any species with greater than ~40 carbons. The most abundant hot spots for both classes are highly aromatic and occupy locations very close to the PAH planar limit. The compositional range for the low-MW GPC aggregate fraction is slightly displaced from the PAH planar limit, but both classes still contain highly aromatic species. The medium-MW GPC fraction, shown in the middle of Figure 6, occupies a compositional range even further displaced from the PAH planar limit. Species present with DBE greater than 20 are more alkylated with a distribution from ~40 to 55 carbons. In the lower DBE range, the hot spot at DBE 6 in the S1 heteroatom class corresponds to a benzothiophene core (8 aromatic carbons) and as many as 40 aliphatic carbons are present as alkyl substitutions. Together, the compositional range spanned by the tailing, low-MW, and medium-MW reconstitutes the distribution of the whole asphaltenes fairly well for both heteroatom classes. The largest aggregate, high-MW fraction continues the observed trends, and the distribution is significantly more aliphatic. The high-MW fraction has the lowest average DBE and the greatest average carbon number for both classes. The compositional range corresponds to compounds that are the most aliphatic, and the distribution becomes less aromatic as aggregate size increases. The most abundant species likely have ~2−4 aromatic rings, as nonaromatics ionize very poorly by APPI, and likely contain very long alkyl chains. It is interesting to note that compounds with DBE 6 and 50 carbons are likely entrained material that coprecipitated with the purified asphaltenes, because they should be soluble in heptane on their own. As shown in Figure 6, the same observations discussed above were also made for the O_1S_1 and O_1S_2 heteroatom classes, which were among the most abundant heteroatom classes in the whole asphaltene prior to fractionation. The average composition shifts to larger, more aliphatic compounds as aggregate size increases.

Note that the compositional range spanned by the whole asphaltenes can be more or less reconstructed from those for the fractions for those heteroatom classes. S_x and O_xS_y classes were among the most abundant prior to fractionation; however, as discussed above, HC and O_x accounted for more than one-half of the relative abundance in the asphaltenes fractions. The isoabundance-contoured plots for the HC, O_1, and O_2 heteroatom classes are included in the Supporting Information to highlight the limitations of fraction collection and analysis by direct infusion for difficult to ionize/analyze samples. Compared to the compositional range spanned prior to fractionation, the distributions for the fractions, shown in Figure S2, could not come close to reconstructing that for the whole asphaltenes. Especially for the O_x classes, the only observable features in the composition of the fractions are almost exclusively hot spots that correspond to chemical contaminant peaks.

The heteroatom class distribution and isoabundance-contoured plots for the HC, S_1, S_2, and O_1S_1 heteroatom classes from the whole crude oil and its corresponding GPC aggregate fractions are included in the Supporting Information. The heteroatom class distribution (Figure S3) shows that the most abundant classes for the whole crude oil were HC, S_1, S_2, and O_1S_1. It is difficult to draw meaningful conclusions from the heteroatom class distributions for the corresponding GPC aggregate fractions alone, but the compositions of the HC, S_1, S_2, and O_1S_1 heteroatom classes are shown in Figure S4 (listed from top to bottom). The composition of the whole crude oil

https://dx.doi.org/10.1021/acs.energyfuels.0c01522
Energy Fuels XXXX, XXX, XXX−XXX

is shown at the far left, and the tailing fraction is shown at the far right. As reported previously[11] and as observed in the asphaltene aggregate fractions, the composition becomes increasingly aliphatic as aggregate size increases. The abundance-weighted average carbon number for the medium-MW fraction is more than double that for the tailing fraction for all four classes, and the average DBE is lower for three out of the four classes. For all four heteroatom classes, any compounds with more than ~40 carbons with DBE less than ~10 elute in the medium- or high-MW aggregate fractions. Note that the composition of the largest aggregate, high-MW fraction is actually higher in aromaticity. The compositional range for the S_1 and S_2 heteroatom classes in the high-MW fraction is similar to that for the tailing fraction. Structural differences similar to those reported by Chacon-Patiño et al. (i.e., archipelago vs island) may account for the differences in aggregation potential.[27] However, the compositional range spanned by the HC and O_1S_1 heteroatom classes in the high-MW fraction more closely resembles that for the asphaltene fraction. Those classes exhibit pseudobimodal distributions with part centered close to the PAH limit in the high-DBE region and long, aliphatic, alkyl substitutions observed in the low-DBE region.

■ CONCLUSIONS

Monomer ion yield and aggregation state were strongly correlated in both the crude oil and the asphaltenes. The monomer ion yields of the two largest aggregate GPC fractions (high MW and medium MW) from the asphaltenes were ~1000 times lower than that of the least aggregated, tailing fraction from the whole crude. Due to the extremely low monomer ion yields in these fractions, analysis was limited to only the most abundant heteroatom classes in the asphaltenes. Note that it is difficult, if not impossible, to determine the extent to which the observed heteroatom classes represent the actual composition of the high- and medium-MW GPC fractions; it is entirely possible that additional heteroatom classes are present but ionize so poorly due to their aggregation state that they are not observed. However, for all of the heteroatom classes that we were able to characterize, both in the whole crude oil and in the purified asphaltenes, we observed a strong correlation between aggregation tendency and more aliphatic compounds. As aggregate size decreased, the composition shifted toward more condensed aromatics. No clear evidence of polar functionalities driving aggregation during the GPC separation was observed. A follow-up study will utilize online GPC with detection by 21 T FT-ICR-MS to overcome the limitations associated with fraction collection and direct infusion experiments.

■ ASSOCIATED CONTENT

Supporting Information

The Supporting Information is available free of charge at https://pubs.acs.org/doi/10.1021/acs.energyfuels.0c01522.

Average and % RSD for the normalized mass recovery from the purified asphaltene sample with THF as diluent and mobile phase (n = 3); positive-ion APPI-derived isoabundance-contoured plots of double-bond equivalents vs carbon number for the HC, O_1, and O_2 heteroatom classes which were most abundant in the high-MW GPC aggregate fraction; positive-ion APPI-derived isoabundance-contoured plots of double-bond equivalents vs carbon number for the HC, O_1, and O_2 heteroatom classes which were most abundant in the high-MW GPC aggregate fraction; heteroatom class distributions from (+) APPI 9.4 T FT-ICR mass spectral analysis of the whole Arabian crude oil and its corresponding GPC fractions; isoabundance contoured plots of double-bond equivalents vs carbon number derived from (+) APPI analysis of the whole crude oil and its GPC aggregate fractions; zoom insets of two mass segments from the broad-band mass spectra of the purified asphaltene and its GPC fractions; average H/C ratios for the heteroatom class groups from the parent whole crude oil and its corresponding GPC aggregate fractions (PDF)

■ AUTHOR INFORMATION

Corresponding Authors

Brice Bouyssiere − *International Joint Laboratory−iC2MC: Complex Matrices Molecular Characterization TRTG, BP 27, Harfleur 76700, France; TOTAL Raffinage Chimie TRTG, BP 27, Harfleur 76700, France; Institut des Sciences Analytiques et de Physico-chimie pour l'Environnement et les Materiaux, Universite de Pau et des Pays de l'Adour, E2S UPPA, CNRS, IPREM UMR5254, Pau 64053, France;* orcid.org/0000-0001-5878-6067; Phone: +33(0) 559 407 752; Email: Brice.bouyssiere@univ-pau.fr; Fax: +33(0) 559 407 781

Alan G. Marshall − *National High Magnetic Field Laboratory and Department of Chemistry and Biochemistry, Florida State University, Tallahassee, Florida 32310, United States;* orcid.org/0000-0001-9375-2532; Phone: 850-644-0529; Email: marshall@magnet.fsu.edu; Fax: 850-644-1366

Authors

Jonathan C. Putman − *National High Magnetic Field Laboratory and Department of Chemistry and Biochemistry, Florida State University, Tallahassee, Florida 32310, United States; Exum Instruments, Denver, Colorado 80223, United States*

Rémi Moulian − *International Joint Laboratory−iC2MC: Complex Matrices Molecular Characterization TRTG, BP 27, Harfleur 76700, France; TOTAL Raffinage Chimie TRTG, BP 27, Harfleur 76700, France; Institut des Sciences Analytiques et de Physico-chimie pour l'Environnement et les Materiaux, Universite de Pau et des Pays de l'Adour, E2S UPPA, CNRS, IPREM UMR5254, Pau 64053, France*

Caroline Barrère-Mangote − *International Joint Laboratory−iC2MC: Complex Matrices Molecular Characterization TRTG, BP 27, Harfleur 76700, France; TOTAL Raffinage Chimie TRTG, BP 27, Harfleur 76700, France*

Ryan P. Rodgers − *National High Magnetic Field Laboratory, Department of Chemistry and Biochemistry, and Future Fuels Institute, Florida State University, Tallahassee, Florida 32310, United States; International Joint Laboratory−iC2MC: Complex Matrices Molecular Characterization TRTG, BP 27, Harfleur 76700, France; Institut des Sciences Analytiques et de Physico-chimie pour l'Environnement et les Materiaux, Universite de Pau et des Pays de l'Adour, E2S UPPA, CNRS, IPREM UMR5254, Pau 64053, France;* orcid.org/0000-0003-1302-2850

Pierre Giusti − *International Joint Laboratory−iC2MC: Complex Matrices Molecular Characterization TRTG, BP 27,*

https://dx.doi.org/10.1021/acs.energyfuels.0c01522
Energy Fuels XXXX, XXX, XXX−XXX

Harfleur 76700, France; TOTAL Raffinage Chimie TRTG, BP 27, Harfleur 76700, France; orcid.org/0000-0002-9569-3158

Complete contact information is available at: https://pubs.acs.org/10.1021/acs.energyfuels.0c01522

Notes

The authors declare no competing financial interest.

■ ACKNOWLEDGMENTS

This work was performed at the National High Magnetic Field Laboratory ICR User Facility, which is supported by the National Science Foundation Division of Chemistry through Cooperative Agreements DMR-1157490 and DMR-1644779, the State of Florida, Conseil Régional d'Aquitaine (20071303002PFM), and FEDER (31486/08011464). The authors thank TOTAL for supplying oil samples and Steven M. Rowland for helpful discussions and feedback.

■ REFERENCES

(1) Becker, C. H.; Gillen, K. T. *Anal. Chem.* **1984**, *56* (9), 1671−1674.
(2) Akbarzadeh, K.; Hammami, A.; Kharrat, A.; Zhang, D.; Allenson, S.; Creek, J.; Kabir, S.; Jamaluddin, A.; Marshall, A. G.; Rodgers, R. P.; Mullins, O. C.; Solbakken, T. *Oilfield Rev.* **2007**, *19* (2), 22−43.
(3) Fan, T.; Buckley, J. S. *Energy Fuels* **2002**, *16* (6), 1571−1575.
(4) Miller, J. T.; Fisher, R. B.; Thiyagarajan, P.; Winans, R. E.; Hunt, J. E. *Energy Fuels* **1998**, *12* (6), 1290−1298.
(5) Rogel, E.; Roye, M.; Vien, J.; Miao, T. *Energy Fuels* **2015**, *29* (4), 2143−2152.
(6) Buenrostro-Gonzalez, E.; Groenzin, H.; Lira-Galeana, C.; Mullins, O. C. *Energy Fuels* **2001**, *15* (4), 972−978.
(7) Orea, M.; Ranaudo, M. A.; Lugo, P.; López, L. *Energy Fuels* **2016**, *30* (10), 8098−8113.
(8) Hansen, B. E.; Malmros, O.; Turner, N. R.; Stenby, E. H.; Andersen, S. I. In *Proceedings of Light Metals*, New Orleans, LA, 2001; pp 559−564.
(9) Lazaro, M. J.; Islas, C. A.; Herod, A. A.; Kandiyoti, R. *Energy Fuels* **1999**, *13* (6), 1212−1222.
(10) Berrueco, C.; Venditti, S.; Morgan, T. J.; Álvarez, P.; Millan, M.; Herod, A. A.; Kandiyoti, R. *Energy Fuels* **2008**, *22* (5), 3265−3274.
(11) Putman, J. C.; Gutiérrez Sama, S.; Barrère-Mangote, C.; Rodgers, R. P.; Lobinski, R.; Marshall, A. G.; Bouyssière, B.; Giusti, P. *Energy Fuels* **2018**, *32*, 12198−12204.
(12) Qiao, P.; Harbottle, D.; Tchoukov, P.; Masliyah, J.; Sjoblom, J.; Liu, Q.; Xu, Z. *Energy Fuels* **2017**, *31*, 3330−3337.
(13) Molnárné Guricza, L.; Schrader, W. *Fuel* **2018**, *215*, 631−637.
(14) Panda, S. K.; Alawani, N. A.; Lajami, A. R.; Al-Qunaysi, T. A.; Muller, H. *Fuel* **2019**, *235*, 1420−1426.
(15) Alawani, N. A.; Panda, S. K.; Lajami, A. R.; Al-Qunaysi, T. A.; Muller, H. *Energy Fuels* **2020**, *34*, 5414−5425.
(16) Ghislain, T.; Molnarne Guricza, L.; Schrader, W. *Rapid Commun. Mass Spectrom.* **2017**, *31* (2016), 495−502.
(17) Xu, H.; Que, G.; Yu, D.; Lu, J. *Energy Fuels* **2005**, *19* (6), 517−524.
(18) López, L.; Lo Mónaco, S.; Richardson, M. *Org. Geochem.* **1998**, *29* (1-3), 613−629.
(19) Gascon, G.; Vargas, V.; Feo, L.; Castellano, O.; Castillo, J.; Giusti, P.; Acavedo, S.; Lienemann, C. P.; Bouyssiere, B. *Energy Fuels* **2017**, *31* (8), 7783−7788.
(20) Desprez, A.; Bouyssiere, B.; Arnaudguilhem, C.; Krier, G.; Vernex-Loset, L.; Giusti, P. *Energy Fuels* **2014**, *28*, 3730−3737.
(21) Gutierrez Sama, S.; Desprez, A.; Krier, G.; Lienemann, C.-P.; Barbier, J. J.; Lobinski, R.; Barrere-Mangote, C.; Giusti, P.; Bouyssiere, B. *Energy Fuels* **2016**, *30* (9), 6907−6912.
(22) Cui, Q.; Nakabayashi, K.; Ma, X.; Miyawaki, J.; Al-Mutairi, A.; Marafi, A. M.; Park, J.-I.; Yoon, S.-H.; Mochida, I. *Energy Fuels* **2017**, *31* (7), 6637−6648.
(23) Ligiero, L. M.; Bouriat, P.; Dicharry, C.; Passade-Boupat, N.; Lalli, P. M.; Rodgers, R. P.; Barrère-Mangote, C.; Giusti, P.; Bouyssiere, B. *Energy Fuels* **2017**, *31* (2), 1065−1071.
(24) Lathe, G. H.; Ruthven, C. R. J. *Biochem. J.* **1956**, *62* (4), 665−674.
(25) Sato, S.; Takanohashi, T.; Tanaka, R. *Energy Fuels* **2005**, *19* (5), 1991−1994.
(26) Prokai, L.; Simonsick, W. J., Jr. *Rapid Commun. Mass Spectrom.* **1993**, *7* (9), 853−856.
(27) Chacón-Patiño, M. L.; Rowland, S. M.; Rodgers, R. P. *Energy Fuels* **2018**, *32* (1), 314−328.
(28) Rowland, S. M.; Robbins, W. K.; Corilo, Y. E.; Marshall, A. G.; Rodgers, R. P. *Energy Fuels* **2014**, *28* (8), 5043−5048.
(29) McKenna, A. M.; Marshall, A. G.; Rodgers, R. P. *Energy Fuels* **2013**, *27* (3), 1257−1267.
(30) Itoh, N.; Aoyagi, Y.; Yarita, T. *J. Chromatogr. A* **2006**, *1131* (1−2), 285−288.
(31) Robb, D. B.; Covey, T. R.; Bruins, a. P. *Anal. Chem.* **2000**, *72* (15), 3653−3659.
(32) Andreatta, G.; Bostrom, N.; Mullins, O. C. *Langmuir* **2005**, *21* (7), 2728−2736.
(33) Giusti, P.; Nuevo Ordonez, Y.; Philippe Lienemann, C.; Schaumloffel, D.; Bouyssiere, B.; Lobinski, R. *J. Anal. At. Spectrom.* **2007**, *22* (1), 88−92.
(34) Caumette, G.; Lienemann, C.-P.; Merdrignac, I.; Paucot, H.; Bouyssiere, B.; Lobinski, R. *Talanta* **2009**, *80* (2), 1039−1043.
(35) Kaiser, N. K.; Quinn, J. P.; Blakney, G. T.; Hendrickson, C. L.; Marshall, A. G. *J. Am. Soc. Mass Spectrom.* **2011**, *22* (8), 1343−1351.
(36) Blakney, G. T.; Hendrickson, C. L.; Marshall, A. G. *Int. J. Mass Spectrom.* **2011**, *306* (2−3), 246−252.
(37) Purcell, J. M.; Hendrickson, C. L.; Rodgers, R. P.; Marshall, A. G. b. *Anal. Chem.* **2006**, *78* (16), 5906−5912.
(38) Xian, F.; Hendrickson, C. L.; Blakney, G. T.; Beu, S. C.; Marshall, A. G. *Anal. Chem.* **2010**, *82* (21), 8807−8812.
(39) Corilo, Y. E. *PetroOrg. Software*; Florida State University: Tallahassee, FL,2017.
(40) ASTM D6560. *Standard Test Method for Determination of Asphaltenes (Heptane Insolubles) in Crude Petroleum and Petroleum Products*; ASTM International: West Conshohocken, PA, 2017; www.astm.org.
(41) Derakhshesh, M.; Bergmann, A.; Gray, M. R. *Energy Fuels* **2013**, *27* (4), 1748−1751.
(42) Strausz, O. P.; Torres, M.; Lown, E. M.; Safarik, I.; Murgich, J. *Energy Fuels* **2006**, *20* (5), 2013−2021.
(43) Chacón-Patiño, M. L.; Vesga-Martínez, S. J.; Blanco-Tirado, C.; Orrego-Ruiz, J. A.; Gómez-Escudero, A.; Combariza, M. Y. *Energy Fuels* **2016**, *30* (6), 4550−4561.
(44) Giusti, P.; Bouyssière, B.; Carrier, H.; Afonso, C. *Energy Fuels* **2018**, *32*, 2641.
(45) Chacón-Patiño, M. L.; Rowland, S. M.; Rodgers, R. P. *Energy Fuels* **2017**, *31* (12), 13509−13518.
(46) Hughey, C. A.; Hendrickson, C. L.; Rodgers, R. P.; Marshall, A. G.; Qian, K. *Anal. Chem.* **2001**, *73* (19), 4676−4681.
(47) Hsu, C. S.; Lobodin, V. V.; Rodgers, R. P.; McKenna, A. M.; Marshall, A. G. *Energy Fuels* **2011**, *25* (5), 2174−2178.
(48) Lobodin, V. V.; Marshall, A. G.; Hsu, C. S. *Anal. Chem.* **2012**, *84* (7), 3410−3416.

energy&fuels

pubs.acs.org/EF Article

Probing Aggregation Tendencies in Asphaltenes by Gel Permeation Chromatography. Part 2: Online Detection by Fourier Transform Ion Cyclotron Resonance Mass Spectrometry and Inductively Coupled Plasma Mass Spectrometry

Jonathan C. Putman, Rémi Moulian, Donald F. Smith, Chad R. Weisbrod, Martha L. Chacón-Patiño, Yuri E. Corilo, Greg T. Blakney, Leah E. Rumancik, Caroline Barrère-Mangote, Ryan P. Rodgers, Pierre Giusti, Alan G. Marshall,* and Brice Bouyssière*

Cite This: https://dx.doi.org/10.1021/acs.energyfuels.0c02158 Read Online

ACCESS | Metrics & More | Article Recommendations

ABSTRACT: This work is the second installment of a study that probes the aggregation behavior of asphaltenes by gel permeation chromatography (GPC). In part 1, analysis of GPC aggregate fractions collected from the 2017 PetroPhase asphaltene sample by direct infusion revealed an inverse correlation between aggregate size and aromaticity. However, characterization of the largest aggregate fractions by direct infusion was hampered by solvent contaminant peaks and dynamic range limitations due to the extremely low ionization efficiencies of the larger, more aliphatic species that comprise those fractions. Here, we couple the GPC separation with online detection by positive atmospheric pressure photoionization ((+)APPI) 21 T Fourier transform ion cyclotron resonance mass spectrometry (FT-ICR MS) to overcome those problems and reveal that the most abundant species that comprise the largest aggregate segment are indeed the most aliphatic. The ability to characterize difficult-to-analyze samples, like asphaltenes, is the first major advantage of online coupling. Another benefit is the increased chromatographic resolution afforded by online coupling, which enables a finer examination in the most aggregated region and reveals a local trend opposed to the global trend. The very first species to elute in the largest aggregates were more condensed polyaromatic compounds, and the larger, more aliphatic species elute shortly thereafter in much greater relative abundance.

INTRODUCTION

Notoriously one of the most problematic components of crude oils—asphaltenes—can complicate every stage of the production chain.[1] On the recovery side, asphaltene deposition in pipelines can require production shutdowns to remove the blockage. On the refinery side, high asphaltene concentrations typically decrease a crude oil's yield and, simultaneously, increase maintenance costs. Asphaltenes are also possibly the most polydisperse and compositionally complex mixture in the world.[2−6] Unfortunately, asphaltenes are not a well-understood chemical compound class partly due to their poor definition: insolubility in an *n*-alkane solution, typically *n*-pentane or *n*-heptane.[7] Based on bulk properties, asphaltenes typically contain higher concentrations of polar heteroatoms and are more aromatic than their parent crude oils.[8−10] On the basis of these typical characteristics, it has long been believed that asphaltene nanoaggregation is driven primarily by $\pi-\pi$ stacking and hydrogen bonding between polar compounds. However, linking chemical functionalities to aggregation potential requires detailed molecular-level information, and the tendency of asphaltenes to aggregate results in very poor ionization efficiency and makes them extremely difficult to analyze.

Despite the challenges associated with the analysis of asphaltenes, recent work has begun to reveal that waxlike interactions between more aliphatic compounds may play a more important role in asphaltene aggregation than previously known. Berrueco et al. hypothesized that the earliest-eluting (most aggregated) molecular weight regime of gel permeation chromatography (GPC) fractions from asphaltenes, petroleum pitch, and coal-derived materials are composed of larger, more aliphatic compounds based on lower fluorescence and UV absorbance in this region.[11−13] GPC aggregate fractions collected from a typical atmospheric residue and characterized by positive-ion atmospheric pressure photoionization 9.4 T Fourier transform ion cyclotron resonance ((+)APPI) FT-ICR) mass spectrometry revealed aromaticity to vary inversely with aggregation potential.[14] The largest, most aggregated fractions were composed of large, very aliphatic compounds that ionize extremely poorly. In interfacially active asphaltenes (~2% subfraction that absorbs to the surface of water droplets), characterization by electrospray ionization mass

Received: June 29, 2020
Revised: August 3, 2020
Published: August 5, 2020

https://dx.doi.org/10.1021/acs.energyfuels.0c02158
Energy Fuels XXXX, XXX, XXX−XXX

spectrometry (ESI-MS) and ^{1}H and ^{13}C nuclear magnetic resonance (NMR) spectroscopy revealed a larger molecular weight distribution in the interfacially active species compared to the whole asphaltenes. The interfacially active asphaltenes were also more aliphatic on average and enriched in sulfoxides compared to the whole asphaltenes.[15] In another study, it has also been shown that unstable asphaltenes have higher binding capacities for alkanes and waxes.[16] In fact, several recent studies have observed similar trends and reported GPC elution based on both mass and H/C ratio, with the more alkylated compounds eluting earliest.[17−19]

Gel permeation chromatography (GPC) can help probe the forces driving asphaltene aggregation by acting as a proxy for studying aggregation in a laboratory. GPC is often coupled online with detection by inductively coupled plasma mass spectrometry (ICP MS), thereby enabling the quantitative determination of individual elements. GPC ICP MS chromatograms are commonly termed size distributions or size profiles. Most commonly, sulfur is monitored along with the most abundant heavy metals in petroleum products (vanadium, nickel, and iron). Heavy metals are of interest due to their potential to deactivate hydrotreatment and hydrocracking catalysts during upgrading and refinery processes. Vanadium, nickel, and iron exist structurally in petroleum as porphyrins (heterocyclic macrocycles with four modified pyrrole subunits).[20,21] Metal-containing petroporphyrins are enriched in precipitated asphaltenes, but their exact role in asphaltene aggregation is unknown.[22] GPC ICP MS chromatograms for porphyrinic metals typically exhibit multimodal/trimodal aggregate size distributions that provide "fingerprints" for petroleum samples.[23,24] The determination of GPC aggregate size profiles can provide insight into specific refinery problems, and the method has been applied to saturates, aromatics, resins, and asphaltene fractions,[24,25] distillation cuts,[23] and isolated interfacial material.[26] However, it is not entirely clear how well GPC aggregation mimics "real-world" asphaltene aggregation in the field because elimination of possible surface effects during GPC separations is difficult, if not impossible.[27,28] GPC elution should be dictated entirely by hydrodynamic volume, and although that ideal may not be achievable, the appropriate choice of mobile phase and column conditions can help to ensure than hydrodynamic volume is the dominant elution mechanism.[13,29] To ensure that we do not infer too much from GPC results on their own, however, we shall discuss results with regard to aggregation tendencies observed during GPC elution.

In the analysis of complex mixtures, especially asphaltenes, ionization biases arise from differences in ionization efficiencies and aggregation tendencies, resulting in the preferential detection of the species that ionize most efficiently. Chromatographic separations help to overcome ionization biases by simplifying the sample matrix,[2,30] but just as important is the choice of ionization method. Positive-ion atmospheric pressure photoionization ((+)APPI) is widely thought to be the most compatible method for asphaltenes.[5,31,32] Despite the well-known ionization biases of aromatic compounds, APPI ionizes more uniformly compared to electrospray, which is why it was selected for this study,[5,33] which is the second installment of a study that investigates the aggregation tendencies and molecular composition of the PetroPhase 2017 asphaltene sample by use of GPC. In part 1, GPC aggregate fractions were collected from the PetroPhase 2017 asphaltene sample and analyzed by direct infusion.[34] Monomer ion yields and aggregation state were strongly correlated. The asphaltene fractions that were most aggregated ionized ∼1000 times less efficiently than the least aggregated fractions in the whole crude oil. For all of the heteroatom classes observed in both the whole crude oil and the asphaltenes, the aggregate state and the relative abundance of larger, more alkylated species were closely correlated. The composition shifted toward more condensed polyaromatic species as aggregation decreased. The results from part 1 suggested that interactions between more aliphatic compounds may be a major contributor to aggregation. However, the extremely low monomer ion yields for these fractions limited our ability to characterize the asphaltenes by direct infusion to only a few of the most abundant heteroatom classes. By coupling the GPC separation with online detection by 21 T FT-ICR MS, this study overcomes some of the challenges and limitations encountered when asphaltene fractions were characterized by direct infusion. To further improve our ability to characterize the most aggregated regions of the GPC profile, which contains compounds with extremely poor ionization efficiencies, 4% (v/v) anisole was added to the postcolumn eluent to act as a dopant for detection by (+)APPI. Tetrahydrofuran (THF) on its own is compatible with (+)APPI, but anisole was added because it has been shown to be a very effective charge exchange dopant to improve ionization for compounds with low ionization efficiencies.[35] We did observe increased sensitivity in the largest aggregate region with the addition of anisole, and we hoped that it would translate to improved compositional coverage. The addition of anisole shifts the ionization process to favor the formation of radical cations; however, no significant differences in the number of species identified or the compositional coverage with anisole were observed.

Very few previous reports have combined chromatographic methods with online detection by FT-ICR MS to characterize petroleum products and/or asphaltenes.[36] Several close mass differences are critical to resolve in the analysis of petroleum products. Two particularly important mass differences are the 3.4 mDa (S_1H_4 vs C_3) and 1.1 mDa ($^{13}C_1H_3{}^{32}S_1$ vs C_4). These close mass differences make online detection by high-resolution MS difficult on a chromatographic time scale. Often, long transients are required to obtain high mass resolving power, and coaddition of time-domain transients is required to increase signal-to-noise ratio to maintain sufficient dynamic range. For that reason, many studies with online detection by high-resolution MS resemble fraction collection and analysis by direct infusion. One of the first studies that coupled a chromatographic separation with online detection by FT-ICR MS for the analysis of petroleum products divided the chromatogram into two main peaks.[37] Size exclusion chromatography has been coupled to ultrahigh-resolution MS to study asphaltenes only a handful of times. An early work by Ghislain et al. observed a ∼50% higher number of molecular formulas assigned than by direct infusion, and despite the entire elution profile taking less than 5 min, they highlighted several examples of structural isomers that were resolved chromatographically.[17] One of the best examples by Guricaz et al. coupled size exclusion chromatography with a research-type LTQ-Orbitrap Elite mass spectrometer to study asphaltene aggregation.[38] The equivalent of six fractions was achieved through the coaddition of data acquisitions across 1 min periods. They also observed elution according to the H/C ratio. Compounds eluted according to the degree of alkylation;

https://dx.doi.org/10.1021/acs.energyfuels.0c02158
Energy Fuels XXXX, XXX, XXX−XXX

the most aliphatic species eluted earliest, in the more aggregated regions.

EXPERIMENTAL SECTION

Instrumentation and Materials. For online FT-ICR MS, the GPC separation was performed with an Alliance e2695 separation module equipped with a WAT 005319 2 μm precolumn inline filter and a 2998 photodiode array (PDA). All Waters HPLC system components were operated with EMPOWER3 software (Waters Corporation, Milford, MA). The GPC column was a Varian PLgel (50 Å, 7.5 × 300 mm^2, 5 μm) HPLC column (Agilent Technologies, Santa Clara, CA). The flow rate was set to 0.20 mL/min with inhibitor-free HPLC grade (≥99.9%) tetrahydrofuran (THF) (Sigma-Aldrich, St. Louis, MO). Column components and detectors were connected with 0.020 in. stainless steel tubing (IDEX Health and Science LLC). When coupled with ICP MS, the GPC separation was performed with an AKTA purifier liquid chromatography system equipped with a UV-900 multiwavelength UV absorbance detector and a Frac-950 fraction collector (GE Healthcare Bio-Sciences, Pittsburgh, PA). For detection by ICP MS, most of the eluent was directed to waste by a postcolumn split, and ~40 μL/min was diverted to the detector (Thermo Scientific Element XRsector field ICP-HRMS). Differences in extracolumnar volumes between the experimental setup for detection with ICP-MS and 21 T FT-ICR MS were calculated theoretically to align the two chromatograms, and the elution times from a tetraphenyl porphyrin standard were monitored by UV−vis (prior to either postcolumn dilution/split); the porphyrin standard was detected by both ICP-MS and FT-ICR MS to verify that the elution times of the two systems were aligned. Experimental conditions for the ICP MS interface and detection have been described extensively in previous works.[14,23,24,39,40]

The APPI source (ThermoFisher Scientific, San Jose, CA) was set to a vaporization temperature of 350 °C, and N_2 was used for the sheath gas (50 psi) and the auxiliary gas (32 mL/min) to avoid sample oxidation. Experiments were performed on a custom-built hybrid dual ion-trap 21 T FT-ICR mass spectrometer described previously.[41,42] Excitation and detection were performed with a Predator data station.[43] Online detection by 21 T FT-ICR MS yields a mass resolving power of 3400000 at m/z 400 for a single-phase mass spectrum (6.2 s transient duration), yielding 6451 unique assigned molecular formulas (120 ppb RMS error).[36] A 3.1 s transient often maximizes sensitivity and improves scan rate, while maintaining sufficient resolving power to separate the 1.1 mDa mass split out to ~m/z 700. In this study we expected to observe species with molecular weights as great as ~1000 Da, so we chose a 4.5 s transient to maintain resolution of the 1.1 mDa mass split. All spectra were phase-corrected for a mass resolving power of ~2500000 at m/z 400.[44] Predator Analysis and PetroOrg were used to perform mass calibration and to assign peaks.[45,46] For each individual mass spectrum, Excel spreadsheets containing relative abundances for all assigned heteroatom classes and groups were exported from PetroOrg. A custom-made python script was used to parse through and consolidate data from these Excel workbooks to generate extracted ion chromatograms (XICs) for individual heteroatom classes.

Purified Asphaltenes. Starting from an Arabian heavy crude oil provided by Total, asphaltenes were isolated by use of the standard ASTM D6560-12 method.[47] As previously reported,[48] four iterations of maceration followed by Soxhlet extraction with clean n-C_7 for 5 h (20 h total) was performed to further purify the asphaltenes and remove occluded material, which can account for up to 50 wt % of the initial asphaltenes.[49,50] The Arabian heavy purified asphaltenes (aka the PetroPhase 2017 Asphaltenes) were obtained as part of an international collaborative effort to study asphaltenes.[51] The same isolation and purification procedures were also performed for Athabasca Bitumen.

RESULTS AND DISCUSSION

GPC Chromatograms for Asphaltenes. The GPC separation of asphaltenes was performed in duplicate to utilize online detection by both ICP MS and 21 T FT-ICR MS. As shown in Figure 1, GPC ICP MS allows the quantitative

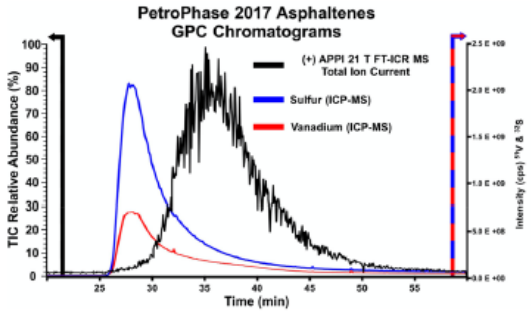

Figure 1. GPC total ion chromatogram (TIC) from (+)APPI 21 T FT-ICR mass spectral analysis of the PetroPhase 2017 asphaltenes plotted in black on the primary axis. Sulfur (blue) and vanadium (red) GPC ICP-MS chromatograms are plotted on the secondary axis on the right.

determination of ^{32}S (blue) and ^{51}V (red) nanoaggregate size distributions. The size profiles exhibit typical asphaltene monomodal distributions that increase sharply on the peak front, are centered at ~28 min, and then decrease slowly on the tailing side until ~55 min. Most of the total sulfur and vanadium elute within the first 5 min of the total exclusion limit in the largest aggregate region (~25−30 min). Figure 1 also shows the (+)APPI total ion chromatogram (TIC) determined by 21 T FT-ICR MS in black. The TIC exhibits a more Gaussian-shaped broad peak that extends from ~25−55 min and is centered at ~36 min.

Figure 2 shows the TIC determined by FT-ICR MS (black) and the corresponding ^{51}V (red) GPC ICP-MS size profile for asphaltenes purified from Athabasca Bitumen. Both of these chromatograms resemble their counterparts from the PetroPhase 2017 asphaltene sample, but the bitumen asphaltenes have higher concentrations of heavy metals. Figure 2 also shows the FT-ICR MS extracted ion chromatogram (XIC) for

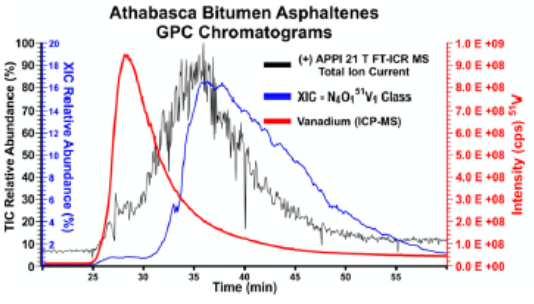

Figure 2. GPC TIC (black) and extracted ion chromatogram (XIC) for the $N_4O_1{}^{51}V_1$ heteroatom class (blue) from the (+)APPI mass spectral analysis of purified Athabasca Bitumen asphaltenes plotted on the left axes. The vanadium (red) GPC ICP-MS chromatogram is plotted on the secondary axis on the right.

https://dx.doi.org/10.1021/acs.energyfuels.0c02158
Energy Fuels XXXX, XXX, XXX−XXX

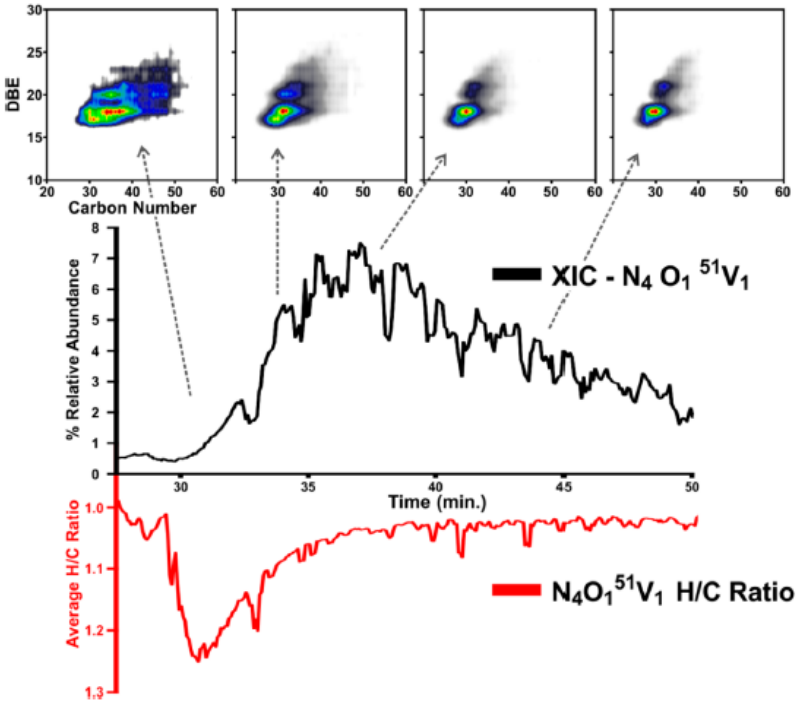

Figure 3. XIC and (+)APPI derived isoabundance color-contoured plots of double-bond equivalents (DBE) vs carbon number shown in order of elution from left to right for the $N_4O_1{}^{51}V_1$ heteroatom class (top) from the analysis of the PetroPhase 2017 asphaltenes. The inverted chromatogram shows the XIC's average H/C ratio (bottom).

the $N_4O_1{}^{51}V_1$ heteroatom class (blue) for comparison. Based on the total ^{52}V signal measured by ICP-MS, the vanadium content of the bitumen asphaltenes is ~1.5 times that of the PetroPhase 2017 asphaltenes. The higher concentration of vanadium makes the bitumen asphaltenes better suited to compare the chromatographic features of the mass profile (GPC ICP-MS) to those of the $N_4O_1{}^{51}V_1$ porphyrin heteroatom class (GPC FT-ICR MS). Approximately half of the total vanadium elutes in the most excluded region, from ~25−30 min; however, the XIC for the $N_4O_1{}^{51}V_1$ heteroatom class (the most abundant of the assigned vanadyl porphyrin classes) increases in relative abundance only slightly and plateaus at ~1% during the most aggregated elution period. The relative abundance begins to increase sharply at ~31 min, after more than half of the total vanadium has already eluted, and reaches its peak maximum of ~16% relative abundance at a time to that for the TIC at ~35 min. From the ~16-fold increase in relative abundance, combined with the ~5-fold decrease in GPC ICP-MS signal for ^{51}V during that time, we can infer qualitatively that the relative ionization efficiencies (aka monomer ion yield) of the vanadyl porphyrins eluting in the largest aggregates is ~80 times lower than those at ~36 min. The difference in monomer ion yield continues to increase with elution time and decreased aggregate size, consistent with previous results.

Online Detection Accesses the Compositional Changes of Asphaltene Species Not Observable by Direct Infusion. In our previous work, we analyzed GPC fractions collected from the same PetroPhase 2017 asphaltene sample by direct infusion with only moderate success. Chemical contaminants up-concentrated during the fraction collection and drying processes made the analysis of fractions collected with THF as the mobile phase impossible (even after several attempts), and results from runs with xylene as the mobile phase were limited to only the most abundance heteroatom classes (S_1, S_2, O_1S_1, and O_1S_2). Coupling the GPC separation with online detection eliminates the contaminant problem. Furthermore, because the dynamic range increases quadratically with magnetic field strength, detection by 21 T FT-ICR MS helped overcome the dynamic range limitations encountered at lower fields. The dynamic range is especially important for difficult-to-analyze samples with low ionization efficiencies (i.e., asphaltenes and their GPC fractions).

With online detection by 21 T FT-ICR MS we can also extract more detailed molecular information than just a heteroatom class relative abundances and gain more insight into why the earliest eluting porphyrins ionize so poorly. For example, Figure 3 shows the XIC for the $N_4O_1{}^{51}V_1$ porphyrin heteroatom class from the PetroPhase 2017 asphaltenes in black. The same XIC is also plotted with the abundance-weighted average H/C ratio as the *y*-axis instead of relative abundance. The average H/C ratio XIC is shown in red with the *y*-axis inverted, and it gives us a measure of aromaticity for the $N_4O_1{}^{51}V_1$ porphyrin heteroatom class.[52] The aromaticity and H/C ratio are inversely related, so the earliest eluting porphyrins are least aromatic, as confirmed by the (+)APPI derived isoabundance color-contoured plots of double-bond

https://dx.doi.org/10.1021/acs.energyfuels.0c02158
Energy Fuels XXXX, XXX, XXX−XXX

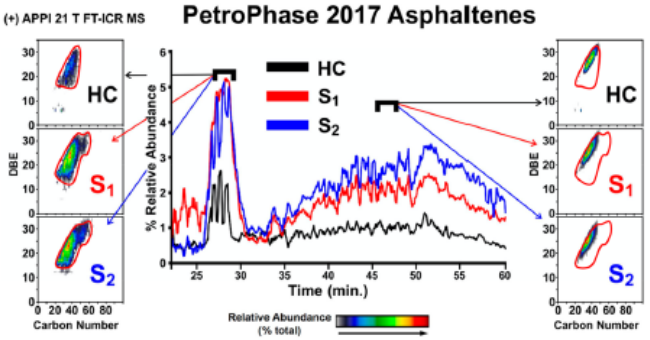

Figure 4. GPC FT-ICR MS extracted ion chromatograms for the hydrocarbon and sulfur heteroatom classes (center). Positive APPI-derived isoabundance contour plots of DBE vs carbon number for the HC class (top), S_1 class (middle), and S_2 class (bottom) with short retention times (left) and long retention times (right). As aggregation decreases, the compositional range for each class moves from more aliphatic species on the left toward condensed polycyclic aromatics on the right.

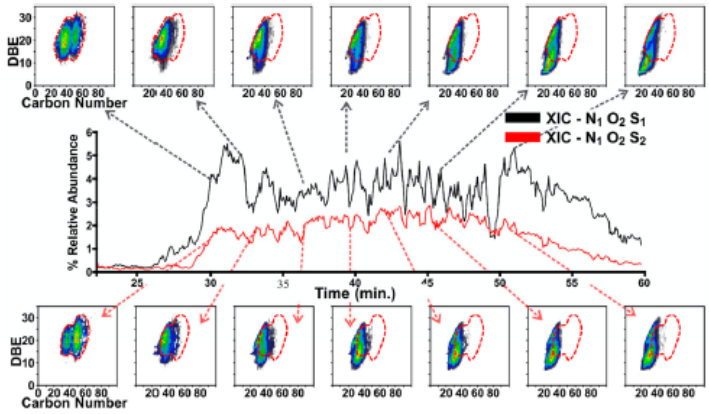

Figure 5. Extracted ion chromatograms and plots of DBE vs carbon number shown in order of elution from left to right for the $N_1O_2S_1$ (top) and $N_1O_2S_2$ (bottom) heteroatom classes from the PetroPhase 2017 asphaltenes. As aggregation decreases, the compositional range shifts toward more condensed aromatics in the high DBE range, and the abundance of lower DBE species increases, possibly indicating a shift in structural motifs (i.e., from thiophenic to sulfidic sulfur).

equivalents vs carbon number for the $N_4O_1{}^{51}V_1$ class (Figure 3, top). The composition of the vanadyl porphyrins eluting in the most aggregated region (leftmost plot) spans the largest carbon number range. As aggregation lessens, the carbon number range narrows and the average H/C ratio decreases to almost 1.0, corresponding to species with very little alkylation on the core, tetrapyrrolic porphyrin structure.[24,53,54] Increased aggregation correlated to decreased aromaticity and greater abundance of more aliphatic species for all of the heteroatom classes observed. Figure 4 confirms that correlation for three of the most abundant heteroatom classes in the whole asphaltenes. GPC FT-ICR MS XICs for the HC, S_1, and S_2 heteroatom classes are shown in black, red, and blue. Plots of carbon number vs DBE for early eluting (left) and later-eluting (right) regions have the distribution for the most aggregated elution period circled in red for comparison. The earliest, most aggregated region spans the widest carbon number range, and as aggregation decreases, the compositional range for all three heteroatom classes moves from more aliphatic species on the left toward condensed polycyclic aromatics on the right.

For the PetroPhase 2017 asphaltene sample, we were able to successfully characterize the S_x heteroatom classes by direct infusion; however, we were not able to obtain molecular information for polyheteroatomic classes, such as $N_xO_yS_z$, in the high molecular weight fraction even after multiple attempts. Online detection grants access to these heteroatom classes by eliminating the need to blow down large volumes of solvents to dry fractions, thereby up-concentrating chemical contaminants. Figure 5 shows the XIC and composition for the $N_1O_2S_1$ and $N_1O_2S_2$ heteroatom classes. The red outlines correspond to the composition of the earliest-eluting species in the largest aggregates. As aggregation decreases, two main trends are apparent. First, in the high DBE range, alkylation decreases, and the composition shifts toward more condensed aromatics. Second, a distribution of lower DBE species emerges as aggregation continues to decrease, which likely indicating a change in the sulfur moiety, possibly from thiophenic (aromatic) to sulfidic (aliphatic) sulfur.

Observations in composition of the O_1S_1, O_1S_2, and O_2S_1 heteroatom classes support the inference that a change in

https://dx.doi.org/10.1021/acs.energyfuels.0c02158
Energy Fuels XXXX, XXX, XXX−XXX

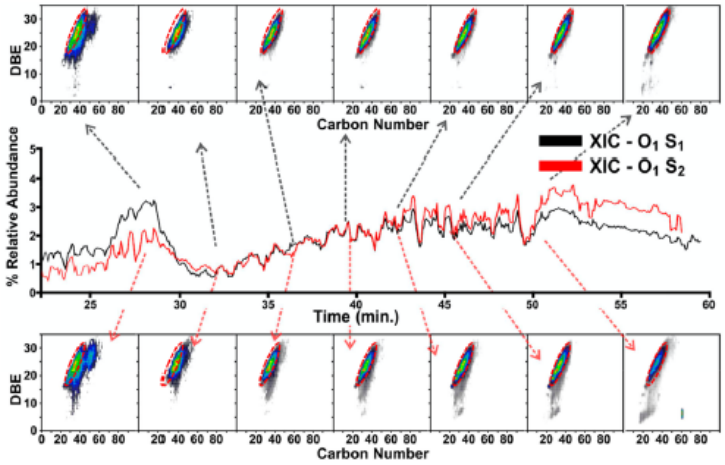

Figure 6. Extracted ion chromatograms and plots of DBE vs carbon number shown in order of elution from left to right for the O_1S_1 (top) and O_1S_2 (bottom) heteroatom classes from the PetroPhase 2017 asphaltenes.

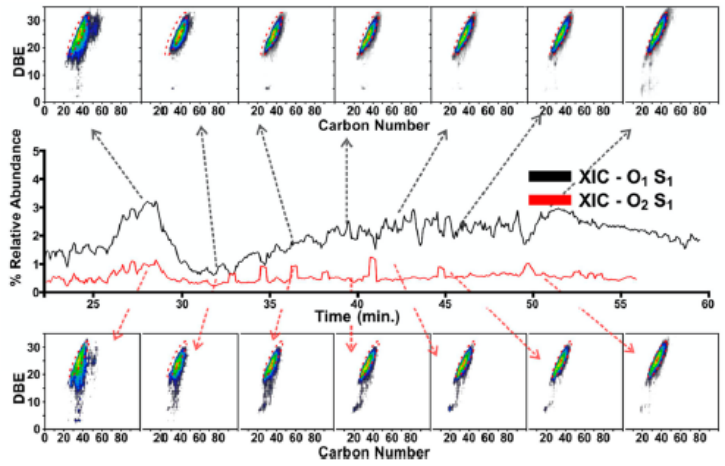

Figure 7. Extracted ion chromatograms and plots of DBE vs carbon number shown in order of elution from left to right for the O_1S_1 (top) and O_2S_1 (bottom) heteroatom classes from the PetroPhase 2017 asphaltenes.

sulfur moieties is likely responsible for the appearance of the second, lower-DBE species in the less aggregated region. Figures 6 and 7 show extracted ion chromatograms and track the composition of those three heteroatom classes. To compare changes with the incorporation of a single oxygen vs a single sulfur heteroatom, both figures show the O_1S_1 XIC in black with the corresponding DBE vs carbon number plots on the top. In black and on the bottom, Figure 6 shows the XIC and composition of the O_1S_2 heteroatom class, whereas Figure 7 shows the XIC and composition of the O_2S_1 heteroatom class. Plots are shown in order of elution from left to right, and the dotted red ovals represent the composition of species that elute latest, in the nonaggregated region. For all three heteroatom classes, the most abundant species in the high DBE region are near the polyaromatic hydrocarbon planar limit and correspond to condensed aromatic compounds with very little alkylation.[55] As aggregate size increases, the degree of alkylation gradually increases. In the largest aggregates, both the O_1S_1 and O_1S_2 heteroatom classes exhibit a bimodal distribution with a second distribution between DBE ~25−30 and ~45−60 carbons. There are also a few species in low abundance with DBE < ~15 that elute with the largest aggregates before ~30 min for both classes. In the O_1S_1 heteroatom class, compounds with DBE < 15 are absent until the latest elution period at ~50 min, but in the O_1S_2 class, low DBE species appear again in low abundance at ~35 min. These species become more numerous, gradually increasing in relative abundance and decreasing in DBE with increasing elution time. The region that elutes last contains the peaks corresponding to species with DBE < 15 for any of the elution regions. Compared to the O_1S_2 class, the opposite trend is observed in the composition of the O_2S_1 heteroatom class in the low-DBE region. As shown in the bottom of Figure 7, the earliest eluting region with the largest

https://dx.doi.org/10.1021/acs.energyfuels.0c02158
Energy Fuels XXXX, XXX, XXX−XXX

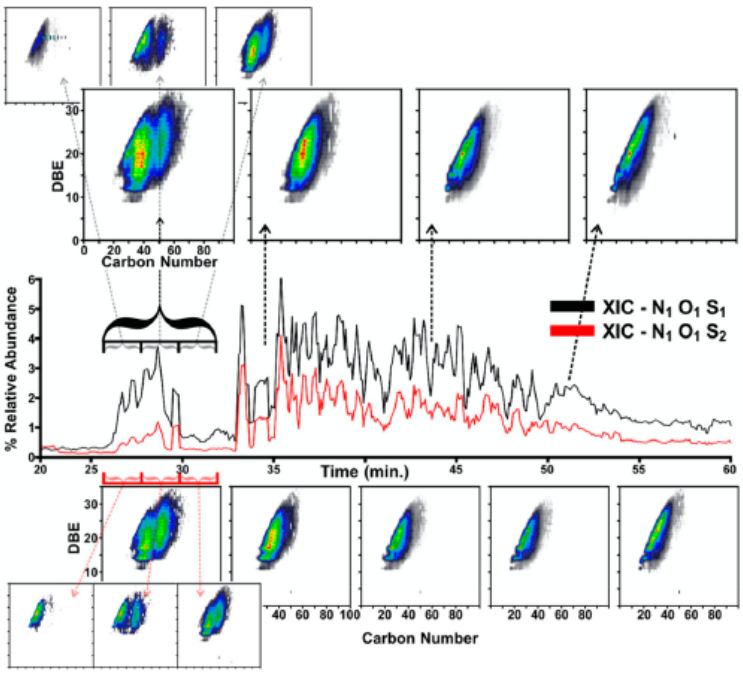

Figure 8. Extracted ion chromatograms and plots of DBE vs carbon number for the PetroPhase 2017 asphaltenes shown in order of elution from left to right for the $N_1O_1S_1$ (top) and $N_1O_1S_2$ (bottom) heteroatom classes. The composition for the most aggregated species exhibits a bimodal distribution. Online detection enables the small overlaid plots to show three discrete segments of that region. The shorter time windows reveal that the first species to elute are actually more aromatic, with DBE ≈ 20−25. Those species are followed closely by more alkylated compounds in much higher relative abundance.

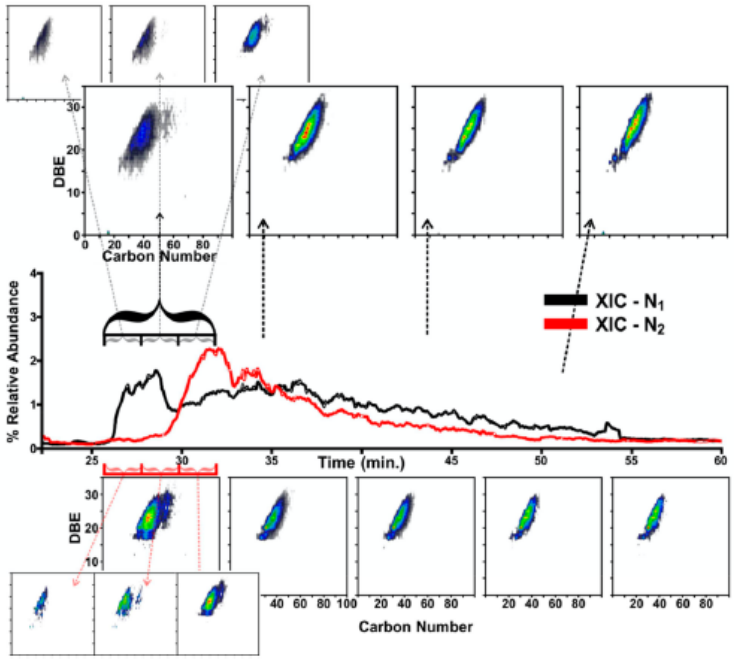

Figure 9. Extracted ion chromatograms and plots of DBE vs carbon number for the PetroPhase 2017 asphaltenes shown in order of elution from left to right for the N_1 (top) and N_2 (bottom) heteroatom classes.

https://dx.doi.org/10.1021/acs.energyfuels.0c02158
Energy Fuels XXXX, XXX, XXX−XXX

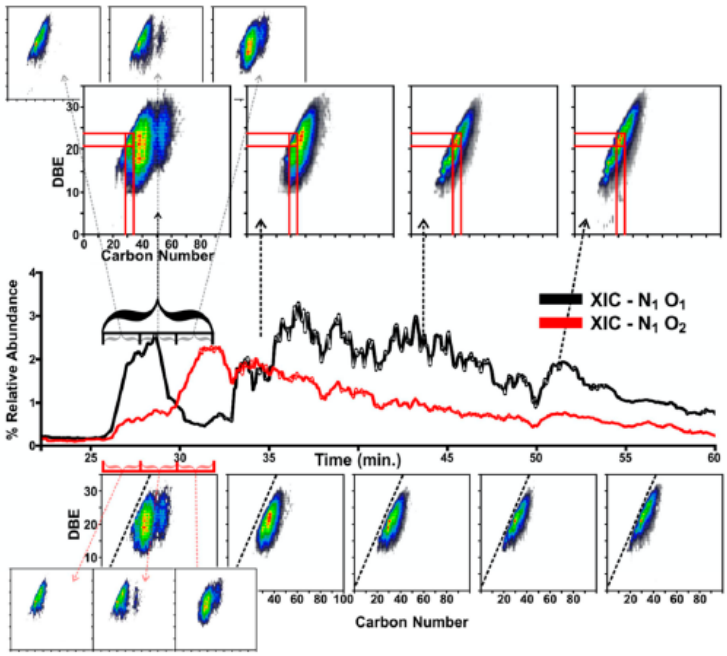

Figure 10. Extracted ion chromatograms and plots of DBE vs carbon number for the PetroPhase 2017 asphaltenes shown in order of elution from left to right for the N_1O_1 (top) and N_1O_2 (bottom) heteroatom classes.

aggregates contains the greatest number of O_2S_1 species with DBE less than 15. As elution time increases, low-DBE O_2S_1 species decrease in number and in relative abundance. On the far right, in the least-aggregated region, only a few O_2S_1 species are observed in extremely low relative abundance.

Improved Chromatographic Resolution with Online Detection Reveals Local Trends That Oppose the Global Trends. The first major advantage with online detection is the ability to track compositional changes for heteroatom classes not observable by direct infusion, making it well suited for analysis of samples with low ionization efficiencies. The second major advantage is the increased chromatographic resolution afforded by online detection. For the $N_1O_1S_1$ and $N_1O_1S_2$ heteroatom classes shown in Figure 8, we observe the same global trends as previously discussed. The XICs for the $N_1O_1S_1$ (black) and $N_1O_1S_2$ (red) heteroatom exhibit a bimodal distribution with a smaller, narrow peak eluting near the total exclusion limit from ~25−30 min and a second, broader, later-eluting hump from ~34−55 min. The isoabundance-contoured plots of DBE vs carbon number on the top correspond to the $N_1O_1S_1$ class, while those on the bottom correspond to the $N_1O_1S_2$ heteroatom class. The plots of DBE vs carbon number directly above and below the XICs show the composition of large elution periods of ~7 min. The longer elution periods reveal the same global trends discussed previously at length. If we were able to successfully track compositional changes for those heteroatom classes by direct infusion (which we were not able to do), we would expect to observe similar global trends. The most aliphatic species elute earliest in the largest aggregates, and aromaticity increases as aggregation lessens at longer elution times. However, the composition of the most aggregated species exhibits a bimodal distribution. Online detection enables the small overlaid plots to reveal three discrete segments of that region. The shorter time windows reveal that the first species to elute are actually more aromatic, with DBE ~ 20−25. Those species are followed closely by more alkylated compounds in much higher relative abundance. Globally, the most aliphatic species elute first in the largest aggregates, but locally, within that region the trend is the opposite. In addition to improving our ability to extract information for difficult-to-analyze samples, the increased chromatographic resolution reveals local trends in most-aggregated region that oppose the global trend for both the $N_1O_1S_1$ and $N_1O_1S_2$ heteroatom classes.

The local trend in the largest aggregates was not limited to polyheteroatomic classes with many polar functional groups. We observed the same local trend in the most aggregated region for all the heteroatom classes we examined. Figure 9 f9 shows the N_1 and N_2 heteroatom classes XICs in black/red and composition on the top/bottom. The XIC for the N_1 heteroatom class reaches its maximum relative abundance of ~2% at ~27 min. Note that the N_2 heteroatom class is offset by ~4 min and stays closer to baseline level during that elution period. At ~30 min, its relative abundance begins to increase, finally reaching its maximum value of just over 2% relative abundance at ~31 min. Globally, the earliest elution window for both heteroatom classes spans the widest carbon number range, and as elution increases and aggregation decreases, the composition shifts toward condensed polyaromatics with very little alkylation. However, locally, within the earliest, most-aggregated elution window, the trend is the opposite. The very first compounds to elute at ~26 min are more aromatic, and by 28 min, the composition has shifted to more aliphatic species with longer alkyl chains in greater abundance.

https://dx.doi.org/10.1021/acs.energyfuels.0c02158
Energy Fuels XXXX, XXX, XXX−XXX

Consistent with the prior discussion, similar trends are observed in the composition of the N_1O_1 and N_1O_2 heteroatom classes, shown in Figure 10. The nonaggregated region is composed of species that correspond to condensed polyaromatic cores, with only short alkyl substitutions. The solid red lines within the carbon number vs DBE plots on the top highlight the most abundant species in the least-aggregated region that elutes last. For the N_1O_1 heteroatom class, these hot spots are located between DBE ~21−24 and carbon numbers ~29−35. In the plots on the bottom that show the composition of the N_1O_2 heteroatom class, the black dashed lines represent the theoretical polyaromatic hydrocarbon limit, or PAH line, and provide an alternative way to compare the changes in aromaticity as a function of aggregate state. In the smallest aggregates, the composition is within ~10 carbons of the PAH line. For both heteroatom classes, as aggregate size increases moving to the left, alkylation increases, and the composition shifts away from the PAH line, and alkylation increases. In the largest aggregate region, species are observed ~40 carbons away from the PAH limit and 60 total carbons in both the N_1O_1 and N_1O_2 heteroatom classes. These species correspond to extremely aliphatic compounds with long alkyl substitutions on the aromatic cores. The compositional space covered by both heteroatom classes exhibits a similar bimodal distribution observed in the most aggregated regions of the $N_xO_yS_z$ and O_xS_y heteroatom classes, and once again, the improved chromatographic resolution afforded by online detection reveals a local trend opposite that of the global trend in this region. The very earliest compounds that elute are actually closer to the PAH limit and are more aromatic. Those species are quickly followed by more alkylated compounds in greater relative abundance.

■ CONCLUSIONS

GPC coupled with online detection successfully overcomes the challenges associated with fraction collection and analysis by direct infusion and reveals that for all heteroatom classes in the PetroPhase 2017 asphaltene sample aggregate size and aromaticity are inversely correlated. The largest aggregate region is composed of the most alkylated species, and the composition shifts toward more aromatic compounds as aggregation decreases. In addition to the ability to characterize samples with extremely low ionization efficiencies, online coupling improves the chromatographic resolution, which enables a closer examination of the most aggregated region. Smaller time segments revealed a local trend in the largest aggregates that opposed the global trend. The very first species to elute in the largest aggregates are actually more aromatic, and more alkylated compounds eluted shortly thereafter in greater relative abundance. Even disregarding the limitations associated with fraction collection and direct infusion, it would be difficult (and certainly impractical) to collect a sufficient number of fractions with short enough time intervals to reveal this local trend in the largest aggregates.

■ AUTHOR INFORMATION

Corresponding Authors

Alan G. Marshall − *National High Magnetic Field Laboratory and Department of Chemistry and Biochemistry, Florida State University, Tallahassee, Florida 32310, United States;* orcid.org/0000-0001-9375-2532; Phone: 1-850-644-0529; Email: marshall@magnet.fsu.edu; Fax: 1-850-644-1366

Brice Bouyssière − *International Joint Laboratory−iC2MC: Complex Matrices Molecular Characterization, TRTG, 76700 Harfleur, France; TOTAL Raffinage Chimie, TRTG, 76700 Harfleur, France; E2S UPPA, CNRS, IPREM, Institut des Sciences Analytiques et de Physico-chimie pour l'Environnement et les Materiaux, UMR5254, Hélioparc, Universite de Pau et des Pays de l'Adour, 64053 Pau, France;* orcid.org/0000-0001-5878-6067; Phone: +33 (0) 559 407 752; Email: brice.bouyssiere@univ-pau.fr; Fax: +33 (0) 559 407 781

Authors

Jonathan C. Putman − *National High Magnetic Field Laboratory and Department of Chemistry and Biochemistry, Florida State University, Tallahassee, Florida 32310, United States; Exum Instruments, Denver, Colorado 80223, United States*

Rémi Moulian − *International Joint Laboratory−iC2MC: Complex Matrices Molecular Characterization, TRTG, 76700 Harfleur, France; TOTAL Raffinage Chimie, TRTG, 76700 Harfleur, France; E2S UPPA, CNRS, IPREM, Institut des Sciences Analytiques et de Physico-chimie pour l'Environnement et les Materiaux, UMR5254, Hélioparc, Universite de Pau et des Pays de l'Adour, 64053 Pau, France*

Donald F. Smith − *National High Magnetic Field Laboratory, Florida State University, Tallahassee, Florida 32310, United States;* orcid.org/0000-0003-3331-0526

Chad R. Weisbrod − *National High Magnetic Field Laboratory, Florida State University, Tallahassee, Florida 32310, United States;* orcid.org/0000-0001-5324-4525

Martha L. Chacón-Patiño − *National High Magnetic Field Laboratory, Florida State University, Tallahassee, Florida 32310, United States;* orcid.org/0000-0002-7273-5343

Yuri E. Corilo − *National High Magnetic Field Laboratory, Florida State University, Tallahassee, Florida 32310, United States*

Greg T. Blakney − *National High Magnetic Field Laboratory, Florida State University, Tallahassee, Florida 32310, United States;* orcid.org/0000-0002-4205-9866

Leah E. Rumancik − *Department of Computer Science, Florida State University, Tallahassee, Florida 32304, United States*

Caroline Barrère-Mangote − *International Joint Laboratory−iC2MC: Complex Matrices Molecular Characterization, TRTG, 76700 Harfleur, France; TOTAL Raffinage Chimie, TRTG, 76700 Harfleur, France*

Ryan P. Rodgers − *National High Magnetic Field Laboratory, Department of Chemistry and Biochemistry, and Future Fuels Institute, Florida State University, Tallahassee, Florida 32310, United States; International Joint Laboratory−iC2MC: Complex Matrices Molecular Characterization, TRTG, 76700 Harfleur, France; E2S UPPA, CNRS, IPREM, Institut des Sciences Analytiques et de Physico-chimie pour l'Environnement et les Materiaux, UMR5254, Hélioparc, Universite de Pau et des Pays de l'Adour, 64053 Pau, France;* orcid.org/0000-0003-1302-2850

Pierre Giusti − *International Joint Laboratory−iC2MC: Complex Matrices Molecular Characterization, TRTG, 76700 Harfleur, France; TOTAL Raffinage Chimie, TRTG, 76700 Harfleur, France;* orcid.org/0000-0002-9569-3158

Complete contact information is available at: https://pubs.acs.org/10.1021/acs.energyfuels.0c02158

https://dx.doi.org/10.1021/acs.energyfuels.0c02158
Energy Fuels XXXX, XXX, XXX−XXX

Notes

The authors declare no competing financial interest.

■ ACKNOWLEDGMENTS

This work was supported by the National Science Foundation Division of Chemistry through Cooperative Agreements No. DMR-11-57490 and DMR-1644779, the State of Florida, Conseil Régional d'Aquitaine (20071303002PFM), and FEDER (31486/08011464). The authors thank TOTAL for supplying oil samples and Steven M. Rowland for helpful discussions and feedback.

■ REFERENCES

(1) Akbarzadeh, K.; Hammami, A.; Kharrat, A.; Zhang, D.; Allenson, S.; Creek, J.; Kabir, S.; Jamaluddin, A.; Marshall, A. G.; Rodgers, R. P.; Mullins, O. C.; Solbakken, T. *Oilf. Rev.* **2007**, *19* (2), 22−43.
(2) Chacón-Patiño, M. L.; Rowland, S. M.; Rodgers, R. P. *Energy Fuels* **2018**, *32* (1), 314−328.
(3) Herod, A. A. *Rapid Commun. Mass Spectrom.* **2010**, *24* (17), 2507−2519.
(4) Herod, A. A.; Bartle, K. D.; Morgan, T. J.; Kandiyoti, R. *Chem. Rev.* **2012**, *112* (7), 3892−3923.
(5) McKenna, A. M.; Marshall, A. G.; Rodgers, R. P. *Energy Fuels* **2013**, *27* (3), 1257−1267.
(6) Purcell, J. M.; Merdrignac, I.; Rodgers, R. P.; Marshall, A. G.; Gauthier, T.; Guibard, I. *Energy Fuels* **2010**, *24*, 2257−2265.
(7) Fan, T.; Buckley, J. S. *Energy Fuels* **2002**, *16* (6), 1571−1575.
(8) Miller, J. T.; Fisher, R. B.; Thiyagarajan, P.; Winans, R. E.; Hunt, J. E. *Energy Fuels* **1998**, *12* (6), 1290−1298.
(9) Rogel, E.; Roye, M.; Vien, J.; Miao, T. *Energy Fuels* **2015**, *29* (4), 2143−2152.
(10) Buenrostro-Gonzalez, E.; Groenzin, H.; Lira-Galeana, C.; Mullins, O. C. *Energy Fuels* **2001**, *15* (4), 972−978.
(11) Hansen, B. E.; Malmros, O.; Turner, N. R.; Stenby, E. H.; Andersen, S. I. In *Proceedings of Light Metals*; New Orleans, LA, 2001; pp 559−564.
(12) Lazaro, M. J.; Islas, C. A.; Herod, A. A.; Kandiyoti, R. *Energy Fuels* **1999**, *13* (6), 1212−1222.
(13) Berrueco, C.; Venditti, S.; Morgan, T. J.; Álvarez, P.; Millan, M.; Herod, A. A.; Kandiyoti, R. *Energy Fuels* **2008**, *22* (5), 3265−3274.
(14) Putman, J. C.; Gutiérrez Sama, S.; Barrère-Mangote, C.; Rodgers, R. P.; Lobinski, R.; Marshall, A. G.; Bouyssière, B.; Giusti, P. *Energy Fuels* **2018**, *32*, 12198.
(15) Qiao, P.; Harbottle, D.; Tchoukov, P.; Masliyah, J.; Sjoblom, J.; Liu, Q.; Xu, Z. *Energy Fuels* **2017**, *31*, 3330−3337.
(16) Orea, M.; Ranaudo, M. A.; Lugo, P.; López, L. *Energy Fuels* **2016**, *30* (10), 8098−8113.
(17) Ghislain, T.; Molnárné Guricza, L.; Schrader, W. *Rapid Commun. Mass Spectrom.* **2017**, *31* (6), 495−502.
(18) Panda, S. K.; Alawani, N. A.; Lajami, A. R.; Al-Qunaysi, T. A.; Muller, H. *Fuel* **2019**, *235*, 1420−1426.
(19) Alawani, N. A.; Panda, S. K.; Lajami, A. R.; Al-Qunaysi, T. A.; Muller, H. *Energy Fuels* **2020**, *34*, 5414.
(20) Xu, H.; Que, G.; Yu, D.; Lu, J. *Energy Fuels* **2005**, *19* (6), 517−524.
(21) López, L.; Lo Mónaco, S.; Richardson, M. *Org. Geochem.* **1998**, *29*, 613−629.
(22) Gascon, G.; Vargas, V.; Feo, L.; Castellano, O.; Castillo, J.; Giusti, P.; Acavedo, S.; Lienemann, C. P.; Bouyssiere, B. *Energy Fuels* **2017**, *31* (8), 7783−7788.
(23) Desprez, A.; Bouyssiere, B.; Arnaudguilhem, C.; Krier, G.; Vernex-loset, L.; Giusti, P. 2014.
(24) Gutierrez Sama, S.; Desprez, A.; Krier, G.; Lienemann, C.-P.; Barbier, J. J.; Lobinski, R.; Barrere-Mangote, C.; Giusti, P.; Bouyssiere, B. *Energy Fuels* **2016**, *30* (9), 6907−6912.
(25) Cui, Q.; Nakabayashi, K.; Ma, X.; Miyawaki, J.; Al-mutairi, A.; Mj, A.; Park, J.; Yoon, S.; Mochida, I. *Energy Fuels* **2017**, *31* (7), 6637.
(26) Ligiero, L. M.; Bouriat, P.; Dicharry, C.; Passade-Boupat, N.; Lalli, P. M.; Rodgers, R. P.; Barrère-Mangote, C.; Giusti, P.; Bouyssiere, B. *Energy Fuels* **2017**, *31* (2), 1065−1071.
(27) Sato, S.; Takanohashi, T.; Tanaka, R. *Energy Fuels* **2005**, *19* (5), 1991−1994.
(28) Prokai, L.; Simonsick, W. J., Jr. *Rapid Commun. Mass Spectrom.* **1993**, *7* (9), 853−856.
(29) Lathe, G. H.; Ruthven, C. R. J. *Biochem. J.* **1956**, *62* (4), 665−674.
(30) Rowland, S. M.; Robbins, W. K.; Corilo, Y. E.; Marshall, A. G.; Rodgers, R. P. *Energy Fuels* **2014**, *28* (8), 5043−5048.
(31) Itoh, N.; Aoyagi, Y.; Yarita, T. *J. Chromatogr. A* **2006**, *1131* (1−2), 285−288.
(32) Robb, D. B.; Covey, T. R.; Bruins, a. P. *Anal. Chem.* **2000**, *72* (15), 3653−3659.
(33) Andreatta, G.; Bostrom, N.; Mullins, O. C. *Langmuir* **2005**, *21* (7), 2728−2736.
(34) Putman, J. C.; Moulian, R.; Barrère-Mangote, C.; Rodgers, R. P.; BOUYSSIERE, B.; Giusti, P.; Marshall, A. G. *Energy Fuels* **2020**, *34*, 8308.
(35) Smith, D. R.; Robb, D. B.; Blades, M. W., 2009.
(36) Putman, J. C.; Smith, D. F.; Weisbrod, C. R.; Rowland, S. M.; Patiño, M. L. C.; Corilo, Y. E.; Blakney, G. T.; Hendrickson, C. L.; Rodgers, R. P.; Marshall, A. G. In *Proceedings of the 67th ASMS Conference on Mass Spectrometry and Allied Topics*, 2019.
(37) Lababidi, S.; Schrader, W. *Rapid Commun. Mass Spectrom.* **2014**, *28* (12), 1345−1352.
(38) Molnárné Guricza, L.; Schrader, W. *Fuel* **2018**, *215*, 631−637.
(39) Giusti, P.; Nuevo Ordonez, Y.; Philippe Lienemann, C.; Schaumloffel, D.; Bouyssiere, B.; Lobinski, R. *J. Anal. At. Spectrom.* **2007**, *22* (1), 88−92.
(40) Caumette, G.; Lienemann, C.-P.; Merdrignac, I.; Paucot, H.; Bouyssiere, B.; Lobinski, R. *Talanta* **2009**, *80* (2), 1039−1043.
(41) Hendrickson, C. L.; Quinn, J. P.; Kaiser, N. K.; Smith, D. F.; Blakney, G. T.; Chen, T.; Marshall, A. G.; Weisbrod, C. R.; Beu, S. C. *J. Am. Soc. Mass Spectrom.* **2015**, *26* (9), 1626−1632.
(42) Smith, D. F.; Podgorski, D. C.; Rodgers, R. P.; Blakney, G. T.; Hendrickson, C. L. *Anal. Chem.* **2018**, *90* (3), 2041−2047.
(43) Blakney, G. T.; Hendrickson, C. L.; Marshall, A. G. *Int. J. Mass Spectrom.* **2011**, *306* (2−3), 246−252.
(44) Xian, F.; Hendrickson, C. L.; Blakney, G. T.; Beu, S. C.; Marshall, A. G. *Anal. Chem.* **2010**, *82* (21), 8807−8812.
(45) Blakney, G. T.; Hendrickson, C. L.; Marshall, A. G. *Int. J. Mass Spectrom.* **2011**, *306* (2−3), 246−252.
(46) Corilo, Y. E. *PetroOrg. Software*; Florida State University: Tallahassee, FL, 2017.
(47) Deleted in proof.
(48) Chacón-Patiño, M. L.; Vesga-Martínez, S. J.; Blanco-Tirado, C.; Orrego-Ruiz, J. A.; Gómez-Escudero, A.; Combariza, M. Y. *Energy Fuels* **2016**, *30* (6), 4550−4561.
(49) Derakhshesh, M.; Bergmann, A.; Gray, M. R. *Energy Fuels* **2013**, *27* (4), 1748−1751.
(50) Strausz, O. P.; Torres, M.; Lown, E. M.; Safarik, I.; Murgich, J. *Energy Fuels* **2006**, *20* (5), 2013−2021.
(51) Giusti, P.; Bouyssière, B.; Carrier, H.; Afonso, C. *Energy Fuels* **2018**, *32*, 2641.
(52) Santos Silva, H.; Sodero, A. C. R.; Korb, J. P.; Alfarra, A.; Giusti, P.; Vallverdu, G.; Béguê, D.; Baraille, I.; Bouyssiere, B. *Fuel* **2017**, *188*, 374−381.
(53) Santos Silva, H.; Sodero, A. C. R.; Korb, J. P.; Alfarra, A.; Giusti, P.; Vallverdu, G.; Béguê, D.; Baraille, I.; Bouyssiere, B. *Fuel* **2017**, *188*, 374−381.
(54) Santos Silva, H.; Alfarra, A.; Vallverdu, G.; Béguê, D.; Bouyssiere, B.; Baraille, I. *Pet. Sci.* **2020**, *17* (3), 797−810.
(55) Hsu, C. S.; Lobodin, V. V.; Rodgers, R. P.; McKenna, A. M.; Marshall, A. G. *Energy Fuels* **2011**, *25* (5), 2174−2178.

https://dx.doi.org/10.1021/acs.energyfuels.0c02158
Energy Fuels XXXX, XXX, XXX−XXX

energy&fuels

pubs.acs.org/EF Article

Compositional Trends for Total Vanadium Content and Vanadyl Porphyrins in Gel Permeation Chromatography Fractions Reveal Correlations between Asphaltene Aggregation and Ion Production Efficiency in Atmospheric Pressure Photoionization

Martha L. Chacón-Patiño, Rémi Moulian, Caroline Barrère-Mangote, Jonathan C. Putman, Chad R. Weisbrod, Greg T. Blakney, Brice Bouyssiere,* Ryan P. Rodgers,* and Pierre Giusti

Cite This: https://dx.doi.org/10.1021/acs.energyfuels.0c03349 Read Online

ACCESS | Metrics & More | Article Recommendations | Supporting Information

ABSTRACT: Fourier transform ion cyclotron resonance mass spectrometry (FT-ICR MS) has exposed the ultracomplexity of fossil fuels, thereby validating the compositional trends that rule petroleum distillation, known as the *Boduszynski Continuum*. Routine FT-ICR MS analysis of a single crude oil sample can reveal tens-of-thousands of unique molecular formulas; however, currently available ionization methods suffer from limitations for such complex mixtures that are not yet completely understood. Simply put, MS detects ions, and thus, it depends heavily on the ability of ion sources to indiscriminately volatilize and subsequently ionize samples of interest. Despite advances in soft ionization methods, the characterization of complex matrices remains a challenge due to the lack of an ion source, commercial or custom-built, that can vaporize and ionize all compounds without bias, save analyte concentration. However, atmospheric pressure photoionization (APPI) has been shown to provide the most uniform ion production for mixtures of petroleum model compounds and real samples, with little to no fragmentation. In this work, we investigated the molecular composition of PetroPhase 2017 asphaltenes and its extrography fractions, with a focus on the total vanadium content and molecular composition of vanadyl porphyrins as a function of aggregate size distribution, accessed through separate experiments: online gel permeation chromatography (GPC) inductively coupled plasma−MS (ICP−MS) and online GPC APPI FT-ICR MS (at 21 T). The results reveal that the extrography separation provides asphaltene fractions (*i.e.*, acetone, Hep/Tol, and Tol/THF/MeOH) enriched in ^{51}V-containing compounds with distinctive aggregate size distributions. The acetone fraction features smaller aggregate sizes, as it elutes later in the GPC chromatogram than Hep/Tol and Tol/THF/MeOH fractions, and overall, presents up to ∼14-fold higher ionization efficiency in APPI. Such behavior suggests a correlation between aggregate size and production efficiency of monomeric ions in APPI. Bulk compositional trends accessed by GPC separation and highlighted by ICP−MS detection indicate that despite multiple separation steps (*i.e.* extrography followed by GPC), APPI FT-ICR MS can only access ∼37% of the total V-containing compounds. Although the more stable/larger aggregates dominate the size distributions of all asphaltene samples studied, it is the weakly aggregated/monomeric species that are preferentially observed by APPI-MS. Tendencies in the molecular composition of vanadyl porphyrins and S/O-containing compounds strongly suggest that London forces might be central in the self-assembly process of asphaltene nanoaggregates to produce more massive clusters. The results demonstrate that the observed compositional trends (albeit limited) can be accessed when coupling advanced chromatographic separations with online high-field FT-ICR MS detection.

INTRODUCTION

"Classic" Asphaltene Chemistry. Asphaltenes comprise arguably the most challenging and complex, naturally occurring mixture, and their importance to upstream production and downstream oil processing have triggered scientific interest for over 50 years.[1−4] Their definition as a solubility class, that is, *n*-heptane-insoluble/toluene-soluble, instead of a specific chemical/structural family, such as saturates, mono-aromatics, or vanadyl porphyrins, and associated complexity have motivated instrumentation advances in analytical chemistry, in particular, atomic force microscopy (AFM),[5,6] and high-magnetic field Fourier transform ion cyclotron resonance mass spectrometry (FT-ICR MS).[7−9]

The "modified Yen model" provides the most popular description of petroleum asphaltenes at the molecular level. Mullins *et al.*[3,10] promoted the notion that asphaltenes are highly-aromatic/single-core molecules (known as "island") that consist of ∼7 fused-aromatic rings and low number/length of alkyl-side chains. Based on bulk properties and low-resolution MS, the authors have suggested that the predominant intermolecular force in asphaltene self-assembly is π-stacking. They also concluded that heteroatom-based interactions, such as hydrogen bonding, have no overall effect in aggregation.[11]

Received: October 6, 2020
Revised: November 17, 2020

The central concept of the modified Yen model is the stepwise association of monomeric species to form aggregates and then larger clusters, which is essentially a colloidal view.[12] These ideas have been recently supported by single-molecule AFM,[5,6] which revealed dominant island structures for various asphaltene samples. However, it is well known that AFM favors the detection of planar/near planar molecules.[13] Regardless of the limitations, some authors suggest that the island model is consistent with reservoir geodynamics,[14,15] but it is critical to point out that it fails to explain several asphaltene properties such as gas-phase fragmentation patterns in MS (tandem-MS),[16,17] the chemistry of thermal cracking products,[18−20] heterogeneous aggregation/solubility,[21,22] and interfacial behavior.[23−25]

Role of FT-ICR MS in Modern Petroleomics. High-field FT-ICR MS is widely viewed as the most advanced analytical tool for comprehensive molecular characterization of ultra-complex mixtures (*e.g.*, crude oil, petroleum distillates, and dissolved organic matter) because of its inherent high resolution and accurate mass measurement capabilities that facilitate the assignment of individual elemental compositions to tens-of-thousands of species in a single sample in a matter of minutes by mass measurement alone.[26,27] For instance, McKenna *et al.*[28] reported the detection of ∼85,000 species in a natural petroleum seep sample in which the authors identified nickel and vanadyl porphyrins with unprecedented mass accuracy. Recent works from the National High Magnetic Field Laboratory have highlighted the utility of the technique to investigate potential asphaltene structural motifs by tandem-MS, which demonstrated that single-core, "island" motifs coexist with those composed of multiple aromatic cores linked by covalent bonds (multicore or "archipelago").[29,30] These findings were also supported by Wittrig,[31] Rüger,[32−34] Nyadong,[35] and Kenttämaa *et al.*[36] Moreover, gas-phase fragmentation studies of geologically diverse asphaltene samples have revealed that the dominance of a particular structural motif (island or archipelago) is sample-dependent and correlates with the chemistry/structure of products from thermal cracking processes. These reports, along with recent findings by Xu,[23,24,37] Harbottle,[38] Clingenpeel,[39] and Jarvis *et al.*,[40] challenge the idea of the uniform dominance of highly aromatic/single-core structures in petroleum asphaltene samples and strongly suggest the existence of abundant multi-core "archipelago" species as well as heptane-insoluble/toluene-soluble compounds with "atypical" low aromaticity but high heteroatom content (*i.e.*, oxygen and sulfur).

Limitations of MS. Although MS has shed light on many of the compositional/structural trends that govern petroleum chemistry,[41−44] it suffers limitations (imposed by ionization methods) that are not entirely understood in complex matrices. Simply put, MS detects ions, and thus, it relies on the ability of ion sources to uniformly volatilize and ionize molecules within a complex sample. Development of "soft" ion sources, such as electrospray ionization (ESI), atmospheric pressure photoionization (APPI), and matrix-assisted laser desorption/ionization, has enabled the MS characterization of non-volatile/labile analytes from proteins to petroleum, creating the fields of proteomics and petroleomics.[45−48] However, the characterization of complex mixtures is still limited by selective ionization due to the absence of an ion source that can completely vaporize and ionize all compounds with no bias other than molar concentration. It is essential to point out that among all commercially available and custom-built[49−51] ion sources capable of coupling to FT-ICR MS, APPI has been shown to provide the most uniform and complete ionization of mixtures of aromatic petroleum model compounds and real-world samples, with little or no fragmentation; it is hypothesized that some aliphatic species (*e.g.*, cycloalkanes) exhibit lower ionization efficiency than aromatic compounds in APPI, but their response factor relative to aromatic species has not been determined.[52,53] For instance, Huba *et al.*[54] tested the ionization trends of a wide range of petroleum standards (*e.g.*, naphthenic acids, 2−7 ring PAHs, nitrogen/sulfur-containing PAHs, furans, and phenols) in APPI, ESI, and atmospheric pressure chemical ionization (APCI). The authors concluded that APPI featured the lowest ion suppression effects, allowing the ionization of the broadest range of model compounds. In another work, Schrader *et al.*[50] used ESI, APPI, APCI, and custom-built atmospheric pressure laser ionization (APLI) to access the molecular composition of North American asphaltenes by FT-ICR MS. The authors concluded that APPI and APLI provided the broadest representation of asphaltenes, revealing the highest number of assigned molecular formulas and the closest H/C, O/C, and N/C ratios to bulk elemental analysis.

Early works by Cho *et al.*[55] demonstrated that petroleum MS characterization suffers considerable ion suppression effects. The authors fractionated an Arabian heavy oil into saturates, aromatics, resins, and asphaltenes and concluded that separate MS analyses enabled the identification of ∼33,000 unique molecular formulas, compared with only ∼18,000 species observed for the unfractionated/whole sample. Recently, Chacón-Patiño *et al.*[30] developed an extrography separation to improve the characterization of petroleum asphaltenes. The method involves asphaltene adsorption on silica gel and subsequent extraction with specific solvents. In the shortened version of the separation, the solid mixture of asphaltenes/SiO_2 is gradually extracted with acetone, Hep/Tol (1:1), and Tol/THF/MeOH (5:5:1). Although the solvent series seems unusual, it enables the initial isolation of highly aromatic/pericondensed structures, with high production efficiency of non-aggregated asphaltene ions in APPI, or high "monomer ion yield" (MIY), which leaves behind the asphaltene compounds that are more difficult to ionize as "monomeric" species. In brief, acetone is a polar solvent, but its predominant intermolar interactions are dipole−dipole; thus, acetone selectively extracts alkyl-deficient polycyclic aromatic hydrocarbons (PAHs) and vanadyl porphyrins.[56] The second solvent mixture, Hep/Tol, assists the isolation of alkyl−aromatic compounds. Finally, Tol/THF/MeOH extracts the species that interact via hydrogen bonding with the SiO_2 silanol groups. MS and tandem-MS studies have demonstrated that asphaltene acetone fractions from diverse oils produce up to ∼50-fold more monomeric ions and contain abundant single-core motifs. In contrast, Tol/THF/MeOH fractions are more difficult to ionize and comprise abundant multicore compounds. The authors performed heptane titrations of toluene solutions composed of the extrography fractions and observed increased precipitation (∼2−10-fold) for the Tol/THF/MeOH fraction.[29,30] Thus, production efficiency of non-aggregated asphaltene ions in APPI, or MIY, was suggested to be affected by asphaltene aggregation. It is critical to point out that in those studies, naturally occurring vanadyl porphyrins ($N_4O_1{}^{51}V_1$ class) were utilized as naturally occurring internal standards; their gas-phase fragmentation was consistent with their known single-core structure.[57]

https://dx.doi.org/10.1021/acs.energyfuels.0c03349
Energy Fuels XXXX, XXX, XXX−XXX

However, they were only detected in the acetone fractions from several different asphaltenes (*e.g.*, Athabasca bitumen, South American heavy oils, Maya, and Arabian heavy), and it was not determined if difficult-to-ionize samples contain vanadium complexes locked into asphaltene aggregates.

GPC to Correlate Petroleum Chemistry and Aggregation. Online gel permeation chromatography (GPC) coupled to elemental analysis [inductively coupled plasma (ICP−MS)] has been useful to understand bulk compositional trends as a function of aggregate size distributions within petroleum samples.[58−60] Sulfur, vanadium, and nickel are usually monitored, and the resulting GPC ICP−MS chromatograms are commonly referred to as size profiles or size distributions.[58,61] Recent studies by GPC strongly suggest that London forces between aliphatic moieties have a central role in petroleum aggregation. For instance, Berrueco *et al.*[62] performed off-line characterization of GPC asphaltene fractions by synchronous UV−fluorescence spectroscopy and concluded that earlier-eluting fractions (most aggregated species) comprised compounds with high content of alkyl-side chains. Conversely, analysis of the later-eluting fractions (less aggregated asphaltenes/free molecules) revealed abundant alkyl-depleted/low-molecular-weight PAHs. In another work, Putman *et al.*[63] performed off-line FT-ICR MS characterization of GPC asphaltene fractions and observed that earlier-eluting compounds were more aliphatic, with MS-derived H/C ratios above 1.2. In contrast, later-eluting fractions revealed abundant highly-aromatic/alkyl-depleted species (H/C < 1.0). The authors observed similar trends for the parent whole crude oil, thereby suggesting that interactions between aliphatic moieties could be central in petroleum and asphaltene aggregation. These results are consistent with the idea that London forces between alkyl side chains drive the self-assembly of asphaltene nanoaggregates to produce more massive clusters, widely reported by Rogel,[64] Carbognani,[65] and Stachowiak *et al.*[66]

It is critical to point out that there is not a clear correlation between asphaltene aggregation in industrial applications (*e.g.*, fouling in production facilities) and GPC elution trends. For example, Muller *et al.*[67,68] fractionated geologically diverse crude oils by GPC and used off-line FT-ICR MS for molecular characterization. The earlier-eluting fractions revealed abundant small aromatic cores (1−3 fused rings) with extensive alkyl substitution, whereas the later-eluting compounds were alkyl-depleted/sizable aromatic structures (5−9 fused rings). The authors suggested possible "non-size" effects for the later-eluting species, that is, the interaction of aromatic cores with the stationary phase. On the other hand, for the earlier-eluting fractions, the alkyl-side chains were suspected to prevent interactions between the aromatic cores and the column. Thus, alkyl-side chain content was suggested as the dominant molecular property that drives petroleum elution in GPC.

Online GPC FT-ICR MS for Petroleum Analysis. GPC fractionation with off-line FT-ICR MS detection is known to be limited by ion suppression effects and complicated by the potential presence of contaminants from repeated fraction collection/solvent evaporation.[63,69] Moreover, for vacuum residues and asphaltenes, it is increasingly difficult to determine if the observed ions reflect the real molecular composition of earlier-eluting/highly aggregated species.

Online molecular-level characterization has recently shown potential to mitigate the issues associated with fraction collection and off-line MS characterization.[69] There are few reports about petroleum analysis by chromatographic methods with online FT-ICR MS detection.[69,70] The reason is simple: close mass splits such as 3.4 mDa (species differing in SH_4 vs C_3 content) and 1.1 mDa ($^{13}CH_3{}^{32}S$ vs C_4), abundant in heavy petroleum and asphaltenes, are a challenge to resolve on a chromatographic time scale. However, the custom-built 21 T FT-ICR mass spectrometer at the National High Magnetic Field Laboratory offers the most suitable option for online LC analysis because of its ultra-high resolving power,[71] mass accuracy, and sensitivity in a single scan, precluding the need for the coaddition of several scans required to yield sufficient resolving power and S/N.

In this work, the interlaboratory sample known as PetroPhase 2017 asphaltenes and its acetone, Hep/Tol, and Tol/THF/MeOH extrography fractions were fractionated by an improved GPC method that uses three columns in series to increase the resolution between earlier and later-eluting fractions. The GPC fractionation was hyphenated with positive-ion APPI 21 T FT-ICR MS characterization. Separate GPC ^{51}V ICP−MS studies were performed for quantification of total vanadium content as a function of aggregate size distribution. The results reveal that extrography yields asphaltene fractions that contain ^{51}V compounds with characteristic elution behavior in GPC. The acetone fraction elutes much later than Hep/Tol and Tol/THF/MeOH, and overall, features up to ∼14-fold higher MIY (or ionization efficiency in APPI), which indicates that nanoaggregate size and production of monomeric ions are correlated. Bulk vanadium content, accessed by GPC ICP−MS, indicates that FT-ICR MS can only access up to ∼37% of ^{51}V-containing compounds; the detected species are preferentially observed in the weakly aggregated GPC subfractions. The molecular composition of vanadyl porphyrins ($N_4O_1{}^{51}V_1$ class), along with S-containing compound classes, strongly suggest that London forces between aliphatic moieties might be central in asphaltene self-assembly.

■ EXPERIMENTAL METHODS

Materials. Asphaltenes were precipitated from an Arabian Heavy Petroleum sample (API = 29.2). High-performance liquid chromatographic (HPLC) grade *n*-heptane (Hep or C_7), toluene (Tol), dichloromethane (DCM), acetone, and methanol (MeOH) were obtained from J.T. Baker and used as received. HPLC-grade tetrahydrofuran (THF) with no solvent stabilizer was purchased from Alfa Aesar. Filter paper Whatman 2, high purity microglass fiber thimbles, and chromatographic-grade silica gel (100−200 mesh, type 60 Å, Fisher Scientific) were used for asphaltene isolation from crude petroleum, asphaltene cleaning, and extrography fractionation.

Asphaltene Precipitation and Extrography Fractionation. Arabian heavy asphaltenes were prepared following a slightly modified version of the standard method D6560-12.[72] The prepared sample is known as "PetroPhase 2017 asphaltenes".[73] In brief, petroleum was mixed with C_7 in a 1:40 ratio v/v. The dropwise addition of heptane was assisted by sonication (110 W, 40 kHz; Bransonic, Danbury, CT, USA) and refluxed heating at 90 °C for 2 h. The mixture was allowed to settle overnight; the precipitated solids were then collected by filtration (Whatman 2 filter paper). Asphaltenes were cleaned by extended Soxhlet extraction with C_7, under N_2 atmosphere, until the solvent appeared colorless (∼150 h). Asphaltenes were further washed by four cycles of crushing/Soxhlet extraction with heptane in order to decrease the concentration of occluded/coprecipitated maltenes. "Purified" asphaltenes were recovered by redissolution in hot toluene, dried under N_2, and stored in the dark.

Asphaltenes were dissolved in DCM and mixed with silica gel (mass loading 1% = 10 mg of asphaltenes per gram of SiO_2). The

https://dx.doi.org/10.1021/acs.energyfuels.0c03349
Energy Fuels XXXX, XXX, XXX−XXX

mixture was dried entirely under N_2 (24 h) and subsequently extracted in a Soxhlet apparatus with acetone, Hep/Tol (1:1, v/v), and Tol/THF/MeOH (5:5:1, v/v/v); each extraction lasts 24 h. The mixture asphaltenes/SiO_2 requires drying under N_2 after each extraction step. The method is known as extrography and involves sample adsorption on a polar adsorbent (*e.g.*, SiO_2, alumina, and cellulose) and extraction with solvents of different polarity or varying intermolecular forces, such as acetone (dipole−dipole interactions) and THF/MeOH (hydrogen bonding).[74]

GPC Coupled to ICP−Low-Resolution MS. Mobile phase was delivered by a Dionex HPLC system equipped with an UltiMate 3000 microflow pump, an UltiMate 3000 autosampler, and a low port-to-port dead-volume microinjection valve. THF was used for sample preparation and mobile phase as it enables the highest sample recovery from the GPC columns (>99 wt %). A Styragel guard column (4.6 mm inner diameter, 30 mm length, 10,000 Da exclusion limit) was used before the GPC columns, and the chromatographic separation was performed by three GPC columns (from 1000 to 2,000,000 Da) connected in series. 100 μL of asphaltene samples (5 mg/mL) was injected and eluted isocratically at 1 mL/min for 90 min. A post-column splitter was used to assure the infusion of 40 μL/min into the ICP−MS. Samples were chromatographically separated and characterized as fresh solutions and prepared 1 h before analysis.

The ICP−MS (Thermo Scientific Element XR) was fitted with a modified DS-5 microflow total consumption nebulizer (CETAC, Omaha, NE), equipped with a custom jacketed glass spray chamber, as reported elsewhere. The spray chamber was thermostatted at 60 °C by a water bath circulator (Neslab RTE-111, Thermo Fisher Scientific, Waltham, MA). The ICP plasma conditions were Ar gas flow at 16 L/min, Ar auxiliary gas flow at 0.9 L/min, and Ar nebulizer gas flow at 0.6 L/min. O_2 (0.08 L/min) was used to avoid carbon deposition. The instrument was equipped with a quartz injector (inner diameter 1.0 mm), Pt sampler (orifice diameter 1.1 mm), and a skimmer with an aperture diameter of 0.8 mm. The ICP−MS was used to access the spectrally interfered isotopes of ^{32}S, ^{51}V, and ^{58}Ni. This work mainly focuses on ^{51}V content. Instrument conditions were optimized weekly by the use of a multielement tuning solution of Ag, Al, B, Ba, Ca, Cd, Co, Cr, Cu, Fe, In, K, Li, Mg, Mn, Mo, Na, Ni, P, Pb, Sc, Si, Sn, Ti, V, Zn, and Y in THF (1.0 ng/g). Mass offset was optimized daily and was applied to the data acquisition method to compensate the mass drift from the magnetic sector. Excel was used for the integration of the obtained chromatograms.

GPC Coupled to (+) APPI 21 T FT-ICR MS. GPC-FT-ICR-MS. For ultra-high-resolution MS studies, the GPC separation was performed with an Alliance e2695 Separation Module (Waters Corporation, Milford, MA) equipped with the same set of three columns used for GPC ICP−MS. The HPLC system was operated with Empower 3 Chromatography Data Software. 100 μL of asphaltene samples (5 mg/mL) was injected and eluted isocratically at 0.5 mL/min. All samples were separated/analyzed at 5 mg/mL. The effect of asphaltene concentration has been reported elsewhere.[75] The GPC effluent was split in 5, and 100 μL/min was directly infused into the ion source. The APPI source (Ion Max, Thermo Fisher Scientific, San Jose, CA) was operated with a vaporizer temperature of 350 °C. N_2 was used as sheath gas (50 psi) and auxiliary gas (32 mL/min) to prevent sample oxidation. Mass spectral analysis was performed with a custom-built 21 T FT-ICR mass spectrometer. Ion populations of 1.5×10^6 charges were externally accumulated in a Velos Pro linear ion trap (Thermo Scientific, San Jose, CA) and ultimately transferred to a dynamically harmonized ICR cell operated with a trapping potential of 6 V.[8,76] Predator data station assisted MS data collection, with 3.1 or 6.2 s transient duration during the chromatographic time frame. These conditions provide a mass resolving power of ~3,400,000 at m/z 400 for a single phased (absorption mode) mass spectrum, facilitating the resolution of the 1.1 mDa mass split ($SH_3{}^{13}C$ vs $^{12}C_4$) at m/z > 800. The large ion population used here is possible only due to the high magnetic field and yields high dynamic range per single scan without compromising the spectral acquisition rate. This promotes the highest chromatographic resolution since spectral averaging is not required. Ion injection times (ITs) were metered by automated gain control (AGC). AGC is a well-described process in which the linear radio frequency ion trap performs a very brief pre-scan to determine the instantaneous flux of ions. This measurement is extrapolated to determine the ion IT required to meet the user defined AGC target (specified in number of fundamental charges). In this study, the AGC target was 1.5×10^6 charges. Predator Software assisted data collection, phase-correction, and internal calibration with abundant hydrocarbon homologous series.[77] PetroOrg Software assisted molecular formula assignment and data visualization by plots of double bond equivalents (DBE = number of rings plus double bonds to carbon) versus carbon number.[78]

RESULTS AND DISCUSSION

GPC ICP−MS Chromatograms for Asphaltene Extrography Fractions. Figure 1 presents the GPC ^{51}V ICP−MS chromatograms for whole PetroPhase 2017 asphaltenes and its acetone, Hep/Tol, and Tol/THF/MeOH extrography fractions. This analytical approach allows for the quantitative determination of ^{51}V-containing nanoaggregate size distributions, along with other metals or heteroatoms such as ^{58}Ni and ^{32}S. The highlighted elution ranges (gray dashed lines) have been previously defined based on the molecular weight distribution of polystyrene standards (*e.g.*, high molecular weight > 10,000 Da, medium molecular weight ~ 1000−10,000 Da, low molecular weight < 1000 Da) and comprise[61,75] high molecular weight (HMW, 20−24 mL elution volume), medium molecular weight (MMW, 24−28 mL), and low molecular weight (LMW, 28−32 mL) species, plus a "tailing" fraction (>32 mL). It is essential to point out that in this study, adsorption effects or strong interaction between asphaltenes and the GPC column have not been considered; therefore, HMW species are assumed to be sizable/stable aggregates, whereas LMW and tailing compounds are ascribed to weakly aggregated or asphaltene "monomers" (free molecules). The tailing fraction, more abundant for the whole sample, comprises non-aggregated vanadium compounds that elute after the full permeation volume and might experience strong adsorption on the stationary phase. It is important to highlight that the V-containing tailing fraction is less pronounced for the extrography fractions. We hypothesize that this behavior is likely due to (1) absence of those compounds due to their irreversible retention on the silica gel particles used for the extrography separation and (2) possible cooperative stabilization between asphaltene fractions when they are part of the

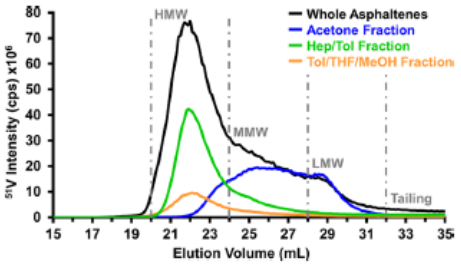

Figure 1. ^{51}V GPC ICP−MS chromatograms for whole PetroPhase 2017 asphaltenes (black) and its extrography fractions: acetone (blue), Hep/Tol (green), and Tol/THF/MeOH (orange). High, medium, and LMW, and tailing elution ranges are highlighted by gray dashed lines.

https://dx.doi.org/10.1021/acs.energyfuels.0c03349
Energy Fuels XXXX, XXX, XXX−XXX

whole sample. Collection of the GPC fractions (*e.g.*, HMW and tailing), followed by solvent evaporation, dilution, and reinjection into the GPC separation system, yielded a nanoaggregate distribution similar to that obtained when the whole sample was injected (*i.e.*, HMW and tailing). Moreover, we have used three GPC columns in series, which enables higher chromatographic resolution and observation of multimodal size profiles, compared to the monomodal-like distributions previously reported by Putman *et al.*[69,79]

The size distribution of the whole PetroPhase 2017 asphaltenes (black) indicates a diverse population of ^{51}V-containing aggregates. The integrated areas of the GPC chromatograms are presented in Table 1 and facilitate sample comparison. For whole asphaltenes, ~59, 27, and 10% of the total area correspond to HMW, MMW, and LMW species, plus a ~3% for the tailing region. Thus, the size GPC profiles for the extrography fractions indicate that the separation reported by Chacón-Patiño[29] yields asphaltene cuts with distinctive aggregation behavior.[80] The acetone fraction, previously shown to contain abundant single-core (island) motifs with a high production efficiency of non-aggregated ions in APPI, or high MIY, mostly reveals MMW (~61%) and LMW (~25%) vanadium-containing species, whereas Hep/Tol and Tol/THF/MeOH fractions, shown to be enriched in multicore (archipelago) structures with a much lower MIY,[29] mostly elute in the HMW region (73/66%).

Table 1. Integrated Areas (%) for the GPC ^{51}V ICP−MS Chromatograms for Whole PetroPhase 2017 Asphaltenes and Its Acetone, Hep/Tol, and Tol/THF/MeOH Extrography Fractions

sample	prior to HMW[a] (%)	HMW (%)	MMW (%)	LMW (%)	tailing (%)
whole PetroPhase 2017 asphaltenes	0.90	59.00	27.06	9.94	3.09
acetone fraction	0.03	13.06	60.70	24.82	1.39
Hep/Tol fraction	0.20	72.91	19.02	4.39	3.48
Tol/THF/MeOH fraction	1.12	66.47	21.20	6.87	4.34

[a]Fraction eluted before the established molecular weight ranges. Material can elute before the defined MW ranges.

In previous work, we accessed the precipitation behavior by titration and the molecular composition via direct-infusion (+) APPI FT-ICR MS, of whole PetroPhase 2017 asphaltenes and its extrography fractions. The results suggested a stronger precipitation tendency in heptane/toluene mixtures for Hep/Tol and Tol/THF/MeOH, whereas acetone featured up to ~20-fold higher stability.[29,80] Thus, ionization efficiency in APPI was linked to asphaltene precipitation, and strong aggregation (low concentration of monomeric species) was suggested as the reason for poor ionization efficiency. Furthermore, ^{51}V-containing compounds, or vanadyl porphyrins ($N_4O_1{}^{51}V_1$) as revealed by (+) APPI FT-ICR MS, were only detected in the acetone fraction. Therefore, the aggregation trends presented in Figure 1 agree with the previously reported precipitation behavior in bulk liquid phase. However, the results here demonstrate that ^{51}V-containing compounds are present in all extrography fractions; GPC elution trends suggest that lack of observation in direct infusion MS experiments is likely due to a prominent aggregation tendency.

GPC Hyphenated to Positive-Ion APPI 21 T FT-ICR MS. The GPC separation system was coupled with an APPI ion source operated in positive mode attached to a custom-built 21 T FT-ICR mass spectrometer. The instrument is equipped with AGC,[8] which determines an appropriate *ion accumulation period* to hit a constant target ion population (1.5×10^6 charges),[81] required for optimal data collection, for each scan during the entire chromatographic run. Figure 2, upper panel, presents the total ion chromatogram (IC) for whole PetroPhase 2017 asphaltenes (gray) measured by (+) APPI FT-ICR MS and also shows the GPC ^{51}V ICP−MS chromatogram (black) for comparison. Although the sample comprises ~59% of ^{51}V-containing HMW compounds (ICP data, integrated areas, Table 1), the total ion current (TIC) is maximum for the MMW species, close to the LMW region limit. Figure 2, lower panel, features the accumulation period (blue) for the whole chromatographic separation, which maxed out for the HMW region, and the elution volumes for which the ^{51}V content, as determined by GPC ICP−MS, are low (<20 mL and tailing). Figure 2, lower panel, also presents the MIY (orange) as a function of elution volume. MIY is calculated by eq 1 and is consistent with the TIC. The results suggest an inverse correlation between the production efficiency of monomeric ions, MIY, and aggregate size.

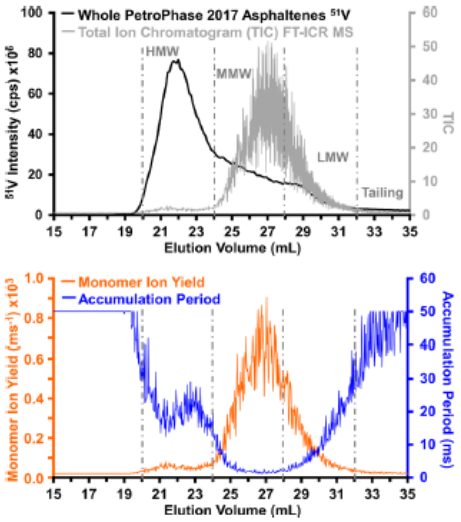

Figure 2. Upper panel: ^{51}V GPC ICP−MS chromatogram for whole PetroPhase 2017 asphaltenes (black) plotted along with the total IC (TIC) derived from (+) APPI 21 T FT-ICR MS (gray). Lower panel: accumulation period (ms) required to hit the target of 1×10^5 charges (blue) and MIY, (orange) throughout the entire GPC separation.

$$\mathrm{MIY} = \frac{1}{\text{accumulation period}} \times 1000\ (\mathrm{ms}^{-1}) \quad (1)$$

Correlation between Aggregation Trends and Production Efficiency of Monomeric Ions in APPI. Figure 3, left panel, presents the MIY (orange) as a function of elution volume for the PetroPhase 2017 asphaltenes extrography fractions; the values are derived from (+) APPI FT-ICR MS (eq 1). Acetone features the most optimal ionization: the MMW species exhibit up to MIY ~2100. Conversely, Hep/Tol

https://dx.doi.org/10.1021/acs.energyfuels.0c03349
Energy Fuels XXXX, XXX, XXX−XXX

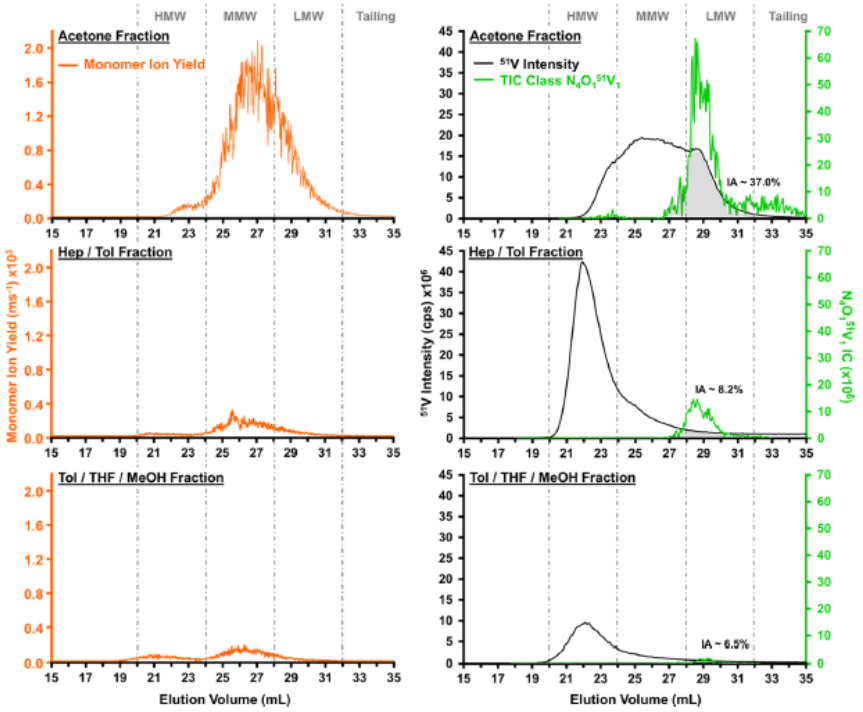

Figure 3. Left: MIY, as a function of elution volume, for the extrography fractions from PetroPhase 2017 asphaltenes. Right: GPC ^{51}V ICP−MS chromatograms (black) plotted along with the ICs for vanadyl porphyrins ($N_4O_1V_1$ class, green). IA are highlighted and suggest that detected $N_4O_1{}^{51}V_1$ species by (+) APPI FT-ICR MS may correspond to ∼37.0, 8.2, and 6.5% of the total vanadium content detected via ICP−MS. Abundant ^{51}V, as measured by ICP, and its limited detection in (+) APPI FT-ICR MS, demonstrate an inverse correlation between aggregate size and MIY.

and Tol/THF/MeOH fractions present a poor production of monomeric ions, with a ∼7−14-fold lower MIY for the elution volumes in which ion accumulation time maxed out. Although most of Hep/Tol and Tol/THF/MeOH ^{51}V-containing species elute in the HMW region (∼73/66% integrated areas), the results suggest that most of the ions derive from MMW and LMW GPC subfractions.

Molecular formulas assigned to the mass spectral peaks based on accurate mass are sorted in compound classes. For instance, all the formulas with carbon, hydrogen, and one sulfur atom comprise the class S_1. Thus, vanadyl porphyrins, with one oxygen, one vanadium, and four nitrogen atoms, make up the class $N_4O_1{}^{51}V_1$. Porphyrins with additional heteroatoms, for example, $N_1O_1S_1{}^{51}V_1$, previously reported by Gray,[82] Qian,[83] and McKenna *et al.*,[84] are in much lower concentration and are the topic of future work. Figure 3, right panel, presents the IC for the $N_4O_1{}^{51}V_1$ class (green) for all the extrography fractions and again, their GPC ^{51}V ICP−MS chromatograms (black) for comparison. The whole sample is included in the Supporting Information Figure S1. $N_4O_1{}^{51}V_1$ species were mostly detected in the LMW and tailing acetone subfractions, despite the majority of the ^{51}V-containing compounds eluted in the MMW region (∼61%, integrated area—ICP−MS), which indeed, presents the highest MIY values. The intersection area (IA) between ^{51}V ICP−MS and $N_4O_1{}^{51}V_1$ FT-ICR MS ICs is highlighted in Figure 3 (gray) and can be used to qualitatively infer the observation window of (+) APPI FT-ICR MS. The results suggest access to only ∼37.0% of the total vanadium content of the acetone fraction. The later extrography fractions follow the same trend: although 73/66% of Hep/Tol and Tol/THF/MeOH species elute in the HMW region, most of the vanadyl porphyrins are detected in the LMW aggregates, and the IAs suggest minimal APPI-MS access to ^{51}V-containing compounds (∼8.2 and ∼6.5%).

Collectively, the results support the notion that GPC can be used to access asphaltene aggregation trends, as the results are consistent with previously reported precipitation/deposition behaviors.[29,85] Lack of FT-ICR MS detection of abundant $N_4O_1{}^{51}V_1$ compounds in the HMW region, despite the high ^{51}V abundance revealed by ICP−MS, confirms that APPI FT-ICR MS analysis of asphaltenes is strongly hampered by aggregation.

Molecular Composition as a Function of Aggregate Size Distribution. Molecular formulas can be sorted by the number of rings and double bonds (DBE) respective to carbon atoms. Figure 4, upper panel, presents the DBE versus carbon number plots for the $N_4O_1{}^{51}V_1$ class for the GPC subfractions from whole PetroPhase 2017 asphaltenes. In these graphs, the color scale represents the relative abundance, normalized within each class for each GPC subfraction. Thus, in Figure 4, the molecular formulas and contour plots result from coadding the scans collected for the corresponding HMW, MMW,

https://dx.doi.org/10.1021/acs.energyfuels.0c03349
Energy Fuels XXXX, XXX, XXX−XXX

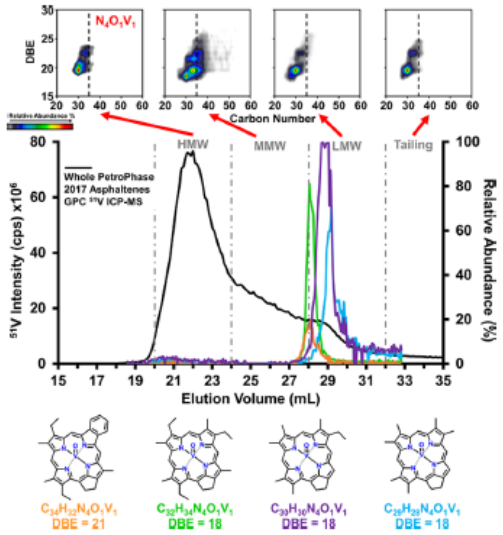

Figure 4. DBE vs carbon number plots for the $N_4O_1{}^{51}V_1$ class for the various GPC regions from whole PetroPhase 2017 asphaltenes (upper panel) and relative abundance as a function of elution volume for the most abundant $N_4O_1{}^{51}V_1$ formulas (middle panel). Data derived from (+) APPI FT-ICR MS characterization. The GPC ^{51}V ICP−MS chromatogram (black) is included for reference, and the most likely molecular structures for the most abundant vanadyl porphyrins are presented in the lower panel.

LMW, and tailing GPC regions. Furthermore, compounds with the same DBE but varying content of carbon number belong to the same homologous series.

In Figure 4, it is important to keep in account that vanadyl porphyrins eluted as HMW aggregates exhibit a *global* relative abundance below 2%; these species reveal a narrow distribution of carbon number (~28−35). We hypothesize that these compounds may exist as "free" porphyrins available on the surface of sizable aggregates and thus remain accessible to APPI FT-ICR MS. Conversely, the abundant $N_4O_1{}^{51}V_1$ species detected in the MMW GPC fraction (up to ~60% of relative abundance, green line) reveal more extended homologous series (carbon number ~27−50), which translates into a higher content of carbon atoms in alkyl-side chains. Finally, the disaggregated/monomeric compounds, LMW/tailing subfractions, exhibit abundant $N_4O_1{}^{51}V_1$ species with decreased alkylation (carbon number ~27−35). We hypothesize that these compounds are likely "free" porphyrins and thus their molecular composition could hint correlations between GPC elution trends and molecular structure. As discussed above, "tailing" species may also experience adsorption on the stationary phase and therefore elute after the full permeation volume. The global compositional trends are consistent with the results reported by Putman *et al.*,[63,69] who concluded that the *most abundant* species in larger aggregates (*e.g.*, MMW) contain more carbon atoms in alkyl-side chains, suggesting that London forces may be fundamental in asphaltene self-association. Several reports[22,86−89] suggest extensive trapping/occlusion of porphyrins within asphaltene aggregates, which is consistent with the abundant detection of vanadium-containing compounds in large/sizable aggregates in this work.

Figure 4, middle panel, presents the relative abundance of the most abundant $N_4O_1{}^{51}V_1$ molecular formulas as a function of elution volume, plotted along with the GPC ^{51}V ICP−MS chromatogram for comparison. The lower panel features the most likely molecular structure for the most abundant species.[90−92] Although the differences in carbon number and DBE are minimal, the results suggest a good chromatographic resolution between the $N_4O_1{}^{51}V_1$ species highlighted in orange/green and purple/blue. The results also indicate that the GPC elution of non-aggregated species is ruled by the presence of side groups (either alkylic or aromatic). More substituted compounds elute earlier, which suggests that steric hindrance around the porphyrin core might prevent a stronger interaction/longer residence period in the stationary phase. Previous studies indicate that the GPC elution order of metal porphyrins mostly depends on the molecular geometry and the presence of exocyclic rings.[93,94] For instance, the vanadyl group (V=O) produces a pyramidal geometry with the porphyrin

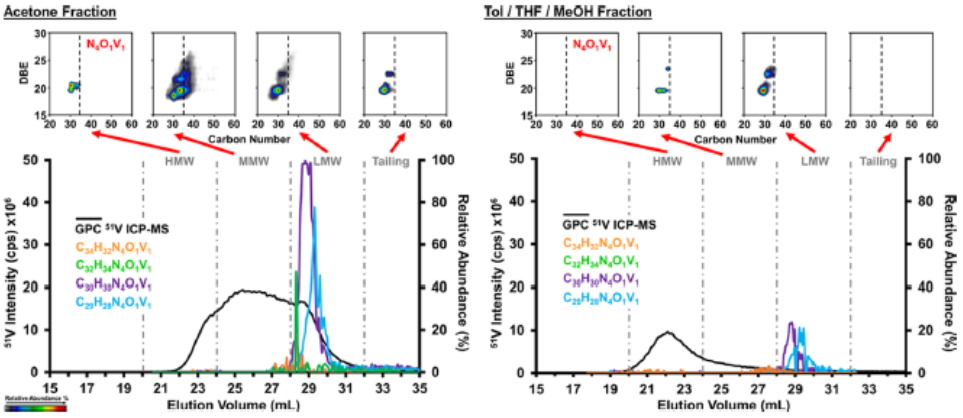

Figure 5. Upper row: DBE vs carbon number plots for the $N_4O_1{}^{51}V_1$ class for all GPC subfractions from acetone (left) and Tol/THF/MeOH (right) extrography fractions from PetroPhase 2017 asphaltenes. Data derived from (+) APPI 21 T FT-ICR MS characterization. Lower row: relative abundance, as a function of elution volume, for the most abundant $N_4O_1{}^{51}V_1$ molecular formulas. The GPC ^{51}V ICP−MS chromatogram (black) is included for reference.

https://dx.doi.org/10.1021/acs.energyfuels.0c03349
Energy Fuels XXXX, XXX, XXX−XXX

core, whereas Ni forms a square-planar complex; thus, vanadyl porphyrins elute earlier. Exocyclic rings are also correlated with less retention: the presence of a five-membered exocyclic ring decreases molecular planarity, precluding strong adsorption on the stationary phase.

Figure 5 presents the compositional range for the $N_4O_1V_1$ class for the various GPC subfractions for the acetone and Tol/THF/MeOH PetroPhase 2017 extrography fractions. The Hep/Tol fraction is included in Supporting Information Figure S2. Figure 5 also shows the relative abundance of the most abundant vanadyl porphyrins as a function of elution volume. The acetone fraction reveals compositional trends similar to those of the whole asphaltene sample (Figure 4). Again, the most abundant species, detected as LMW aggregates (74 molecular formulas), reveal a narrower carbon number distribution than the MMW vanadyl porphyrins (134 molecular formulas). The results support the notion that sizable aggregates (MMW) are likely enriched with more alkyl-substituted compounds.

It is important to point out that in previous work, we reported the molecular composition of PetroPhase 2017 asphaltenes, accessed by direct-infusion (+) APPI FT-ICR MS. Vanadyl porphyrins were only observed in whole asphaltenes and the acetone fraction. However, in this work, Hep/Tol (Figure S2) and Tol/THF/MeOH fractions reveal abundant $N_4O_1{}^{51}V_1$ compounds in the "monomeric" LMW region. We hypothesize that cooperative aggregation effects during direct-infusion MS analysis of complete extrography fractions prevent the detection of vanadyl porphyrins.[29] In this work, LMW Tol/THF/MeOH species reveal 27 $N_4O_1{}^{51}V_1$ formulas, and one prominent homologous series of 7 species (DBE 18) was detected in the MMW aggregates. The results confirm that separation by aggregate size distribution coupled to online FT-ICR MS detection, help to mitigate, to some extent, selective ionization.

Figure 6 presents the molecular composition for $N_4O_1{}^{51}V_1$ and $N_4O_2{}^{51}V_1$ classes of various elution ranges for the LMW region for the acetone fraction. The results indicate that the structural diversity narrows as a function of elution volume. Earlier-eluting $N_4O_1{}^{51}V_1$ species (upper row, Figure 6a) exhibit up to ~38 carbon atoms and DBE ~26, which translates into a higher content of carbon atoms in alkyl-side chains (up to ~10) and more exocyclic rings. Possible structures are shown in Figure 6b, based on previous reports.[57,83,95] The last elution range (31−32 mL) only presents three prominent homologous series, and the majority of the detected species feature DBE = 19. The lower row of Figure 6a shows the compositional range of vanadyl porphyrins with an additional oxygen atom. The slightly higher DBE values, more evident for the first elution range (28−29 mL), suggest that oxygen may be incorporated as a ketone functionality or a furan ring (Figure 6b, right). In general, the content of side groups decreases for later-eluting compounds, which support the idea that exocyclic rings and alkyl-side chains hinder stronger interaction/longer residence on the GPC column. These results also agree with findings by Reynolds, Caumette, and Mironov *et al.*, who found that vanadyl porphyrins could elute late in the GPC separation of vacuum residues and asphaltenes.[60,94,96−98]

Compositional Trends for Sulfur/Oxygen-Containing Heteroatomic Groups. Figure 7, upper row, presents the GPC ^{32}S ICP−MS chromatograms for acetone (left) and Tol/THF/MeOH (right) extrography fractions, along with the ICs (APPI FT-ICR MS) for selected S-containing heteroatomic

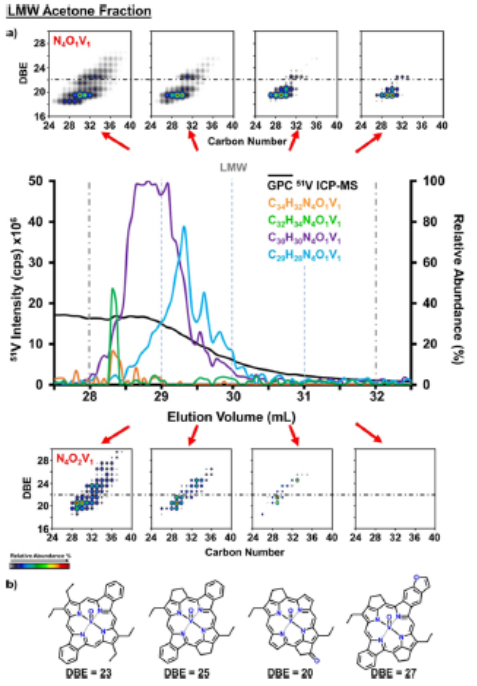

Figure 6. (a) DBE vs carbon number plots for $N_4O_1{}^{51}V_1$ and $N_4O_2{}^{51}V_1$ classes of various elution ranges for the LMW region for the acetone fraction; (b) suggested molecular structure for high DBE vanadyl porphyrins.

groups. For instance, the group S_x comprises S_1, S_2, S_3, S_4, and S_5 classes, and the group S_xO_y contains all the classes with both S and O atoms, such as S_1O_1, S_1O_2, S_1O_3, S_2O_1, and S_2O_2, among others. The results indicate that ^{32}S-containing compounds (S_x, S_xO_y, and $N_xO_yS_x$) follow trends similar to those for ^{51}V species: MMW and LMW regions reveal the highest sulfur abundance in (+) APPI FT-ICR MS, whereas quantitative data (GPC ^{32}S ICP−MS) points to much higher S amounts in the HMW aggregates, not effectively captured by MS detection. Table 2 includes the integrated areas for ^{32}S (ICP−MS), which facilitate sample comparison.

Figure 7, lower row, presents combined DBE versus carbon number plots for S-containing heteroatomic groups for the various GPC subfractions. Abundance-weighted H/C ratios are included and assist data interpretation. The compositional trends indicate that sizable/medium aggregates, HMW and MMW, contain abundant alkyl-enriched compounds with H/C ratios much higher (up to H/C ~ 1.37) than commonly reported values for asphaltenes[99,100] and the LMW/tailing subfractions (H/C ~ 0.60−0.89). For both extrography fractions, HMW and MMW regions reveal longer homologous series, with up to ~40 carbon atoms in alkyl-side chains, and low-DBE (<15) S_xO_y compounds. Readers should keep into account that asphaltenes are classically defined as highly aromatic species with an average of ~7 fused aromatic rings,[3] which translates into DBE values of 19−21.[17,101] We hypothesize that abundant oxygen-containing/polarizable functionalities, such as sulfoxides, rule the intermolecular forces responsible for the stronger aggregation of low-DBE/"atypical" compounds.[74,102,103] Furthermore, it is challenging

https://dx.doi.org/10.1021/acs.energyfuels.0c03349
Energy Fuels XXXX, XXX, XXX−XXX

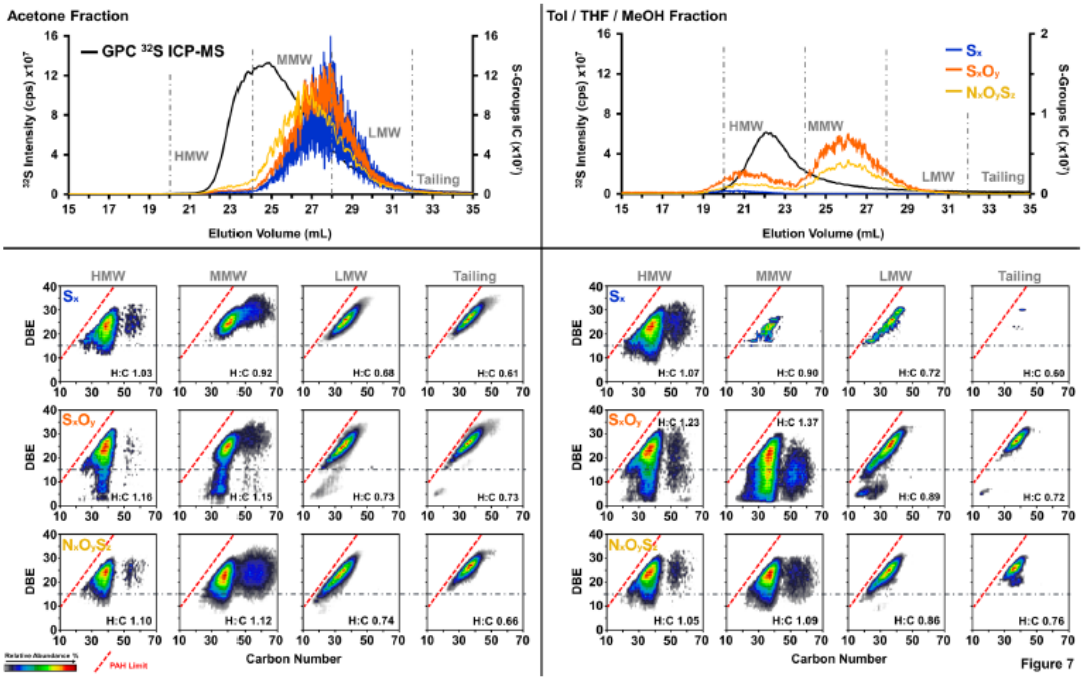

Figure 7

Figure 7. Upper row: GPC ^{32}S ICP–MS and ICs for S-containing groups for acetone (left) and Tol/THF/MeOH (right). Lower row: DBE vs carbon number plots for S_x, S_xO_y, and $N_xO_yS_z$ groups. Abundance-weighted H/C ratios facilitate subfraction comparison.

Table 2. IAs (%) for the GPC ^{32}S ICP–MS Chromatograms for Whole PetroPhase 2017 Asphaltenes and Its Acetone, Hep/Tol, and Tol/THF/MeOH Extrography Fractions

sample	prior to HMW[a] (%)	HMW (%)	MMW (%)	LMW (%)	tailing (%)
whole PetroPhase 2017 asphaltenes	1.11	64.64	25.52	6.12	2.61
acetone fraction	0.07	23.07	63.16	12.13	1.57
Hep/Tol fraction	3.09	65.78	20.70	5.86	4.57
Tol/THF/MeOH fraction	1.27	68.23	20.24	6.41	3.85

[a]Fraction eluted before the established molecular weight ranges. Material can elute before the defined MW ranges.

to establish the extent to which the detected heteroatom classes represent the real molecular composition of HMW/MMW aggregates. However, the abundance weighted H/C ratios suggest that the detected "atypical" species are likely abundant: their higher H/C ratios offset the substantial lower values of the LMW and tailing species.

The trends highlighted in Figure 7 are consistent with previous works by Putman *et al.*[63,69] who investigated the molecular composition of asphaltenes as a function of aggregate size and suggested that London forces between aliphatic moieties might be central in asphaltene self-assembly. In support of this hypothesis, for instance, Tanaka *et al.*[104] performed molecular dynamics simulations on model asphaltene compounds to understand the role of aliphatic chains and polar functionalities on the stability of aggregates upon heating. Simulations for structures in which aliphatic side chains were removed and heteroatoms were replaced with carbon revealed that dissociation occurred at much lower temperatures. The authors also pointed out that coal molecules are comprised of smaller aromatic cores and fewer aliphatic carbons, whereas asphaltenes reveal higher content of longer alkyl side chains attached to bigger aromatic cores. Therefore, differences in solubility in common solvents for coal and asphaltenes should be ruled by alkyl-chain and heteroatom content, and thus, it seems plausible that aliphatic side chains and polar groups can affect the aggregate stability. The authors concluded that removal of alkyl side chains caused a decrease in the interaction energy, likely, in part, because of lack of London forces between aliphatic side chains, which decreased the stability of the aggregated structures. Furthermore, entanglement of long aliphatic chains was also suggested to stabilize the aggregates. Supporting Information, Figure S3, includes the DBE versus carbon number plots for S-containing groups for the GPC subfractions from whole PetroPhase 2017 asphaltenes and its Hep/Tol extrography fraction, which exhibit DBE and carbon number tendencies consistent with acetone and Tol/THF/MeOH.

All the samples feature an interesting trend for the PAH limit, which is highlighted by the red dashed line in the DBE versus carbon number plots of Figure 7 and is defined as the highest possible DBE value, at a given carbon number, for fossil hydrocarbons with a planar molecular structure. The PAH limit is determined by eq 2[105−107] and dictates that the DBE of planar hydrocarbons do not exceed the ~90% of its carbon number. Species close to the PAH limit, to the right, are highly aromatic/pericondensed; molecular formulas with DBE values above the limit are inherent to fullerene-like structures. Figures 7 and S3 indicate that the compositional

https://dx.doi.org/10.1021/acs.energyfuels.0c03349
Energy Fuels XXXX, XXX, XXX−XXX

range moves toward the PAH limit as a function of elution volume, suggesting that weakly-aggregated/monomeric species contain abundant highly aromatic/pericondensed "classical" asphaltenes.

$$\mathrm{DBE} = 0.899 \times \text{carbon number} \quad (2)$$

Figure 8, upper row, presents the compositional range of S-containing groups for the complete acetone extrography

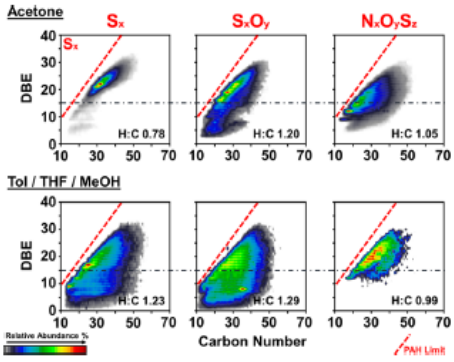

Figure 8. Compositional range for S-containing heteroatom groups accessed by direct infusion (+) APPI FT-ICR MS for complete acetone (upper row) and Tol/THF/MeOH (lower row) fractions extrography fractions.

fraction, derived from direct-infusion (+) APPI FT-ICR MS characterization.[29] The results confirm the preferential access to highly-aromatic/hydrogen-deficient S_x compounds, similar to the species observed in the LMW and tailing GPC subfractions, which comprise only ~14% of the total sulfur content (GPC ^{32}S ICP–MS, Table 2). Furthermore, direct infusion MS hints some of the S_xO_y and $N_xO_yS_z$ species that feature a higher content of carbon atoms in alkyl-side chains and slightly lower DBE values, detected in the MMW GPC region (~63% sulfur content). Figure 8, lower row, presents the composition of the complete Tol/THF/MeOH extrography fraction and reveals low-DBE S_x and S_xO_y compounds with H/C ratios somehow similar to those observed in HMW/MMW GPC regions (~88% sulfur content). Collectively, the results indicate that the species revealed by direct infusion MS are determined by both ionization efficiency (MIY) and actual concentration. LMW/tailing Tol/THF/MeOH S-containing compounds, although they ionize more efficiently, are in minimal abundance and thus do not dominate the compositional range revealed by direct infusion MS.

Implications for Novel Aggregation Models for Petroleum Asphaltenes. The online GPC ICP–MS (V^{51}) analysis of the whole PetroPhase 2017 asphaltene and its extrography fractions confirmed the success of the fractionation procedure in the isolation of fractions with varying degrees of aggregation. Specifically, the acetone extrography fraction was the most unaggregated fraction and comprised most of the MMW/LMW V^{51} containing species. Conversely, the Hep/Tol and Tol/THF/MeOH extrography fractions were shifted to lower elution volumes and resided in the HMW (large aggregate size) region of the GPC chromatogram. Comparison of the quantitative GPC ICR-MS (V^{51}) to that of an identical GPC separation coupled online to a 21 T FT-ICR mass spectrometer revealed several trends that support prior offline observations: (1) despite high V^{51} ICP–MS concentrations in the HMW region, very few vanadyl porphyrins were detected by MS. (2) The vanadyl porphyrins detected by MS in the HMW region of the GPC chromatogram were of the lowest carbon number and similar to those detected in the LMW/tailing fraction. (3) Vanadyl porphyrins had the widest carbon number ranges at the end of the MMW/beginning of the LMW region and progressively dropped in carbon number with elution volume (from end of MMW to the final tailing fraction). (4) The MIY of the HMW fraction was more than ~10-fold lower than that of the medium and LMW regions despite 2-fold higher V^{51} concentrations. (5) The overlap in measure V^{51} concentrations and TIC (by MS) for vanadyl porphyrins was greatest for the LMW region of the GPC chromatogram. (6) Similar experiments monitoring S^{32} revealed a greater overlap between the ICP and FT-ICR MS results in the MMW region compared to vanadyl porphyrins and exposed sulfur-containing species that are not detected in offline analysis of the GPC fractions. (7) The offline MS analysis of the GPC fractions most closely resembles that of the LMW/tailing fraction. Collectively, the results support prior observations that aggregation is most likely responsible for the extremely low MIY in the APPI MS analysis of high and MMW regions of the GPC chromatogram. Simply, these species appear to exist as stable aggregates, and thus the amount of unaggregated material available for ionization/detection in the $200 < m/z < 2000$ range is very low. Whether the aggregates are ionized and available for detection at much higher m/z values is not known.[108] The most striking result is the comparison of the vanadyl porphyrins to the sulfur species detected in the HMW/MMW regions. The vanadyl porphyrins are at their lowest carbon numbers in these fractions (close to the PAH limit), whereas the sulfur species are displaced from the PAH line with their widest carbon number and DBE ranges. The vanadyl porphyrins reach their greatest width in carbon number ranges at the end of the medium/beginning of the LMW region but progressively compress their carbon number range as elution progresses through the LMW and into the tailing fraction. Sulfur-containing species exhibit similar behavior and end closest to the PAH line in the tailing fractions. Given that previous tandem MS experiments have demonstrated the island fragmentation behavior of the PetroPhase 2017 asphaltene acetone fraction and archipelago fragmentation of the Hep/Tol and Tol/THF/MeOH fractions, the same MIY trends as a function of extrography fraction (acetone, high MIY and Tol/THF/MeOH, lowest MIY), and revealed that the stability trend for heptane titration of a toluene solution of extrography fractions is acetone (most stable), Hep/Tol (less stable), to Tol/THF/MeOH (least stable); the results presented herein strongly suggest that the archipelago dominant Hep/Tol and Tol/THF/MeOH extrography fractions of the PetroPhase 2017 asphaltenes are strongly aggregated and a large fraction of the vanadyl porphyrin species remain locked inside the aggregate and are thus unavailable for ionization/detection by MS. Those porphyrins that are available are alkyl deficient and most likely absorbed to the aggregate surface. Unaggregated porphyrins are readily detected in the LMW/tailing fractions and elute from higher alkylated to lower alkylated species as previous observed with other GPC/FT-ICR MS studies. Conversely, sulfur-containing species are most highly alkylated in the HMW/MMW regions and compress quickly in their carbon number distribution widths in the LMW/tailing fraction. If one assumes that this

https://dx.doi.org/10.1021/acs.energyfuels.0c03349
Energy Fuels XXXX, XXX, XXX−XXX

contradictory behavior between the observed vanadyl porphyrins and sulfur-containing species is attributable to species that are absorbed on the aggregate surface (vanadyl porphyrins) to some fraction of those present in the aggregate (sulfur species), the large differences in the widths of their corresponding carbon number distribution (~5 for vanadyl porphyrins compared to ~40 for sulfur-containing species) supports the importance of London forces between alkane moieties in stable aggregates.

CONCLUDING REMARKS

The interlaboratory sample known as PetroPhase 2017 asphaltenes and its extrography fractions were separated via GPC into four fractions: HMW (aggregates), MMW, LMW (non-aggregated/monomers), and "tailing" (free species). The separation was hyphenated to elemental analysis by $^{51}V/^{32}S$-ICP-MS (quantitative) and APPI 21 T-FT-ICR-MS (molecular formula assignment).

Quantitative results via ICP−MS and compositional features accessed by FT-ICR MS indicate:

- Extrography yields asphaltene fractions with distinctive aggregation behavior. Acetone reveals abundant MMW and LMW species, whereas Hep/Tol and Tol/THF/MeOH are enriched with highly aggregated compounds (HMW).
- Ion production (as detected by APPI FT-ICR MS) is inversely proportional to aggregate size (determined by GPC). The acetone fraction, shown to aggregate to a lesser extent than Tol/THF/MeOH, reveals the highest production efficiency of non-aggregated V/S-containing compounds.
- ICs for specific molecular formulas, mostly detected in the monomeric GPC fractions, suggest that alkyl-chain content and exocyclic rings govern the elution behavior of free/non-aggregated porphyrins. "Free"/highly substituted vanadyl porphyrins elute earlier likely because of their decreased interaction with the GPC column.
- Compositional trends for S-containing molecules indicate that HMW/MMW aggregates contain abundant species with a higher content of carbon atoms in alkyl-side chains. For these GPC fractions, oxygen-rich compounds (SO_x classes) feature low DBE values. Conversely, non-aggregated/monomeric GPC fractions (LMW/tailing) reveal abundant highly aromatic, likely pericondensed, alkyl-depleted molecules.
- These structural features suggest that alkyl-side chain moieties and polarizable functionalities could have a central role in asphaltene aggregation. In other words, π-stacking is not the dominant intermolecular force that rules petroleum aggregation.
- The results indicate that APPI MS characterization is highly limited by aggregation, and advanced separations, as well as online FT-ICR MS detection, are required to overcome these limitations.

ASSOCIATED CONTENT

Supporting Information

The Supporting Information is available free of charge at https://pubs.acs.org/doi/10.1021/acs.energyfuels.0c03349.

MIY and ^{51}V GPC ICP−MS chromatogram for whole PetroPhase 2017 asphaltenes; compositional range for vanadyl porphyrins for all GPC subfractions and ICs for selected $N_4O_1{}^{51}V_1$ molecular formulas for Hep/Tol PetroPhase 2017 asphaltenes; GPC ^{32}S ICP−MS and ICs for S-containing groups for whole PetroPhase 2017 asphaltenes and its Hep/Tol fraction; and DBE versus carbon number plots for S_x, S_xO_y, and $N_xO_yS_z$ groups (PDF)

AUTHOR INFORMATION

Corresponding Authors

Brice Bouyssiere − *International Joint Laboratory iC2MC: Complex Matrices Molecular Characterization, Total Research & Technology, Gonfreville, 76700 Harfleur, France; Université de Pau et des Pays de l'Adour, E2S UPPA, CNRS, IPREM, Institut des Sciences Analytiques et de Physico-chimie pour l'Environnement et les Materiaux, UMR5254, Hélioparc, 64053 Pau, France;* orcid.org/0000-0001-5878-6067; Email: brice.bouyssiere@univ-pau.fr

Ryan P. Rodgers − *Ion Cyclotron Resonance Program, National High Magnetic Field Laboratory and Future Fuels Institute, Florida State University, Tallahassee, Florida 32310, United States; International Joint Laboratory iC2MC: Complex Matrices Molecular Characterization, Total Research & Technology, Gonfreville, 76700 Harfleur, France; Université de Pau et des Pays de l'Adour, E2S UPPA, CNRS, IPREM, Institut des Sciences Analytiques et de Physico-chimie pour l'Environnement et les Materiaux, UMR5254, Hélioparc, 64053 Pau, France;* orcid.org/0000-0003-1302-2850; Email: rodgers@magnet.fsu.edu

Authors

Martha L. Chacón-Patiño − *Ion Cyclotron Resonance Program, National High Magnetic Field Laboratory, Florida State University, Tallahassee, Florida 32310, United States; International Joint Laboratory iC2MC: Complex Matrices Molecular Characterization, Total Research & Technology, Gonfreville, 76700 Harfleur, France;* orcid.org/0000-0002-7273-5343

Rémi Moulian − *International Joint Laboratory iC2MC: Complex Matrices Molecular Characterization, Total Research & Technology, Gonfreville, 76700 Harfleur, France; Université de Pau et des Pays de l'Adour, E2S UPPA, CNRS, IPREM, Institut des Sciences Analytiques et de Physico-chimie pour l'Environnement et les Materiaux, UMR5254, Hélioparc, 64053 Pau, France*

Caroline Barrère-Mangote − *International Joint Laboratory iC2MC: Complex Matrices Molecular Characterization, Total Research & Technology, Gonfreville, 76700 Harfleur, France; TOTAL Raffinage Chimie, TRTG, 76700 Harfleur, France*

Jonathan C. Putman − *Ion Cyclotron Resonance Program, National High Magnetic Field Laboratory, Florida State University, Tallahassee, Florida 32310, United States*

Chad R. Weisbrod − *Ion Cyclotron Resonance Program, National High Magnetic Field Laboratory, Florida State University, Tallahassee, Florida 32310, United States;* orcid.org/0000-0001-5324-4525

Greg T. Blakney − *Ion Cyclotron Resonance Program, National High Magnetic Field Laboratory, Florida State University, Tallahassee, Florida 32310, United States;* orcid.org/0000-0002-4205-9866

Pierre Giusti − *International Joint Laboratory iC2MC: Complex Matrices Molecular Characterization, Total Research & Technology, Gonfreville, 76700 Harfleur, France;*

https://dx.doi.org/10.1021/acs.energyfuels.0c03349
Energy Fuels XXXX, XXX, XXX−XXX

TOTAL Raffinage Chimie, TRTG, 76700 Harfleur, France; orcid.org/0000-0002-9569-3158

Complete contact information is available at: https://pubs.acs.org/10.1021/acs.energyfuels.0c03349

Notes

The authors declare no competing financial interest.

■ ACKNOWLEDGMENTS

A portion of this work was performed at the National High Magnetic Field Laboratory ICR User Facility, which is supported by the National Science Foundation Division of Chemistry through Cooperative Agreements DMR-1157490 and DMR-1644779, and the State of Florida; and Conseil Régional d'Aquitaine (20071303002PFM), and FEDER (31486/08011464). The authors thank TOTAL and Professor Marianny Combariza, Industrial University of Santander–Colombia, for supplying the PetroPhase 2017 asphaltenes.

■ REFERENCES

(1) Molnárné Guricza, L.; Schrader, W. New Separation Approach for Asphaltene Investigation: Argentation Chromatography Coupled with Ultrahigh-Resolution Mass Spectrometry. *Energy Fuels* **2015**, *29*, 6224–6230.

(2) Moir, M. E. *Asphaltenes, What Art Thou?: Asphaltenes and the Boduszynski Continuum*; ACS Symposium Series; American Chemical Society, 2018.

(3) Mullins, O. C. The Modified Yen Model. *Energy Fuels* **2010**, *24*, 2179–2207.

(4) Gray, M. R. Whatsoever things are true: Hypothesis, artefact, and bias in chemical engineering research. *Can. J. Chem. Eng.* **2020**, 1–14.

(5) Schuler, B.; Meyer, G.; Peña, D.; Mullins, O. C.; Gross, L. Unraveling the Molecular Structures of Asphaltenes by Atomic Force Microscopy. *J. Am. Chem. Soc.* **2015**, *137*, 9870–9876.

(6) Schuler, B.; Fatayer, S.; Meyer, G.; Rogel, E.; Moir, M.; Zhang, Y.; Harper, M. R.; Pomerantz, A. E.; Bake, K. D.; Witt, M.; et al. Heavy Oil Based Mixtures of Different Origins and Treatments Studied by Atomic Force Microscopy. *Energy Fuels* **2017**, *31*, 6856–6861.

(7) Kaiser, N. K.; Quinn, J. P.; Blakney, G. T.; Hendrickson, C. L.; Marshall, A. G. A Novel 9.4 Tesla FTICR Mass Spectrometer with Improved Sensitivity, Mass Resolution, and Mass Range. *J. Am. Soc. Mass Spectrom.* **2011**, *22*, 1343–1351.

(8) Hendrickson, C. L.; Quinn, J. P.; Kaiser, N. K.; Smith, D. F.; Blakney, G. T.; Chen, T.; Marshall, A. G.; Weisbrod, C. R.; Beu, S. C. 21 Tesla Fourier Transform Ion Cyclotron Resonance Mass Spectrometer: A National Resource for Ultrahigh Resolution Mass Analysis. *J. Am. Soc. Mass Spectrom.* **2015**, *26*, 1626–1632.

(9) Niles, S. F.; Chacón-Patiño, M. L.; Smith, D. F.; Rodgers, R. P.; Marshall, A. G. Comprehensive Compositional and Structural Comparison of Coal and Petroleum Asphaltenes Based on Extrography Fractionation Coupled with Fourier Transform Ion Cyclotron Resonance MS and MS/MS Analysis. *Energy Fuels* **2020**, *34*, 1492–1505.

(10) Mullins, O. C.; Sabbah, H.; Eyssautier, J.; Pomerantz, A. E.; Barré, L.; Andrews, A. B.; Ruiz-Morales, Y.; Mostowfi, F.; McFarlane, R.; Goual, L.; Lepkowicz, R.; Cooper, T.; Orbulescu, J.; Leblanc, R. M.; Edwards, J.; Zare, R. N. Advances in Asphaltene Science and the Yen–Mullins Model. *Energy Fuels* **2012**, *26*, 3986–4003.

(11) Mullins, O. C. The Asphaltenes. *Annu. Rev. Anal. Chem.* **2011**, *4*, 393–418.

(12) Barré, L.; Espinat, D.; Rosenberg, E.; Scarsella, M. Colloidal Structure of Heavy Crudes and Asphaltene Solutions. *Rev. Inst. Fr. Pét.* **1997**, *52*, 161–175.

(13) Chen, P.; Joshi, Y. V.; Metz, J. N.; Yao, N.; Zhang, Y. Conformational Analysis of Nonplanar Archipelago Structures on a Cu (111) Surface by Molecular Imaging. *Energy Fuels* **2020**, *34*, 12135–12141.

(14) Schuler, B.; Zhang, Y.; Liu, F.; Pomerantz, A. E.; Andrews, A. B.; Gross, L.; Pauchard, V.; Banerjee, S.; Mullins, O. C. Overview of Asphaltene Nanostructures and Thermodynamic Applications. *Energy Fuels* **2020**, DOI: 10.1021/acs.energyfuels.0c00874.

(15) Zuo, J. Y.; Jackson, R.; Agarwal, A.; Herold, B.; Kumar, S.; De Santo, I.; Dumont, H.; Ayan, C.; Beardsell, M.; Mullins, O. C. Diffusion Model Coupled with the Flory-Huggins-Zuo Equation of State and Yen-Mullins Model Accounts for Large Viscosity and Asphaltene Variations in a Reservoir Undergoing Active Biodegradation. *Energy Fuels* **2015**, *29*, 1447–1460.

(16) Chacón-Patiño, M. L.; Rowland, S. M.; Rodgers, R. P. Advances in Asphaltene Petroleomics. Part 1: Asphaltenes Are Composed of Abundant Island and Archipelago Structural Motifs. *Energy Fuels* **2017**, *31*, 13509–13518.

(17) Podgorski, D. C.; Corilo, Y. E.; Nyadong, L.; Lobodin, V. V.; Bythell, B. J.; Robbins, W. K.; McKenna, A. M.; Marshall, A. G.; Rodgers, R. P. Heavy Petroleum Composition. 5. Compositional and Structural Continuum of Petroleum Revealed. *Energy Fuels* **2013**, *27*, 1268–1276.

(18) Savage, P. E.; Klein, M. T.; Kukes, S. G. Asphaltene Reaction Pathways. 1. Thermolysis. *Ind. Eng. Chem. Process Des. Dev.* **1985**, *24*, 1169–1174.

(19) Karimi, A.; Qian, K.; Olmstead, W. N.; Freund, H.; Yung, C.; Gray, M. R. Quantitative Evidence for Bridged Structures in Asphaltenes by Thin Film Pyrolysis. *Energy Fuels* **2011**, *25*, 3581–3589.

(20) Rueda-Velásquez, R. I.; Freund, H.; Qian, K.; Olmstead, W. N.; Gray, M. R. Characterization of Asphaltene Building Blocks by Cracking under Favorable Hydrogenation Conditions. *Energy Fuels* **2013**, *27*, 1817–1829.

(21) Gray, M. R.; Tykwinski, R. R.; Stryker, J. M.; Tan, X. Supramolecular Assembly Model for Aggregation of Petroleum Asphaltenes. *Energy Fuels* **2011**, *25*, 3125–3134.

(22) Castillo, J.; Vargas, V. Metal Porphyrin Occlusion: Adsorption during Asphaltene Aggregation. *Pet. Sci. Technol.* **2016**, *34*, 873–879.

(23) Qiao, P.; Harbottle, D.; Tchoukov, P.; Masliyah, J.; Sjöblom, J.; Liu, Q.; Xu, Z. Fractionation of Asphaltenes in Understanding Their Role in Petroleum Emulsion Stability and Fouling. *Energy Fuels* **2017**, *31*, 3330–3337.

(24) Yang, F.; Tchoukov, P.; Dettman, H.; Teklebrhan, R. B.; Liu, L.; Dabros, T.; Czarnecki, J.; Masliyah, J.; Xu, Z. Asphaltene Subfractions Responsible for Stabilizing Water-in-Crude Oil Emulsions. Part 2: Molecular Representations and Molecular Dynamics Simulations. *Energy Fuels* **2015**, *29*, 4783–4794.

(25) Natarajan, A.; Kuznicki, N.; Harbottle, D.; Masliyah, J.; Zeng, H.; Xu, Z. Understanding Mechanisms of Asphaltene Adsorption from Organic Solvent on Mica. *Langmuir* **2014**, *30*, 9370–9377.

(26) Hsu, C. S.; Hendrickson, C. L.; Rodgers, R. P.; McKenna, A. M.; Marshall, A. G. Petroleomics: Advanced Molecular Probe for Petroleum Heavy Ends. *J. Mass Spectrom.* **2011**, *46*, 337–343.

(27) Rodgers, R. P.; Marshall, A. G. Petroleomics: Advanced Characterization of Petroleum-Derived Materials by Fourier Transform Ion Cyclotron Resonance Mass Spectrometry (FT-ICR MS). In *Asphaltenes, Heavy Oils, and Petroleomics*; Mullins, O. C., Sheu, E. Y., Hammam, A., Marshall, A. G., Eds.; Springer, 2007; pp 63–93.

(28) McKenna, A. M.; Williams, J. T.; Putman, J. C.; Aeppli, C.; Reddy, C. M.; Valentine, D. L.; Lemkau, K. L.; Kellermann, M. Y.; Savory, J. J.; Kaiser, N. K.; et al. Unprecedented Ultrahigh Resolution FT-ICR Mass Spectrometry and Parts-per-Billion Mass Accuracy Enable Direct Characterization of Nickel and Vanadyl Porphyrins in Petroleum from Natural Seeps. *Energy Fuels* **2014**, *28*, 2454–2464.

(29) Chacón-Patiño, M. L.; Rowland, S. M.; Rodgers, R. P. Advances in Asphaltene Petroleomics. Part 2: Selective Separation Method That Reveals Fractions Enriched in Island and Archipelago Structural Motifs by Mass Spectrometry. *Energy Fuels* **2018**, *32*, 314–328.

(30) Chacón-Patiño, M. L.; Rowland, S. M.; Rodgers, R. P. Advances in Asphaltene Petroleomics. Part 3. Dominance of Island or Archipelago Structural Motif Is Sample Dependent. *Energy Fuels* **2018**, *32*, 9106−9120.
(31) Wittrig, A. M.; Fredriksen, T. R.; Qian, K.; Clingenpeel, A. C.; Harper, M. R. Single Dalton Collision-Induced Dissociation for Petroleum Structure Characterization. *Energy Fuels* **2017**, *31*, 13338−13344.
(32) Rüger, C. P.; Miersch, T.; Schwemer, T.; Sklorz, M.; Zimmermann, R. Hyphenation of Thermal Analysis to Ultrahigh-Resolution Mass Spectrometry (Fourier Transform Ion Cyclotron Resonance Mass Spectrometry) Using Atmospheric Pressure Chemical Ionization For Studying Composition and Thermal Degradation of Complex Materials. *Anal. Chem.* **2015**, *87*, 6493−6499.
(33) Rüger, C. P.; Grimmer, C.; Sklorz, M.; Neumann, A.; Streibel, T.; Zimmermann, R. Combination of Different Thermal Analysis Methods Coupled to Mass Spectrometry for the Analysis of Asphaltenes and Their Parent Crude Oils: Comprehensive Characterization of the Molecular Pyrolysis Pattern. *Energy Fuels* **2017**, *32*, 2699−2711.
(34) Rüger, C. P.; Neumann, A.; Sklorz, M.; Schwemer, T.; Zimmermann, R. Thermal Analysis Coupled to Ultrahigh Resolution Mass Spectrometry with Collision Induced Dissociation for Complex Petroleum Samples: Heavy Oil Composition and Asphaltene Precipitation Effects. *Energy Fuels* **2017**, *31*, 13144−13158.
(35) Nyadong, L.; Lai, J.; Thompsen, C.; LaFrancois, C. J.; Cai, X.; Song, C.; Wang, J.; Wang, W. High-Field Orbitrap Mass Spectrometry and Tandem Mass Spectrometry for Molecular Characterization of Asphaltenes. *Energy Fuels* **2018**, *32*, 294−305.
(36) Dong, X.; Zhang, Y.; Milton, J.; Yerabolu, R.; Easterling, L.; Kenttämaa, H. I. Investigation of the relative abundances of single-core and multicore compounds in asphaltenes by using high-resolution in-source collision-activated dissociation and medium-energy collision-activated dissociation mass spectrometry with statistical considerations. *Fuel* **2019**, *246*, 126−132.
(37) Qiao, P.; Harbottle, D.; Li, Z.; Tang, Y.; Xu, Z. Interactions of Asphaltene Subfractions in Organic Media of Varying Aromaticity. *Energy Fuels* **2018**, *32*, 10478.
(38) Ballard, D. A.; Chacón-Patiño, M. L.; Qiao, P.; Roberts, K. J.; Rae, R.; Dowding, P. J.; Xu, Z.; Harbottle, D. Molecular Characterization of Strongly- and Weakly-Interfacially Active Asphaltenes by High-Resolution Mass Spectrometry. *Energy Fuels* **2020**, *34*, 13966.
(39) Clingenpeel, A. C.; Rowland, S. M.; Corilo, Y. E.; Zito, P.; Rodgers, R. P. Fractionation of Interfacial Material Reveals a Continuum of Acidic Species That Contribute to Stable Emulsion Formation. *Energy Fuels* **2017**, *31*, 5933−5939.
(40) Jarvis, J. M.; Robbins, W. K.; Corilo, Y. E.; Rodgers, R. P. Novel Method to Isolate Interfacial Material. *Energy Fuels* **2015**, *29*, 7058−7064.
(41) Boduszynski, M. M. Composition of Heavy Petroleums. 1. Molecular Weight, Hydrogen Deficiency, and Heteroatom Concentration as a Function of Atmospheric Equivalent Boiling Point up to 1400 °F (760 °C). *Energy Fuels* **1987**, *1*, 2−11.
(42) McKenna, A. M.; Purcell, J. M.; Rodgers, R. P.; Marshall, A. G. Heavy Petroleum Composition. 1. Exhaustive Compositional Analysis of Athabasca Bitumen HVGO Distillates by Fourier Transform Ion Cyclotron Resonance Mass Spectrometry: A Definitive Test of the Boduszynski Model. *Energy Fuels* **2010**, *24*, 2929−2938.
(43) McKenna, A. M.; Blakney, G. T.; Xian, F.; Glaser, P. B.; Rodgers, R. P.; Marshall, A. G. Heavy Petroleum Composition. 2. Progression of the Boduszynski Model to the Limit of Distillation by Ultrahigh-Resolution FT-ICR Mass Spectrometry. *Energy Fuels* **2010**, *24*, 2939−2946.
(44) Chacón-Patiño, M. L.; Rowland, S. M.; Rodgers, R. P. The Compositional and Structural Continuum of Petroleum from Light Distillates to Asphaltenes: The Boduszynski Continuum Theory As Revealedby FT-ICR Mass Spectrometry. In *The Boduszynski Continuum: Contributions to the Understanding of the Molecular Composition of Petroleum*; Ovalles, C., Moir, M. E., Eds.; ACS Symposium Series; American Chemical Society: Washington, DC, 2018; Vol. *1282*, pp 113−171.
(45) Rodgers, R. P.; Schaub, T. M.; Marshall, A. G. Petroleomics: MS Returns to Its Roots. *Anal. Chem.* **2005**, *77*, 20 A−27 A.
(46) Qian, K.; Edwards, K. E.; Diehl, J. H.; Green, L. A. Fundamentals and Applications of Electrospray Ionization Mass Spectrometry for Petroleum Characterization. *Energy Fuels* **2004**, *18*, 1784−1791.
(47) Purcell, J. M.; Hendrickson, C. L.; Rodgers, R. P.; Marshall, A. G. Atmospheric Pressure Photoionization Proton Transfer for Complex Organic Mixtures Investigated by Fourier Transform Ion Cyclotron Resonance Mass Spectrometry. *J. Am. Soc. Mass Spectrom.* **2007**, *18*, 1682−1689.
(48) Ramírez-Pradilla, J. S.; Blanco-Tirado, C.; Hubert-Roux, M.; Giusti, P.; Afonso, C.; Combariza, M. Y. Comprehensive Petroporphyrin Identification in Crude Oils Using Highly Selective Electron Transfer Reactions in MALDI-FTICR-MS. *Energy Fuels* **2019**, *33*, 3899−3907.
(49) Gaspar, A.; Zellermann, E.; Lababidi, S.; Reece, J.; Schrader, W. Characterization of Saturates, Aromatics, Resins, and Asphaltenes Heavy Crude Oil Fractions by Atmospheric Pressure Laser Ionization Fourier Transform Ion Cyclotron Resonance Mass Spectrometry. *Energy Fuels* **2012**, *26*, 3481−3487.
(50) Gaspar, A.; Zellermann, E.; Lababidi, S.; Reece, J.; Schrader, W. Impact of Different Ionization Methods on the Molecular Assignments of Asphaltenes by FT-ICR Mass Spectrometry. *Anal. Chem.* **2012**, *84*, 5257−5267.
(51) Pomerantz, A. E.; Hammond, M. R.; Morrow, A. L.; Mullins, O. C.; Zare, R. N. Two-Step Laser Mass Spectrometry of Asphaltenes. *J. Am. Chem. Soc.* **2008**, *130*, 7216−7217.
(52) Gutiérrez Sama, S.; Farenc, M.; Barrère-Mangote, C.; Lobinski, R.; Afonso, C.; Bouyssière, B.; Giusti, P. Molecular Fingerprints and Speciation of Crude Oils and Heavy Fractions Revealed by Molecular and Elemental Mass Spectrometry: Keystone between Petroleomics, Metallopetroleomics, and Petrointeractomics. *Energy Fuels* **2018**, *32*, 4593−4605.
(53) Farenc, M.; Corilo, Y. E.; Lalli, P. M.; Riches, E.; Rodgers, R. P.; Afonso, C.; Giusti, P. Comparison of Atmospheric Pressure Ionization for the Analysis of Heavy Petroleum Fractions with Ion Mobility-Mass Spectrometry. *Energy Fuels* **2016**, *30*, 8896−8903.
(54) Huba, A. K.; Huba, K.; Gardinali, P. R. Understanding the Atmospheric Pressure Ionization of Petroleum Components: The Effects of Size, Structure, and Presence of Heteroatoms. *Sci. Total Environ.* **2016**, *568*, 1018−1025.
(55) Cho, Y.; Na, J.-G.; Nho, N.-S.; Kim, S.; Kim, S. Application of Saturates, Aromatics, Resins, Asphaltenes Crude Oil Fractionation for Detailed Chemical Characterization of Heavy Crude Oils by Fourier Transform Ion Cyclotron Resonance Mass Spectrometry Equipped with Atmospheric Pressure Photoionization. *Energy Fuels* **2012**, *26*, 2558−2565.
(56) Buenrostro-Gonzalez, E.; Andersen, S. I.; Garcia-Martinez, J. A.; Lira-Galeana, C. Solubility/Molecular Structure Relationships of Asphaltenes in Polar and Nonpolar Media. *Energy Fuels* **2002**, *16*, 732−741.
(57) Zhang, Y.; Schulz, F.; Rytting, B. M.; Walters, C. C.; Kaiser, K.; Metz, J. N.; Harper, M. R.; Merchant, S. S.; Mennito, A. S.; Qian, K.; et al. Elucidating the Geometric Substitution of Petroporphyrins by Spectroscopic Analysis and Atomic Force Microscopy Molecular Imaging. *Energy Fuels* **2019**, *33*, 6088−6097.
(58) Gutierrez Sama, S.; Desprez, A.; Krier, G.; Lienemann, C. P.; Barbier, J.; Lobinski, R.; Barrere-Mangote, C.; Giusti, P.; Bouyssiere, B. Study of the Aggregation of Metal Complexes with Asphaltenes Using Gel Permeation Chromatography Inductively Coupled Plasma High-Resolution Mass Spectrometry. *Energy Fuels* **2016**, *30*, 6907−6912.
(59) Ligiero, L. M.; Bouriat, P.; Dicharry, C.; Passade-Boupat, N.; Lalli, P. M.; Rodgers, R. P.; Barrère-Mangote, C.; Giusti, P.; Bouyssiere, B. Characterization of Crude Oil Interfacial Material

https://dx.doi.org/10.1021/acs.energyfuels.0c03349
Energy Fuels XXXX, XXX, XXX−XXX

Isolated by the Wet Silica Method. Part 1: Gel Permeation Chromatography Inductively Coupled Plasma High-Resolution Mass Spectrometry Analysis. *Energy Fuels* **2017**, *31*, 1065−1071.
(60) Caumette, G.; Lienemann, C.-P.; Merdrignac, I.; Bouyssiere, B.; Lobinski, R. Fractionation and Speciation of Nickel and Vanadium in Crude Oils by Size Exclusion Chromatography-ICP MS and Normal Phase HPLC-ICP MS. *J. Anal. At. Spectrom.* **2010**, *25*, 1123−1129.
(61) Desprez, A.; Bouyssiere, B.; Arnaudguilhem, C.; Krier, G.; Vernex-Loset, L.; Giusti, P. Study of the Size Distribution of Sulfur, Vanadium, and Nickel Compounds in Four Crude Oils and Their Distillation Cuts by Gel Permeation Chromatography Inductively Coupled Plasma High-Resolution Mass Spectrometry. *Energy Fuels* **2014**, *28*, 3730−3737.
(62) Berrueco, C.; Venditti, S.; Morgan, T. J.; Álvarez, P.; Millan, M.; Herod, A. A.; Kandiyoti, R. Calibration of Size-Exclusion Chromatography Columns with 1-Methyl-2-Pyrrolidinone (NMP)/Chloroform Mixtures as Eluent: Applications to Petroleum-Derived Samples. *Energy Fuels* **2008**, *22*, 3265−3274.
(63) Putman, J. C.; Moulian, R.; Barrère-Mangote, C.; Rodgers, R. P.; Bouyssiere, B.; Giusti, P.; Marshall, A. G. Probing Aggregation Tendencies in Asphaltenes by Gel Permeation Chromatography. Part 1: Online Inductively Coupled Plasma Mass Spectrometry and Offline Fourier Transform Ion Cyclotron Resonance Mass Spectrometry. *Energy Fuels* **2020**, *34*, 8308−8315.
(64) Carbognani, L.; Rogel, E. Solvent Swelling of Petroleum Asphaltenes. *Energy Fuels* **2002**, *16*, 1348−1358.
(65) Carbognani, L.; Rogel, E. Solid Petroleum Asphaltenes Seem Surrounded by Alkyl Layers. *Pet. Sci. Technol.* **2003**, *21*, 537−556.
(66) Stachowiak, C.; Viguié, J.-R.; Grolier, J.-P. E.; Rogalski, M. Effect of N-Alkanes on Asphaltene Structuring in Petroleum Oils. *Langmuir* **2005**, *21*, 4824−4829.
(67) Alawani, N. A.; Panda, S. K.; Lajami, A. R.; Al-Qunaysi, T. A.; Muller, H. Characterization of Crude Oils through Alkyl Chain-Based Separation by Gel Permeation Chromatography and Mass Spectrometry. *Energy Fuels* **2020**, *34*, 5414−5425.
(68) Panda, S. K.; Alawani, N. A.; Lajami, A. R.; Al-Qunaysi, T. A.; Muller, T. Characterization of Aromatic Hydrocarbons and Sulfur Heterocycles in Saudi Arabian Heavy Crude Oil by Gel Permeation Chromatography and Ultrahigh Resolution Mass Spectrometry. *Fuel* **2019**, *235*, 1420.
(69) Putman, J. C.; Moulian, R.; Smith, D. F.; Weisbrod, C. R.; Chacón-Patiño, M. L.; Corilo, Y. E.; Blakney, G. T.; Rumancik, L. E.; Rodgers, C. P.; Giusti, P.; et al. Probing Aggregation Tendencies in Asphaltenes by Gel Permeation Chromatography. Part 2: Online Inductively Coupled Plasma Mass Spectrometry and Offline Fourier Transform Ion Cyclotron Resonance Mass Spectrometry. *Energy Fuels* **2020**, *34*, 10915.
(70) Molnárné Guricza, L.; Schrader, W. Optimized Asphaltene Separation by Online Coupling of Size Exclusion Chromatography and Ultrahigh Resolution Mass Spectrometry. *Fuel* **2018**, *215*, 631−637.
(71) Smith, D. F.; Podgorski, D. C.; Rowland, S. M.; Hendrickson, C. L. 21 Tesla FT-ICR Mass Spectrometer for Complex Mixture Analysis. *Proceedings of the ASMS Asilomar Conference 2016 Pacific Grove, CA, USA, October 14−18*, 2016.
(72) Chacón-Patiño, M. L.; Vesga-Martínez, S. J.; Blanco-Tirado, C.; Orrego-Ruiz, J. A.; Gómez-Escudero, A.; Combariza, M. Y. Exploring Occluded Compounds and Their Interactions with Asphaltene Networks Using High-Resolution Mass Spectrometry. *Energy Fuels* **2016**, *30*, 4550−4561.
(73) Giraldo-Dávila, D.; Chacón-Patiño, M. L.; McKenna, A. M.; Blanco-Tirado, C.; Combariza, M. Y. Correlations between Molecular Composition and Adsorption, Aggregation, and Emulsifying Behaviors of PetroPhase 2017 Asphaltenes and Their Thin-Layer Chromatography Fractions. *Energy Fuels* **2018**, *32*, 2769.
(74) Chacón-Patinõ, M. L.; Smith, D. F.; Hendrickson, C. L.; Marshall, A. G.; Rodgers, R. P. Advances in Asphaltene Petroleomics. Part 4. Compositional Trends of Solubility Subfractions Reveal That Polyfunctional Oxygen-Containing Compounds Drive Asphaltene Chemistry. *Energy Fuels* **2020**, *34*, 3013−3030.
(75) Gascon, G.; Vargas, V.; Feo, L.; Castellano, O.; Castillo, J.; Giusti, P.; Acavedo, S.; Lienemann, C.-P.; Bouyssiere, B. Size Distributions of Sulfur, Vanadium, and Nickel Compounds in Crude Oils, Residues, and Their Saturate, Aromatic, Resin, and Asphaltene Fractions Determined by Gel Permeation Chromatography Inductively Coupled Plasma High-Resolution Mass Spectrometry. *Energy Fuels* **2017**, *31*, 7783−7788.
(76) Kaiser, N. K.; Savory, J. J.; Hendrickson, C. L. Controlled Ion Ejection from an External Trap for Extended m/z Range in FT-ICR Mass Spectrometry. *J. Am. Soc. Mass Spectrom.* **2014**, *25*, 943−949.
(77) Blakney, G. T.; Hendrickson, C. L.; Marshall, A. G. Predator Data Station: A Fast Data Acquisition System for Advanced FT-ICR MS Experiments. *Int. J. Mass Spectrom.* **2011**, *306*, 246−252.
(78) Corilo, Y. E. *PetroOrg Software*; Florida State University; all rights reserved, 2013. http://www.petroorg.com.
(79) Putman, J. C.; Moulian, R.; Smith, D. F.; Weisbrod, C. R.; Chacón-Patiño, M. L.; Corilo, Y. E.; Blakney, G. T.; Rumancik, L. E.; Barrère-Mangote, C.; Rodgers, R. P.; et al. Probing Aggregation Tendencies in Asphaltenes by Gel Permeation Chromatography. Part 2: Online Detection by Fourier Transform Ion Cyclotron Resonance Mass Spectrometry and Inductively Coupled Plasma Mass Spectrometry. *Energy Fuels* **2020**, *34*, 10915−10925.
(80) Acevedo, N.; Moulian, R.; Chacon-Patino, M. L.; Mejia, A.; Radji, S.; Daridon, J.-L.; Mangote, C.; Giusti, P.; Rodgers, R. P.; Piscitelli, V.; et al. Understanding Asphaltene Fraction Behavior through Combined Quartz Crystal Resonator Sensor, FT-ICR MS, GPC ICP HR-MS and AFM Characterization. Part I: Extrography Fractionations. *Energy Fuels* **2020**, *34*, 13903.
(81) Kalli, A.; Smith, G. T.; Sweredoski, M. J.; Hess, S. Evaluation and Optimization of Mass Spectrometric Settings during Data-Dependent Acquisition Mode: Focus on LTQ-Orbitrap Mass Analyzers. *J. Proteome Res.* **2013**, *12*, 3071−3086.
(82) Zhao, X.; Shi, Q.; Gray, M. R.; Xu, C. New Vanadium Compounds in Venezuela Heavy Crude Oil Detected by Positive-Ion Electrospray Ionization Fourier Transform Ion Cyclotron Resonance Mass Spectrometry. *Nature* **2014**, *4*, 5373.
(83) Qian, K.; Fredriksen, T. R.; Mennito, A. S.; Zhang, Y.; Harper, M. R.; Merchant, S.; Kushnerick, J. D.; Rytting, B. M.; Kilpatrick, P. K. Evidence of Naturally-Occurring Vanadyl Porphyrins Containing Multiple S and O Atoms. *Fuel* **2019**, *239*, 1258−1264.
(84) Putman, J. C.; Rowland, S. M.; Corilo, Y. E.; McKenna, A. M. Chromatographic Enrichment and Subsequent Separation of Nickel and Vanadyl Porphyrins from Natural Seeps and Molecular Characterization by Positive Electrospray Ionization FT-ICR Mass Spectrometry. *Anal. Chem.* **2014**, *86*, 10708−10715.
(85) Lin, Y.-J.; Cao, T.; Chacón-Patiño, M. L.; Rowland, S. M.; Rodgers, R. P.; Yen, A.; Biswal, S. L. Microfluidic Study of the Deposition Dynamics of Asphaltene Subfractions Enriched with Island and Archipelago Motifs. *Energy Fuels* **2019**, *33*, 1882−1891.
(86) Evdokimov, I. N.; Fesan, A. A.; Losev, A. P. Occlusion of Foreign Molecules in Primary Asphaltene Aggregates from Near-UV-Visible Absorption Studies. *Energy Fuels* **2017**, *31*, 1370−1375.
(87) Milordov, D. V.; Usmanova, G. S.; Yakubov, M. R.; Yakubova, S. G.; Romanov, G. V. Comparative Analysis of Extractive Methods of Porphyrin Separation from Heavy Oil Asphatenes. *Chem. Technol. Fuels Oils* **2013**, *49*, 232−238.
(88) Dechaine, G. P.; Gray, M. R. Chemistry and Association of Vanadium Compounds in Heavy Oil and Bitumen, and Implications for Their Selective Removal. *Energy Fuels* **2010**, *24*, 2795−2808.
(89) Novelli, J. M.; Medina, J. C.; Lena, L.; Ruiz, J. M.; Vincent, E. J. Vanadium in Heavy Petroleum Crudes. *Collect. Colloq. Semin. (Inst. Fr. Pet.)* **1984**, *40*, 169−172.
(90) McKenna, A. M.; Purcell, J. M.; Rodgers, R. P.; Marshall, A. G. Identification of Vanadyl Porphyrins in a Heavy Crude Oil and Raw Asphaltene by Atmospheric Pressure Photoionization Fourier Transform Ion Cyclotron Resonance (FT-ICR) Mass Spectrometry. *Energy Fuels* **2009**, *23*, 2122−2128.

https://dx.doi.org/10.1021/acs.energyfuels.0c03349
Energy Fuels XXXX, XXX, XXX−XXX

(91) Ali, M. F.; Perzanowski, H.; Bukhari, A.; Al-haji, A. A. Nickel and Vanadyl Porphyrins in Saudi Arabian Crude Oils. *Energy Fuels* **1993**, *7*, 179−184.
(92) Qian, K.; Edwards, K. E.; Mennito, A. S.; Walters, C. C.; Kushnerick, J. D. Enrichment, Resolution, and Identification of Nickel Porphyrins in Petroleum Asphaltene by Cyclograph Separation and Atmospheric Pressure Photoionization Fourier Transform Ion Cyclotron Resonance Mass Spectrometry. *Anal. Chem.* **2010**, *82*, 413−419.
(93) Rosell-Melé, A.; Maxwell, J. R. Rapid Characterization of Metallo Porphyrin Classes in Natural Extracts by Gel Permeation Chromatography/Atmospheric Pressure Chemical Ionization/Mass Spectrometry. *Rapid Commun. Mass Spectrom.* **1996**, *10*, 209−213.
(94) Biggs, W. R.; Fetzer, J. C.; Brown, R. J.; Reynolds, J. G. Characterization of Vanadium Compounds in Selected Crudes I. Porphyrin and Non-Porphyrin Separation. *Liq. Fuels Technol.* **1985**, *3*, 397−421.
(95) Zhao, X.; Shi, Q.; Gray, M. R.; Xu, C. New Vanadium Compounds in Venezuela Heavy Crude Oil Detected by Positive-Ion Electrospray Ionization Fourier Transform Ion Cyclotron Resonance Mass Spectrometry. *Nature* **2014**, *4*, 5373.
(96) Caumette, G.; Lienemann, C.-P.; Merdrignac, I.; Bouyssiere, B.; Lobinski, R. Element Speciation Analysis of Petroleum and Related Materials. *J. Anal. At. Spectrom.* **2009**, *24*, 263−276.
(97) Reynolds, J. G.; Biggs, W. R. Effects of Asphaltene Precipitation and a Modified D 2007 Separation on the Molecular Size of Vanadium-and Nickel-Containing Compounds in Heavy Residua. *Fuel Sci. Technol. Int.* **1986**, *4*, 749−777.
(98) Mironov, N. A.; Milordov, D. V.; Abilova, G. R.; Yakubova, S. G.; Yakubov, M. R. Methods for Studying Petroleum Porphyrins (Review). *Pet. Chem.* **2019**, *59*, 1077−1091.
(99) Ancheyta, J.; Trejo, F.; Rana, M. S. Definition and Structure of Asphaltenes. *Asphaltene Chemical Transformation during Hydroprocessing of Heavy Oils*; CRC Press, Taylor & Francis Group: Boca Raton, FL, USA, 2010; pp 1−86.
(100) McKenna, A. M.; Marshall, A. G.; Rodgers, R. P. Heavy Petroleum Composition. 4. Asphaltene Compositional Space. *Energy Fuels* **2013**, *27*, 1257−1267.
(101) Ruiz-Morales, Y. HOMO-LUMO Gap as an Index of Molecular Size and Structure for Polycyclic Aromatic Hydrocarbons (PAHs) and Asphaltenes: A Theoretical Study. I. *J. Phys. Chem. A* **2002**, *106*, 11283−11308.
(102) McKenna, A. M.; Chacón-Patiño, M. L.; Weisbrod, C. R.; Blakney, G. T.; Rodgers, R. P. Molecular-Level Characterization of Asphaltenes Isolated from Distillation Cuts. *Energy Fuels* **2019**, *33*, 2018−2029.
(103) Santos Silva, H.; Alfarra, A.; Vallverdu, G.; Bégué, D.; Bouyssiere, B.; Baraille, I. Asphaltene Aggregation Studied by Molecular Dynamics Simulations: Role of the Molecular Architecture and Solvents on the Supramolecular or Colloidal Behavior. *Pet. Sci.* **2019**, *16*, 669−684.
(104) Takanohashi, T.; Sato, S.; Saito, I.; Tanaka, R. Molecular Dynamics Simulation of the Heat-Induced Relaxation of Asphaltene Aggregates. *Energy Fuels* **2003**, *17*, 135−139.
(105) Lobodin, V. V.; Marshall, A. G.; Hsu, C. S. Compositional Space Boundaries for Organic Compounds. *Anal. Chem.* **2012**, *84*, 3410−3416.
(106) Cho, Y.; Kim, Y. H.; Kim, S. Planar Limit-Assisted Structural Interpretation of Saturates/Aromatics/Resins/Asphaltenes Fractionated Crude Oil Compounds Observed by Fourier Transform Ion Cyclotron Resonance Mass Spectrometry. *Anal. Chem.* **2011**, *83*, 6068−6073.
(107) Hsu, C. S.; Lobodin, V. V.; Rodgers, R. P.; McKenna, A. M.; Marshall, A. G. Compositional Boundaries for Fossil Hydrocarbons. *Energy Fuels* **2011**, *25*, 2174−2178.
(108) McKenna, A. M.; Donald, L. J.; Fitzsimmons, J. E.; Juyal, P.; Spicer, V.; Standing, K. G.; Marshall, A. G.; Rodgers, R. P. Heavy Petroleum Composition. 3. Asphaltene Aggregation. *Energy Fuels* **2013**, *27*, 1246−1256.

https://dx.doi.org/10.1021/acs.energyfuels.0c03349
Energy Fuels XXXX, XXX, XXX−XXX

Comme précédemment étudié, le vanadium présent dans l'asphaltène est réparti sur une large plage de taille d'agrégats allant d'un million de dalton à quelques centaines de dalton. En ce qui concerne les fractions extrographie analysées par GPC-ICP MS, le vanadium est contenu pour les fractions Heptane/Toluène et Toluène/THF/MeOH dans les hauts poids moléculaires. Alors que pour la fraction acétone le vanadium est contenu dans les agrégats moléculaire moyen et faible.

Du côté du couplage GPC-FT-ICR MS, les porphyrines de vanadium sont visibles uniquement dans les fractions à poids moléculaires moyen et faible. Pour la fraction Acétone, les résultats montrent en effet que plusieurs porphyrines sont trouvées en grande quantité et sont séparées (dans la région des bas poids moléculaire) en fonction de leur taille. En ce qui concerne la fraction Toluène/THF/MeOH, très peu de porphyrines sont visibles alors qu'une grande quantité de vanadium est présent dans l'échantillon.

Malgré l'utilisation d'une double séparation, la fraction contenant du vanadium dans les hauts poids moléculaires reste trop complexe pour être analysée par la spectrométrie de masse à très haute résolution.

As previously studied, vanadium in asphaltene is distributed over a wide range of aggregate sizes from one million daltons to a few hundred daltons. For the extrographic fractions analysed by GPC-ICP MS, vanadium is contained in the Heptane/Toluene and Toluene/THF/MeOH fractions in the high molecular weights. Whilst for the Acetone fraction vanadium is contained in the medium and low molecular aggregates.

On the GPC-FT-ICR MS coupling side, vanadium porphyrins are visible only in the medium and low molecular weight fractions. For the Acetone fraction, the results indeed show that several porphyrins are found in large quantities and are separated (in the low molecular weight region) according to their size. For the Toluene/THF/MeOH fraction, very few porphyrins are visible while a large amount of vanadium is present in the sample.

Despite the use of double separation, the vanadium-containing fraction in the high molecular weight range remains too complex to be analysed by very high-resolution mass spectrometry.

Conclusion chapitre II

La première partie de ce chapitre sur le couplage de technique de séparation, d'analyse élémentaire et moléculaire a permis d'obtenir des informations complémentaires sur les échantillons de la chaine de raffinage des huiles.

La deuxième partie de ce chapitre a montré que la séparation par extrographie suivis de techniques d'analyses par GPC-ICP MS, FT-ICR MS et QCR permettaient de mettre en évidence des différences sur deux asphaltènes provenant de pétroles différents la ou les techniques d'analyses classiques ne le permettaient pas.

Enfin, la troisième partie de ce chapitre a montré qu'un couplage GPC-FT-ICR MS en ligne était possible. Il est apparu que les composés contenus dans les plus hauts poids moléculaires sont plus aliphatiques que le reste de l'échantillon. Cependant, malgré cela en plus de la séparation par extrographie, des informations sur les porphyrines de vanadium restent inaccessibles. Cela pose la question de quelle portion des échantillons pétroliers est capables d'analyser les appareils à spectrométrie de masse haute résolution.

Dans le prochain chapitre de cette thèse, un autre type de séparation non pas par taille des agrégats mais par polarité sera utilisé dans le but de simplifier la matrice pétrolière. Ensuite les techniques d'analyses UV, ICP MS et FT-ICR MS seront utilisées dans le but d'analyser les fractions préalablement séparées et notamment la partie des hauts poids moléculaire qui contient les porphyrines.

The first part of this chapter on the coupling of separation techniques, elemental and molecular analysis has provided additional information on samples from the oil refining chain.

The second part of this chapter showed that the separation by extrography followed by GPC-ICP MS, FT-ICR MS and QCR analysis techniques made it possible to highlight differences on two asphaltenes coming from different oils when the conventional analysis techniques did not allow it.

Finally, the third part of this chapter showed that an on-line GPC-FT-ICR MS coupling was possible. It appeared that the compounds contained in the highest molecular weights were more aliphatic than the rest of the sample. However, despite this, in addition to extrographic separation, information on vanadium porphyrins remains inaccessible. This raises the question of how much of the oil samples are capable of analysis by high resolution mass spectrometry apparatus.

In the next chapter of this thesis another type of separation not by aggregate size but by polarity will be used to simplify the petroleum matrix. Then UV, ICP MS and FT-ICR MS analysis techniques will be used to analyze the previously separated fractions and in particular the high molecular weight part which contains porphyrins.

Chapitre III : Développement d'une méthode séparation des produits pétroliers en fonction de la polarité des composés/agrégats

Comme présenté dans le chapitre I, l'HPTLC permet la séparation de composés de polarités différentes. Cette méthode présente les avantages d'être peu consommatrice d'échantillon et de solvants. Les plaques sont certes à usage unique mais il est possible de déposer jusqu'à 25 échantillons par plaque (20 cm X 10 cm) ce qui en fait une technique peu couteuse. La séparation par HPTLC permet une séparation par affinité chimique qui vient compléter la séparation par GPC présentée dans le chapitre II ou la séparation par extrographie. La faible consommation d'échantillon de l'HPTLC permet de facilement séparer les échantillons déjà fractionnés par une autre technique de séparation comme la GPC ou l'extrographie. Habituellement les plaques HPTLC utilisés pour l'analyse de produit pétroliers sont à base de silice. L'utilisation d'adsorbant moins polaire comme la cellulose pourrait améliorer la détection des molécules présentes.

La première partie de ce chapitre se consacrera au fractionnement des asphaltènes par GPC préparative pour isoler des fractions contenant des agrégats de différentes tailles de l'Asphaltène 2017, déjà étudiés au chapitre II partie III. Ces fractions ont ensuite été séparées par HPTLC pour obtenir plus d'informations sur le vanadium présent dans les différents agrégats. L'analyse a été effectuée par UV et par LA-ICP MS

La deuxième partie de ce chapitre se concentrera sur le couplage d'une séparation par extrographie avec une séparation par HPTLC de l'asphaltène 2017. Ici une analyse élémentaire par LA-ICP MS sera effectuée ainsi qu'une analyse moléculaire par MALDI-FT-ICR MS dans le but de suivre la présence des porphyrines de vanadium dans chacune des fractions de l'asphaltène.

As presented in Chapter I, HPTLC allows the separation of compounds of different polarities. This method has the advantages of being low in sample and solvent consumption. Although the plates are single-use plates, up to 25 samples can be deposited per plate (20 cm X 10 cm), making it an inexpensive technique. HPTLC separation allows separation by chemical affinity to complement the GPC separation described in Chapter II or extrographic separation. The low sample consumption of HPTLC makes it easy to separate samples already fractionated by another separation technique such as GPC or extrography. Usually HPTLC plates used for the analysis of petroleum products are silica-based. The use of less polar adsorbents such as cellulose could improve the detection of the molecules present.

The first part of this chapter will focus on asphaltene fractionation by preparative GPC to isolate fractions containing aggregates of different sizes from Asphaltene 2017, already discussed in Chapter II Part III. These fractions were then separated by HPTLC to obtain more information on the vanadium present in the different aggregates. The analysis was carried out by UV and LA-ICP MS

The second part of this chapter will focus on coupling an extrographic separation with HPTLC separation of asphaltene 2017. Here an elemental analysis by LA-ICP MS will be carried out as well as a molecular analysis by MALDI-FT-ICR MS to monitor the presence of vanadium porphyrins in each of the asphaltene fractions.

Partie I : Apport de l'HPTLC dans le cadre de la séparation des asphaltènes sur plaques de cellulose couplé à une analyse par UV et LA-ICP MS.

Cette partie a fait l'objet d'un article publié dans le journal *Energy and Fuels* de l'*American Chemical Society* (ACS). Cet article a été laissé tel qu'il a été publié aux références suivantes :

R. Moulian *et al.*, « Speciation of Metals in Asphaltenes by High-Performance Thin-Layer Chromatography and Laser Ablation Inductively Coupled Plasma-Mass Spectrometry », *Energy & Fuels*, vol. 33, n° 7, p. 6060-6068, juill. 2019, doi: 10.1021/acs.energyfuels.9b00676.

Cet article décrit dans un premier temps une comparaison entre une séparation HPTLC sur plaque de silice et une séparation sur plaque de cellulose en utilisant comme échantillon l'asphaltènes 2017. Les solvants utilisés sont un mélange de dichlorométhane et de méthanol qui permet d'éluer jusqu'au front de solvant les porphyrines de vanadium libres. Ensuite l'asphaltène 2017 a été fractionné par taille grâce à la GPC puis chacune des fractions ainsi que l'échantillon complet ont été séparées par HPTLC.

Toutes les fractions obtenues ont été analysées par UV dans le but notamment de suivre la présence de porphyrines de vanadium à 420 nm et par LA-ICP MS afin de suivre la présence de vanadium. En effet la présence de vanadium sous-entend la présence de porphyrines. Or la quantité de vanadium présent au point de dépôt ou au front de solvant en fonction des fraction GPC nous renseigne sur la proportion porphyrines libres en fonction des fractions GPC. Un signal UV à 420 nm, présent au front de solvant signifie que les porphyrines ont été éluées et sont plus facilement accessibles alors signal UV absent au point de dépôt signifierait que les porphyrines sont plus difficilement accessibles.

This section was the subject of an article published in the American Chemical Society (ACS) journal Energy and Fuels. This article has been left as published in the following references:

R. Moulian et al, "Speciation of Metals in Asphaltenes by High-Performance Thin-Layer Chromatography and Laser Ablation Inductively Coupled Plasma-Mass Spectrometry", Energy & Fuels, vol. Energy & Fuels, Vol. 33, No. 7, p. 6060 6068, July 2019, doi: 10.1021/acs.energyfuels.9b00676.

This paper first describes a comparison between HPTLC separation on silica plate and separation on cellulose plate using asphaltenes 2017 as a sample. The solvents used are a mixture of dichloromethane and methanol to elute free vanadium porphyrins to the solvent front. Then the asphaltene 2017 was fractionated by size using GPC and then each of the fractions as well as the complete sample were separated by HPTLC.

All fractions obtained were analysed by UV to monitor the presence of vanadium porphyrins at 420 nm and by LA-ICP MS to monitor the presence of vanadium. Indeed the presence of vanadium implies the presence of porphyrins. The amount of vanadium present at the deposition point or at the solvent front as a function of the GPC fractions gives us information on the proportion of free porphyrins as a function of the GPC fractions. A UV signal at 420 nm, present at the solvent front means that the porphyrins have been eluted and are more easily accessible then a UV signal absent at the deposition point would mean that the porphyrins are more difficult to access.

energy&fuels

Article

Cite This: Energy Fuels 2019, 33, 6060−6068

pubs.acs.org/EF

Speciation of Metals in Asphaltenes by High-Performance Thin-Layer Chromatography and Laser Ablation Inductively Coupled Plasma-Mass Spectrometry

Rémi Moulian,[†,‡,§] Sara Gutierrez Sama,[†,‡,§] Carole Garnier,[‡] Sandra Mounicou,[†] Maxime Enrico,[†] Xavier Jaurand,[∥] Ryszard Lobinski,[†,§] Pierre Giusti,[‡,§] Brice Bouyssiere,*[,†,§] and Caroline Barrère-Mangote*[,‡,§]

[†]CNRS/University of Pau/E2S, Institut des Sciences Analytiques et de Physico-Chimie pour l'Environnement et les Materiaux, UMR5254, Hélioparc- 2 Av Pr Angot, 64000 Pau, France

[‡]TOTAL Refining and Chemicals, Total Research and Technologies, Gonfreville, BP 27, 76700 Harfleur, France

[§]TOTAL RC, CNRS, Univ. Pau, Univ. Rouen, International Joint Laboratory − C2MC: Complex Matrices Molecular Characterization, TRTG, BP 27, 76700 Harfleur, France

[∥]Centre Technologique des Microstructures, Université Claude Bernard Lyon1, 5 rue Raphael Dubois-Bâtiment Darwin B, F-69622 Villeurbanne, Cedex, France

Supporting Information

ABSTRACT: Asphaltenes are considered to be the most problematic components of heavy oils because they can self-aggregate which leads to precipitation and causes various problems during oil recovery, transportation, and refining. The contribution of the porphyrins present in asphaltenes to the aggregation was previously studied by gel permeation chromatography inductively coupled plasma-mass spectrometry (GPC-ICP MS). The molecular weight of asphaltene aggregates was shown to be increased by free metal-containing porphyrins (corresponding to the lower molecular weight fraction) interacting with the aggregate's surfaces by weak forces. The characterization of free porphyrins within the asphaltenes is therefore for the understanding of the mechanism of the aggregation, coprecipitation, and demetalation processes. Here, we developed a method for the separation of free porphyrins from asphaltenes on the basis of their polarity using high-performance thin-layer chromatography (HPTLC). This technique, using disposable plates, is particularly well suited for asphaltene analysis since it eliminates the risk of clogging typical of column chromatography. Cellulose plates were used in this study. The lower polarity of their hydroxyl groups limit the irreversible adsorption and improves the detection limit by the ICP-MS. Two well-separated peaks were obtained from purified asphaltene (Asphaltene 2017; Asphaltene Characterization Interlaboratory Study for PetroPhase 2017. In *Proceedings of the 18th International Conference on Pretroleum Phase Behavior and Fouling*, Le Havre, France, June 11−15, 2017; Total, the University of Pau, and the University of Rouen-Normandy: Le Havre, France, 2017.) and its corresponding whole crude oil and C5 and C7 fractions. The distribution of vanadium due to migration was determined by laser ablation (LA) ICP MS. The eluted fraction contained the free porphyrins, whereas the major fraction did not migrate and corresponded to trapped porphyrins. A comparison with the signal obtained by UV densitometry allowed the ratio between the inorganic and organic material to be measured.

INTRODUCTION

The composition of asphaltenes, the most polar fraction of a petroleum matrix, remains largely unknown. Speight[1] defined asphaltenes as the fraction that precipitates in the presence of alkanes but is soluble in hot toluene. The asphaltenes that precipitate in *n*-pentane, *n*-hexane, and *n*-heptane are referred to as C5, C6, and C7 asphaltenes, respectively. Asphaltenes contain a wide variety of molecules with different aromaticities, high polarities, and high contents of heteroatoms and metals (Ni, V···).[2−4] These properties allow asphaltenes to self-aggregate in fairly concentrated solutions, leading to macro-aggregation that results in precipitation in organic media.[5−7] The nano and macroaggregation need to be understood to avoid problematic effects, such as pipe clogging. Also, nanoaggregation may be linked to the efficiency in catalytic processes via pore size.

Thin-layer chromatography (TLC), usually with silica plates, has been extensively[8−18] used for the characterization of petroleum samples. For instance, Cebolla et al.[8] used silica gel plates impregnated with berberine to separate SARA components (saturates, asphaltenes, resins, aromatics) of petroleum samples. Berberine was necessary to detect saturated compounds.[8] Sharma et al.[9] used TLC-FID (Iatroscan) to perform SARA separations with a standard deviation below 3.5%. Furthermore, Jarne et al.[10] used modified silica gel plates impregnated with caffeine to separate petroleum products according to their number of rings. Mateos et al.[11] used silica gel plates impregnated with a solution of

Received: March 6, 2019
Revised: June 11, 2019
Published: June 11, 2019

DOI: 10.1021/acs.energyfuels.9b00676
Energy Fuels 2019, 33, 6060−6068

coralyne cation, which is more sensitive than berberine for many compounds. The use of TLC with single-use plates for asphaltene characterization can avoid the damage to chromatography columns caused by irreversible adsorption of the polar compounds present onto the stationary phase and asphaltene precipitation. Recently, Chacon-Patino et al.[12] and Giraldo-Davila et al.[13] used silica gel plates to separate asphaltene samples. They used a mixture of DCM/MeOH and then toluene to separate asphaltenes in three fractions.[12,13] This technique can also be used on the preparative scale to separate fractions that can then be scratched, extracted with solvents, and further analyzed by other techniques.[14] Vorapalawut et al.[15] used TLC in conjunction with LA-ICP-MS for SARA separation with silica-based plates for the speciation of sulfur, vanadium, and nickel from the SARA fractions of petroleum samples. Chirinos et al.[16] also used this hyphenated technique for the rapid determination of the vanadium/nickel ratio in different samples of asphaltenes.[16] Although silica-based plates are typically used for HPTLC for hydrocarbon-type analyses, these plates are affected by irreversible adsorption at the application point due to the high polarity of the silanol groups present, and this effect is most dramatic in asphaltene analysis. The use of less polar sorbents, such as cellulose, could allow a more robust speciation of asphaltene. The use of sorbents that are not based on silica could facilitate the detection of certain analyte molecules by eliminating the high silica signal derived from the plate in LA-ICP-MS. Several authors have used TLC for the separation of porphyrins and metalloporphyrins. In 1978, Hajibrahim et al.[17] used preparative TLC for the separation of carotenoids and porphyrins for further analysis. In 1989, van Berkel et al.[18] used liquid chromatography to obtain vanadyl porphyrin- and nickel porphyrin-enriched fractions from bitumen samples. Then, they used TLC with silica-based plates to separate the different porphyrins in each of the previous fraction. All the Ni porphyrins eluted with heptane/DCM 3/2% v/v, while vanadyl porphyrins need a more polar solvent, such as 100% DCM. Vargas et al.[19] used liquid chromatography to obtain fractions of crude oil with different mixtures of solvent ((1) hexane/DCM 9/1; (2) hexane/DCM 3/1; (3) hexane/DCM 1/1; (4) DCM/acetone 1/1; (5) DCM/methanol 4/1; (6) chloroform/methanol/water 65/25/4). In the second step, they used HPTLC by doing a SARA separation in order to determine what they had in each of the different fractions. They concluded that fractions 4, 5, and 6 are retained at the application point and correspond to asphaltene. At the same time, they used UV analysis to analyze each fraction and concluded that free vanadyl porphyrins are more present in fraction 3.

This study aims to test for the first time the use of cellulose-based HPTLC plates for asphaltene speciation and to compare the results with those achieved with classic silica-based plates. The efficiency of the method for separating free porphyrins from aggregates is assessed by the analysis of samples previously separated by GPC.[20−22] GPC is a widely used technique for the characterization of petroleum samples due to its ability to separate compounds by their hydrodynamic volume, molecular size, and/or aggregation state. This separation strategy uses a different principle to the polarity-based separation usually achieved on silica stationary phases. Deelchand et al.[23] proposed an off-line hyphenation of TLC and GPC techniques involving a preparative TLC separation of petroleum residue and pitch on silica-based plates followed by characterization of the fractions by UV, mass spectrometry, and GPC. They obtained lower molecular weights and higher mobilities on the plates. Similar results were obtained by the same group for other samples.[15]

In this work, high-performance (HP) TLC is proposed for the speciation of asphaltenes, particularly for the separation and detection of "free porphyrins." The porphyrins are detected by element specific techniques, such as laser ablation-inductively coupled plasma-mass spectrometry (LA-ICP-MS) and UV densitometry. Most of the vanadium and nickel ions in asphaltenes are part of porphyrin complexes (tetrapyrrolic complexes mainly of vanadyl (VO^{2+}) and nickel(II) ions).[24] Although porphyrins can be free in solution, they can also be trapped into nanoaggregates of asphaltenes, making them difficult to separate and analyze with UV−visible spectrophotometry.[24,25] Improving the understanding the porphyrins's role associated with asphaltene nanoaggregates by different types of interactions[26,27] in the aggregation process is the main objective of this study. For this purpose, our recently developed method using GPC and HPTLC characterization is applied to different asphaltene samples obtained from the same crude oil with different alkanes, as well as to the Asphaltene 2017 reference sample.

EXPERIMENTAL SECTION

Samples, Materials, and Reagents. *Samples.* Asphaltene 2017 (from a Middle East crude oil, with a vanadium content of 640 ppm) from the interlaboratory study of the PetroPhase congress, and its preparative GPC fractions,[21] asphaltenes C5 and C7, were studied. The three samples (A2017, AC7, and AC5) came from the same crude oil. The difference between A2017 and AC7 is that A2017 is washed more after the precipitation (see the complete procedure https://petrophase2017.sciencesconf.org/resource/page/id/10). Asphaltene 2017 is obtained first by the ASTM D6560-12 method and then by a Soxhlet wash with heptane for 5 h. This step is repeated until the material extracted from asphaltene is below 0.2 mg/200 mL heptane. Two reference molecules (5,10,15,20-tetraphenyl-21H,23H-vanadyl porphyrin and 5,10,15,20-tetraphenyl-21H-23H-porphine nickel, purity 95%, Merck, Frankfurter Strasse 250, Darmstadt 64293, Germany) were used.

Solvents. Tetrahydrofuran (THF, HPLC grade, without stabilizer, Lichrosolv, Merck, Frankfurter Strasse 250, Darmstadt 64293, Germany) was used as the solvent for sample preparation. To facilitate the release of porphyrins, the solutions of the whole asphaltenic samples were subjected to ultrasound for 1 h. Dichloromethane (DCM) and methanol (MeOH) (HPLC grade, Lichrosolv, Merck, Frankfurter Strasse 250, Darmstadt 64293, Germany) were used to develop the HPTLC plates. Toluene, heptane, and pentane were used to prepare Asphaltenes 2017, C7, and C5.

HPTLC Plates. Classic HPTLC silica gel plates (thickness of 0.15−0.2 mm, Merck, Frankfurter Strasse 250, Darmstadt 64293, Germany) and cellulose HPTLC glass plates (thickness of 0.06−0.11 mm, Merck, Frankfurter Strasse 250, Darmstadt 64293, Germany), with dimensions of 20 cm × 10 cm without fluorescent indicators were used. The cellulose stationary phase is thinner and contains smaller, more uniform particles than silica gel for faster separation, better separation efficiency, better resolution, and more sensitive detection.[28]

Instrumentation. *HPTLC.* The HPTLC procedure was carried out with the following instrumentation from Camag. The sample application and sample development were performed using an Automatic TLC Sampler 4 (ATS4) and an Automated Multiple Development 2 (AMD2), respectively. UV absorbance chromatograms were monitored at a wavelength of 280 nm with a D2&W lamp by a TLC scanner. UV spectra from 190 to 900 nm were obtained using the same device. Finally, a TLC visualizer was used to obtain a

DOI: 10.1021/acs.energyfuels.9b00676
Energy Fuels 2019, 33, 6060−6068

picture of the plate under 366 nm UV light after development. Peak area data were collected using WinCATS software.

HPTLC plates were cleaned with DCM and THF and dried at 110 °C for 10 min prior to sample deposition. The samples were deposited 10 mm from the bottom of the plate. A high-strength mobile phase (DCM/MeOH, 99.5:0.5) was used to completely elute the free porphyrins, so they could be characterized separately from the rest of the material. The plate was developed in a single step until the solvent front reached 50 mm.[29]

The nickel and vanadyl porphyrins were calibrated by depositing six different amounts of the complexes, from 0.00537 to 1.08 μg for vanadyl porphyrins and from 0.0054 to 1.08 μg for nickel porphyrins. Furthermore, three different amounts of Asphaltene 2017, C5, and C7 (1, 3, and 5 μg) were deposited. All the details are available in Table S2 of the Supporting Information. The calibration standards and the samples were deposited on three cellulose plates for repeatability and on a silica plate for comparison. The repeatability of the method was calculated, and the differences between silica and cellulose were determined.

Additionally, Asphaltene 2017 (1, 2.5, and 5 μg) and its GPC fractions (1, 2.5, and 5 μg) were deposited on another cellulose plate.

LA-ICP MS. Element specific analysis of the developed HPTLC plate was carried out by LA-ICP MS using a New Wave Research UP-213 Nd:YAG laser (ESI, Fremont, CA) coupled with ICP MS (7700 series, Agilent, Santa Clara, CA) under the operating conditions given in Table 1. The instrument was equipped with a Fassel-type quartz torch shielded with a grounded Pt electrode and a quartz bonnet. A standard quartz injector (1.75 mm i.d.) was used. An ablation chamber was installed on a three-axis translation stage and coupled to the ICP torch using a 60 cm Tygon tube (5.0 mm i.d.). The ablated material was swept by the carrier gas (helium) and mixed with the spectrometer makeup gas (argon) prior to introduction into the plasma. Ni sampler (orifice diameter of 1.1 mm) and skimmer (orifice diameter of 0.8 mm) cones were used.[15] The laser beam followed a linear trajectory throughout the migration (see Table S1 for repeatability on one sample). The distribution of ^{51}V compounds was controlled. To fit within the ablation cell, plates were cut to dimensions of 9 × 10 cm. FIJI[30,31] image processing software was used to precisely determine the area of each spot of sample on the solvent front and normalize all the results obtained by UV and LA-ICP MS.

Table 1. LA-ICP MS Operating Parameters

Agilent 7700 Series ICP MS	
plasma Ar gas flow rate (L min^{-1})	15
auxiliary Ar gas flow rate (L min^{-1})	1
measured isotope	^{13}C, ^{32}S, ^{51}V, ^{58}Ni, ^{60}Ni
analysis time (s)	506
New Wave Research UP-213 LA	
wavelength (nm)	213
pulse energy (mJ)	0.45 (50%)
fluence (J cm^{-2})	3.5
spot size (μm)	200
repetition rate (Hz)	20
scan speed (μms^{-1})	100
carrier He gas flow rate (L min^{-1})	0.5

Preparative GPC. Fractionation was carried out following the method of Putman et al.[21] Briefly, we used three Shodex (Showa Denko, Japan) polystyrene−divinylbenzene (PS/DVB) preparative gel permeation columns (20 mm i.d., 300 mm length), i.e., KF2001 (particle size: 6 μm, exclusion limit: 1500 Da), KF2002.5 (particle size: 6 μm, exclusion limit: 20000 Da), and KF2004 (particle size: 7 μm, exclusion limit: 400000 Da) connected in series with a KF-LG precolumn for protection. The column temperature was not controlled.

The preparative GPC system was calibrated with nine polystyrene standards with Mw values ranging from 630 to 2350000 Da using a refractive index detector. The equation of the mass calibration curve was log (Mw) = $-1.10^{-5}x^3 + 0.0048x^2 - 0.7188x + 40.614$ ($R > 0.9988$), where x is the elution volume.

One milliliter of the asphaltene solution diluted 100 times in THF (Sigma-Aldrich) was injected into the column by means of an injection loop connected to an external 6-way valve. Xylene was used as the mobile phase instead of THF, and the eluent was delivered at a flow rate of 3 mL/min by a Dionex high-performance liquid chromatography (HPLC) system with an UltiMate 3000 microflow pump.

Fractions of different molecular weights were collected at the outlet of the preparative columns, and the fractions contained the high-molecular-weight aggregates (HMW), medium-molecular-weight (MMW) compounds, low-molecular-weight (LMW) compounds, and the tailing fraction of compounds retained on the stationary phase. The peak corresponding to the porphyrinic solution was observed in the LMW fraction; thus, the free porphyrins are expected to be present in this fraction.

RESULTS AND DISCUSSION

Reference Metalloporphyrins. As shown by Chirinos et al.,[16] in order to obtain measurable LA-ICP-MS signals using classic Si-based plates, several tens of micrograms of crude oil are typically deposited. This amount of sample does not allow good quality migrations in HPTLC because of the thin layer of sorbent (approximately 100 μm vs 250 μm for classic TLC[15,16]). Cellulose plates represent an interesting alternative for achieving suitable migration. Indeed, unlike silica, cellulose is a polar sorbent with alcohol and ether functional groups that is suitable for adsorption chromatography. Moreover, the use of cellulose plates improves the detection in ICP MS by removing the intense silica interferences and improving the plasma stability. Figure 1 compares silica- and cellulose-based HPTLC plates with 1 μg of each reference vanadyl and nickel porphyrin deposited. The detections were carried out by LA-ICP MS. The ^{51}V signal intensities from the two kinds of HPTLC plates differed by a factor of 10 (Figure 1a). As

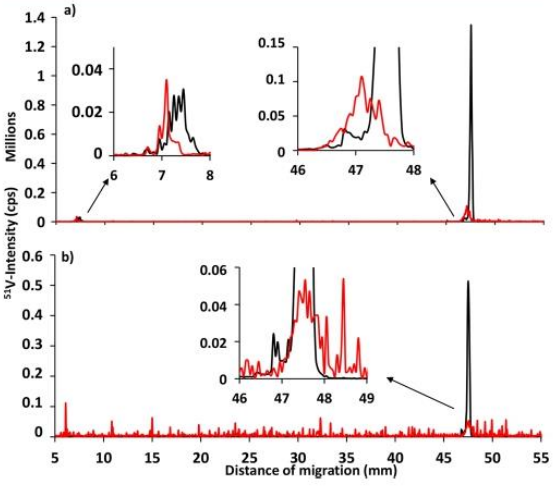

Figure 1. (a) ^{51}V signal and (b) ^{58}Ni signal from LA-ICP-MS of a one-step (40 mm) development with silica (red line) and cellulose (black line) HPTLC plates with DCM/MeOH 99.5/0.5% v/v of 1 μg of the reference porphyrin mixture.

DOI: 10.1021/acs.energyfuels.9b00676
Energy Fuels 2019, 33, 6060−6068

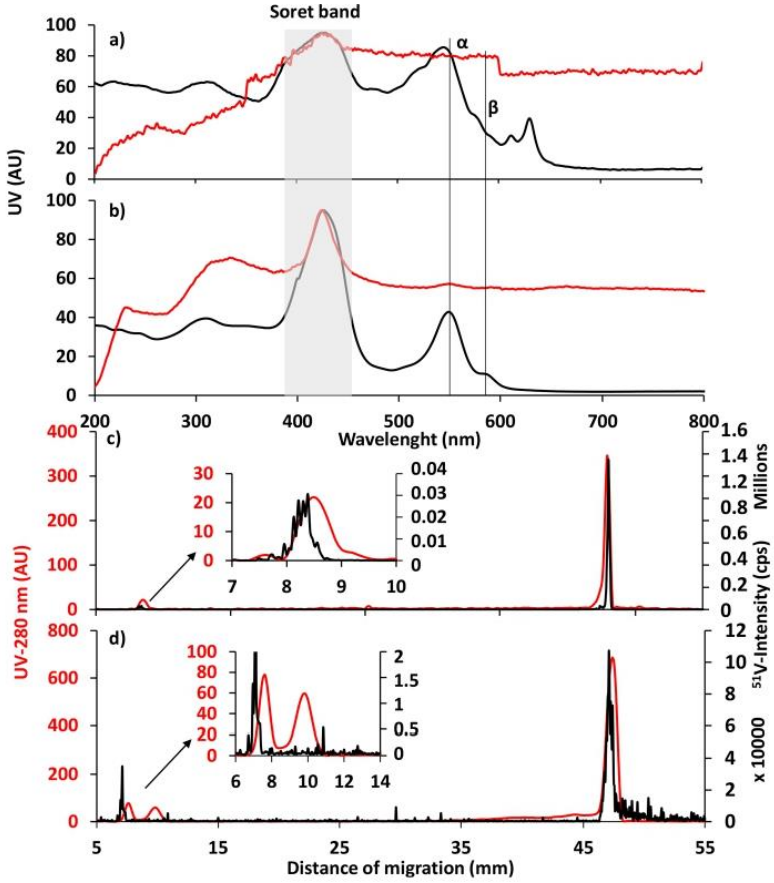

Figure 2. Densitometry UV spectrum of the (black line) eluted and (red line) noneluted fractions of the reference porphyrin mixture on cellulose (a) and silica (b) HPTLC plates. The UV signal at 280 nm (red line) and the ^{51}V signal (black line) from LA-ICP-MS of the reference porphyrin mixture on cellulose (c) and silica (d) HPTLC plates.

expected, vanadyl porphyrins quantitatively elute at the solvent front on the cellulose plate (black line). In comparison, only 85% of these species migrate with the solvent front (red line) on silica-based plates, indicating that a significant fraction remained at the application point. Similar results were obtained for nickel porphyrins (Figure 1b). Our observations confirm that cellulose interacts less with the porphyrin samples than does the silica gel. Moreover, the ^{58}Ni LA-ICP MS signal is half as intense as the vanadium signal (V has a lower ionization potential (6,7) than Ni (7,6) and thus has a better detection limit in ICP MS). From the chromatographic point of view, the separation of the components is likely to be the result of their different solubilities in the solvent. Our purpose is to understand what migrates or does not migrate with a mixture like DCM/MeOH.

This unexpected retention of porphyrins at the application point could be due to irreversible adsorption, as previously observed in our laboratory for polar compounds on silica plates. Several authors reported the degradation of metalloporphyrins on silica-based TLC plates, but degradation preferentially occurred for Ni porphyrins, as shown by Ali et al.[32] and van Berkel et al.[18] To better understand this phenomenon, UV−vis densitometry spectra were recorded directly at the application point and at the solvent front on the two plates (Figure 2). Even when the UV spectra were recorded from the solid HPTLC plate rather than in solution, the expected absorption bands for the porphyrins were observed in the spectra of the eluted fractions on the plates with a large Soret band at approximately 425 nm (gray band), a α band at approximately 545 nm, and an β band at approximately 575 nm (Figure 2 (a, b vertical black lines)). The wavelengths of the maximum intensities of these bands were close to those reported by Freeman et al.[33] for benzo vanadyl porphyrins. The spectra obtained from the noneluted fractions on the plates are shown in Figure 2 (a, b red lines). The spectrum obtained from the cellulose plate was noisier, and no characteristic absorption bands indicating the presence of the vanadium porphyrin complexes at the application point were observed. In contrast to that, the spectrum obtained at the application point from the silica-based plate was similar to the spectra obtained for the porphyrins at the elution front, suggesting that a portion of the analyte was adsorbed at the application point. Futhermore, when a cellulose plate was used (Figure 2 (c)), the UV signal (red line) at the deposition point was only 1% of the total signal. Note that in the case of the LA-ICP-MS ^{51}V signal (black line), the signal at the deposition point was 6% of the total. This would mean that there is 6% of the vanadium at the application point but that it is not inside a

DOI: 10.1021/acs.energyfuels.9b00676
Energy Fuels 2019, 33, 6060−6068

porphyrin. Opposite that, on silica, as shown in Figure 2 (d), at the application point, 15% of the vanadium and 18% of the UV signal have been detected. This would mean that on silica, more vanadium is retain and at least a portion is vanadyl porphyrin.

Vanadium calibration when the cellulose plates were used showed that the reference porphyrin moved with the front solvent (Figure 3). The spead of the peaks at the solvent front

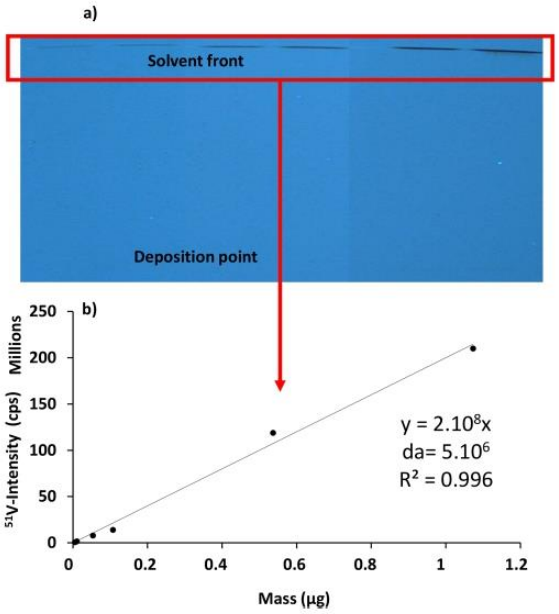

Figure 3. (a) Picture at 280 nm of the cellulose plate after separation of the vanadyl porphyrins. (b) Six-point calibration curve obtained with vanadyl porphyrin by LA-ICP-MS after image processing.

and the absence of peaks in the middle of the plate can be explained by a "solubility mode" separation rather than a classic chromatographic separation. Indeed we could suppose that, on the cellulose phase with very polar solvent as DCM/MeOH, all molecules that have been dissolved are eluted without any retention. This plate was analyzed by LA-ICP MS, but the size of the eluted spot from the different migration trials and on different plates differed because the spot spread out. To solve this problem, we used image processing software (FIJI) to determine the area of each spot of the eluted and noneluted fractions. The laser-ablated area together with ICP MS signal data allowed the correction of the data (Figure S1). FIJI was used for the treatment of all the plates.

The calibration curve obtained for vanadyl porphyrin (shown in Figure 3b) was $y = 2 \times 10^8 x$ ($\pm 5.5 \times 10^6$) with $R^2 = 0.994$ and $F = 1325$. This calibration curve was prepared for a single cellulose plate. The others calibration curves on plate 2 and 3 are given in Figure S2. The results of the interplate repeatability are given in Table 2. These results indicate that the relative standard deviation from one plate to another could be up to 25%, probably resulting from differences in migration and plate quality. For this reason, calibration points were added to each plate (A, B, and C) and were used to calibrate the quantification data.

GPC Fractions of Asphaltene 2017. Our previous work[20] using GPC showed that heavy petroleum samples could be separated into four fractions, referred to as the high-molecular-weight (HMW), medium-molecular-weight (MMW), low-molecular-weight (LMW), and tailing fractions for analytes having interactions with the stationary phase (unexpected separation mechanism in GPC), as proposed in Figure 4. Note that by GPC-ICP-MS, our reference vanadyl porphyrins each lead to a sharp peak in the LMW area,[20,22] as shown in Figure 4.

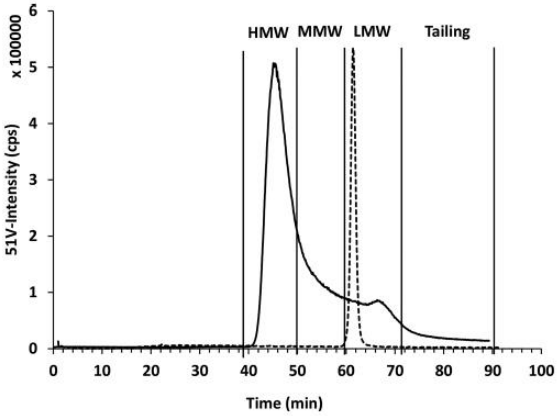

Figure 4. Chromatogram of vanadium in Asphaltene 2017 from GPC-ICP-MS (black line) and vanadyl porphyrin (dotted line). Fraction limits were set at 39−49 min for HMW, 49−60 min for MMW, 60−70 min for LMW, and 71−91 min for tailing based on the trimodal distribution seen in chromatograms of V-containing aggregates.

A 1 mL aliquot of Asphaltene 2017 diluted in THF was fractionated according to this method. The obtained chromatogram is shown in Figure 4, and the corresponding mass balance is given in Table 3. There is no correlation between the mass of the fraction and quantity of vanadium, and most of the metal species and total material are part of the HMW fraction. However, the percent of vanadium in the LMW fraction is higher than the percent of total material in this fraction.

Table 2. Calibration with Vanadyl Porphyrins

vanadium (µg)	area A	area B	area C	average	standard deviation (%)
0.00537	524304	676552	706549	635802	15
0.0108	1456995	1404246	896046	1252429	24
0.0537	7797726	7976937	6050314	7274992	14
0.108	13860441	16379744	12440338	14226841	14
0.537	118697108	162436773	108242613	129792165	22
1.08	209863919	231665273	169634752	203721315	15

DOI: 10.1021/acs.energyfuels.9b00676
Energy Fuels 2019, 33, 6060−6068

Table 3. Mass Balance of Asphaltene 2017 and ^{51}V Repartition in the Collected GPC Fractions Obtained by GPC-ICP-MS

	Injected Quantity	HMW	MMW	LMW	Tailing	Recovery
mass of Asphaltene 2017 (mg)	9.0	4.8	2.3	0.9	0.2	8.2
mass of Asphaltene 2017 (%)		53.3	25.6	10.0	2.2	91.1
vanadium by GPC-ICP-MS (%)		52.3	26.9	15.0	5.8	100

The different GPC fractions were deposited on HPTLC cellulose plates and developed using the same procedure as was used for the porphyrins. The plates were analyzed by LA-ICP MS and by UV densitometry at 280 nm. A picture of the plate and the LA-ICP MS chromatograms are given in Figure 5, and

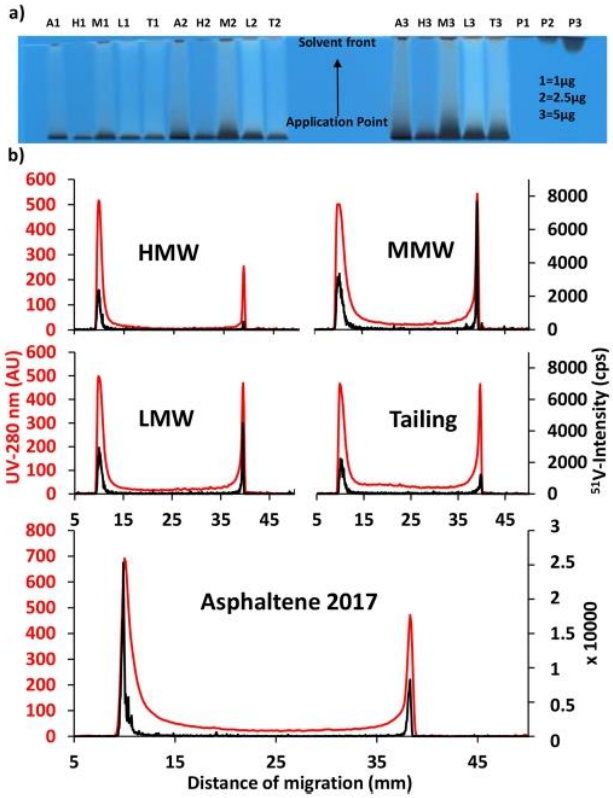

Figure 5. (a) Picture at 280 nm of the cellulose plate after migration. (b) LA-ICP-MS chromatograms (black line) and UV spectra (red line) of the one-step development on cellulose HPTLC plates with DCM/MeOH of 1 μg of the preparative GPC fractions of Asphaltene 2017.

the various measured areas are given in Table 4. Figure 5 shows that for all GPC fractions, a portion of the sample remains at the application point and a portion migrates with the solvent front. Surprisingly, even for the LMW fraction, which is considered the free porphyrin part of the sample, 65% of the vanadium remains at the application point, as indicated in Table 4. This result means that the LMW fraction is not only made of porphyrins similar to our porphyrin standards and that these porphyrins are more polar (polar side chains) or they can reaggregate. However, Deelchand et al.[23] observed the same trend; higher molecular weight fractions showed lower mobilities on the HPTLC plate. The same tendency is observed for deposits of 2.5 and 5 μg (Table S3).

We can also follow the ratio between LA and UV (Table 4). For the MMW and LMW fractions of Asphaltene 2017, the ratio of the eluted part of LA/UV is between 600 and 800. However, the ratio is approximately 300 for the HMW fraction. Thus, the eluted MMW and LMW fractions are more concentrated in vanadium than the HMW is.

An UV−vis spectrum for each peak was recorded to obtain structural information on the molecules present, and the spectra are given Figure 6. The spectrum obtained for the noneluted part, drawn in red, is similar for each fraction. This spectrum, with a maximum intensity at approximately 240 nm that decreases continuously until 800 nm, is characteristic of highly polyaromatic compounds. These spectra are similar to those obtained by Bonoldi et al.[34] for an asphaltene diluted in THF. However, unlike in the work of Bonoldi et al.,[34] no peaks were observed at approximately 400 nm, which is the wavelength of the porphyrin Soret band. On the other hand, large peaks were observed in LA-ICP-MS at the application point, indicating the presence of vanadium. As proposed by Evdokimov et al.,[25] this could be due to the occlusion of porphyrins inside the aggregates, which would prevent the detection of their characteristic UV−vis absorption bands. Furthermore, the spectra obtained from the eluted parts (black line) differed depending on the fraction. For the HMW fraction (Figure 6), the signal between 300 and 400 nm is weaker. For the MMW, LMW, and T fractions, we can see the Soret band of the porphyrins at 420 nm, especially for the LMW fraction (represented by a star). This result suggests that separation by HPTLC allows the isolation of the free porphyrins contained in the MMW, LMW, and T fractions from the rest of the material.

Asphaltenes 2017, C7, and C5. The distribution of the ^{51}V species in Asphaltene 2017, Asphaltene C7, and Asphaltene C5 was controlled using the same methodology, and the distributions are given in Figure 7 and Table 5. As shown in Figure 7, again only two peaks were observed. The fraction of the asphaltene with the greatest affinity for the plate has a higher vanadium content than the eluted fraction (Table 5), meaning that the largest portion of the metal would be in the aggregates. Table 5 shows that the ratios between LA/UV for the application point of asphaltene varied. For Asphaltene C7 and 2017, the ratio is close to 1800. This would mean that the molecules removed during the washing do not stay at the application point or are not aromatics (as UV mostly detects aromatic compounds). Therefore, for Asphaltene C5, the ratio is close to 1300, this would mean that in Asphaltene C5 there is more organic aromatic matter than in the others asphaltenes. For the eluted part, the ratio between LA/UV for Asphaltene 2017 is close to 900 instead of 500 for C5 and C7. This would mean that precipitate asphaltene with C7 and wash it allow a better migration of metallic compounds.

The calibration curves shown in Table 2 were used to calculate the concentrations of vanadium in Asphaltene 2017, C5, and C7 (Table S4). The average concentration on the three different plates with three different depositions was approximately 642 ppm, which is in good agreement with the concentration obtained by the ATSM method (640 ppm). Thus, HPTLC-LA-ICP-MS with a cellulose plate allowed us to

DOI: 10.1021/acs.energyfuels.9b00676
Energy Fuels 2019, 33, 6060−6068

Table 4. Area and Percentages of Noneluted and Eluted Material from 1 μg of Each Fraction for UV and ^{51}V by LA-ICP-MS After Image Processing

	area			percentage			
sample	noneluted	eluted	total	noneluted	eluted	LA/UV noneluted	LA/UV eluted
			UV				
A 2017	1311	588	2556	77	23		
HMW	1152	232	1354	83	17		
MMW	2113	704	2814	75	25		
LMW	1446	754	2200	66	34		
T	1654	966	2540	63	37		
porphyrins	5	395	400	1	99		
			LA-ICP-MS				
A 2017	3317643	469063	3786707	88	12	2530	798
HMW	692888	63514	756402	92	8	601	274
MMW	1609144	609555	2218699	73	27	762	866
LMW	900274	482428	1382702	65	35	623	639
T	839530	297053	1136583	74	26	508	307
porphyrins	13610088	209863919	223474007	6	94	2722018	531301

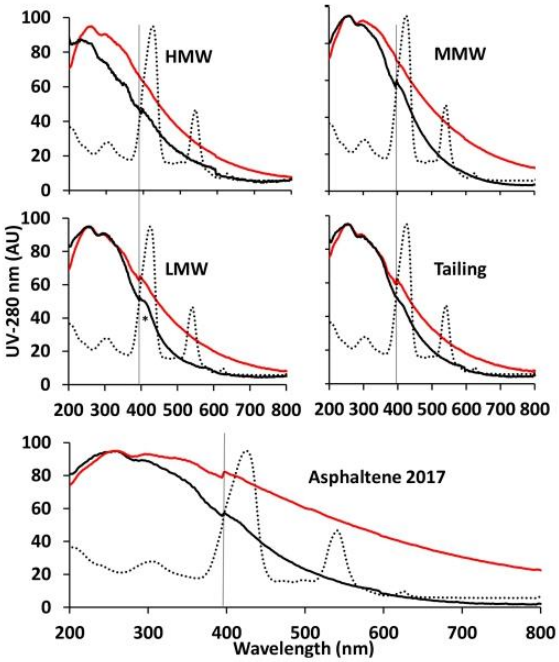

Figure 6. UV spectra of 1 μg of each preparative GPC fraction, i.e., HMW, MMW, LMW and T, of Asphaltene 2017 and the total Asphaltene 2017 at the application point (red line) and at the solvent front (black line). Dotted lines represent the vanadyl porphyrin. Vertical lines represent a change in the lamp setting on the device. The Soret band corresponding to free porphyrins is indicated with a star. .

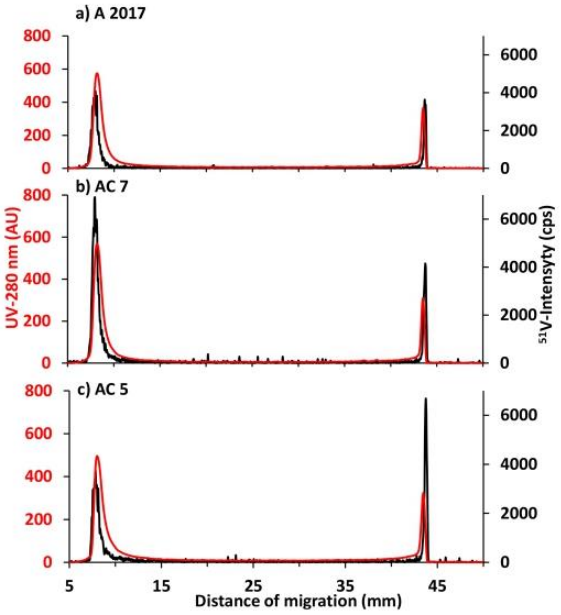

Figure 7. LA-ICP-MS (black line) and UV (red line) chromatograms of the one-step development on cellulose HPTLC plates with DCM/MeOH of 1 μg of Asphaltene 2017 (a), Asphaltene C7 (b), and Asphaltene C5 (c).

calculate the concentration of vanadium in the asphaltene sample. According to the results, the concentration in Asphaltene C7 has an average of 611 ppm vanadium is close to that in Asphaltene 2017, which has an average of 642 ppm of vanadium. However, Asphaltene C5 is less concentrated (464 ppm), meaning that during the precipitation of asphaltene, heptane promotes more coprecipitation of metals than nonmetallic compounds.

■ CONCLUSIONS

In this work, instead of classic Si-based sorbents, cellulose plates were used for HPTLC analysis of petroleum samples. Cellulose leads to 10-fold more intense signals with less noise than silica gel when the plates are analyzed by LA-ICP MS and allows the quantification of vanadium forms in asphaltene samples. Two well-separated peaks were obtained for purified asphaltene (Asphaltene 2017)[35] and its corresponding fractions. The eluted fraction was found to contain free porphyrins, whereas the fraction that remained at the application point (the major fraction) corresponded to trapped or highly polar porphyrins and was the most difficult part to

DOI: 10.1021/acs.energyfuels.9b00676
Energy Fuels 2019, 33, 6060−6068

Table 5. Average of the Areas and Percentages of Noneluted and Eluted Material from 5 μg of Each Asphaltene Sample on Three Different Plates for UV and ^{51}V by LA-ICP-MS After Image Processing

	area			percentage			
sample	noneluted	eluted	total	noneluted	eluted	ratio LA/UV roneluted	ratio LA/UV eluted
				UV			
A 2017	3926	954	4880	80	20		
AC 7	3875	935	4810	81	19		
AC 5	3644	1175	4819	76	24		
porphyrins	5	395	400	1	99		
				LA-ICP-MS			
A 2017	7307202	918289	8225490	89	11	1861	963
AC 7	6878423	433202	7311625	94	6	1775	463
AC 5	4932036	581532	5513568	89	11	1353	495
porphyrins	13610088	209863919	223474007	6	94	2722018	531301

remove. These results suggest that is separation could be used to pilot efficient processes using a hydrodemetalation step. Moreover, the differences between Asphaltene 2017, C7, and C5 can be determined by comparing their UV and LA-ICP MS data as a function of the nature of the asphaltene. The concentration in vanadium is higher in asphaltene precipitated with heptane, and there is less organic matter in Asphaltene 2017.

■ ASSOCIATED CONTENT

Supporting Information

The Supporting Information is available free of charge on the ACS Publications website at DOI: 10.1021/acs.energyfuels.9b00676.

(Figure S1) Processing data with FIJI; (Figure S2) calibration curve for each plate A, B, and C; (Table S1) intensity of three replicates on the same spot (AC5 3 μg) by LA-ICP-MS; (Table S2) mass deposit for asphaltene and porphyrins samples; (Table S3) results obtained for 1, 2.5, and 5 μg of deposit of A2017 and fractions by UV and LA-ICP-MS; and (Table S4) concentration obtained by HPTLC-LA-ICP-MS after image processing (PDF)

■ AUTHOR INFORMATION

Corresponding Authors

*E-mail: caroline.mangote@total.com. Tel.: +33 (0) 235 551 102.

*E-mail: brice.bouyssière@univ-pau.fr. Tel.: +33 (0) 559 407 752.

ORCID

Pierre Giusti: 0000-0002-9569-3158

Brice Bouyssiere: 0000-0001-5878-6067

Notes

The authors declare no competing financial interest.

■ ACKNOWLEDGMENTS

This work was supported by the Conseil Régional d'Aquitaine (20071303002PFM) and FEDER (31486/08011464). The authors thank TOTAL for supplying the oil samples.

■ REFERENCES

(1) Speight, J. G. Petroleum asphaltenes - Part 1: asphaltenes, resins and the structure of petroleum. *Oil Gas Sci. Technol.* **2004**, *59*, 467−477.

(2) Strausz, O. P.; Peng, P. A.; Murgich, J. About the colloidal nature of asphaltenes and the MW of covalent monomeric units. *Energy Fuels* **2002**, *16*, 809−822.

(3) Leyva, C.; Ancheyta, J.; Berrueco, C.; Millán, M. Chemical characterization of asphaltenes from various crude oils. *Fuel Process. Technol.* **2013**, *106*, 734−738.

(4) Pereira, T. M. C.; Vanini, G.; Oliveira, E. C. S.; Cardoso, F. M. R.; Fleming, F. P.; Neto, A. C.; Lacerda, V.; Castro, E. V. R.; Vaz, B. G.; Romão, W. An evaluation of the aromaticity of asphaltenes using atmospheric pressure photoionization Fourier transform ion cyclotron resonance mass spectrometry − APPI(±)FT-ICR MS. *Fuel* **2014**, *118*, 348−357.

(5) McKenna, A. M.; Marshall, A. G.; Rodgers, R. P. Heavy petroleum composition. 4. Asphaltene compositional space. *Energy Fuels* **2013**, *27*, 1257−1267.

(6) Barrera, D. M.; Ortiz, D. P.; Yarranton, H. W. Molecular weight and density distributions of asphaltenes from crude oils. *Energy Fuels* **2013**, *27*, 2474−2487.

(7) Yarranton, H. W.; Ortiz, D. P.; Barrera, D. M.; Baydak, E. N.; Barré, L.; Frot, D.; Eyssautier, J.; Zeng, H.; Xu, Z.; Dechaine, G.; Becerra, M.; Shaw, J. M.; McKenna, A. M.; Mapolelo, M. M.; Bohne, C.; Yang, Z.; Oake, J. On the size distribution of self-associated asphaltenes. *Energy Fuels* **2013**, *27*, 5083−5106.

(8) Cebolla, V. L.; Membrado, L.; Domingo, M. P.; Henrion, P.; Garriga, R.; González, P.; Cossío, F. P.; Arrieta, A.; Vela, J. Quantitative applications of fluorescence and ultraviolet scanning densitometry for compositional analysis of petroleum products in thin-layer chromatography. *J. Chromatogr. Sci.* **1999**, *37*, 219−226.

(9) Sharma, B. K.; Sarowha, S. L. S.; Bhagat, S. D.; Tiwari, R. K.; Gupta, S. K.; Venkataramani, P. S. Hydrocarbon group type analysis of petroleum heavy fractions using the TLC-FID technique. *Fresenius' J. Anal. Chem.* **1998**, *360*, 539−544.

(10) Jarne, C.; Cebolla, V. L.; Membrado, L.; Le Mapihan, K.; Giusti, P. High-performance thin-layer chromatography using automated multiple development for the separation of heavy petroleum products according to their number of aromatic rings. *Energy Fuels* **2011**, *25*, 4586−4594.

(11) Mateos, E.; Cebolla, V. L.; Membrado, L.; Vela, J.; Galvez, E. M.; Matt, M.; Cossio, F. P. Coralyne cation, a fluorescent probe for general detection in planar chromatography. *J. Chromatogr. A* **2007**, *1146*, 251−257.

(12) Chacón-Patiño, M. L.; Blanco-Tirado, C.; Orrego-Ruiz, J. A.; Gómez-Escudero, A.; Combariza, M. Y. High resolution mass spectrometric view of asphaltene−SiO_2 interactions. *Energy Fuels* **2015**, *29*, 1323−1331.

(13) Giraldo-Dávila, D.; Chacón-Patiño, M. L.; McKenna, A. M.; Blanco-Tirado, C.; Combariza, M. Y. Correlations between molecular composition and adsorption, aggregation, and emulsifying behaviors of petrophase 2017 asphaltenes and their thin-layer chromatography fractions. *Energy Fuels* **2018**, *32*, 2769−2780.

(14) Li, W.; Morgan, T. J.; Herod, A. A.; Kandiyoti, R. Thin-layer chromatography of pitch and a petroleum vacuum residue. Relation

between mobility and molecular size shown by size-exclusion chromatography. *J. Chromatogr. A* **2004**, *1024*, 227−243.
(15) Vorapalawut, N.; Martinez Labrador, M.; Pohl, P.; Caetano, M.; Chirinos, J.; Arnaudguilhem, C.; Bouyssiere, B.; Shiowatana, J.; Lobinski, R. Application of TLC and LA ICP SF MS for speciation of S, Ni and V in petroleum samples. *Talanta* **2012**, *97*, 574−578.
(16) Chirinos, J.; Oropeza, D.; González, J.; Ranaudo, M.; Russo, R. E. Determination of Vanadium/Nickel proportionality in the asphaltene fraction of crude oil using thin-layer chromatography with femtosecond laser ablation−inductively coupled plasma−mass spectrometry. *Energy Fuels* **2013**, *27*, 2431−2436.
(17) Hajibrahim, S. K.; Tibbetts, P. J. C.; Watts, C. D.; Maxwell, J. R.; Eglinton, G.; Colin, H.; Guiochon, G. Analysis of carotenoid and porphyrin pigments of geochemical interest by high-performance liquid chromatography. *Anal. Chem.* **1978**, *50*, 549−553.
(18) Van Berkel, G. J.; Quirke, J. M. E.; Filby, R. H. The Henryville Bed of the New Albany shale—I. Preliminary characterization of the Nickel and Vanadyl porphyrins in the bitumen. *Org. Geochem.* **1989**, *14*, 119−128.
(19) Vargas, V.; Castillo, J.; Ocampo Torres, R.; Bouyssiere, B.; Lienemann, C.-P. Development of a chromatographic methodology for the separation and quantification of V, Ni and S compounds in petroleum products. *Fuel Process. Technol.* **2017**, *162*, 37−44.
(20) Gutierrez Sama, S.; Desprez, A.; Krier, G.; Lienemann, C.-P.; Barbier, J.; Lobinski, R.; Barrere-Mangote, C.; Giusti, P.; Bouyssiere, B. Study of the aggregation of metal complexes with asphaltenes using gel permeation chromatography inductively coupled plasma high-resolution mass spectrometry. *Energy Fuels* **2016**, *30*, 6907−6912.
(21) Putman, J. C.; Gutiérrez Sama, S.; Barrère-Mangote, C.; Rodgers, R. P.; Lobinski, R.; Marshall, A. G.; Bouyssière, B.; Giusti, P. Analysis of petroleum products by gel permeation chromatography coupled online with inductively coupled plasma mass spectrometry and offline with fourier transform ion cyclotron resonance mass spectrometry. *Energy Fuels* **2018**, *32*, 12198.
(22) Desprez, A. *Caractérisation moléculaire et élémentaire des produits pétroliers lourds*. Ph.D. Thesis, University of Pau, Pau, France, 2014.
(23) Deelchand, J. P.; Naqvi, Z.; Dubau, C.; Shearman, J.; Lazaro, M. J.; Herod, A. A.; Read, H.; Kandiyoti, R. Planar chromatographic separation of petroleum residues and coal-derived liquids. *J. Chromatogr. A* **1999**, *830*, 397−414.
(24) Zhao, X.; Xu, C.; Shi, Q. Porphyrins in heavy petroleums: a review. *Structure and Modeling of Complex Petroleum Mixtures* **2016**, 39−70.
(25) Evdokimov, I. N.; Fesan, A. A.; Losev, A. P. Occlusion of foreign molecules in primary asphaltene aggregates from near-UV−visible absorption studies. *Energy Fuels* **2017**, *31*, 1370−1375.
(26) Caumette, G.; Lienemann, C.-P.; Merdrignac, I.; Bouyssiere, B.; Lobinski, R. Element speciation analysis of petroleum and related materials. *J. Anal. At. Spectrom.* **2009**, *24*, 263−276.
(27) Barrow, M. P.; McDonnell, L. A.; Feng, X.; Walker, J.; Derrick, P. J. Determination of the nature of naphthenic acids present in crude oils using nanospray fourier transform ion cyclotron resonance mass spectrometry: the continued battle against corrosion. *Anal. Chem.* **2003**, *75*, 860−866.
(28) Striegel, M. F.; Hill, J. *Thin-layer Chromatography for Binding Media Analysis*. Getty Conservation Institute: Los Angeles, CA, 1996.
(29) Poole, C. F.; Dias, N. C. Practitioner's guide to method development in thin-layer chromatography. *J. Chromatogr. A* **2000**, *892*, 123−142.
(30) Rueden, C. T.; Schindelin, J.; Hiner, M. C.; DeZonia, B. E.; Walter, A. E.; Arena, E. T.; Eliceiri, K. W. ImageJ2: ImageJ for the next generation of scientific image data. *BMC Bioinformatics* **2017**, *18* (1), 1.
(31) Schindelin, J.; Arganda-Carreras, I.; Frise, E.; Kaynig, V.; Longair, M.; Pietzsch, T.; Preibisch, S.; Rueden, C.; Saalfeld, S.; Schmid, B.; Tinevez, J.-Y.; White, D. J.; Hartenstein, V.; Eliceiri, K.; Tomancak, P.; Cardona, A.; et al. Fiji: An open source platform for biological image analysis. *Nat. Methods* **2012**, *9* (7), 676−682.
(32) Ali, M. F.; Perzanowski, H.; Bukhari, A.; Al-Haji, A. A. Nickel and vanadyl porphyrins in Saudi Arabian crude oils. *Energy Fuels* **1993**, *7*, 179−184.
(33) Freeman, D. H.; Saint Martin, D. C.; Boreham, C. J. Identification of metalloporphyrins by third-derivative UV/VIS diode array spectroscopy. *Energy Fuels* **1993**, *7*, 194−199.
(34) Bonoldi, L.; Flego, C.; Galasso, L. Beyond the average molecule description of asphaltenes: hyphenated gel permeation chromatography and spectroscopic analyses. *Energy Fuels* **2016**, *30*, 3630−3636.
(35) PetroPhase. Asphaltene Characterization Interlaboratory Study for PetroPhase 2017. In *Proceedings of the 18th International Conference on Pretroleum Phase Behavior and Fouling*, Le Havre, France, June 11−15, 2017; Total, the University of Pau, and the University of Rouen-Normandy: Le Havre, France, 2017.

DOI: 10.1021/acs.energyfuels.9b00676
Energy Fuels 2019, 33, 6060−6068

Dans cet article plusieurs points ont été abordés. Dans un premier temps il a été montré qu'une analyse quantitative du vanadium est possible sur plaque de cellulose avec seulement 1 µg d'échantillon déposé.

Ensuite, l'étalon de porphyrine de vanadium utilisé migre jusqu'au front de solvant. Or seule une partie du vanadium présent dans l'asphaltène 2017 migre. Lorsque le développement HPTLC est effectué sur les différentes fractions GPC de l'asphaltène, il a été montré que dans les fractions agrégées (haut poids moléculaire) la quantité de vanadium qui reste au point de dépôt est très importante. Au contraire dans la fraction GPC de bas poids moléculaire, contenant les porphyrines libres, la quantité de vanadium qui migre est plus importante. De plus sur la partie qui a migré de la fraction GPC des bas poids moléculaires, la bande de Soret obtenue par UV et caractéristique des porphyrines apparait.

Ces résultats suggèrent que les porphyrines libres se retrouvent au front de solvant, alors que celles difficilement accessibles restent au point de dépôt. Si cela est confirmé, il peut être intéressant d'analyser plusieurs échantillons et de quantifier la proportion de porphyrines libres pour chacun d'entre eux dans le but de mettre en lien les résultats avec les procédés de dé-metallation.

Dans la seconde partie de ce chapitre, les mêmes plaques HPTLC en cellulose seront utilisées mais cette fois ci la séparation HPTLC sera couplée à la séparation par extrographie. De plus l'analyse se fera non seulement par UV et LA-ICP MS, mais aussi par MALDI-FT-ICR MS ce qui permettra une analyse moléculaire afin d'identifier les porphyrines en fonction des fractions.

In this article several points have been addressed. Firstly, it was shown that a quantitative analysis of vanadium is possible on a cellulose plate with only 1 µg of deposited sample.

Then the vanadium porphyrin standard used migrates to the solvent front. However, only part of the vanadium present in asphaltene 2017 migrates. When HPTLC development is carried out on the different GPC fractions of the asphaltene, it has been shown that in the aggregate (high molecular weight) fractions the amount of vanadium remaining at the deposition point is very large. In contrast, in the low molecular weight GPC fraction, containing free porphyrins, the amount of vanadium which migrates is greater. In addition, on the migrated part of the low molecular weight GPC fraction, the Soret band obtained by UV light and characteristic of porphyrins appears.

These results suggest that free porphyrins are found at the solvent front, while those that are difficult to access remain at the deposition point. If this is confirmed, it may be interesting to analyze several samples and quantify the proportion of free porphyrins for each of them in order to link the results with the de-metallation processes.

In the second part of this chapter, the same cellulose HPTLC plates will be used but this time the HPTLC separation will be coupled with the extrographic separation. In addition to UV and LA-ICP MS, the analysis will also be done by MALDI-FT-ICR MS which will allow a molecular analysis to identify porphyrins according to fractions.

Partie II : Apport de l'HPTLC dans le cadre de la séparation des asphaltènes sur plaques de cellulose, analyse par MALDI-FT-ICR MS

Cette partie a fait l'objet d'un article publié dans le journal *Energy and Fuels* de l'*American Chemical Society* (ACS). Cet article a été laissé tel qu'il a été publié.

Ici la séparation par extrographie est couplée à une séparation par HPTLC dans le cadre de l'analyse de l'asphaltène 2017. De plus l'analyse se fera par UV, par LA-ICP MS et par une analyse moléculaire par MALDI-FT-ICR MS dans le but d'identifier les porphyrines de vanadium dans chacune des fractions.

Dans la partie précédente, le vanadium contenu dans la fraction GPC des hauts poids moléculaires a peu migré. Or après séparation par extrographie, l'addition de la fraction C7/Tol et Tol/THF/MeOH forment la fraction des hauts poids moléculaires. Il est attendu que le vanadium présent dans au moins une de ces deux fractions migre peu par HPTLC et au contraire celui présent dans la fraction acétone migre en grande partie. L'objectif ici est de non seulement de confirmer la théorie que la séparation par HPTLC permet une séparation des porphyrines libres du reste des porphyrines. Mais aussi d'identifier les porphyrines facilement accessibles et celles difficilement accessibles grâce à une matrice promouvant l'ionisation des porphyrines. Si les porphyrines qui restent au point de dépôt de la plaque HPTLC sont différentes de celles qui migrent, cela serait une information importante pour les processus de démétallation.

.

This section was the subject of an article published to the American Chemical Society (ACS) journal Energy and Fuels. This article has been left as published.

Here extrographic separation is coupled with HPTLC separation in the analysis of asphaltene 2017. In addition the analysis will be done by UV, LA-ICP MS and molecular analysis by MALDI-FT-ICR MS in order to identify the vanadium porphyrins in each of the fractions.

In the previous section the vanadium in the high molecular weight GPC fraction has migrated little. However, after separation by extrographic separation, the addition of the C7/Tol and Tol/THF/MeOH fractions form the high molecular weight fraction. Vanadium in at least one of these two fractions is expected to migrate little by HPTLC and vanadium in the acetone fraction is expected to migrate largely. The objective here is not only to confirm the theory that separation by HPTLC allows a separation of free porphyrins from the rest of the porphyrins. But also to identify the porphyrins that are easily accessible and those that are difficult to access thanks to a matrix promoting porphyrin ionization. If the porphyrins that remain at the deposition point of the HPTLC plate are different from those that migrate, this would be important information for demetallation processes.

energy&fuels

pubs.acs.org/EF

Article

Speciation of Metals in Asphaltenes by High-Performance Thin-Layer Chromatography and Solid−Liquid Extraction Hyphenated with Elemental and Molecular Identification

Rémi Moulian, Martha Chacón-Patiño, Oscar Lacroix-Andrivet, Sandra Mounicou, Anna Luiza Mendes Siqueira, Carlos Afonso, Ryan Rodgers, Pierre Giust, Brice Bouyssiere,* and Caroline Barrère-Mangote*

Cite This: *Energy Fuels* 2020, 34, 12449−12456

Read Online

ACCESS | Metrics & More | Article Recommendations | Supporting Information

ABSTRACT: Asphaltenes are among the most challenging components in petroleum processing because they contain high amounts of heteroatoms (i.e., S, N, O, V, and Ni) thought to be responsible for strong aggregation tendencies, precipitation, and fouling problems. The role of vanadium- and nickel-containing petroleum compounds (i.e., petroporphyrins) in aggregation and fouling is not completely understood because asphaltene composition and structure is still a subject of debate in the petroleum chemistry community. Characterization of asphaltenes, namely, molecular analysis that employs no chromatographic separation, often fails to reveal their comprehensive composition. The work herein presents asphaltene fractionation by (1) solid/liquid extraction, which allows for separation of single-core ("island") and multicore ("archipelago") structural motifs and by (2) high-performance thin layer chromatography (HPTLC) with cellulose as the stationary phase and DCM/MeOH as the eluent, which facilitates access to petroporphyrins. Characterization is performed by laser ablation inductively coupled plasma mass spectrometry (LA-ICP-MS) and matrix-assisted laser desorption ionization Fourier transform ion cyclotron resonance mass spectrometry (MALDI FT-ICR MS). The results demonstrate that even with multiple separation steps, a large quantity of vanadyl porphyrins remains inaccessible for molecular analysis by MALDI FT-ICR MS, which raises the question of what portion of a complex sample of asphaltene can be revealed by ultrahigh resolution mass spectrometry. Furthermore, the results show that easily accessible porphyrins migrate with the solvent front in HPTLC. Thus, HPTLC can be used to isolate and identify "free" porphyrins not locked into asphaltene aggregates; however, further development of separation methods is required to access the most difficult and problematic asphaltene fractions, which do not migrate and impose analytical challenges due to their stronger aggregation tendency.

INTRODUCTION

Asphaltenes are well known for their negative impact on petroleum production, transportation, storage, and refining. Asphaltenes contain a wide diversity of molecules with different degrees of aromaticity, heteroatom contents, and molecular structure. For instance, Fourier transform ion cyclotron resonance mass spectrometry (FT-ICR MS) has revealed asphaltene molecules with either single-core or multicore structures that contain only hydrogen and carbon (hydrocarbons or the HC class) as well as species with up to three or more heteroatoms (e.g., vanadyl porphyrins or the $N_4O_1V_1$ class, sulfur-containing molecules or the S_3 class, and oxygen-rich compounds or the O_4 class).[1−6] Thus, the combined effects of aromaticity, heteroatom content, and molecular structure trigger multiple intermolecular interactions, such as pi-stacking, hydrogen bonding, acid−base conjugations, and London dispersion forces between asphaltenes. The synergy between multiple intermolecular interactions results in strong aggregation and ultimate precipitation of a wide compositional range of species, from those with no heteroatoms (HC class) to high heteroatom-containing species.[7−9] It is believed that metals present in asphaltenes are mainly present in porphyrinic complexes,[10−12] i.e., nickel and vanadyl porphyrins are tetrapyrrole-based metal complexes. The actual structures of nickel and vanadyl porphyrins are the result of geochemical modifications of the chlorophyll molecule. The chlorophyll structure changed over geological time during fossil crude oil formation via demetalation, aromatization, and peripheral addition of sulfur or oxygen.[13,14] These transformations yielded several structurally different porphyrin families of the types $N_4O_1V_1$, $N_4O_2V_1$, $N_4O_3V_1$, $N_4O_1V_1S_1$, and N_4Ni_1, as shown in Figure 1.

Understanding the molecular composition of porphyrins and other metal complexes that trigger issues in refinery processes is critical to the petroleum industry. For this purpose, it is essential to fractionate asphaltenes before molecular-level analysis because direct "dilute-and-shoot" studies of such a complex matrix usually do not reveal a great part of the information. As shown by Evdokimov et al.,[15,16] even with the

Received: July 28, 2020
Revised: September 22, 2020
Published: September 23, 2020

https://dx.doi.org/10.1021/acs.energyfuels.0c02525
Energy Fuels 2020, 34, 12449−12456

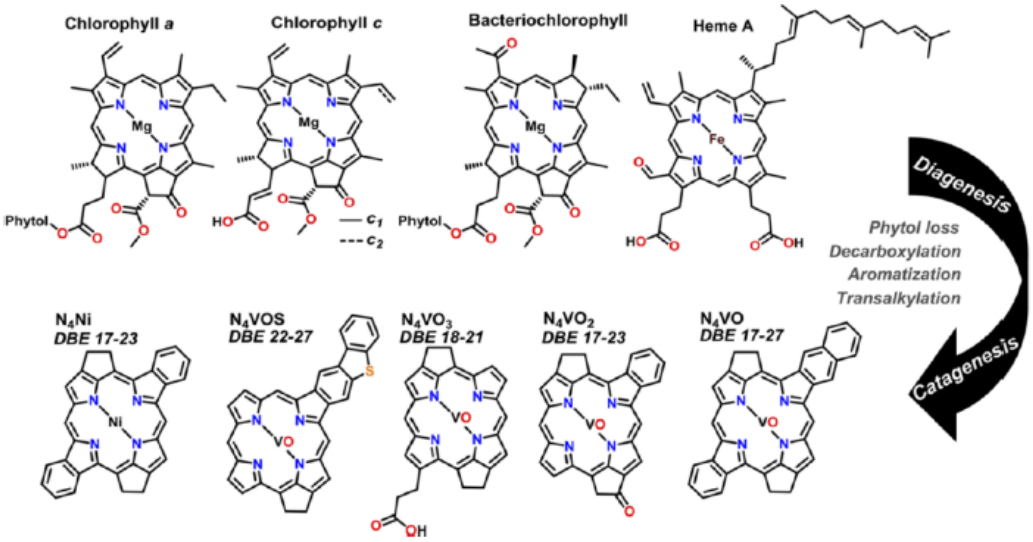

Figure 1. Scheme of geochemical transformation of chlorophylls.[4]

abundant presence of petroporphyrins, the Soret band, characteristic of porphyrinic complexes in ultraviolet absorption spectra, is not always detected in the sample spectrum, the detection of which depends on the dilution factor. Furthermore, with MS techniques such as matrix-assisted laser desorption ionization (MALDI) FT-ICR MS, the matrix, ionization efficiency, and ion suppression effects usually conceal the molecular level of difficult-to-ionize compounds. Recently, Chacón-Patiño et al.[17] and Giraldo-Davila et al.[18] used silica gel thin-layer chromatography plates to separate asphaltene samples and achieve a more complete molecular characterization. The authors used a mixture of DCM/MeOH, followed by toluene, to separate asphaltenes into three fractions enriched in alkyl-aromatic compounds, polar species, and non-eluted asphaltenes. This technique can also be used on the preparative scale to separate fractions that can then be extracted with solvents and further analyzed by other techniques (Li et al.[19]). Furthermore, asphaltene samples can also be separated prior to high-performance thin layer chromatography (HPTLC) analysis. For example, Chacón-Patiño et al.[5,20,21] reported asphaltene fractionation by a solid−liquid extraction strategy using silica gel as an adsorbent and subsequent Soxhlet extraction; this method is known as extrography. The authors demonstrated that extrography allows for the separation of asphaltenes according to their structural motif, multicore or archipelago (composed of several aromatic cores linked by covalent bonds) and single-core or island (composed of one aromatic core with alkyl side chains). According to these results, island compounds are easily accessed by atmospheric pressure photoionization FT-ICR MS; conversely, archipelago molecules are more difficult to ionize, due in part to their relatively stronger aggregation trends.[22]

The use of TLC or HPLTC allows for more comprehensive elemental information for petroleum fractions.[23,24] For instance, Chirinos et al.[25] used laser ablation ICP-MS to achieve rapid determination of the ratio between nickel and vanadium in asphaltene samples after a separation step with HPTLC. Moreover, the use of HPTLC plates also allows for molecular analysis by LDI/MALDI FT-ICR MS; for example, Cho et al.[26] demonstrated that LDI FT-ICR MS can be used to quantify porphyrins in petroleum samples. Additionally, Pradilla et al.[27] developed a MALDI matrix to promote selective ionization or petroporphyrins via electron transfer reactions. The authors used a novel matrix to analyze asphaltenes after an HPTLC separation step. The results revealed the selective ionization of petroporphyrins and an increased number of molecular formulas compared to those identified in previous studies.[4]

In this work, two successive separation steps, extrography and HPTLC, were coupled with elemental laser ablation inductively coupled plasma mass spectrometry (LA-ICP-MS) and molecular detection (MALDI FT-ICR MS) to characterize metals contained in one asphaltene reference sample, referred to as Asphaltene 2017. The purpose was to determine which fractions contained vanadium and the kinds of porphyrins present in these fractions.

■ EXPERIMENTAL SECTION

Samples and Reagents. *Samples.* Asphaltene 2017 (from a Middle Eastern crude oil; vanadium content: 640 ppm) from the interlaboratory study of the Petrophase 2017 Conference[28] and its extrography fractions, prepared as reported by Chacon-Patiño,[5,20] were studied. Asphaltene 2017 was obtained by a slightly modified version of the ASTM D6560-12 method. A cleaning step, via four cycles of maceration and Soxhlet extraction with heptane, was employed to decrease the amount of occluded/coprecipitated maltenes.

Solvents. Tetrahydrofuran (THF, HPLC grade, without stabilizer, Lichrosolv, Merck, Frankfurter Strasse 250, Darmstadt 64293, Germany) was used as the solvent for sample preparation and for MALDI analyses. Dichloromethane (DCM) and methanol (MeOH) (HPLC grade, Lichrosolv, Merck, Frankfurter Strasse 250, Darmstadt 64293, Germany) were used to develop the HPTLC plates. Toluene, heptane, and pentane were used to prepare Petrophase 2017 asphaltenes. Acetone, toluene, heptane, THF, and methanol of HPLC grade were used to prepare extrography fractions from Asphaltene 2017.

Solid/Liquid Extraction Samples. Extrography fractionation was carried out following a method reported elsewhere.[20] Briefly, a Soxhlet

https://dx.doi.org/10.1021/acs.energyfuels.0c02525
Energy Fuels 2020, 34, 12449−12456

apparatus was used to perform three successive extractions. Approximately 150 mg of asphaltenes was dissolved in dichloromethane, and 15 g of silica was then added to the solution. Subsequently, the mixture was completely dried under nitrogen, and the dried mixture was Soxhlet extracted with acetone, toluene/heptane (50/50 Hep/Tol, v/v), and toluene/tetrahydrofuran/methanol (47.5/47.5/5 Tol/THF/MeOH, v/v/v).

Instrumentation. *HPTLC Plates.* Cellulose HPTLC glass plates (Merck, thickness 0.15−0.2 mm, Frankfurter Strasse 250, Darmstadt 64293, Germany) that were 20 cm × 10 cm in size and did not contain fluorescent indicators were used. The HPTLC procedure was carried out with the following instrumentation protocol from CAMAG. Sample application and sample development were performed using an automatic TLC Sampler 4 (ATS4) and automated multiple development 2 (AMD2) equipment. UV absorbance chromatograms were acquired at a wavelength of 280 nm with a D2 and W lamp TLC scanner. UV spectra from 190 to 900 nm were obtained using the same device. Finally, a TLC visualizer was used to obtain images of the cellulose plate under 366 nm UV light after development. Peak area data were determined using WinCATS software.

HPTLC plates were cleaned with DCM and THF and dried at 110 °C for 10 min prior to sample deposition. All the samples were deposited 10 mm from the bottom of the plate. A high eluent-strength mobile phase (DCM/MeOH, 99.5:0.5) was used. The plate was developed in a single step until the solvent front reached 50 mm. Whole Petrophase 2017 and its extrography fractions were deposited two times per HPTLC plate on three different plates that were developed as described above for subsequent analysis by LA-ICP-MS.

Developed HPTLC separations for whole Petrophase 2017 and its three extrography fractions were also subjected to MALDI FT-ICR MS analysis. After separation, the different samples were scratched from the plates, and extraction using THF was performed and mixed with a custom synthesized MALDI matrix (matrix/sample ratio of 1) developed by the Combariza Research Group.[4,27,29] The MALDI matrix facilitated porphyrin ionization by electron transfer reactions and is known as α-cyanophenylenevinylene (α-CNPV-CH3).

LA-ICP-MS. Element-specific analyses of the developed HPTLC plates were carried out by LA-ICP-MS using a New Wave Research UP-213 Nd:YAG laser (ESI, Fremont, CA) coupled with ICP-MS (7700 series, Agilent, Santa Clara, CA)[24] under the operating conditions given in Table 1. The instrument was equipped with a Fassel-type quartz torch shielded with a grounded Pt electrode and a quartz bonnet; a standard quartz injector (1.75 mm i.d.) was used. An ablation chamber was installed on a three-axis translation stage and coupled to the ICP torch using a 60 cm Tygon tube (5.0 mm i.d.). The ablated material was swept by the carrier gas (helium) and mixed with the spectrometer makeup gas (argon) prior to introduction into the plasma. Ni sampler (orifice diameter: 1.1 mm) and skimmer (orifice diameter: 0.8 mm) cones were optimized for the analyses.[24] The laser beam followed a linear trajectory throughout the migration. To fit within the ablation cell, plates were cut to dimensions of 9 × 10 cm^2. Each sample on the three different plates was analyzed in triplicate.

Table 1. LA-ICP MS Operating Parameters

Agilent 7700 Series ICP MS	
plasma Ar gas flow rate (L min^{-1})	15
auxiliary Ar gas flow rate (L min^{-1})	1
measured isotope	^{13}C, ^{32}S, ^{51}V, ^{58}Ni, ^{60}Ni
analysis time (s)	506
New Wave Research UP-213 LA	
wavelength (nm)	213
fluence (J cm^{-2})	0.85
spot size (μm)	200
scan speed (μ ms^{-1})	100
carrier He gas flow rate (L min^{-1})	0.8

MALDI FT-ICR MS. A hybrid quadrupole FT-ICR instrument (SolariXR, Bruker Daltonics, Bremen, Germany) equipped with a 12 T superconducting magnet was equipped with an LDI/MALDI source with a Nd:YAG × 3 solid-state laser (355 nm).[30] Broadband mass spectra were acquired over a mass range of m/z 147−1000 with an accumulation of 200 scans. The signal was digitalized with 8 M points, resulting in a transient length of 3.4 s; this gave a resolving power number of 0.9×10^6 at m/z 400. Instrument control and data acquisition were facilitated by DataAnalysis (ver. 4.4); OriginPro (ver. 2016) was used to process and visualize the data. From the molecular formulas determined from the accurate mass measurements (typically <0.2 ppm), double bond equivalent (DBE) values were calculated as shown in eq 1 (c, carbon number; h, hydrogen number; n, nitrogen number).[31]

$$\mathrm{DBE} = c - \frac{h}{2} + \frac{n}{2} + 1 \quad (1)$$

RESULTS

HPTLC Results. Four asphaltene samples, the whole Petrophase 2017 asphaltene sample (A2017) and its three extrography fractions (acetone, Hep/Tol, and Tol/THF/MeOH), were separated via HPTLC and analyzed with a UV densitometer. UV analysis at 280 nm of the developed HPTLC plates (Figure 2 A) demonstrates that the samples were separated into two major fractions, eluted and non-eluted. Figure 2 B features the complete UV spectra for the eluted and non-eluted fractions. The results demonstrate that all non-eluted fractions have a similar spectrum, in which the absorbance reaches a maximum at ∼240 nm and then decreases continuously until ∼800 nm. However, the eluted HPTLC fractions present different trends. For instance, the Tol/THF/MeOH extrography fraction features an absorption spectrum with a weaker signal between 400 and 600 nm than those of the other fractions. Eluted species from whole PetroPhase 2017 and its Hep/Tol extrography fraction present similar absorption spectra. Finally, the acetone extrography fraction shows the Soret band (∼420 nm, indicated with a star), which is characteristic of porphyrins.

Table 2 shows the results for average quantification for the three developed HPTLC plates. Combined with the data shown in Figure 2, the results indicate that only ∼9% of the Tol/THF/MeOH extrography fraction migrates up to the solvent front. For the acetone fraction, there is 53% migration. Whole asphaltenes and their Hep/Tol fraction present a similar migration of 28% and 23%, respectively. The results suggest that species in the acetone fraction are less prone to strong adsorption issues on polar surfaces such as cellulose.

Trends of Elemental Composition as a Function of Migration. HPTLC plates were analyzed by LA-ICP-MS to quantify vanadium in the eluted/non-eluted fractions. The results are presented in Figure 3 and Figure S1 and are summarized in Table 3; the results corroborate compositional similarities between whole PetroPhase 2017 asphaltenes and its Hep/Tol extrography fraction (panels A and C). For both samples, ^{51}V is present at the deposition point (non-eluted fraction) and the solvent front (eluted species). Regarding the acetone fraction, Figure 3 B demonstrates that all vanadium-containing compounds migrated with the solvent front. Conversely, the Tol/THF/MeOH fraction revealed vanadium compounds that remained in the non-eluted HPTLC fraction. The quantitative results shown in Table 3 demonstrate that

https://dx.doi.org/10.1021/acs.energyfuels.0c02525
Energy Fuels 2020, 34, 12449−12456

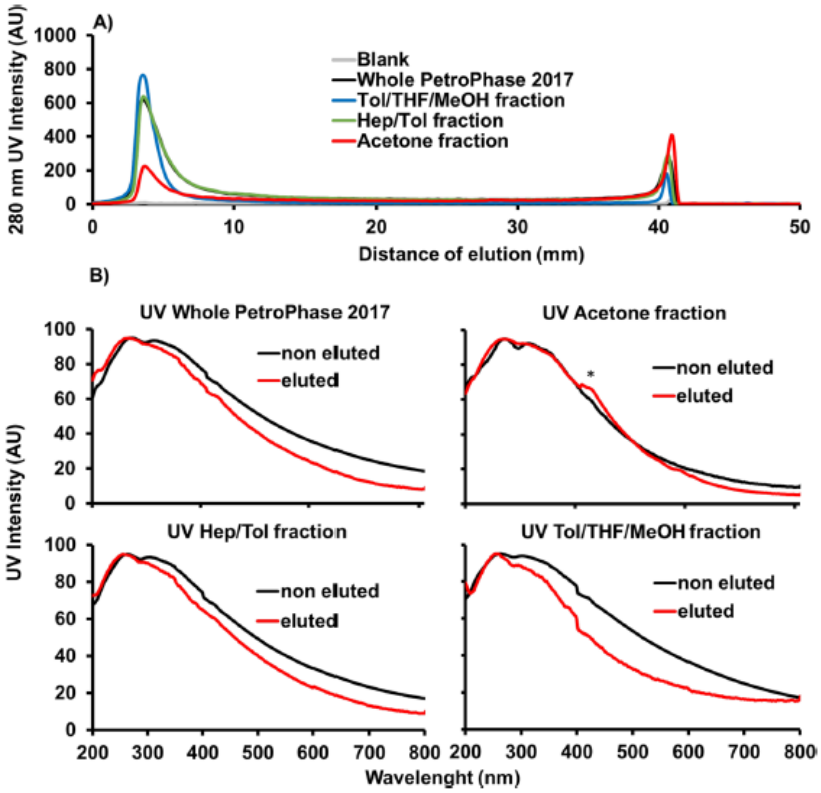

Figure 2. UV chromatograms at 280 nm (A) and UV spectra (D) and chromatograms (B) obtained by HPTLC-UV at 280 nm for all four samples and a blank.

Table 2. Results for UV Analysis at 280 nm for All Four Samples with the Average Intensity for a Total of Six Replicates and the RSD

area 280 nm	area at non-eluted point	area at eluted point	RSD at non-eluted point (%)	RSD at eluted point (%)
whole PetroPhase 2017	19000 (72%)	8000 (28%)	11.1	23.4
Tol/THF/MeOH fraction	15000 (91.2%)	1000 (8.8%)	7.4	16.9
Hep/Tol fraction	19000 (76.9%)	6000 (23.1%)	6.6	19.8
acetone fraction	6000 (47%)	8000 (53%)	6.6	20.7

~100% of ^{51}V-containing compounds (~20000 cps) in the acetone fraction migrated to the solvent front, whereas 100% of vanadium species in the Tol/THF/MeOH (~30000 cps) fraction remained non-eluted.

Molecular-Level Characterization by FT-ICR MS. MALDI FT-ICR MS characterization was facilitated by the use of a novel matrix designed to favor electron transfer reactions for the efficient ionization of metal complexes, such as vanadyl porphyrins.[4,27] This MALDI matrix is a phenylenevinylene derivative that allows for greater ion abundances of porphyrin-like molecules and limits the ionization of other compounds, such as alkyl-substituted PAHs, which are also present in asphaltenes. MALDI FT-ICR spectra were collected for all samples at the deposition point (non-eluted fraction) and the solvent front (eluted fraction). Molecular formulas were assigned to the mass spectral peaks and sorted by heteroatom class (e.g., $N_4O_1V_1$ or vanadyl porphyrins), carbon number, and double bond equivalents (DBE = number of rings plus double bonds). At the sample deposition point (non-eluted fraction), porphyrins were not detected in the whole asphaltene sample or in all extrography fractions. Thus, at the deposition point, vanadium-containing compounds detected by LA-ICP-MS were not ionized (as monomers) by MALDI, even when a specific matrix designed to enhance the ionization of vanadyl porphyrins was utilized. The results highlight the limitations of mass spectrometry to access the complete molecular composition of one of the most complex/challenging samples, the asphaltenes.

Figure 4 presents isoabundance color-contoured plots of DBE versus carbon number for vanadyl porphyrins ($N_4O_1V_1$ class) and heteroatom-substituted counterparts ($N_4O_2V_1$ and $N_4O_1S_1V_1$ classes) for all eluted HPTLC fractions. In these plots, the color scale represents the relative abundance. For the $N_4O_1V_1$ class (Figure 4 A), the most abundant components (red data points) for all samples present the same carbon number (29/30) and DBE values (18). Molecular formula for DBE for all the samples are presented in Table S1. Thus, the

https://dx.doi.org/10.1021/acs.energyfuels.0c02525
Energy Fuels 2020, 34, 12449−12456

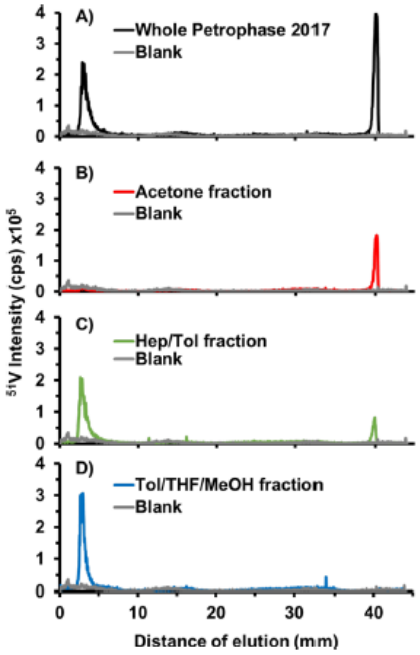

Figure 3. Chromatograms obtained by HPTLC-LA-ICP-MS analysis at *mass* 51 for all four samples and a blank.

Table 3. Results for LA-ICP-MS Analysis at *mass* 51 for All Four Samples with the Average Intensity for a Total of Six Replicates and the RSD

area ^{51}V	area at non-eluted point	area at eluted point	RSD at non-eluted point (%)	RSD at eluted point (%)
whole Petrophase 2017	552000 (78.9%)	148000 (21.1%)	11.4	9.8
Tol/THF/MeOH fraction	667000 (100%)	0 (0%)	6.3	0.0
Hep/Tol fraction	500000 (95.8%)	22000 (4.2%)	2.3	31.9
acetone fraction	0 (0%)	143000 (100%)	0.0	4.1

results suggest that the PetroPhase 2017 asphaltene sample contains abundant DPEP-type porphyrins.

For the whole PetroPhase 2017 asphaltene sample, 146 molecular formulas were found; the most abundant compounds feature DBE values of 17 and 18, which indicates the dominance of Etio and DPEP porphyrins. The Hep/Tol and Tol/THF/MeOH extrography fractions only revealed 44 and 7 porphyrins species. Conversely, the acetone fraction featured the highest content of vanadyl porphyrins, as revealed by 254 molecular formulas obtained via mass spectrometry. In Figure 4 B, porphyrins with one additional oxygen atom were found only in whole asphaltenes and the acetone fraction with a 3.3- and 2.2-fold lower relative abundance than the $N_4O_1V_1$ class. Figure 4 C indicates that porphyrins with one sulfur atom, detected only in the acetone fraction, have abundant homologous series with DBE values from 22 to 30 and carbon numbers between 25 and 50. The higher DBE values are consistent with S incorporated as, e.g., thiophene and benzothiophene peripheral groups.

DISCUSSION

In Figure 2 B, the spectra obtained for the non-eluted fractions for all samples are remarkably similar and are characteristic of a complex mixture of polyaromatic compounds. For the eluted HPTLC fractions, the Soret band at 420 nm was evident only in the acetone extrography fraction. As shown by Evdokimov et al.,[15] porphyrins can be "invisible" in UV−vis spectroscopy due to aggregation. Thus, our results suggest that separation by HPTLC allows for the isolation of porphyrins that are not bound in asphaltene aggregates, as already proposed in our previous paper.[32]

For the whole PetroPhase 2017 sample, the results obtained by UV (Figure 2) and laser ablation (Figure 3) are quite similar to our previous results.[32] Indeed, nearly 80% of the vanadium remained at the deposition point (Table 3, LA-ICP-MS analysis). In that work, the Asphaltene 2017 sample was also analyzed by MALDI FT-ICR MS, but no porphyrins were detected at the deposition point. The results suggest that vanadium-containing molecules, such as porphyrins (whole asphaltenes/deposition point), are present but are not easily accessible, likely because of aggregation. These results are consistent with the UV spectroscopy behavior. Putman et al.[33] has reported limitations in MS characterization of asphaltenes due to the low ionization efficiency of specific chromatography fractions. In this work, according to Table 3 and Figure 4 A, approximately 80% of molecules containing vanadium could not be identified via ultrahigh-resolution mass spectrometry. This raises questions about what portion can be analyzed with such techniques even with previous separation steps. Furthermore, in Figure 4 B, porphyrins with one additional oxygen atom were found only in the PetroPhase 2017 sample and the acetone fraction in both cases at the eluted point with a lower relative abundance (3.34 and 2.25 times less). The UV results for the Hep/Tol fraction were quite similar (Figure 2) to those of the whole PetroPhase 2017 sample. However, according to elemental analysis, vanadium was present at a lower concentration at the eluted point (5%) for the Hep/Tol fraction than for the whole PetroPhase 2017 sample (20%). In MALDI-FT-ICR MS, the abundance of porphyrins at the eluted point was lower in the Hep/Tol fraction than in the whole sample. Collectively, the results suggest that the whole PetroPhase 2017 asphaltene sample and the Hep/Tol extrography fraction contained free and aggregate-bound porphyrins.

HPTLC-LA-ICP-MS analysis (Figure 3 D) of the Tol/THF/MeOH extrography fraction indicates that ^{51}V is present only at the deposition point; however, no Soret band was detected by UV−vis spectroscopy (Figure 2 B). For MALDI FT-ICR MS experiments, despite the use of the custom MALDI matrix for selective ionization of metal complexes, no porphyrins were detected at the deposition point. Thus, non-eluted vanadium-containing compounds are not easily accessible and could be trapped into asphaltene aggregates that prevent their detection by UV−vis spectroscopy and as monomers in FT-ICR MS. The eluted fraction (~8.8% in UV) from Tol/THF/MeOH presents a vanadium content below the LA-ICP-MS detection limit. However, it reveals 7 $N_4O_1V_1$ molecular formulas; such compounds could be completely "free" or present on the aggregate surface and therefore

https://dx.doi.org/10.1021/acs.energyfuels.0c02525
Energy Fuels 2020, 34, 12449−12456

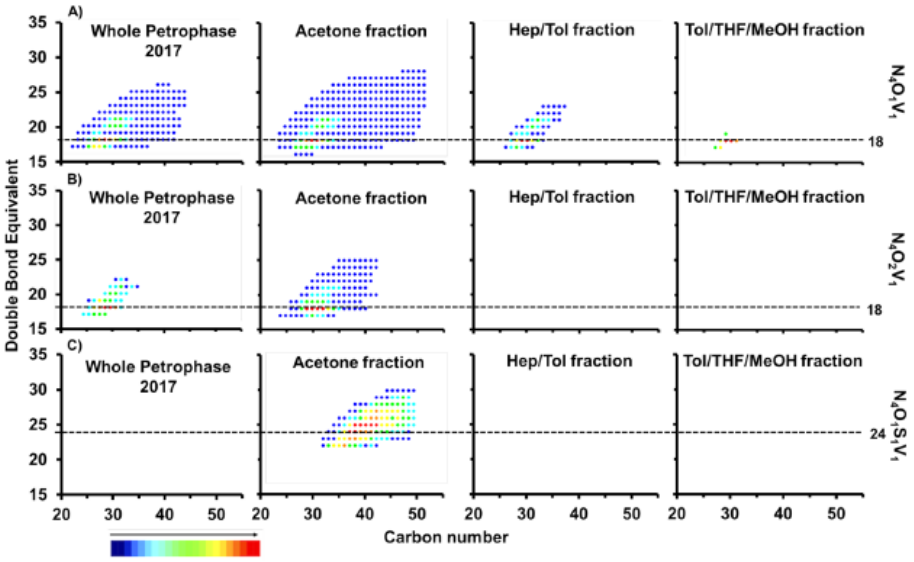

Figure 4. DBE/# maps of $V_1O_1N_4$ (A), $V_1O_2N_4$ (B), and $V_1O_1N_4S_1$ (C) for all four samples by MALDI FT-ICR MS at the eluted point.

available for MS analyses. As reported by Chacon-Patiño,[20] the Tol/THF/MeOH extrography fraction contains abundant multicore motifs (archipelago) and heteroatom-rich compounds. This fraction exhibits stronger aggregation trends and may comprise the most problematic asphaltene species that are likely responsible for demetalation problems in refineries.

Conversely, the acetone fraction presents the highest intensities for the three different types of porphyrins (Figure 4), and the Soret band present in the UV–vis spectrum (Figure 2) at the eluted point suggests a high amount of easily accessible porphyrins. The most abundant molecular formulas have the same carbon number and DBE values as those found for other samples (whole asphaltenes, Hep/Tol, and Tol/THF/MeOH). These results suggest that the easily accessible porphyrins are likely the same compounds in all four samples and were concentrated in the acetone fraction, which exhibits weaker adsorption on polar surfaces (i.e., cellulose) and weaker aggregation tendencies than for the other solvents; therefore, it is likely that porphyrins were not locked into aggregates in this fraction. Furthermore, the UV results in Figure 2 A suggest that a portion of the sample (47%) remained at the deposition point, but no vanadium was found by the elemental LA-ICP-MS and molecular-level FT-ICR-MS analyses. These results suggest that Soxhlet extraction, coupled with HPTLC, allows for the separation of free porphyrins from those that are locked into asphaltene aggregates. The results indicate that the vanadium present in the acetone extrography fraction is easily accessible and constitutes free porphyrins. Chacon-Patiño et al.[5] demonstrated that acetone fractions from geologically diverse asphaltene samples are enriched in single-core or island-type asphaltenes.[20] Therefore, the results indicate that vanadyl porphyrins in the acetone fraction exhibit weak intermolecular interactions with asphaltene aggregates mostly comprised of single-core motifs; HPTLC separation by cellulose plates and DCM solvent can disrupt those interactions. Conversely, vanadyl porphyrins linked to multi-core-type asphaltenes in the Tol/THF/MeOH extrography fraction are strongly linked to the nanoaggregates, which precludes their elution during HPTLC separation.

■ CONCLUSIONS

Our previous works[32] using GPC-HPTLC with LA-ICP-MS suggest that porphyrins that migrate until they reach the solvent front using DCM/MeOH were more accessible as free porphyrins than those that remained at the deposition point. Here, extrography followed by HPTLC separation was used on asphaltene samples. Then, molecular and elemental detection to analyze vanadium and vanadyl porphyrins was successfully used. The combination of molecular and elemental analyses proved that a large quantity of porphyrins remained inaccessible to molecular analyses because of matrix effects and ionization preferences and that these porphyrins are linked to archipelago asphaltenes. The MALDI FT-ICR MS analyses showed that in all the samples, porphyrins that migrate until they reach the solvent front are easier to analyze than those that remain at the deposition point. The acetone fraction showed a great quantity of easily ionizable porphyrins that migrated entirely until they reached the solvent front. These results suggest that there was a high quantity of free porphyrins or porphyrins with weak interactions with the island nanoaggregates in the acetone fraction. In contrast, the Tol/THF/MeOH fraction, which contains a great quantity of vanadium, remains at the deposition point and gives almost no signal by MALDI-FT-ICR MS, which proves the strong interaction between porphyrins and archipelago-type nanoaggregates or an effective occlusion of the porphyrins into the nanoaggregates. These results suggest that when ultrahigh-resolution mass spectrometry is used on asphaltene samples, even after previously using a separation step, only a part of the molecular complex structure can be revealed. Further works should concentrate on the non-eluted part of the Hep/Tol and Tol/THF/MeOH fractions to determine the kinds of porphyrins present and their links with the asphaltene matrices.

https://dx.doi.org/10.1021/acs.energyfuels.0c02525
Energy Fuels 2020, 34, 12449−12456

■ ASSOCIATED CONTENT

Supporting Information

The Supporting Information is available free of charge at https://pubs.acs.org/doi/10.1021/acs.energyfuels.0c02525.

(Figure S1) Six point calibration with vanadyl porphyrins after HPTLC separation and concentration obtained for the four samples by HPTLC-LA-ICP-MS; (Table S1) molecular formula, mass error, and signal-to-noise ratio for all the vanadyl porphyrins signal at DBE 18 for all four samples (PDF)

■ AUTHOR INFORMATION

Corresponding Authors

Caroline Barrère-Mangote − *TOTAL Refining and Chemicals, Total Research and Technologies Gonfreville, BP 27, 76700 Harfleur, France; International Joint Laboratory - iC2MC, Complex Matrices Molecular Characterization, TRTG, BP 27, 76700 Harfleur, France*; Phone: +33 (0) 235 551 102; Email: caroline.mangote@total.com

Brice Bouyssiere − *Universite de Pau et des Pays de l'Adour, E2S UPPA, CNRS, IPREM, Institut des Sciences Analytiques et de Physico-chimie pour l'Environnement et les Materiaux, UMR5254, Helioparc 64053, Pau, France; International Joint Laboratory - iC2MC, Complex Matrices Molecular Characterization, TRTG, BP 27, 76700 Harfleur, France*; orcid.org/0000-0001-5878-6067; Phone: +33 (0) 559 407 752; Email: brice.bouyssiere@univ-pau.fr

Authors

Rémi Moulian − *Universite de Pau et des Pays de l'Adour, E2S UPPA, CNRS, IPREM, Institut des Sciences Analytiques et de Physico-chimie pour l'Environnement et les Materiaux, UMR5254, Helioparc 64053, Pau, France; TOTAL Refining and Chemicals, Total Research and Technologies Gonfreville, BP 27, 76700 Harfleur, France; International Joint Laboratory - iC2MC, Complex Matrices Molecular Characterization, TRTG, BP 27, 76700 Harfleur, France*

Martha Chacón-Patiño − *International Joint Laboratory - iC2MC, Complex Matrices Molecular Characterization, TRTG, BP 27, 76700 Harfleur, France; National High Magnetic Field Laboratory, Florida State University, Tallahassee, Florida 32310, United States*; orcid.org/0000-0002-7273-5343

Oscar Lacroix-Andrivet − *International Joint Laboratory - iC2MC, Complex Matrices Molecular Characterization, TRTG, BP 27, 76700 Harfleur, France; Normandie Université, COBRA, UMR 6014 et FR 3038, Université de Rouen, INSA de Rouen, CNRS, IRCOF, 76136 Mont Saint Aignan Cedex, France; TOTAL Marketing Services, Research Center, 69360 Solaize, France*

Sandra Mounicou − *Universite de Pau et des Pays de l'Adour, E2S UPPA, CNRS, IPREM, Institut des Sciences Analytiques et de Physico-chimie pour l'Environnement et les Materiaux, UMR5254, Helioparc 64053, Pau, France; International Joint Laboratory - iC2MC, Complex Matrices Molecular Characterization, TRTG, BP 27, 76700 Harfleur, France*

Anna Luiza Mendes Siqueira − *International Joint Laboratory - iC2MC, Complex Matrices Molecular Characterization, TRTG, BP 27, 76700 Harfleur, France; TOTAL Marketing Services, Research Center, 69360 Solaize, France*

Carlos Afonso − *International Joint Laboratory - iC2MC, Complex Matrices Molecular Characterization, TRTG, BP 27, 76700 Harfleur, France; Normandie Université, COBRA, UMR 6014 et FR 3038, Université de Rouen, INSA de Rouen, CNRS, IRCOF, 76136 Mont Saint Aignan Cedex, France*; orcid.org/0000-0002-2406-5664

Ryan Rodgers − *Universite de Pau et des Pays de l'Adour, E2S UPPA, CNRS, IPREM, Institut des Sciences Analytiques et de Physico-chimie pour l'Environnement et les Materiaux, UMR5254, Helioparc 64053, Pau, France; International Joint Laboratory - iC2MC, Complex Matrices Molecular Characterization, TRTG, BP 27, 76700 Harfleur, France; National High Magnetic Field Laboratory and Department of Chemistry and Biochemistry, Florida State University, Tallahassee, Florida 32310, United States; Future Fuels Institute, Tallahassee, Florida 32310-4005, United States*; orcid.org/0000-0003-1302-2850

Pierre Giust − *TOTAL Refining and Chemicals, Total Research and Technologies Gonfreville, BP 27, 76700 Harfleur, France; International Joint Laboratory - iC2MC, Complex Matrices Molecular Characterization, TRTG, BP 27, 76700 Harfleur, France*; orcid.org/0000-0002-9569-3158

Complete contact information is available at: https://pubs.acs.org/10.1021/acs.energyfuels.0c02525

Notes

The authors declare no competing financial interest.

■ ACKNOWLEDGMENTS

The authors would like to thank TOTAL for supplying the oil samples. Work performed at the National High Magnetic Field Laboratory ICR User Facility was supported by the National Science Foundation Division of Chemistry through Cooperative Agreements DMR-1157490 and DMR-1644779 and the state of Florida. This work was also supported by Conseil Régional d'Aquitaine (20071303002PFM) and FEDER (31486/08011464). The authors would like to thank the E.U. for funding via the ERC PRIMCHEM project (636829). This work was supported at the Chimie Organique Bioorganique Réactivité Analyse (COBRA) laboratory by the European Regional Development Fund (ERDF)N°31708, the Région Normandie, and the Laboratoire LabEx SynOrg (ANR-11-LABX-0029). The authors would also like to thank Professor Marianny Y. Combariza, University of Santander-Colombia, for providing the matrix used for MALDI analysis during this work.

■ REFERENCES

(1) Strausz, O. P.; Peng, P.; Murgich, J. About the Colloidal Nature of Asphaltenes and the MW of Covalent Monomeric Units. *Energy Fuels* **2002**, *16* (4), 809−822.

(2) Leyva, C.; Ancheyta, J.; Berrueco, C.; Millán, M. Chemical characterization of asphaltenes from various crude oils. *Fuel Process. Technol.* **2013**, *106*, 734−738.

(3) Pereira, T. M. C.; Vanini, G.; Oliveira, E. C. S.; Cardoso, F. M.R.; Fleming, F. P.; Neto, A. C.; Lacerda, V.; Castro, E. V. R.; Vaz, B. G.; Romao, W. An evaluation of the aromaticity of asphaltenes using atmospheric pressure photoionization Fourier transform ion cyclotron resonance mass spectrometry − APPI(±)FT-ICR MS. *Fuel* **2014**, *118*, 348−357.

(4) Ramírez-Pradilla, J. S.; Blanco-Tirado, C.; Hubert-Roux, M.; Giusti, P.; Afonso, C.; Combariza, M. Y. Comprehensive Petroporphyrin Identification in Crude Oils Using Highly Selective Electron Transfer Reactions in MALDI-FTICR-MS. *Energy Fuels* **2019**, 33, 3899.

(5) Chacón-Patiño, M. L.; Rowland, S. M.; Rodgers, R. P. Advances in Asphaltene Petroleomics. Part 3. Dominance of Island or

Archipelago Structural Motif Is Sample Dependent. *Energy Fuels* **2018**, *32* (9), 9106−9120.
(6) Ghislain, T.; Molnárné Guricza, L.; Schrader, W. Characterization of crude oil asphaltenes by coupling size-exclusion chromatography directly to an ultrahigh-resolution mass spectrometer: Characterization of crude oil asphaltenes. *Rapid Commun. Mass Spectrom.* **2017**, *31* (6), 495−502.
(7) McKenna, A. M.; Marshall, A. G.; Rodgers, R. P. Heavy Petroleum Composition. 4. Asphaltene Compositional Space. *Energy Fuels* **2013**, *27* (3), 1257−1267.
(8) Yarranton, H. W.; Ortiz, D. P.; Barrera, D. M.; Baydak, E. N.; Barre, L.; Frot, D.; Eyssautier, J.; Zeng, H.; Xu, Z.; Dechaine, G.; Becerra, M.; Shaw, J. M.; McKenna, A. M.; Mapolelo, M. M.; Bohne, C.; Yang, Z.; Oake, J. On the Size Distribution of Self-Associated Asphaltenes. *Energy Fuels* **2013**, *27* (9), 5083−5106.
(9) Gray, M. R.; Tykwinski, R. R.; Stryker, J. M.; Tan, X. Supramolecular Assembly Model for Aggregation of Petroleum Asphaltenes. *Energy Fuels* **2011**, *25* (7), 3125−3134.
(10) Borisova, Y. Y.; Tazeeva, E. G.; Mironov, N. A.; Borisov, D. N.; Yakubova, S. G.; Abilova, G. R.; Sinyashin, K. O.; Yakubov, M. R. Role of Vanadylporphyrins in the Flocculation and Sedimentation of Asphaltenes of Heavy Oils with High Vanadium Content. *Energy Fuels* **2017**, *31* (12), 13382−13391.
(11) Santos Silva, H.; Sodero, A. C. R.; Korb, J.-P.; Alfarra, A.; Giusti, P.; Vallverdu, G.; Begue, D.; Baraille, I.; Bouyssiere, B. The role of metalloporphyrins on the physical-chemical properties of petroleum fluids. *Fuel* **2017**, *188*, 374−381.
(12) Freeman, D. H.; Saint Martin, D. C.; Boreham, C. J. Identification of metalloporphyrins by third-derivative UV/VIS diode array spectroscopy. *Energy Fuels* **1993**, *7* (2), 194−199.
(13) Filby, R. H.; Van Berkel, G. J. Geochemistry of Metal Complexes in Petroleum, Source Rocks, and Coals: An Overview. *Metal Complexes in Fossil Fuels* **1987**, *344*, 2−39.
(14) Lash, T. D. Geochemical origins of sedimentary benzoporphyrins and tetrahydrobenzoporphyrins. *Energy Fuels* **1993**, *7* (2), 166−171.
(15) Evdokimov, I. N.; Eliseev, N. Yu.; Akhmetov, B. R. Assembly of asphaltene molecular aggregates as studied by near-UV/visible spectroscopy. *J. Pet. Sci. Eng.* **2003**, *37* (3−4), 135−143.
(16) Evdokimov, I. N.; Fesan, A. A.; Losev, A. P. Occlusion of Foreign Molecules in Primary Asphaltene Aggregates from Near-UV−Visible Absorption Studies. *Energy Fuels* **2017**, *31* (2), 1370−1375.
(17) Chacón-Patiño, M. L.; Blanco-Tirado, C.; Orrego-Ruiz, J. A.; Gómez-Escudero, A.; Combariza, M. Y. High Resolution Mass Spectrometric View of Asphaltene−SiO_2 Interactions. *Energy Fuels* **2015**, *29* (3), 1323−1331.
(18) Giraldo-Dávila, D.; Chacón-Patiño, M. L.; McKenna, A. M.; Blanco-Tirado, C.; Combariza, M. Y. Correlations between Molecular Composition and Adsorption, Aggregation, and Emulsifying Behaviors of PetroPhase 2017 Asphaltenes and Their Thin-Layer Chromatography Fractions. *Energy Fuels* **2018**, *32* (3), 2769−2780.
(19) Li, W.; Morgan, T. J.; Herod, A. A.; Kandiyoti, R. Thin-layer chromatography of pitch and a petroleum vacuum residue. *Journal of Chromatography A* **2004**, *1024* (1−2), 227−243.
(20) Chacón-Patiño, M. L.; Rowland, S. M.; Rodgers, R. P. Advances in Asphaltene Petroleomics. Part 2: Selective Separation Method That Reveals Fractions Enriched in Island and Archipelago Structural Motifs by Mass Spectrometry. *Energy Fuels* **2018**, *32* (1), 314−328.
(21) Chacón-Patiño, M. L.; Rowland, S. M.; Rodgers, R. P. Advances in Asphaltene Petroleomics. Part 1: Asphaltenes Are Composed of Abundant Island and Archipelago Structural Motifs. *Energy Fuels* **2017**, *31* (12), 13509−13518.
(22) Chacón-Patiño, M. L.; Rowland, S. M.; Rodgers, R. P. The Compositional and Structural Continuum of Petroleum from Light Distillates to Asphaltenes: The Boduszynski Continuum Theory As Revealed by FT-ICR Mass Spectrometry. *ACS Symp. Ser.* **2018**, *1282*, 113−171.
(23) Günther, D.; Horn, I.; Hattendorf, B. Recent trends and developments in laser ablation-ICP-mass spectrometry. *Fresenius' J. Anal. Chem.* **2000**, *368* (1), 4−14.
(24) Vorapalawut, N.; Martinez Labrador, M.; Pohl, P.; Caetano, M.; Chirinos, J.; Arnaudguilhem, C.; Bouyssiere, B.; Shiowatana, J.; Lobinski, R. Application of TLC and LA ICP SF MS for speciation of S, Ni and V in petroleum samples. *Talanta* **2012**, *97*, 574−578.
(25) Chirinos, J.; Oropeza, D.; González, J.; Ranaudo, M.; Russo, R. E. Determination of Vanadium/Nickel Proportionality in the Asphaltene Fraction of Crude Oil Using Thin-Layer Chromatography with Femtosecond Laser Ablation−Inductively Coupled Plasma−Mass Spectrometry. *Energy Fuels* **2013**, *27* (5), 2431−2436.
(26) Cho, Y.; Witt, M.; Jin, J. M.; Kim, Y. H.; Nho, N.-S.; Kim, S. Evaluation of Laser Desorption Ionization Coupled to Fourier Transform Ion Cyclotron Resonance Mass Spectrometry To Study Metalloporphyrin Complexes. *Energy Fuels* **2014**, *28* (11), 6699−6706.
(27) Ramírez-Pradilla, J. S.; Blanco-Tirado, C.; Combariza, M. Y. Electron-Transfer Ionization of Nanoparticles, Polymers, Porphyrins, and Fullerenes Using Synthetically Tunable α-Cyanophenylenevinylenes as UV MALDI-MS Matrices. *ACS Appl. Mater. Interfaces* **2019**, *11* (11), 10975−10987.
(28) Putman, J. C.; Gutierrez Sama, S.; Barrere-Mangote, C.; Rodgers, R. P.; Lobinski, R.; Marshall, A. G.; Bouyssiere, B.; Giusti, P. Analysis of Petroleum Products by Gel Permeation Chromatography Coupled Online with Inductively Coupled Plasma Mass Spectrometry and Offline with Fourier Transform Ion Cyclotron Resonance Mass Spectrometry. *Energy Fuels* **2018**, *32*, 12198.
(29) Giraldo-Dávila, D.; Chacón-Patiño, M. L.; Ramirez-Pradilla, J. S.; Blanco-Tirado, C.; Combariza, M. Y. Selective ionization by electron-transfer MALDI-MS of vanadyl porphyrins from crude oils. *Fuel* **2018**, *226*, 103−111.
(30) Lacroix-Andrivet, O.; Hubert-Roux, M.; Mendes Siqueira, A. L.; Bai, Y.; Afonso, C. Comparison of Silica and Cellulose Stationary Phases to Analyze Bitumen by High-Performance Thin-Layer Chromatography Coupled to Laser Desorption Ionization Fourier Transform Ion Cyclotron Resonance Mass Spectrometry. *Energy Fuels* **2020**, *34*, 9296.
(31) Kim, S.; Kramer, R. W.; Hatcher, P. G. Graphical Method for Analysis of Ultrahigh-Resolution Broadband Mass Spectra of Natural Organic Matter, the Van Krevelen Diagram. *Anal. Chem.* **2003**, *75* (20), 5336−5344.
(32) Moulian, R.; Sama, S. G.; Garnier, C.; Mounicou, S.; Enrico, M.; Jaurand, X.; Lobinski, R.; Giusti, P.; Bouyssiere, B.; Barrere-Mangote, C. Speciation of Metals in Asphaltenes by High-Performance Thin-Layer Chromatography and Laser Ablation Inductively Coupled Plasma-Mass Spectrometry. *Energy Fuels* **2019**, *33* (7), 6060−6068.
(33) Putman, J. C.; Moulian, R.; Barrere-Mangote, C.; Rodgers, R. P.; Bouyssiere, B.; Giusti, P.; Marshall, A. G. Probing Aggregation Tendencies in Asphaltenes by Gel Permeation Chromatography. Part 1: Online Inductively Coupled Plasma Mass Spectrometry and Offline Fourier Transform Ion Cyclotron Resonance Mass Spectrometry. *Energy Fuels* **2020**, *34*, 8308.

https://dx.doi.org/10.1021/acs.energyfuels.0c02525
Energy Fuels 2020, 34, 12449−12456

Comme attendu le vanadium présent dans la fraction Tol/THF/MeOH migre peu par HPTLC et au contraire celui présent dans la fraction Acétone migre en grande partie. De plus de nombreuses porphyrines ont été identifiées majoritairement sur la fraction acétone mais sur les deux autres fractions aussi. Cependant toutes les porphyrines identifiées l'ont été au front de solvant.

Malgré le fait que la majorité du Vanadium (sur l'ensemble des fractions) reste au point de dépôt, aucune porphyrine n'a pu y être identifiée. Ces résultats soutiennent la théorie que les porphyrines présentent au point d'application sont plus difficilement accessibles. Cette séparation par HPTLC a été faite sur un seul échantillon d'asphaltène (ici A2017), maintenant il serait intéressant de faire de même sur plusieurs échantillons d'asphaltène provenant de plusieurs pétroles différents avec des comportements différents en HDM. La suite de la recherche sur les porphyrines de vanadium dans les asphaltènes devrait se concentrer sur ces porphyrines difficilement accessibles.

As expected the vanadium present in the Tol/THF/MeOH fraction migrates little by HPTLC and on the contrary the vanadium present in the Acetone fraction migrates largely. In addition many porphyrins have been identified mainly on the Acetone fraction but on the other two fractions as well. However, all the porphyrins identified were identified on the solvent front.

Despite the fact that the majority of the vanadium (on all fractions) remains at the deposition point, no porphyrins could be identified there. These results support the theory that porphyrins at the point of application are more difficult to access. This separation by HPTLC was done on a single asphaltene sample (here A2017), now it would be interesting to do the same on several asphaltene samples coming from several different oils with different HDM behaviors. Further research on vanadium porphyrins in asphaltenes should focus on those porphyrins which are not easily accessible.

Conclusion chapitre III

Pour conclure ce chapitre, la séparation par HPTLC sur plaque de cellulose dans le cadre de l'analyse quantitative du vanadium présent dans les produits pétroliers a montré être plus efficace (limite de détection inférieure) que sur plaque de silice.

La migration sur plaque de cellulose avec un mélange DCM/MeOH permet d'isoler les porphyrines libres des porphyrines plus difficilement accessibles. De plus la faible consommation d'échantillon de cette technique permet d'utiliser seulement quelques µg d'échantillon déjà fractionné par d'autres techniques (GPC, extrographie).

Enfin l'analyse moléculaire après séparation par HPTLC montre que sur le front de solvant et quel que soit la fraction analysée, des porphyrines similaires ont été retrouvées. Cependant malgré une présence importante de vanadium, aucune porphyrine n'a pu être identifiée sur la partie des fractions qui est restée au point de dépôt des plaques HPTLC. Le vanadium étant très majoritairement contenu dans les porphyrines, ces porphyrines sont certainement présentes au point de dépôt mais non disponible pour l'ionisation. Cela correspondrait à la partie des porphyrines la plus difficile à enlever lors des traitements de dé-métallation.

Tout comme dans le chapitre II présentant le couplage de la GPC et d'un FT-ICR MS, la spectrométrie de masse n'a pas permis une analyse complète d'un échantillon pétrolier déjà séparé par deux techniques de séparation différentes.

Il est dorénavant clair que l'enjeu principal de la suite des travaux est de réussir à fractionner/désagréger les composés se trouvant dans la fraction des hauts poids moléculaire/ fraction Tol/THF/MeOH. La suite des travaux se concentrera sur le vanadium présent dans les porphyrines les plus difficilement accessibles afin de les identifier.

To conclude this chapter, separation by HPTLC on cellulose plate in the quantitative analysis of vanadium in petroleum products has been shown to be more effective (lower limit of detection) than on silica plate.

Migration on cellulose plate with a DCM/MeOH mixture allows isolation of free porphyrins from the more difficult porphyrins. Moreover the low sample consumption of this technique allows to use only a few µg of sample already fractionated by other techniques (GPC, extrography).

Finally the molecular analysis after separation by HPTLC shows that on the solvent front and whatever the fraction analysed, similar porphyrins were found. However, despite a significant presence of vanadium, no porphyrins could be identified on the part of the fractions which remained at the point of deposition of the HPTLC plates. As vanadium is overwhelmingly contained in the porphyrins, these porphyrins are certainly present at the deposition point but not available for ionisation. This would correspond to the most difficult part of the porphyrins to remove during de-metallation treatments.

As in Chapter II presenting the coupling of the GPC and an FT-ICR MS, mass spectrometry did not allow a complete analysis of a petroleum sample already separated by two different separation techniques.

It is now clear that the main challenge for further work is to successfully fractionate/disaggregate the compounds in the high molecular weight/Tol/THF/MeOH fraction. Further work will focus on the vanadium present in the most difficult porphyrins in order to identify them.

Chapitre IV : Développement d'une méthode de désagrégation par dopage en argent

Dans le chapitre II et III de cette thèse, des couplages entre techniques de séparation GPC et HPTLC avec une séparation par extrographie couplés avec des techniques d'analyse de masses ont été présentés. Cependant une partie des porphyrines de vanadium des asphaltènes reste invisible à la spectrométrie de masse à cause de l'agrégation.

Dans ce chapitre IV le but est de désagréger les agrégats de hauts poids moléculaires pour enfin avoir accès aux porphyrines de vanadium contenues à l'intérieur. Dans ce chapitre, sera présenté une étude menée sur l'effet d'ajout d'argent dans des échantillons pétroliers avant analyse par GPC-ICP MS. En effet, d'après les travaux de Lobodin *et al*[181] le triflate d'argent se complexe notamment avec un certain nombre de composés soufrés sinon inaccessibles. Si une partie des composés difficilement accessible est libérée cela pourrait permettre de les analyser et de les identifier.

Ce chapitre a fait l'objet d'un article publié dans le journal *Energy and Fuels* de l'*American Chemical Society* (ACS). Cet article a été laissé tel qu'il a été publié.

Dans un premier temps, une étude sur la quantité d'agent dopant nécessaire et la cinétique de complexation a été effectuée. Puis un dopage en argent a été effectué sur 5 résidus atmosphérique différents dans le but de mettre en évidence des différences de complexation avec l'argent.

In chapter II and III of this thesis, couplings between GPC and HPTLC separation techniques with extrographic separation coupled with mass analysis techniques were presented. However, some of the vanadium porphyrins in asphaltenes remain invisible to mass spectrometry due to aggregation.

In this chapter IV the aim is to disaggregate the high molecular weight aggregates to gain access to the vanadium porphyrins contained therein. In this chapter a study on the effect of adding silver to petroleum samples prior to analysis by GPC-ICP MS will be presented. Indeed, according to the work of Lobodin et al [181] silver triflate is complexed in particular with a certain number of sulphur compounds if not inaccessible. If a part of the compounds that are difficult to access is released, this could make it possible to analyze and identify them.

This chapter was the subject of an article published to the journal Energy and Fuels of the American Chemical Society (ACS). This article has been left as published.

As a first step, a study on the amount of doping agent required and the complexation kinetics was carried out. Then a silver spiking was performed on 5 different atmospheric residues to demonstrate differences in complexation with silver.

energy&fuels

pubs.acs.org/EF Article

Understanding the Vanadium−Asphaltene Nanoaggregate Link with Silver Triflate Complexation and GPC ICP-MS Analysis

Remi Moulian, Fang Zheng, Germain Salvato Vallverdu, Caroline Barrere-Mangote, Quan Shi, Pierre Giusti, and Brice Bouyssiere*

Cite This: https://dx.doi.org/10.1021/acs.energyfuels.0c02505 Read Online

ACCESS | Metrics & More | Article Recommendations | Supporting Information

ABSTRACT: The effect of silver triflate (AgOTf) on the interaction between vanadium and asphaltene nanoaggregates was investigated by gel permeation chromatography inductively coupled plasma high-resolution mass spectrometry (GPC ICP-HR-MS). The results showed that disaggregation of some vanadium compounds linked to asphaltene nanoaggregates occurred when silver triflate was added. Ag^+ can partially move some porphyrins from the high-molecular-weight (HMW) region to the low-molecular-weight (LMW) region. It was inferred that the interaction between Ag^+ and the porphyrins surroundings led to a decrease in the size of the nanoaggregates (HMW region) and an increase in the "free" V porphyrin compounds (MMW and LMW regions). Asphaltenes from a similar origin, presenting the same vanadium GPC ICP-MS profile, gave different GPC ICP-MS profiles after AgOTf addition, which could be linked to the difference in geochemistry of the samples.

INTRODUCTION

Crude oil is a complex mixture mainly composed of carbon and hydrogen and contains a certain amount of heteroatoms as well as metals.[1] It is well-known that many metals in crude oil exist in the form of metalloporphyrins, which are considered to come from chlorophyll and heme via demetalation, saponification, decarburization, reduction, aromatization, decarboxylation, and metal chelation during long-term geological evolution.[2,3] Metal compounds in crude oil have many negative effects on petroleum refining.[4] Crude oil with a high metal content is liable to cause lead fouling of the furnace tube and catalyst deactivation during the catalytic process.[5] Nickel and vanadium elements are the most abundant metals in crude oils and are present mainly in the form of porphyrins, which are very stable and difficult to remove.

The composition and properties of petroporphyrins have always been one of the most important issues in petrochemistry. Many analytical techniques have been used to characterize the metal compounds in crude oil and its derivatives. Ultraviolet−Visible (UV−vis) spectroscopy is commonly used to identify and quantify petroporphyrins due to its high sensitivity for detecting the electronic absorption of UV−vis radiation of metalloporphyrins.[6] The emergence of mass spectrometry technology has led to new developments in the identification of petroporphyrins.[7−11] However, these techniques are inoperative for the quantitative analysis of metal compounds in heavy oil components, especially in the presence of asphaltenes. This is mainly due to the aggregation between metal compounds and asphaltene molecules, which leads to the formation of metal compounds with high molecular weights (HMWs) or even supramolecules.[12,13] Coupling gel permeation chromatography (GPC) with inductively coupled plasma high-resolution mass spectrometry (ICP-HR-MS) enables the identification of the large sizes associated with the study of metal- and sulfur-containing compounds in heavy fractions of crude oil.[14,15] The distribution of V and Ni in crude oils and residues could be divided into high-, medium-, and low-molecular-weight (HMW, MMW, and LMW) components, and quantitative studies could be performed for further investigation.[14]

The driving forces contributing to aggregations in crude oil include $\pi-\pi$ stacking (electrostatic and/or van der Waals forces),[16] hydrogen bonding,[17] acid−base interactions,[18] and coordination interactions.[19] Recently, Zhang et al. prposed a pancake model for the interpretation of asphaltene aggregation behavior, in which the free radical was considered as a force contribution.[33] However, most of the relevant studies were focused on the analysis of apparent phenomena because of the complexity of the petroleum matrix.[20,21] Aggregation involving petroporphyrins is caused by a variety of forces due to the diversity of their substituents.[22]

Because of these aggregations, the analysis of petroporphyrins is a complex task, as most of the identified compounds are free porphyrins, and all the aggregated compounds are still unknown.

Silver has already been used in molecular mass spectrometry to enhance the ionization of heavy aromatic compounds[23,24] and sulfur-containing species.[25]

In this study, GPC ICP-MS was used to monitor the effect of complexation with silver ions on the nanoaggregation between vanadium and asphaltene. Each of the nitrogen and

Received: July 27, 2020
Revised: October 4, 2020

https://dx.doi.org/10.1021/acs.energyfuels.0c02505
Energy Fuels XXXX, XXX, XXX−XXX

oxygen atoms of the functional groups in asphaltenes has one pair of electrons available for complexation with silver ions. In association with the relatively low energy barrier of nucleus formation, it is probable that silver ions allow for the reduction of aggregation between metal compounds and asphaltene to occur at room temperature.[26,27] Atmospheric residue (AR) represents the relatively heavy fraction with a high concentration of vanadium and nickel that was used as a feed in the hydrodemetalation process. Thus, investigation of five atmospheric residues from different sources was performed, showing that silver triflate, AgOTf, can partially move some porphyrins from the high-molecular-weight region to the low-molecular-weight region.

EXPERIMENTAL SECTION

Chemicals. Tetrahydrofuran (THF), ACS-grade multisolvent GPC, stabilized with 250 ppm butyl butylated hydroxytoluene (BHT) (Scharlau), was used for dilution and as the mobile phase for gel permeation chromatography. Spiking with silver was performed using AgOTf (Sigma-Aldrich).

Samples. Five different atmospheric residues were used: AR1, AR2, and AR3 were from Arabian crude oil, AR4 was from African crude oil, and AR5 was from western European crude oil.

Solutions were prepared in 30 mL vials washed with THF and dried under nitrogen before use. The different atmospheric residues were diluted 50 times in THF. To study the effect of concentration, the addition of 1, 10, 100, and 1000 ppm AgOTf was performed. For the kinetic study, the addition of 1000 ppm AgOTf was performed. For the five different ARs, 100 ppm AgOtf was added.

GPC ICP-HR-MS/UV. The chromatographic system was composed of a Dionex high-performance liquid chromatography (HPLC) system with an UltiMate 3000 microflow pump, an UltiMate 3000 autosampler, a low port-to-port dead-volume microinjection valve, and an Ultimate UV system (following the 420 nm wavelength). Three GPC columns (from 1000 to 600 000 Da) connected in series were used. A Styragel guard column (4.6 mm inner diameter, 30 mm length, 10 000 Da exclusion limit) was used before the columns, and the flow rate was 1 mL·min^{-1} for 90 min. A splitter of 1/20 was used to send only 40 μL·min^{-1} into a double focusing sector field inductively coupled plasma mass spectrometer (Element XR, Thermo Fisher Scientific) ICP-HR-MS. Samples were analyzed as fresh solutions prepared a few hours before injection, except when the kinetic studies were conducted.

The mass spectrometer was fitted with a modified DS-5[28−30] microflow total consumption nebulizer (CETAC) mounted with a laboratory-made, single-pass, jacketed glass spray chamber.[14,31] The chamber was thermostated at 60 °C by water using a temperature-controlled water bath circulator (Neslab RTE-111, Thermo Fisher Scientific). An Ar gas flow was used at 16 L·min^{-1} for the plasma, at 0.9 L·min^{-1} for the auxiliary gas, and at 0.6 L·min^{-1} for the nebulizer gas. An O_2 gas flow was used to avoid carbon deposition at 0.08 L·min^{-1}. The instrument was equipped with a quartz injector (inner diameter: 1.0 mm), Pt sampler (orifice diameter: 1.1 mm), and skimmer (orifice diameter: 0.8 mm) cones. ICP-HR-MS was used to obtain the spectrally interfered isotopes of ^{32}S and ^{51}V. Excel was used for the integration of the chromatographic peaks obtained. Table 1 and Table 2 present the main GPC and ICP-MS parameters.

Table 1. GPC Parameters

GPC parameters	
flow rate	1 mL·min^{-1}
pressure	58 bar
injection volume	20 μL
solvent	THF

Table 2. ICP-HR-MS Parameters

ICP-HR-MS parameters	
auxilary gas flow rate	0.575 L·min^{-1}
O_2 flow rate	0.08 L·min^{-1}
isotopes analyzed	^{32}S, ^{51}V, ^{56}Fe, and ^{109}Ag
acquisition time	90 min

RESULTS AND DISCUSSION

Stability of the GPC ICP-MS Profile during Analysis. This study focused on the effect of the complexing agent AgOTf on the GPC ICP-MS profile. In this case, reproducibility of the GPC ICP-MS chromatogram is an important factor that can impact the interpretation of the results. This reproducibility was already studied by Sama et al.[31] but was performed again to evaluate the method throughout the process. Figure 1 and Table 3 show the ^{51}V and ^{32}S signal reproducibility for three injections of AR-1 during the 2 d analytical sequence. This showed that both the ^{32}S and ^{51}V profiles were the same and that the reproducibility of the method on the total area was better than 95%, proving that, for the rest of the study, a change of more than 5% in the profile could not be attributed to instrument instability.

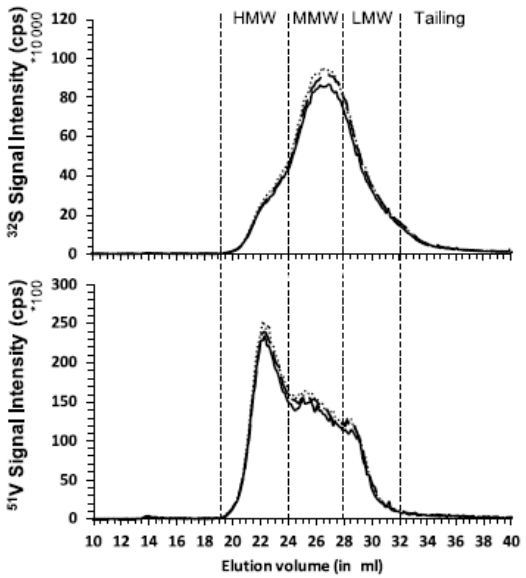

Figure 1. Stability study on ^{32}S and ^{51}V GPC ICP-HR-MS chromatograms of AR-1 samples.

Table 3. Reproducibility of ^{32}S and ^{51}V Analysis after Three Injections of AR-1

	total area	
AR-1 injection	sulfur	vanadium
1	5 929 573	147 137
2	6 107 879	152 612
3	5 562 053	139 584
mean	5 866 501	146 444
SD in %	4.7	4.5

https://dx.doi.org/10.1021/acs.energyfuels.0c02505
Energy Fuels XXXX, XXX, XXX−XXX

Addition of AgOTf in an Atmospheric Residue (AR-1). AgOTf was first added at increasing concentrations (1−1000 ppm) to an atmospheric residue. GPC ICP-MS analyses were performed rapidly after the addition of AgOTf. Table 4 shows

Table 4. Evolution of Total ^{32}S and ^{51}V Peak Areas in the AR-1 Chromatogram during the Addition of AgOTf

	total area	
AgOTf in ppm	sulfur	vanadium
1	5 483 645	137 481
10	5 278 516	132 577
100	5 206 841	126 332
1000	5 103 962	119 271
mean	5 268 241	128 915
SD in %	3.05	6.12

that the addition of AgOTf did not change the total ^{32}S and ^{51}V peak areas in the obtained chromatograms. (As the S added by AgOTf represents less than 0.5% of the total S in the sample, we did not account for this S addition.) This proved that any modification in the S and V profiles was directly linked to the addition of AgOTf.

Figure 2 and Table S1 show the S, V, and Ag chromatograms obtained after the addition of different AgOTf concentrations. Increasing the concentration of AgOTf led to

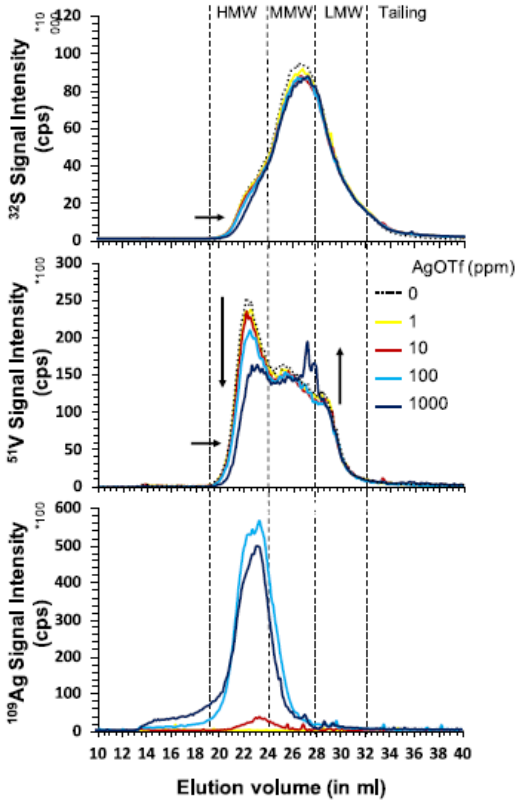

Figure 2. ^{109}Ag, ^{32}S, and ^{51}V GPC ICP-HR-MS chromatograms with increasing concentrations of AgOTf mixed with sample AR-1.

a decrease in the area in the HMW region of the chromatogram with a proportional increase, as the total area was stable during all silver additions, in the MMW region. The last silver addition led to the appearance of a peak on the ^{51}V chromatogram in the MMW/LMW regions.

Concerning the silver signal, a peak, mostly in the HMW region, appeared. A signal was also observed at a very high molecular weight before the HMW region, proving that some very large aggregates were present that cannot be detected due to the lack of sensitivity of the conventional GPC-UV detector. At that retention time, the ^{51}V signal was slightly higher than the background signal but was not counted as a new aggregation fraction.

Influence of Time Reaction of AgOTf Addition to AR-1. ^{32}S and ^{51}V profiles are very similar for these three reaction times, proving that disaggregation for these elements did not change in function of the time. Figure 3 and Table S2 show the

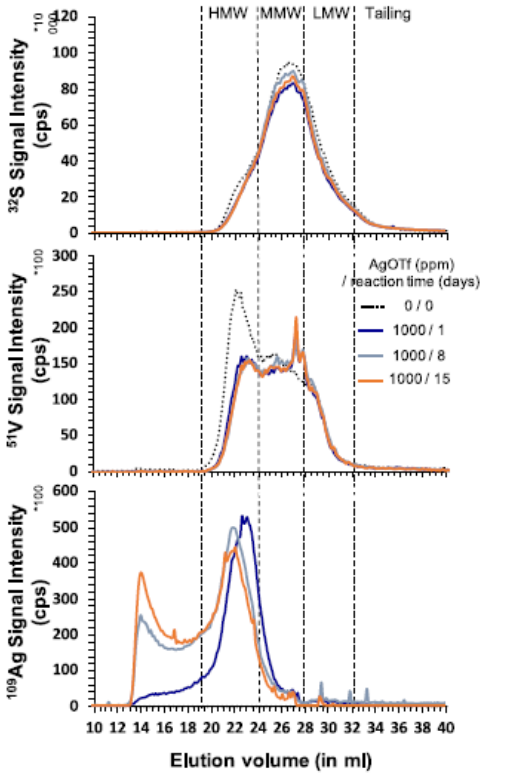

Figure 3. ^{109}Ag, ^{32}S, and ^{51}V GPC ICP-HR-MS chromatograms with 1000 ppm AgOTf mixed with AT-1 samples at different times.

chromatograms for the solution after 1, 8, and 15 d of reaction. The ^{51}V species by AgOTf was not impacted by time. The same results as those of the concentration study were obtained, with a decrease in HMW compounds and an increase in MMW/LMW compounds.

Concerning the Ag profile, a similar chromatogram was obtained to that presented in Figure 2 after a 1 d reaction. For a longer reaction time (8 and 15 d), a strong increase in the very large aggregate region was observed without any modification of the ^{32}S and ^{51}V profiles. Thus, these changes

https://dx.doi.org/10.1021/acs.energyfuels.0c02505
Energy Fuels XXXX, XXX, XXX−XXX

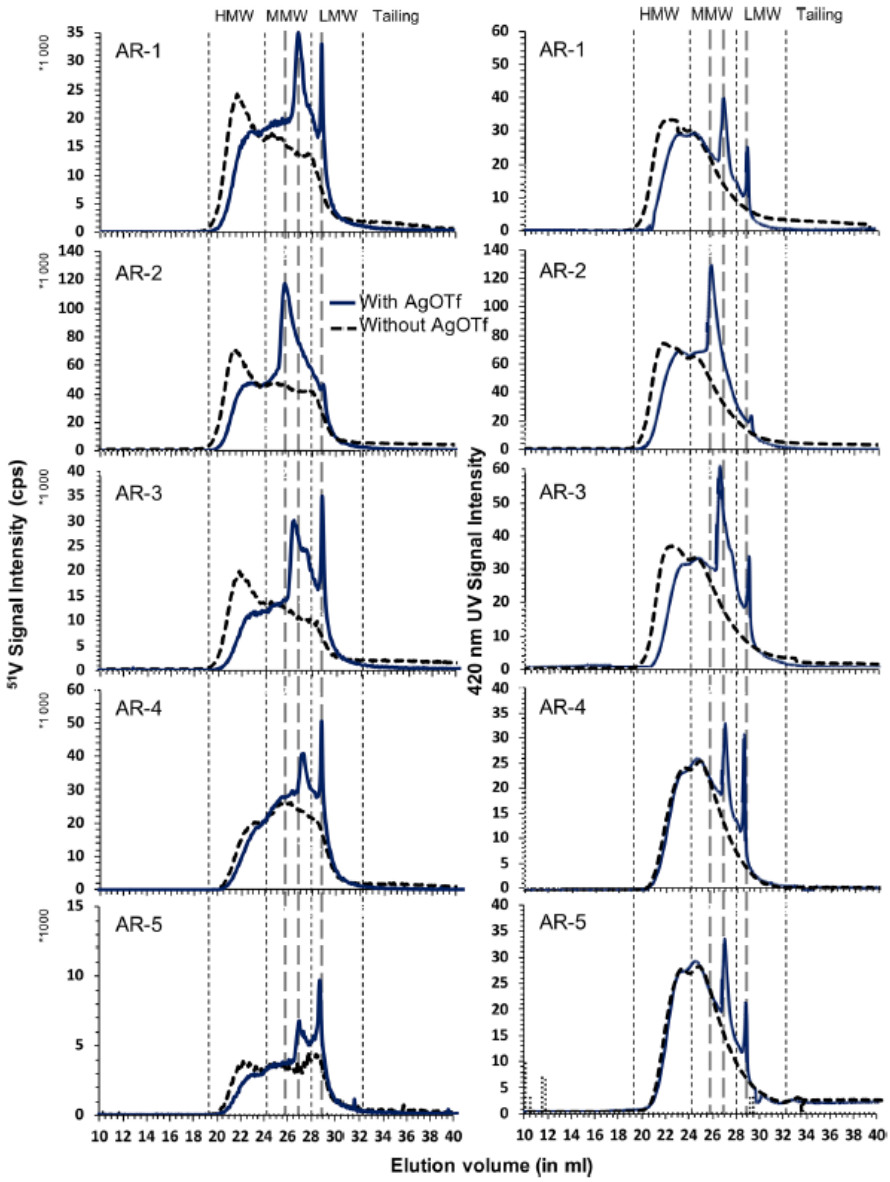

Figure 4. ^{51}V and 420 nm GPC ICP-HR-MS/UV chromatograms of five ARs with and without the addition of AgOTf (at 100 ppm).

in the Ag profile could not be linked to a disaggregation process. As Ag can also react strongly with aromatic compounds,[24] this slow increase in the Ag profile in the very-high-molecular-weight (vHMW) region was linked to the kinetics of the complexation reaction with vHMW aggregates. The molecular complexity of this large aggregate might inhibit interaction with AgOTf, which may be due to the difficulty of accessing $\pi-\pi$ stacking of the aromatic compounds.

After these preliminary studies on the concentration and kinetics of AgOTf complexation, an excess of silver was detected in the GPC column. These results led to contamination by silver in the analysis of samples without silver. Thus, for the rest of the study, we decided to limit the silver addition to 100 ppm and ran all the other analyses with a new set of GPC columns.

Application on Five Different Atmospheric Residues. The developed methodology was applied to five different atmospheric residues. As shown in the vanadium profile in Figure 4, for all five ARs, the addition of AgOTf led to an increase in ^{51}V peaks in the MMW and LMW regions. For the optimization study, the quantitative results (Table 5) proved that the total areas were similar to and without AgOTf addition (3−10% differences between both conditions for the five ARs). These quantitative data also showed a decrease in the percentage of HMW compounds and an increase in those of MMW and LMW compounds. According to the retention

https://dx.doi.org/10.1021/acs.energyfuels.0c02505
Energy Fuels XXXX, XXX, XXX−XXX

Table 5. HMW, MMW, LMW Regions and Percentages of ^{51}V in the Chromatograms of Five AR Samples

sample		HMW area (%)	MMW area (%)	LMW area (%)	tailing area (%)	total area
AR-1	no AgOTf	51 400 (34.6)	53 000 (35.7)	34 400 (23.1)	9800 (6.6)	148 600
	AgOTf	27 470 (17.8)	59 950 (38.9)	63 100 (41.0)	3550 (2.3)	154 070
					diff (%)	3.6
AR-2	no AgOTf	166 690 (35.1)	160 100 (33.8)	115 990 (24.5)	31 530 (6.6)	474 310
	AgOTf	87 750 (17.5)	235 850 (47.0)	168 510 (33.6)	9270 (1.8)	501 380
					diff (%)	5.4
AR-3	no AgOTf	42 340 (33.4)	43 880 (34.6)	28 000 (22.1)	12 700 (10.0)	126 920
	AgOTf	17 525 (12.5)	54 620 (39.0)	63 800 (45.6)	4095 (2.9)	140 040
					diff (%)	9.4
AR-4	no AgOTf	31 670 (16.2)	83 570 (42.7)	66 700 (34.1)	13 770 (7.0)	195 710
	AgOTf	23 825 (11.6)	90 420 (44.0)	88 110 (42.8)	3315 (1.6)	205 670
					diff (%)	4.8
AR-5	no AgOTf	7700 (22.1)	12 300 (35.3)	12 200 (35.0)	2630 (7.6)	34 830
	AgOTf	4540 (12.0)	13 300 (35.1)	18 900 (49.8)	1200 (3.2)	37 940
					diff (%)	8.2

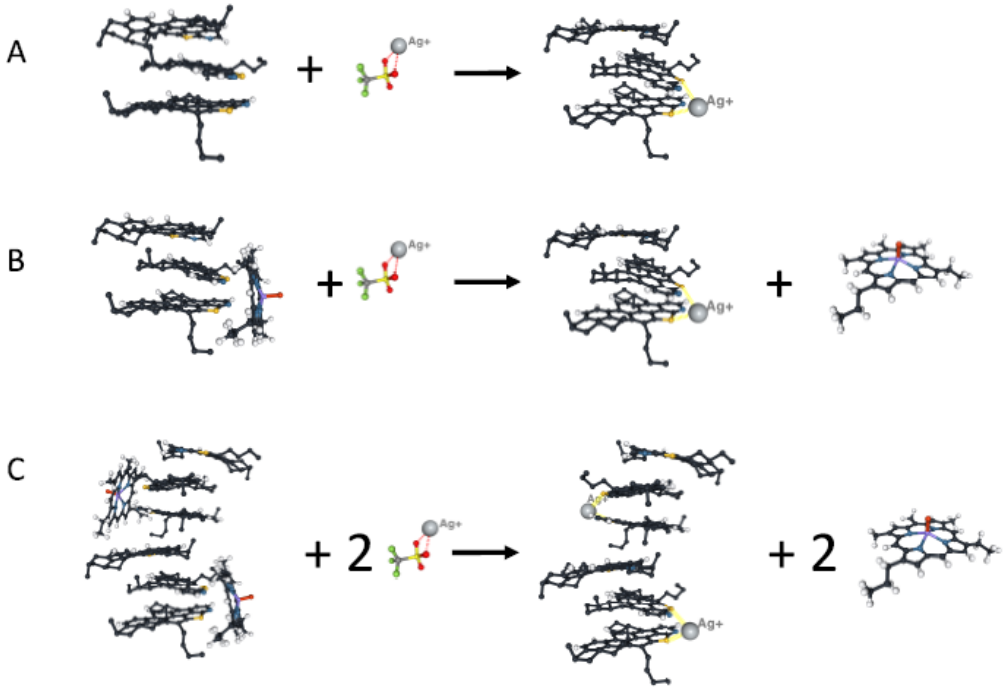

Figure 5. Representation of the possible reactions with AgOTf.

time, we could see that three vanadium peaks appeared (blue line), two in the MMW region and one in the LMW region. According to the UV chromatograms of the same samples (Figure 4, right panel), a peak also appeared on the 420 nm UV chromatogram. The UV 420 nm signal is linked to the Soret adsorption band for porphyrin compounds and to a modification of the background signal from the sample. Thus, the three peaks that appeared after AgOTf addition might be free porphyrins that originated from HMW nanoaggregates.

As presented in Figure 5, AgOTf addition led to different complexation reactions:

- complexation with S species without metal in the molecule and thus without desagregation (Figure 5A).
- complexation with S moieties on the side chain of porphyrin molecules. This reaction was not observed in our experiment, as no Ag was linked to the V signal (Figures 2 and 3).
- substitution of one or two porphyrin molecules by Ag on small aggregates (Figure 5B) or large aggregates (Figure 5C).

In Figure 4, there is a shift in the right side of the chromatogram in the HMW region for all AR samples (black dotted line vs the solid blue line). This shift may be attributed

https://dx.doi.org/10.1021/acs.energyfuels.0c02505
Energy Fuels XXXX, XXX, XXX−XXX

to the interaction with AgOTf, which led to a decrease of the size of the aggregates. Our hypothesis is that silver takes the place of some porphyrins on the surrounding nanoaggregates (Figure 5B,C), leading to a decrease in the size of the nanoaggregates (which can be seen in the HMW region of the chromatogram) and an increase of "free" V porphyrin compounds (which can be seen by the appearance of peaks in the MMW and LMW regions). The same results can be observed for iron and nickel (Figure S1). On a quantification point of view, Table 5 confirms that ^{51}V in the HMW region of the chromatogram decreased in all AR samples, and that in the LMW region increased, with a similar total ^{51}V area in all chromatograms. These results confirm that there was disaggregation of vanadium molecules due to AgOTf addition in the samples.

Concerning the sulfur species, Figure S1 also shows a shift of peaks in the HMW region to the right and a small increase in the peaks in the MMW region for AR-1, AR-2, and AR-3, proving that some small S species were also surrounding the nanoaggregates.

Comparison of Three Samples from the Same Region. AR-1, AR-2, and AR-3 were three atmospheric residues of the same origin (Arabian heavy crude oil) with different amounts of vanadium. According to the normalized vanadium chromatograms in Figure 6, obtained without the addition of AgOTf, the three ARs had similar profiles. It was previously published that the GPC profile can be linked to the origin of a crude oil.[32] Despite the fact that these three ARs are from a similar origin with a similar ^{51}V GPC ICP-MS profile, the addition of AgOTf led to three different profiles. AR-1 and AR-3 had the same low-molecular-weight peak, and the three ARs had three different peaks in the MMW region in terms of retention time. Thus, the addition of AgOTf in atmospheric residues of similar origin presenting similar GPC ICP-MS profiles can lead to some important differences in terms of porphyrin release by nanoaggregates. Despite a similar origin and a similar overall GPC profile, this method can be used to show sample differences from a geological point of view.

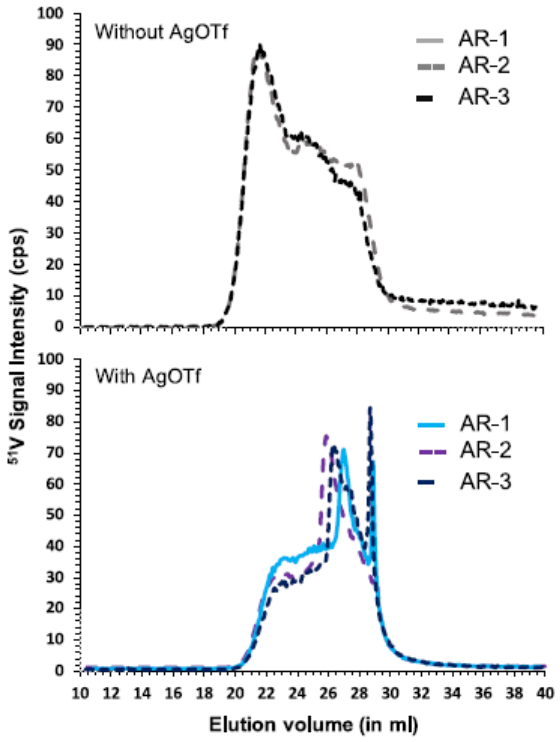

Figure 6. Normalized ^{51}V GPC ICP-HR-MS chromatograms of AR-1, AR-2, and AR-3 with and without the addition of AgOTf (at 100 ppm).

CONCLUSION

The addition of a complexing agent, AgOTF, followed by GPC ICP-MS analysis revealed that some of the vanadium was linked to aggregated molecules. GPC proved that the hydrodynamic volume of the aggregates decreased after the release of vanadium (and Ni or Fe) compounds but was still at a high-molecular-weight retention time. Depending on the atmospheric residue, this loose hydrodynamic volume was different, proving that more than one vanadium molecule can be chelated to these aggregates.

For atmospheric residues with a similar origin, the addition of AgOTF can, for similar original GPC profiles, yield different profiles, showing that different families (and sizes) of vanadium molecules are aggregated around HMW nanoaggregates, which could be linked to the history of the product.

ASSOCIATED CONTENT

Supporting Information

The Supporting Information is available free of charge at https://pubs.acs.org/doi/10.1021/acs.energyfuels.0c02505.

^{32}S, ^{56}Fe, and ^{60}Ni GPC ICP HR MS chromatograms of five AT with and without AgOTf (at 100 ppm). Evolution of ^{32}S, ^{51}V, and ^{109}Ag peak areas in the AR-1 chromatogram during the addition of AgOTf. Evolution of ^{32}S, ^{51}V, and ^{109}Ag peak areas in the AR-1 chromatogram in function of time (PDF)

AUTHOR INFORMATION

Corresponding Author

Brice Bouyssiere − *E2S UPPA, CNRS, IPREM, Institut des 843 Sciences Analytiques et de Physico-chimie pour l'Environnement et les Materiaux, UMR5254, Helioparc, Universite de Pau et des Pays de l'Adour, 64053 Pau, France; International Joint Laboratory C2MC: Complex Matrices Molecular Characterization, Total Research & Technology, Harfleur F-76700, France;* orcid.org/0000-0001-5878-6067; Phone: +33 (0) 559 407 752; Email: brice.bouyssiere@univ-pau.fr

Authors

Remi Moulian − *E2S UPPA, CNRS, IPREM, Institut des 843 Sciences Analytiques et de Physico-chimie pour l'Environnement et les Materiaux, UMR5254, Hélioparc, Universite de Pau et des Pays de l'Adour, 64053 Pau, France; International Joint Laboratory C2MC: Complex Matrices Molecular Characterization and , Total Research & Technology, Harfleur F-76700, France*

Fang Zheng − *E2S UPPA, CNRS, IPREM, Institut des 843 Sciences Analytiques et de Physico-chimie pour l'Environnement et les Materiaux, UMR5254, Hélioparc, Universite de Pau et des Pays de l'Adour, 64053 Pau, France; International Joint*

https://dx.doi.org/10.1021/acs.energyfuels.0c02505
Energy Fuels XXXX, XXX, XXX−XXX

Laboratory C2MC: Complex Matrices Molecular Characterization, Total Research & Technology, Harfleur F-76700, France; State Key Laboratory of Heavy Oil Processing, China University of Petroleum, Beijing 102249, China

Germain Salvato Vallverdu − *E2S UPPA, CNRS, IPREM, Institut des 843 Sciences Analytiques et de Physico-chimie pour l'Environnement et les Materiaux, UMR5254, Helioparc, Universite de Pau et des Pays de l'Adour, 64053 Pau, France; International Joint Laboratory C2MC: Complex Matrices Molecular Characterization, Total Research & Technology, Harfleur F-76700, France;* orcid.org/0000-0003-1116-8776

Caroline Barrere-Mangote − *International Joint Laboratory C2MC: Complex Matrices Molecular Characterization and , Total Research & Technology, Harfleur F-76700, France*

Quan Shi − *State Key Laboratory of Heavy Oil Processing, China University of Petroleum, Beijing 102249, China;* orcid.org/0000-0002-1363-1237

Pierre Giusti − *International Joint Laboratory C2MC: Complex Matrices Molecular Characterization and , Total Research & Technology, Harfleur F-76700, France;* orcid.org/0000-0002-9569-3158

Complete contact information is available at: https://pubs.acs.org/10.1021/acs.energyfuels.0c02505

Notes

The authors declare no competing financial interest.

■ ACKNOWLEDGMENTS

This work was supported by Conseil Régional d'Aquitaine (20071303002PFM) and FEDER (31486/08011464).

■ REFERENCES

(1) Liang, W. *Petroleum Chemistry;* China University of Petroleum Press: Beijing, China, 2009.

(2) Treibs, A. Chlorophyll- und Häminderivate in Bituminösen Gesteinen, Erdölen, Erdwachsen und Asphalten. Ein Beitrag zur Entstehung des Erdöls. *Justus Liebigs Ann. Chem.* **1934**, *510*, 42−62.

(3) Treibs, A. Chlorophyll- und Häminderivate in Organischen Mineralstoffen. *Angew. Chem.* **1936**, *49*, 682−686.

(4) Yen, T. F. *Role of Trace Metals in Petroleum;* Ann Arbor Science Publishers: Ann Arbor, MI, 1975.

(5) Filby, R. H.; Branthaver, J. F. *Metal Complexes in Fossil Fuels: Geochemistry, Characterization, and Processing;* American Chemical Society: Washington, DC, 1987.

(6) Dunning, H. N.; Moore, J. W. Porphyrin Research and Origin of Petroleum. *AAPG Bull.* **1957**, *41*, 2403−2412.

(7) Gallegos, E. J.; Sundararaman, P. Mass Spectrometry of Geoporphyrins. *Mass Spectrom. Rev.* **1985**, *4*, 55−85.

(8) McKenna, A. M.; Purcell, J. M.; Rodgers, R. P.; Marshall, A. G. Identification of Vanadyl Porphyrins, in a Heavy Crude Oil and Raw Asphaltene by Atmospheric Pressure Photoionization Fourier Transform Ion Cyclotron Resonance (FT-ICR) Mass Spectrometry. *Energy Fuels* **2009**, *23*, 2122−2128.

(9) Qian, K.; Mennito, A. S.; Edwards, K. E.; Ferrughelli, D. T. Observation of Vanadyl Porphyrins and Sulfur-Containing Vanadyl Porphyrins in a Petroleum Asphaltene by Atmospheric Pressure Photonionization Fourier Transform Ion Cyclotron Resonance Mass Spectrometry. *Rapid Commun. Mass Spectrom.* **2008**, *22*, 2153−2160.

(10) Zhao, X.; Liu, Y.; Xu, C.; Yan, Y.; Zhang, Y.; Zhang, Q.; Zhao, S.; Chung, K.; Gray, M. R.; Shi, Q. Separation and Characterization of Vanadyl Porphyrins in Venezuela Orinoco Heavy Crude Oil. *Energy Fuels* **2013**, *27*, 2874−2882.

(11) Zheng, F.; Hsu, C. S.; Zhang, Y.; Sun, Y.; Wu, Y.; Lu, H.; Sun, X.; Shi, Q. Simultaneous Detection of Vanadyl, Nickel, Iron, and Gallium Porphyrins in Marine Shales from the Eagle Ford Formation, South Texas. *Energy Fuels* **2018**, *32*, 10382−10390.

(12) Dickie, J. P.; Yen, T. F. Macrostructures of the Asphaltic Fractions by Various Instrumental Methods. *Anal. Chem.* **1967**, *39*, 1847−1852.

(13) Acevedo, S.; Guzmán, K.; Labrador, H.; Carrier, H.; Bouyssiere, B.; Lobinski, R. Trapping of Metallic Porphyrins by Asphaltene Aggregates: A Size Exclusion Microchromatography With High-Resolution Inductively Coupled Plasma Mass Spectrometric Detection Study. *Energy Fuels* **2012**, *26*, 4968−4977.

(14) Desprez, A.; Bouyssiere, B.; Arnaudguilhem, C.; Krier, G.; Vernex-Loset, L.; Giusti, P. Study of the Size Distribution of Sulfur, Vanadium, and Nickel Compounds in Four Crude Oils and Their Distillation Cuts by Gel Permeation Chromatography Inductively Coupled Plasma High-Resolution Mass Spectrometry. *Energy Fuels* **2014**, *28*, 3730−3737.

(15) Gascon, G.; Vargas, V.; Feo, L.; Castellano, O.; Castillo, J.; Giusti, P.; Acavedo, S.; Lienemann, C.-P.; Bouyssiere, B. Size Distributions of Sulfur, Vanadium, and Nickel Compounds in Crude Oils, Residues, and Their Saturate, Aromatic, Resin, and Asphaltene Fractions Determined by Gel Permeation Chromatography Inductively Coupled Plasma High-Resolution Mass Spectrometry. *Energy Fuels* **2017**, *31*, 7783−7788.

(16) Gray, M. R.; Tykwinski, R. R.; Stryker, J. M.; Tan, X. Supramolecular Assembly Model for Aggregation of Petroleum Asphaltenes. *Energy Fuels* **2011**, *25*, 3125−3134.

(17) Gawrys, K. L.; Blankenship, G. A.; Kilpatrick, P. K. On the Distribution of Chemical Properties and Aggregation of Solubility Fractions in Asphaltenes. *Energy Fuels* **2006**, *20*, 705−714.

(18) Östlund, J.-A.; Nydén, M.; Auflem, I. H.; Sjöblom, J. Interactions between Asphaltenes and Naphthenic Acids. *Energy Fuels* **2003**, *17*, 113−119.

(19) Stoyanov, S. R.; Yin, C.-X.; Gray, M. R.; Stryker, J. M.; Gusarov, S.; Kovalenko, A. Computational and Experimental Study of the Structure, Binding Preferences, and Spectroscopy of Nickel(II) and Vanadyl Porphyrins in Petroleum. *J. Phys. Chem. B* **2010**, *114*, 2180−2188.

(20) Yarranton, H. W.; Ortiz, D. P.; Barrera, D. M.; Baydak, E. N.; Barré, L.; Frot, D.; Eyssautier, J.; Zeng, H.; Xu, Z.; Dechaine, G.; et al. On the Size Distribution of Self-Associated Asphaltenes. *Energy Fuels* **2013**, *27*, 5083−5106.

(21) Mullins, O. C. The Modified Yen Model. *Energy Fuels* **2010**, *24*, 2179−2207.

(22) Zhao, X.; Shi, Q.; Gray, M. R.; Xu, C. New Vanadium Compounds in Venezuela Heavy Crude Oil Detected by Positive-ion Electrospray Ionization Fourier Transform Ion Cyclotron Resonance Mass Spectrometry. *Sci. Rep.* **2015**, *4*, 5373.

(23) Roussis, S. G.; Proulx, R. Probing the Molecular Weight Distributions of Non-Boiling Petroleum Fractions by Ag+ Electrospray Ionization Mass Spectrometry. *Rapid Commun. Mass Spectrom.* **2004**, *18*, 1761−1775.

(24) Roussis, S. G.; Proulx, R. Molecular Weight Distributions of Heavy Aromatic Petroleum Fractions by Ag+ Electrospray Ionization Mass Spectrometry. *Anal. Chem.* **2002**, *74*, 1408−1414.

(25) Lobodin, V. V.; Juyal, P.; McKenna, A. M.; Rodgers, R. P.; Marshall, A. G. Silver Cationization for Rapid Speciation of Sulfur-Containing Species in Crude Oils by Positive Electrospray Ionization Fourier Transform Ion Cyclotron Resonance Mass Spectrometry. *Energy Fuels* **2014**, *28*, 447−452.

(26) Lim, P. Y.; Liu, R. S.; She, P. L.; Hung, C. F.; Shih, H. C. Synthesis of Ag Nanospheres Particles in Ethylene Glycol by Electrochemical-Assisted Polyol Process. *Chem. Phys. Lett.* **2006**, *420*, 304−308.

(27) Aziz, S.; Abidin, Z.; Arof, A. Influence of Silver Ion Reduction on Electrical Modulus Parameters of Solid Polymer Electrolyte Based on Chitosan-Silver Triflate Electrolyte Membrane. *eXPRESS Polym. Lett.* **2010**, *4*, 300−310.

(28) Caumette, G.; Lienemann, C. P.; Merdrignac, I.; Paucot, H.; Bouyssiere, B.; Lobinski, R. Sensitivity Improvement in ICP MS

Analysis of Fuels and Light Petroleum Matrices Using a Microflow Nebulizer and Heated Spray Chamber Sample Introduction. *Talanta* **2009**, *80*, 1039−1043.
(29) Giusti, P.; Lobinski, R.; Szpunar, J.; Schaumlöffel, D. Development of a Nebulizer for a Sheathless Interfacing of NanoHPLC and ICPMS. *Anal. Chem.* **2006**, *78*, 965−971.
(30) Bouyssiere, B.; Ordonez, Y. N.; Lienemann, C. P.; Schaumlöffel, D.; Lobinski, R. Determination of Mercury in Organic Solvents and Gas Condensates by μflow-Injection - Inductively Coupled Plasma Mass Spectrometry Using a Modified Total Consumption Micronebulizer Fitted with Single Pass Spray Chamber. *Spectrochim. Acta, Part B* **2006**, *61*, 1063−1068.
(31) Gutierrez Sama, S.; Desprez, A.; Krier, G.; Lienemann, C. P.; Barbier, J.; Lobinski, R.; Barrere-Mangote, C.; Giusti, P.; Bouyssiere, B. Study of the Aggregation of Metal Complexes with Asphaltenes Using Gel Permeation Chromatography Inductively Coupled Plasma High-Resolution Mass Spectrometry. *Energy Fuels* **2016**, *30*, 6907−6912.
(32) Caumette, G.; Lienemann, C. P.; Merdrignac, I.; Bouyssiere, B.; Lobinski, R. Fractionation and Speciation of Nickel and Vanadium in Crude Oils by Size Exclusion Chromatography-ICP MS and Normal Phase HPLC-ICP MS. *J. Anal. At. Spectrom.* **2010**, *25*, 1123−1129.
(33) Zhang, H.; Siskin, M.; Gray, M. R.; Walters, C. C.; Rodgers, R. P. Mechanisms of Asphaltene Aggregation: Puzzles and a New Hypothesis. *Energy Fuels* **2020**, *34*, 9094.

https://dx.doi.org/10.1021/acs.energyfuels.0c02505
Energy Fuels XXXX, XXX, XXX−XXX

Conclusion chapitre IV

Plusieurs points sont à noter, premièrement il a été montré par analyse GPC-ICP MS que l'argent une partie des molécules contenant du vanadium présentes dans les agrégats de plus hauts poids moléculaire et ce vanadium se retrouve élué par GPC dans des poids moléculaires plus faibles. De plus l'argent se retrouve élué dans les plus hauts poids moléculaires, ce qui suggère qu'il se fixe sur des agrégats présents dans le pétrole. Il est probable que l'argent remplace une partie des porphyrines de vanadium se trouvant dans les agrégats. Ces dernières se retrouvent éluée dans la zone des porphyrines libres.

De plus lorsque l'on compare les analyses des 5 résidus atmosphérique dopés, les temps de rétention du vanadium contenues dans les porphyrines désagrégées, ces derniers varie d'une minute à deux ce qui correspond à une différence de quelques centaines de Dalton. Comme vu dans la partie 2 du chapitre II ces résultats suggèrent que ce ne sont pas les mêmes types de porphyrines avec des groupements carbonés différents et cela en fonction de l'échantillon. Ces résultats sont à mettre en parallèle avec les procédés de démétallation dans le but de corréler la présence majoritaire d'une porphyrine avec la difficulté relative au processus démétallation.

De plus il serait intéressant de faire ces mêmes expériences suivis d'une analyse moléculaire afin d'identifier toutes ces porphyrines initialement contenues dans les parties les plus difficiles à analyser.

Several points should be noted, firstly it has been shown by GPC-ICP MS analysis that silver is part of the vanadium-containing molecules present in higher molecular weight aggregates and this vanadium is eluted by GPC in lower molecular weights. In addition silver is eluted in the higher molecular weights suggesting that it binds to aggregates present in petroleum. It is likely that silver replaces some of the vanadium porphyrins in the aggregates. The aggregates elute into the free porphyrin zone.

Furthermore when comparing the analyses of the 5 spiked atmospheric residues, the retention times of vanadium contained in the disaggregated porphyrins vary from one minute to two which corresponds to a difference of a few hundred Dalton. As seen in Part 2 of Chapter II these results suggest that they are not the same types of porphyrins with different carbon groupings depending on the sample. These results should be compared with the demetallation process in order to correlate the majority presence of a porphyrin with the relative difficulty of the demetallation process.

Moreover it would be interesting to do these same experiments followed by a molecular analysis in order to identify all these porphyrins initially contained in the most difficult parts to analyze.

Conclusion Générale

L'objectif principal de ces travaux a été de coupler plusieurs techniques de séparation avec des analyses élémentaire et moléculaire.

L'analyse élémentaire par GPC ICP HR MS pour l'étude de la distribution en taille des agrégats sur des composés d'asphaltènes donne des informations pour les activités de raffinage mais n'est pas toujours suffisante utilisée seule. Des couplages combinant différentes techniques de séparation sont nécessaires pour pouvoir expliquer les différences de comportement entre deux échantillons pétroliers. Cela est confirmé par l'étude par GPC-FT-ICR MS et GPC-ICP MS grâce à laquelle des informations sur la composition des molécules et la taille des agrégats, obtenues lors d'une séparation préalable par GPC, ont pu être mises en relation. Les agrégats les plus grands contiennent des molécules plus aliphatiques que les agrégats les plus petits. Le couplage GPC-FT-ICR MS est cependant limitée pour l'étude complète des agrégats de grandes tailles, car comme lors de l'étude des porphyrines du vanadium, une grande partie de l'information reste inaccessible.

Une méthode HPTLC basée sur une seule étape de migration et qui permet une analyse élémentaire et moléculaire a été développée. La migration sur plaque de cellulose avec un mélange DCM/MeOH permet d'isoler les porphyrines libres des porphyrines plus difficilement accessibles. Enfin l'analyse moléculaire après séparation par HPTLC est possible elle aussi. Sur le front de solvant et quel que soit la fraction analysée, des porphyrines similaires ont été retrouvées. Cependant malgré une présence importante de vanadium, aucune porphyrine n'a pu être identifier sur la partie des fractions qui est restée au point de dépôt des plaques HPTLC et qui correspond aux agrégats haut poids moléculaire. Le vanadium étant très majoritairement contenue dans les porphyrines, ces porphyrines sont certainement présentes au point de dépôt mais non disponible pour l'ionisation certainement dû à l'agrégation. Cela correspondrait à la partie des porphyrines la plus difficile à enlever lors des traitements de démétallation.

Pour finir, dans le but d'analyser la partie des échantillons pétroliers la plus agrégée qui jusqu'à présent reste inaccessible, une méthode à base de dopage d'argent a été développée. L'analyse d'échantillons dopés à l'argent par GPC-ICP MS met en évidence le fait que l'argent permet de désagréger une partie du vanadium contenu dans les agrégats de grandes tailles. Il apparait aussi, lorsque cette méthode a été appliqué à cinq échantillons pétroliers différents, que le pic de vanadium qui apparait dans les poids moléculaire faible change en fonction de l'échantillon. Cela pourrait être due au fait qu'en fonction de l'échantillon, les porphyrines majoritairement présentes dans les hauts poids moléculaires sont différentes.

Par la suite, la désagrégation d'une partie du vanadium contenu dans les hauts poids moléculaires pourrait permettre leur analyse par spectrométrie de masse. De plus, la mise en relation d'un type de porphyrine majoritaire présent dans la partie du pétrole la plus agrégée avec l'efficacité des traitements d'hydrodemetallation permettrait d'apporter de précieux renseignements. Cela pourrait en effet permettre de déterminer rapidement si un pétrole sera plus complexe à raffiner qu'un autre et aider à l'optimisation des unités en conséquence.

The main objective of this work was to couple several separation techniques with elemental and molecular analyses.

Elemental analysis by GPC ICP HR MS for the study of the size distribution of aggregates on asphaltene compounds provides information for refining operations but is not always sufficient when used alone. Couplings combining different separation techniques are needed to explain differences in behaviour between two petroleum samples. This is confirmed by the study by GPC-FT-ICR MS and GPC-ICP MS in which information on molecular composition and aggregate size, obtained during prior GPC separation, was linked. Larger aggregates contain more aliphatic molecules than smaller aggregates. However, GPC-FT-ICR MS coupling is limited for the full study of large aggregates because, as in the study of vanadium porphyrins, much of the information remains inaccessible.

An HPTLC method based on a single migration step which allows elemental and molecular analysis has been developed. Cellulose plate migration with a DCM/MeOH mixture allows the isolation of free porphyrins from the more difficult to access porphyrins. Finally, molecular analysis after separation by HPTLC is also possible. On the solvent front and whatever the fraction analyzed, similar porphyrins were found. However, in spite of a significant presence of vanadium, no porphyrin could be identified on the part of the fractions which remained at the point of deposition of the HPTLC plates and which corresponds to the high molecular weight aggregates. As vanadium is overwhelmingly contained in the porphyrins, these porphyrins are certainly present at the deposition point but not available for ionisation certainly due to aggregation. This would be the most difficult part of the porphyrins to remove during demetallation treatments.

Finally, in order to analyse the most aggregated part of the oil samples which remains inaccessible until now, a silver spiking method has been developed. The analysis of silver spiked samples by GPC-ICP MS shows that silver allows some of the vanadium in the larger aggregates to be disaggregated. It also appears, when this method has been applied to five different petroleum samples, that the vanadium peak which appears in the low molecular weights changes with the sample. This could be due to the fact that depending on the sample, the porphyrins predominantly present in the high molecular weights are different.

Subsequently, the disaggregation of some of the vanadium in the high molecular weights could allow their analysis by mass spectrometry. In addition, linking a type of porphyrin predominantly present in the most aggregated part of the oil to the efficiency of hydrodemetallation treatments would provide valuable information. This could allow to quickly determine if one oil will be more complex to refine than another and help optimize the units accordingly.

Références Bibliographiques :

[1] B. P. Tissot et D. H. Welte, *Petroleum formation and occurrence*, 2nd, rev.enl. ed éd. Berlin ; New York: Springer-Verlag, 1984.

[2] G. Caumette, C.-P. Lienemann, I. Merdrignac, B. Bouyssiere, et R. Lobinski, « Element speciation analysis of petroleum and related materials », *Journal of Analytical Atomic Spectrometry*, vol. 24, nº 3, p. 263, 2009, doi: 10.1039/b817888g.

[3] C. Duyck *et al.*, « The determination of trace elements in crude oil and its heavy fractions by atomic spectrometry », *Spectrochimica Acta Part B: Atomic Spectroscopy*, vol. 62, nº 9, p. 939-951, sept. 2007, doi: 10.1016/j.sab.2007.04.013.

[4] P. A. Mello, J. S. F. Pereira, M. F. Mesko, J. S. Barin, et E. M. M. Flores, « Sample preparation methods for subsequent determination of metals and non-metals in crude oil—A review », *Analytica Chimica Acta*, vol. 746, p. 15-36, oct. 2012, doi: 10.1016/j.aca.2012.08.009.

[5] M. D. Lewan et J. B. Maynard, « Factors controlling enrichment of vanadium and nickel in the bitumen of organic sedimentary rocks », *Geochimica et Cosmochimica Acta*, vol. 46, nº 12, p. 2547-2560, déc. 1982, doi: 10.1016/0016-7037(82)90377-5.

[6] M. F. Ali et S. Abbas, « A review of methods for the demetallization of residual fuel oils », *Fuel Processing Technology*, vol. 87, nº 7, p. 573-584, juill. 2006, doi: 10.1016/j.fuproc.2006.03.001.

[7] M. P. Barrow, L. A. McDonnell, X. Feng, J. Walker, et P. J. Derrick, « Determination of the Nature of Naphthenic Acids Present in Crude Oils Using Nanospray Fourier Transform Ion Cyclotron Resonance Mass Spectrometry: The Continued Battle Against Corrosion », *Analytical Chemistry*, vol. 75, nº 4, p. 860-866, févr. 2003, doi: 10.1021/ac020388b.

[8] M. M. Boduszynski, « Composition of heavy petroleums. 2. Molecular characterization », *Energy & Fuels*, vol. 2, nº 5, p. 597-613, sept. 1988, doi: 10.1021/ef00011a001.

[9] J. Reynolds, « NICKEL IN PETROLEUM REFINING », *Petroleum Science and Technology*, vol. 19, nº 7-8, p. 979-1007, janv. 2001, doi: 10.1081/LFT-100106915.

[10] M. R. Gray, « The Desulfurization of Heavy Oils and Residua, 2nd Edition By James G. Speight, Marcel Dekker: New York; 2000. 480 pp. ISBN 0-8247-8921. $175.00. », *Energy & Fuels*, vol. 14, nº 6, p. 1333-1333, nov. 2000, doi: 10.1021/ef000034s.

[11] J. H. Wang et W. Z. Zhao, « Research on corrosivity of narrow distillate oil of crude oil with naphthenic acid and sulfur », *Materials and Corrosion*, vol. 58, nº 4, p. 290-292, avr. 2007, doi: 10.1002/maco.200604025.

[12] O. Yépez, « Influence of different sulfur compounds on corrosion due to naphthenic acid », *Fuel*, vol. 84, nº 1, p. 97-104, janv. 2005, doi: 10.1016/j.fuel.2004.08.003.

[13] I. Merdrignac et D. Espinat, « Physicochemical Characterization of Petroleum Fractions: the State of the Art », *Oil & Gas Science and Technology - Revue de l'IFP*, vol. 62, nº 1, p. 7-32, janv. 2007, doi: 10.2516/ogst:2007002.

[14] G. Caumette, C.-P. Lienemann, I. Merdrignac, B. Bouyssiere, et R. Lobinski, « Fractionation and speciation of nickel and vanadium in crude oils by size exclusion chromatography-ICP MS and normal phase HPLC-ICP MS », *Journal of Analytical Atomic Spectrometry*, vol. 25, nº 7, p. 1123, 2010, doi: 10.1039/c003455j.

[15] N. Vorapalawut *et al.*, « Application of TLC and LA ICP SF MS for speciation of S, Ni and V in petroleum samples », *Talanta*, vol. 97, p. 574-578, août 2012, doi: 10.1016/j.talanta.2012.04.040.

[16] A. J. G. Barwise, « Role of nickel and vanadium in petroleum classification », *Energy & Fuels*, vol. 4, nº 6, p. 647-652, nov. 1990, doi: 10.1021/ef00024a005.

[17] H. Xie, K. Huang, J. Liu, X. Nie, et L. Fu, « Determination of trace elements in residual oil by high-resolution inductively coupled plasma mass spectrometry », *Analytical and Bioanalytical Chemistry*, vol. 393, nº 8, p. 2075-2080, avr. 2009, doi: 10.1007/s00216-009-2658-3.

[18] J. S. F. Pereira *et al.*, « Determination of metals and metalloids in light and heavy crude oil by ICP-MS after digestion by microwave-induced combustion », *Microchemical Journal*, vol. 96, nº 1, p. 4-11, sept. 2010, doi: 10.1016/j.microc.2009.12.016.

[19] Y. Y. Borisova *et al.*, « Role of Vanadylporphyrins in the Flocculation and Sedimentation of Asphaltenes of Heavy Oils with High Vanadium Content », *Energy & Fuels*, vol. 31, nº 12, p. 13382-13391, déc. 2017, doi: 10.1021/acs.energyfuels.7b02544.

[20] H. Santos Silva *et al.*, « The role of metalloporphyrins on the physical-chemical properties of petroleum fluids », *Fuel*, vol. 188, p. 374-381, janv. 2017, doi: 10.1016/j.fuel.2016.10.065.

[21] M. F. Ali, H. Perzanowski, A. Bukhari, et A. A. Al-Haji, « Nickel and vanadyl porphyrins in Saudi Arabian crude oils », *Energy & Fuels*, vol. 7, nº 2, p. 179-184, mars 1993, doi: 10.1021/ef00038a003.

[22] J. Castillo et V. Vargas, « Metal porphyrin occlusion: Adsorption during asphaltene aggregation », *Petroleum Science and Technology*, vol. 34, nº 10, p. 873-879, mai 2016, doi: 10.1080/10916466.2016.1170846.

[23] D. H. Freeman, D. C. Saint Martin, et C. J. Boreham, « Identification of metalloporphyrins by third-derivative UV/VIS diode array spectroscopy », *Energy & Fuels*, vol. 7, nº 2, p. 194-199, mars 1993, doi: 10.1021/ef00038a006.

[24] X. Zhao *et al.*, « Separation and Characterization of Vanadyl Porphyrins in Venezuela Orinoco Heavy Crude Oil », *Energy & Fuels*, vol. 27, nº 6, p. 2874-2882, juin 2013, doi: 10.1021/ef400161p.

[25] M. Derakhshesh, A. Bergmann, et M. R. Gray, « Occlusion of Polyaromatic Compounds in Asphaltene Precipitates Suggests Porous Nanoaggregates », *Energy & Fuels*, vol. 27, nº 4, p. 1748-1751, avr. 2013, doi: 10.1021/ef3012189.

[26] F. Chen, Q. Zhu, Z. Xu, X. Sun, et S. Zhao, « Metal Porphyrin Adsorption onto Asphaltene in Pentane Solution: A Comparison between Vanadyl and Nickel Etioporphyrins », *Energy & Fuels*, vol. 31, nº 4, p. 3592-3601, avr. 2017, doi: 10.1021/acs.energyfuels.6b03100.

[27] F. Chen, Q. Liu, Z. Xu, X. Sun, Q. Shi, et S. Zhao, « Adsorption Kinetics and Thermodynamics of Vanadyl Etioporphyrin on Asphaltene in Pentane », *Energy & Fuels*, vol. 27, nº 11, p. 6408-6418, nov. 2013, doi: 10.1021/ef400533t.

[28] M. E. Pena, A. Manjarréz, et A. Campero, « Distribution of vanadyl porphyrins in a Mexican offshore heavy crude oil », *Fuel Processing Technology*, vol. 46, nº 3, p. 171-182, mars 1996, doi: 10.1016/0378-3820(95)00053-4.

[29] D. Acevedo, L. F. D'Elia Camacho, J. Moncada, et Z. Puentes, « Electrochemically assisted demetallisation of model metalloporphyrins and crude oil porphyrinic extracts in emulsified media, by using active permeated atomic hydrogen », *Fuel*, vol. 92, nº 1, p. 264-270, févr. 2012, doi: 10.1016/j.fuel.2011.08.015.

[30] B. Wu, J. Zhu, et X. Li, « Distribution of calcium, nickel, iron, and manganese in super-heavy oil from Liaohe Oilfield, China », *Petroleum Science*, vol. 11, nº 4, p. 590-595, déc. 2014, doi: 10.1007/s12182-014-0376-8.

[31] M. S. Luz et P. V. Oliveira, « Non-chromatographic method for separation and determination of Fe, Ni and V porphyrins in crude oil », *Talanta*, vol. 199, p. 147-154, juill. 2019, doi: 10.1016/j.talanta.2019.01.096.

[32] M. J. Teräväinen, J. M. H. Pakarinen, K. Wickström, et P. Vainiotalo, « Comparison of the Composition of Russian and North Sea Crude Oils and Their Eight Distillation Fractions Studied by Negative-Ion Electrospray Ionization Fourier Transform Ion Cyclotron Resonance Mass Spectrometry: The Effect of Suppression », *Energy & Fuels*, vol. 21, nº 1, p. 266-273, janv. 2007, doi: 10.1021/ef060294v.

[33] Y. Pan, Y. Liao, Q. Shi, et C. S. Hsu, « Acidic and Neutral Polar NSO Compounds in Heavily Biodegraded Oils Characterized by Negative-Ion ESI FT-ICR MS », *Energy & Fuels*, vol. 27, nº 6, p. 2960-2973, juin 2013, doi: 10.1021/ef400191h.

[34] L. Wang *et al.*, « Characterization of Acidic Compounds in Heavy Petroleum Resid by Fractionation and Negative-Ion Electrospray Ionization Fourier Transform Ion Cyclotron Resonance Mass Spectrometry Analysis », *Energy & Fuels*, vol. 27, nº 8, p. 4555-4563, août 2013, doi: 10.1021/ef400459m.

[35] M. M. Mapolelo, R. P. Rodgers, G. T. Blakney, A. T. Yen, S. Asomaning, et A. G. Marshall, « Characterization of naphthenic acids in crude oils and naphthenates by electrospray ionization FT-ICR mass spectrometry », *International Journal of Mass Spectrometry*, vol. 300, nº 2-3, p. 149-157, mars 2011, doi: 10.1016/j.ijms.2010.06.005.

[36] C. A. Hughey, R. P. Rodgers, A. G. Marshall, K. Qian, et W. K. Robbins, « Identification of acidic NSO compounds in crude oils of different geochemical origins by negative ion electrospray Fourier transform ion cyclotron resonance mass spectrometry », *Organic Geochemistry*, vol. 33, nº 7, p. 743-759, juill. 2002, doi: 10.1016/S0146-6380(02)00038-4.

[37] Q. Shi, S. Zhao, Z. Xu, K. H. Chung, Y. Zhang, et C. Xu, « Distribution of Acids and Neutral Nitrogen Compounds in a Chinese Crude Oil and Its Fractions: Characterized by Negative-Ion Electrospray Ionization Fourier Transform Ion Cyclotron Resonance Mass Spectrometry », *Energy & Fuels*, vol. 24, nº 7, p. 4005-4011, juill. 2010, doi: 10.1021/ef1004557.

[38] Y. Zhang, C. Xu, Q. Shi, S. Zhao, K. H. Chung, et D. Hou, « Tracking Neutral Nitrogen Compounds in Subfractions of Crude Oil Obtained by Liquid Chromatography Separation Using Negative-Ion Electrospray Ionization Fourier Transform Ion Cyclotron Resonance Mass Spectrometry », *Energy & Fuels*, vol. 24, nº 12, p. 6321-6326, déc. 2010, doi: 10.1021/ef1011512.

[39] T. Zhang *et al.*, « Transformation of Nitrogen Compounds in Deasphalted Oil Hydrotreating: Characterized by Electrospray Ionization Fourier Transform-Ion Cyclotron Resonance Mass Spectrometry », *Energy & Fuels*, vol. 27, nº 6, p. 2952-2959, juin 2013, doi: 10.1021/ef400154u.

[40] H. Sabbah, A. L. Morrow, A. E. Pomerantz, et R. N. Zare, « Evidence for Island Structures as the Dominant Architecture of Asphaltenes », *Energy & Fuels*, vol. 25, nº 4, p. 1597-1604, avr. 2011, doi: 10.1021/ef101522w.

[41] F. McKay, P. J. Amend, et R. Latham, « Composition of petroleum heavy ends I. Separation of petroleum >675”C residues », p. 3.

[42] D. M. Jewell, J. H. Weber, J. W. Bunger, Henry. Plancher, et D. R. Latham, « Ion-exchange, coordination, and adsorption chromatographic separation of heavy-end petroleum distillates », *Analytical Chemistry*, vol. 44, nº 8, p. 1391-1395, juill. 1972, doi: 10.1021/ac60316a003.

[43] O. P. Strausz, P. Peng, et J. Murgich, « About the Colloidal Nature of Asphaltenes and the MW of Covalent Monomeric Units », *Energy & Fuels*, vol. 16, nº 4, p. 809-822, juill. 2002, doi: 10.1021/ef0002795.

[44] T. M. C. Pereira *et al.*, « An evaluation of the aromaticity of asphaltenes using atmospheric pressure photoionization Fourier transform ion cyclotron resonance mass spectrometry – APPI(±)FT-ICR MS », *Fuel*, vol. 118, p. 348-357, févr. 2014, doi: 10.1016/j.fuel.2013.10.062.

[45] C. Leyva, J. Ancheyta, C. Berrueco, et M. Millán, « Chemical characterization of asphaltenes from various crude oils », *Fuel Processing Technology*, vol. 106, p. 734-738, févr. 2013, doi: 10.1016/j.fuproc.2012.10.009.

[46] S. Gutierrez Sama *et al.*, « Study of the Aggregation of Metal Complexes with Asphaltenes Using Gel Permeation Chromatography Inductively Coupled Plasma High-Resolution Mass Spectrometry », *Energy & Fuels*, vol. 30, nº 9, p. 6907-6912, sept. 2016, doi: 10.1021/acs.energyfuels.6b00559.

[47] D. M. Barrera, D. P. Ortiz, et H. W. Yarranton, « Molecular Weight and Density Distributions of Asphaltenes from Crude Oils », *Energy & Fuels*, vol. 27, nº 5, p. 2474-2487, mai 2013, doi: 10.1021/ef400142v.

[48] H. W. Yarranton *et al.*, « On the Size Distribution of Self-Associated Asphaltenes », *Energy & Fuels*, vol. 27, nº 9, p. 5083-5106, sept. 2013, doi: 10.1021/ef400729w.

[49] A. M. McKenna *et al.*, « Heavy Petroleum Composition. 3. Asphaltene Aggregation », *Energy & Fuels*, vol. 27, nº 3, p. 1246-1256, mars 2013, doi: 10.1021/ef3018578.

[50] M. R. Gray, R. R. Tykwinski, J. M. Stryker, et X. Tan, « Supramolecular Assembly Model for Aggregation of Petroleum Asphaltenes », *Energy & Fuels*, vol. 25, nº 7, p. 3125-3134, juill. 2011, doi: 10.1021/ef200654p.

[51] S. Acevedo, K. Guzmán, H. Labrador, H. Carrier, B. Bouyssiere, et R. Lobinski, « Trapping of Metallic Porphyrins by Asphaltene Aggregates: A Size Exclusion Microchromatography With High-Resolution Inductively Coupled Plasma Mass Spectrometric Detection Study », *Energy & Fuels*, vol. 26, nº 8, p. 4968-4977, août 2012, doi: 10.1021/ef3002857.

[52] Z. Liao, H. Zhou, A. Graciaa, A. Chrostowska, P. Creux, et A. Geng, « Adsorption/Occlusion Characteristics of Asphaltenes: Some Implication for Asphaltene Structural Features », *Energy & Fuels*, vol. 19, nº 1, p. 180-186, janv. 2005, doi: 10.1021/ef049868r.

[53] J. J. Adams, « Asphaltene Adsorption, a Literature Review », *Energy & Fuels*, vol. 28, nº 5, p. 2831-2856, mai 2014, doi: 10.1021/ef500282p.

[54] O. C. Mullins, « The Asphaltenes », *Annual Review of Analytical Chemistry*, vol. 4, nº 1, p. 393-418, juill. 2011, doi: 10.1146/annurev-anchem-061010-113849.

[55] O. C. Mullins, « The Modified Yen Model † », *Energy & Fuels*, vol. 24, nº 4, p. 2179-2207, avr. 2010, doi: 10.1021/ef900975e.

[56] J. P. Dickie et T. F. Yen, « ctures of the Asphaltic Fractions b », p. 6.

[57] O. C. Mullins *et al.*, « Advances in Asphaltene Science and the Yen–Mullins Model », *Energy & Fuels*, vol. 26, nº 7, p. 3986-4003, juill. 2012, doi: 10.1021/ef300185p.

[58] H. Sabbah *et al.*, « Comparing Laser Desorption/Laser Ionization Mass Spectra of Asphaltenes and Model Compounds », *Energy & Fuels*, vol. 24, nº 6, p. 3589-3594, juin 2010, doi: 10.1021/ef100402g.

[59] A. K. Ghosh, P. Chaudhuri, B. Kumar, et S. S. Panja, « Review on aggregation of asphaltene vis-a-vis spectroscopic studies », *Fuel*, vol. 185, p. 541-554, déc. 2016, doi: 10.1016/j.fuel.2016.08.031.

[60] M. L. Chacón-Patiño, S. J. Vesga-Martínez, C. Blanco-Tirado, J. A. Orrego-Ruiz, A. Gómez-Escudero, et M. Y. Combariza, « Exploring Occluded Compounds and Their

Interactions with Asphaltene Networks Using High-Resolution Mass Spectrometry », *Energy & Fuels*, vol. 30, nº 6, p. 4550-4561, juin 2016, doi: 10.1021/acs.energyfuels.6b00278.

[61] M. Yasar, D. M. Trauth, et M. T. Klein, « Asphaltene and Resid Pyrolysis. 2. The Effect of Reaction Environment on Pathways and Selectivities », *Energy & Fuels*, vol. 15, nº 3, p. 504-509, mai 2001, doi: 10.1021/ef0000577.

[62] P. E. Savage, M. T. Klein, et S. G. Kukes, « Asphaltene reaction pathways. 3. Effect of reaction environment », *Energy & Fuels*, vol. 2, nº 5, p. 619-628, sept. 1988, doi: 10.1021/ef00011a003.

[63] F. Trejo et J. Ancheyta, « Characterization of Asphaltene Fractions from Hydrotreated Maya Crude Oil », *Industrial & Engineering Chemistry Research*, vol. 46, nº 23, p. 7571-7579, nov. 2007, doi: 10.1021/ie0700213.

[64] C. P. Rüger, C. Grimmer, M. Sklorz, A. Neumann, T. Streibel, et R. Zimmermann, « Combination of Different Thermal Analysis Methods Coupled to Mass Spectrometry for the Analysis of Asphaltenes and Their Parent Crude Oils: Comprehensive Characterization of the Molecular Pyrolysis Pattern », *Energy & Fuels*, vol. 32, nº 3, p. 2699-2711, mars 2018, doi: 10.1021/acs.energyfuels.7b02762.

[65] F. Alvarez-Ramírez et Y. Ruiz-Morales, « Island versus Archipelago Architecture for Asphaltenes: Polycyclic Aromatic Hydrocarbon Dimer Theoretical Studies », *Energy & Fuels*, vol. 27, nº 4, p. 1791-1808, avr. 2013, doi: 10.1021/ef301522m.

[66] M. L. Chacón-Patiño, S. M. Rowland, et R. P. Rodgers, « Advances in Asphaltene Petroleomics. Part 2: Selective Separation Method That Reveals Fractions Enriched in Island and Archipelago Structural Motifs by Mass Spectrometry », *Energy & Fuels*, vol. 32, nº 1, p. 314-328, janv. 2018, doi: 10.1021/acs.energyfuels.7b03281.

[67] M. L. Chacón-Patiño, S. M. Rowland, et R. P. Rodgers, « Advances in Asphaltene Petroleomics. Part 1: Asphaltenes Are Composed of Abundant Island and Archipelago Structural Motifs », *Energy & Fuels*, vol. 31, nº 12, p. 13509-13518, déc. 2017, doi: 10.1021/acs.energyfuels.7b02873.

[68] M. L. Chacón-Patiño, S. M. Rowland, et R. P. Rodgers, « Advances in Asphaltene Petroleomics. Part 3. Dominance of Island or Archipelago Structural Motif Is Sample Dependent », *Energy & Fuels*, vol. 32, nº 9, p. 9106-9120, sept. 2018, doi: 10.1021/acs.energyfuels.8b01765.

[69] E. Furimsky, « Selection of catalysts and reactors for hydroprocessing », *Applied Catalysis A: General*, vol. 171, n° 2, p. 177-206, juill. 1998, doi: 10.1016/S0926-860X(98)00086-6.

[70] J. Ancheyta, M. S. Rana, et E. Furimsky, « Hydroprocessing of heavy petroleum feeds: Tutorial », *Catalysis Today*, vol. 109, n° 1-4, p. 3-15, nov. 2005, doi: 10.1016/j.cattod.2005.08.025.

[71] J. M. Oelderik, S. T. Sie, et D. Bode, « Progress in the catalysis of the upgrading of petroleum residue », *Applied Catalysis*, vol. 47, n° 1, p. 1-24, févr. 1989, doi: 10.1016/S0166-9834(00)83258-3.

[72] S. K. Maity, J. Ancheyta, L. Soberanis, et F. Alonso, « Catalysts for hydroprocessing of Maya heavy crude », *Applied Catalysis A: General*, vol. 253, n° 1, p. 125-134, oct. 2003, doi: 10.1016/S0926-860X(03)00499-X.

[73] S. K. Maity, J. Ancheyta, M. S. Rana, et P. Rayo, « Effect of phosphorus on activity of hydrotreating catalyst of Maya heavy crude », *Catalysis Today*, vol. 109, n° 1-4, p. 42-48, nov. 2005, doi: 10.1016/j.cattod.2005.08.010.

[74] M. Breysse, P. Afanasiev, C. Geantet, et M. Vrinat, « Overview of support effects in hydrotreating catalysts », *Catalysis Today*, vol. 86, n° 1-4, p. 5-16, nov. 2003, doi: 10.1016/S0920-5861(03)00400-0.

[75] S. K. Maity, J. Ancheyta, L. Soberanis, et F. Alonso, « Alumina-silica binary mixed oxide used as support of catalysts for hydrotreating of Maya heavy crude », *Applied Catalysis A: General*, vol. 250, n° 2, p. 231-238, sept. 2003, doi: 10.1016/S0926-860X(03)00292-8.

[76] M. S. Rana, J. Ancheyta, S. K. Maity, et P. Rayo, « Maya crude hydrodemetallization and hydrodesulfurization catalysts: An effect of TiO2 incorporation in Al2O3 », *Catalysis Today*, vol. 109, n° 1-4, p. 61-68, nov. 2005, doi: 10.1016/j.cattod.2005.08.016.

[77] M. S. Rana, J. Ancheyta, P. Rayo, et S. K. Maity, « Effect of alumina preparation on hydrodemetallization and hydrodesulfurization of Maya crude », *Catalysis Today*, vol. 98, n° 1-2, p. 151-160, nov. 2004, doi: 10.1016/j.cattod.2004.07.029.

[78] C. J. Pereira, W.-C. Cheng, J. W. Beeckman, et W. Suarez, « Performance of the minilith—a shaped hydrodemetallation catalyst », *Applied Catalysis*, vol. 42, n° 1, p. 47-60, août 1988, doi: 10.1016/S0166-9834(00)80075-5.

[79] M. S. Rana, V. Sámano, J. Ancheyta, et J. A. I. Diaz, « A review of recent advances on process technologies for upgrading of heavy oils and residua », *Fuel*, vol. 86, nº 9, p. 1216-1231, juin 2007, doi: 10.1016/j.fuel.2006.08.004.

[80] G. Gascon, J. Negrin, V. Garcia-Montoto, S. Acevedo, C.-P. Lienemann, et B. Bouyssiere, « Simplification of Heavy Matrices by Liquid–Liquid Extraction: Part I—How to Separate LMW, MMW, and HMW Compounds in Maltene Fractions of V, Ni, and S Compounds », *Energy Fuels*, vol. 33, nº 3, p. 1922-1927, mars 2019, doi: 10.1021/acs.energyfuels.8b03974.

[81] G. Gascon, J. Negrín, V. G. Montoto, S. Acevedo, C.-P. Lienemann, et B. Bouyssiere, « Simplification of Heavy Matrices by Liquid–Solid Extraction: Part II—How to Separate the LMW, MMW, and HMW Compounds in Asphaltene Fractions for V, Ni, and S Compounds », *Energy Fuels*, vol. 33, nº 9, p. 8110-8117, sept. 2019, doi: 10.1021/acs.energyfuels.9b01511.

[82] J. Sherma, « Handbook of Thin-Layer Chromatography », p. 1356.

[83] L. R. Snyder, « Classification off the Solvent Properties of Common Liquids », *Journal of Chromatographic Science*, vol. 16, nº 6, p. 223-234, juin 1978, doi: 10.1093/chromsci/16.6.223.

[84] S. Nyiredy, « Planar Chromatographic Method Development Using the PRISMA Optimization System and Flow Charts », *Journal of Chromatographic Science*, vol. 40, nº 10, p. 553-563, nov. 2002, doi: 10.1093/chromsci/40.10.553.

[85] F. P. Cossío *et al.*, « Berberine Cation: A Fluorescent Chemosensor for Alkanes and Other Low-Polarity Compounds. An Explanation of This Phenomenon », *Organic Letters*, vol. 2, nº 15, p. 2311-2313, juill. 2000, doi: 10.1021/ol006075p.

[86] V. L. Cebolla *et al.*, « Quantitative Applications of Fluorescence and Ultraviolet Scanning Densitometry for Compositional Analysis of Petroleum Products in Thin-Layer Chromatography », *Journal of Chromatographic Science*, vol. 37, nº 6, p. 219-226, juin 1999, doi: 10.1093/chromsci/37.6.219.

[87] E. Mateos *et al.*, « Coralyne cation, a fluorescent probe for general detection in planar chromatography », *Journal of Chromatography A*, vol. 1146, nº 2, p. 251-257, avr. 2007, doi: 10.1016/j.chroma.2007.01.138.

[88] C. Jarne, V. L. Cebolla, L. Membrado, K. Le Mapihan, et P. Giusti, « High-Performance Thin-Layer Chromatography Using Automated Multiple Development for the Separation of Heavy Petroleum Products According to Their Number of Aromatic Rings », *Energy & Fuels*, vol. 25, nº 10, p. 4586-4594, oct. 2011, doi: 10.1021/ef200940g.

[89] M. L. Chacón-Patiño, C. Blanco-Tirado, J. A. Orrego-Ruiz, A. Gómez-Escudero, et M. Y. Combariza, « High Resolution Mass Spectrometric View of Asphaltene–SiO_2 Interactions », *Energy & Fuels*, vol. 29, nº 3, p. 1323-1331, mars 2015, doi: 10.1021/ef502335b.

[90] D. Giraldo-Dávila, M. L. Chacón-Patiño, A. M. McKenna, C. Blanco-Tirado, et M. Y. Combariza, « Correlations between Molecular Composition and Adsorption, Aggregation, and Emulsifying Behaviors of PetroPhase 2017 Asphaltenes and Their Thin-Layer Chromatography Fractions », *Energy & Fuels*, vol. 32, nº 3, p. 2769-2780, mars 2018, doi: 10.1021/acs.energyfuels.7b02859.

[91] W. Li, T. J. Morgan, A. A. Herod, et R. Kandiyoti, « Thin-layer chromatography of pitch and a petroleum vacuum residue », *Journal of Chromatography A*, vol. 1024, nº 1-2, p. 227-243, janv. 2004, doi: 10.1016/j.chroma.2003.10.020.

[92] J. Chirinos, D. Oropeza, J. González, M. Ranaudo, et R. E. Russo, « Determination of Vanadium/Nickel Proportionality in the Asphaltene Fraction of Crude Oil Using Thin-Layer Chromatography with Femtosecond Laser Ablation–Inductively Coupled Plasma–Mass Spectrometry », *Energy & Fuels*, vol. 27, nº 5, p. 2431-2436, mai 2013, doi: 10.1021/ef3020052.

[93] S. K. Hajibrahim *et al.*, « Analysis of carotenoid and porphyrin pigments of geochemical interest by high-performance liquid chromatography », *Analytical Chemistry*, vol. 50, nº 4, p. 549-553, avr. 1978, doi: 10.1021/ac50026a004.

[94] G. J. Van Berkel, J. M. E. Quirke, et R. H. Filby, « The Henryville Bed of the New Albany shale—I. Preliminary characterization of the nickel and vanadyl porphyrins in the bitumen », *Organic Geochemistry*, vol. 14, nº 2, p. 119-128, janv. 1989, doi: 10.1016/0146-6380(89)90066-1.

[95] « Modern Size-Exclusion Liquid Chromatography », p. 512.

[96] P. Pohl *et al.*, « Multielement molecular size fractionation in crude oil and oil residue by size exclusion microchromatography with high resolution inductively coupled plasma mass spectrometric detection (HR ICP MS) », *Journal of Analytical Atomic Spectrometry*, vol. 25, nº 12, p. 1974, 2010, doi: 10.1039/c0ja00076k.

[97] M. Rietjens et M. Nieuwpoort, « An analysis of crude oil–acid reaction products by size-exclusion chromatography », *Fuel*, vol. 80, nº 1, p. 33-40, janv. 2001, doi: 10.1016/S0016-2361(00)00073-9.

[98] J.-I. Park, A. Al-Mutairi, A. M. J. Marafie, S.-H. Yoon, I. Mochida, et X. Ma, « The characterization of metal complexes in typical Kuwait atmospheric residues using both GPC

coupled with ICP–MS and HT GC–AED », *Journal of Industrial and Engineering Chemistry*, vol. 34, p. 204-212, févr. 2016, doi: 10.1016/j.jiec.2015.11.011.

[99] G. Gascon *et al.*, « Size Distributions of Sulfur, Vanadium, and Nickel Compounds in Crude Oils, Residues, and Their Saturate, Aromatic, Resin, and Asphaltene Fractions Determined by Gel Permeation Chromatography Inductively Coupled Plasma High-Resolution Mass Spectrometry », *Energy & Fuels*, vol. 31, nº 8, p. 7783-7788, août 2017, doi: 10.1021/acs.energyfuels.7b00527.

[100] D. Berek, « Size exclusion chromatography - A blessing and a curse of science and technology of synthetic polymers », *Journal of Separation Science*, vol. 33, nº 3, p. 315-335, févr. 2010, doi: 10.1002/jssc.200900709.

[101] J. H. Aubert et M. Tirrell, « On the Origins of Flow-Rate Dependence of Elution Volume in Gel Permeation Chromatography », *Separation Science and Technology*, vol. 15, nº 2, p. 123-130, mars 1980, doi: 10.1080/01496398008056086.

[102] J. H. Aubert et M. Tirrell, « Flow Rate Dependence of Elution Volumes in Size Exclusion Chromatography: A Review », *Journal of Liquid Chromatography*, vol. 6, nº sup002, p. 219-249, août 1983, doi: 10.1080/01483918308062875.

[103] W. Cheng et D. Hollis, « Flow-rate effect on elution volume in size-exclusion chromatography », *Journal of Chromatography A*, vol. 408, p. 9-19, janv. 1987, doi: 10.1016/S0021-9673(01)81786-6.

[104] J. G. Reynolds et W. R. Biggs, « Application of size exclusion chromatography coupled with element-specific detection to the study of heavy crude oil and residua processing », *Accounts of Chemical Research*, vol. 21, nº 9, p. 319-326, sept. 1988, doi: 10.1021/ar00153a001.

[105] S. Gutiérrez Sama, C. Barrère-Mangote, B. Bouyssière, P. Giusti, et R. Lobinski, « Recent trends in element speciation analysis of crude oils and heavy petroleum fractions », *TrAC Trends in Analytical Chemistry*, vol. 104, p. 69-76, juill. 2018, doi: 10.1016/j.trac.2017.10.014.

[106] G. Brusotti, E. Calleri, R. Colombo, G. Massolini, F. Rinaldi, et C. Temporini, « Advances on Size Exclusion Chromatography and Applications on the Analysis of Protein Biopharmaceuticals and Protein Aggregates: A Mini Review », *Chromatographia*, vol. 81, nº 1, p. 3-23, janv. 2018, doi: 10.1007/s10337-017-3380-5.

[107] R. H. Fish, J. J. Komlenic, et B. K. Wines, « Characterization and comparison of vanadyl and nickel compounds in heavy crude petroleums and asphaltenes by reverse-phase

and size-exclusion liquid chromatography/graphite furnace atomic absorption spectrometry », *Analytical Chemistry*, vol. 56, nº 13, p. 2452-2460, nov. 1984, doi: 10.1021/ac00277a043.

[108] S. Gutiérrez Sama *et al.*, « Molecular Fingerprints and Speciation of Crude Oils and Heavy Fractions Revealed by Molecular and Elemental Mass Spectrometry: Keystone between Petroleomics, Metallopetroleomics, and Petrointeractomics », *Energy & Fuels*, vol. 32, nº 4, p. 4593-4605, avr. 2018, doi: 10.1021/acs.energyfuels.7b03218.

[109] J. Barbier, C.-P. Lienemann, A. Le Masle, P. Chatron-Michaud, B. Guichard, et M. Digne, « New Insights into Resid Desulfurization Processes: Molecular Size Dependence of Catalytic Performances Quantified by Size Exclusion Chromatography-ICP/MS », *Energy & Fuels*, vol. 27, nº 11, p. 6567-6574, nov. 2013, doi: 10.1021/ef401540f.

[110] J. Barbier *et al.*, « Monitoring the behaviour and fate of nickel and vanadium complexes during vacuum residue hydrotreatment and fraction separation », *Fuel Processing Technology*, vol. 119, p. 185-189, mars 2014, doi: 10.1016/j.fuproc.2013.11.004.

[111] W. R. Biggs, R. J. Brown, et J. C. Fetzer, « Elemental profiles of hydrocarbon materials by size-exclusion chromatography/inductively coupled plasma atomic emission spectrometry », *Energy & Fuels*, vol. 1, nº 3, p. 257-262, mai 1987, doi: 10.1021/ef00003a006.

[112] I. Merdrignac, C. Truchy, E. Robert, I. Guibard, et S. Kressmann, « Size Exclusion Chromatography: Characterization of Heavy Petroleum Residues. Application to Resid Desulfurization Process », *Petroleum Science and Technology*, vol. 22, nº 7-8, p. 1003-1022, janv. 2004, doi: 10.1081/LFT-120038725.

[113] A. Desprez, B. Bouyssiere, C. Arnaudguilhem, G. Krier, L. Vernex-Loset, et P. Giusti, « Study of the Size Distribution of Sulfur, Vanadium, and Nickel Compounds in Four Crude Oils and Their Distillation Cuts by Gel Permeation Chromatography Inductively Coupled Plasma High-Resolution Mass Spectrometry », *Energy & Fuels*, vol. 28, nº 6, p. 3730-3737, juin 2014, doi: 10.1021/ef500571f.

[114] L. M. Ligiero *et al.*, « Characterization of Crude Oil Interfacial Material Isolated by the Wet Silica Method. Part 1: Gel Permeation Chromatography Inductively Coupled Plasma High-Resolution Mass Spectrometry Analysis », *Energy & Fuels*, vol. 31, nº 2, p. 1065-1071, févr. 2017, doi: 10.1021/acs.energyfuels.6b02899.

[115] V. Vargas, J. Castillo, R. Ocampo Torres, B. Bouyssiere, et C.-P. Lienemann, « Development of a chromatographic methodology for the separation and quantification of V, Ni and S compounds in petroleum products », *Fuel Processing Technology*, vol. 162, p. 37-44, juill. 2017, doi: 10.1016/j.fuproc.2017.03.027.

[116] J. C. Suatoni et R. E. Swab, « Preparative Hydrocarbon Compound Type Analysis by High Performance Liquid Chromatography », *Journal of Chromatographic Science*, vol. 14, nº 11, p. 535-537, nov. 1976, doi: 10.1093/chromsci/14.11.535.

[117] L. G. Galya et J. C. Suatoni, « Rapid Sara Seprations by High Performance Liqid Chromatography », *Journal of Liquid Chromatography*, vol. 3, nº 2, p. 229-242, janv. 1980, doi: 10.1080/01483918008060167.

[118] L. Molnárné Guricza et W. Schrader, « Optimized asphaltene separation by online coupling of size exclusion chromatography and ultrahigh resolution mass spectrometry », *Fuel*, vol. 215, p. 631-637, mars 2018, doi: 10.1016/j.fuel.2017.11.054.

[119] S. K. Panda, N. A. Alawani, A. R. Lajami, T. A. Al-Qunaysi, et H. Muller, « Characterization of aromatic hydrocarbons and sulfur heterocycles in Saudi Arabian heavy crude oil by gel permeation chromatography and ultrahigh resolution mass spectrometry », *Fuel*, vol. 235, p. 1420-1426, janv. 2019, doi: 10.1016/j.fuel.2018.07.118.

[120] L. Bonoldi, C. Flego, et L. Galasso, « Beyond the Average Molecule Description of Asphaltenes: Hyphenated Gel Permeation Chromatography and Spectroscopic Analyses », *Energy & Fuels*, vol. 30, nº 5, p. 3630-3636, mai 2016, doi: 10.1021/acs.energyfuels.5b02094.

[121] T. J. Morgan, A. George, P. Alvarez, A. A. Herod, M. Millan, et R. Kandiyoti, « Isolation of Size Exclusion Chromatography Elution-Fractions of Coal and Petroleum-Derived Samples and Analysis by Laser Desorption Mass Spectrometry », *Energy & Fuels*, vol. 23, nº 12, p. 6003-6014, déc. 2009, doi: 10.1021/ef9006966.

[122] W. A. Burgess, J. J. Pittman, R. K. Marcus, et M. C. Thies, « Structural Identification of the Monomeric Constituents of Petroleum Pitch », *Energy & Fuels*, vol. 24, nº 8, p. 4301-4311, août 2010, doi: 10.1021/ef1002556.

[123] F. A. Ali, N. Ghaloum, et A. Hauser, « Structure Representation of Asphaltene GPC Fractions Derived from Kuwaiti Residual Oils », *Energy & Fuels*, vol. 20, nº 1, p. 231-238, janv. 2006, doi: 10.1021/ef050130z.

[124] J. C. Putman *et al.*, « Analysis of Petroleum Products by Gel Permeation Chromatography Coupled Online with Inductively Coupled Plasma Mass Spectrometry and Offline with Fourier Transform Ion Cyclotron Resonance Mass Spectrometry », *Energy & Fuels*, nov. 2018, doi: 10.1021/acs.energyfuels.8b02788.

[125] R. S. Houk, « Mass spectrometry of inductively coupled plasmas », *Analytical Chemistry*, vol. 58, nº 1, p. 97A-105A, janv. 1986, doi: 10.1021/ac00292a003.

[126] R. M. de Souza, A. L. S. Meliande, C. L. P. da Silveira, et R. Q. Aucélio, « Determination of Mo, Zn, Cd, Ti, Ni, V, Fe, Mn, Cr and Co in crude oil using inductively coupled plasma optical emission spectrometry and sample introduction as detergentless microemulsions », *Microchemical Journal*, vol. 82, nº 2, p. 137-141, avr. 2006, doi: 10.1016/j.microc.2006.01.005.

[127] S. D. Olsen, S. Westerlund, et R. G. Visser, « Analysis of Metals in Condensates and Naphtha by Inductively Coupled Plasma Mass Spectrometry », *The Analyst*, vol. 122, nº 11, p. 1229-1234, 1997, doi: 10.1039/a704017b.

[128] J. L. Todolí et J. M. Mermet, « Elemental analysis of liquid microsamples through inductively coupled plasma spectrochemistry », *TrAC Trends in Analytical Chemistry*, vol. 24, nº 2, p. 107-116, févr. 2005, doi: 10.1016/j.trac.2004.11.005.

[129] J. L. Todolí et J. M. Mermet, « Sample introduction systems for the analysis of liquid microsamples by ICP-AES and ICP-MS », *Spectrochimica Acta Part B: Atomic Spectroscopy*, vol. 61, nº 3, p. 239-283, mars 2006, doi: 10.1016/j.sab.2005.12.010.

[130] D. R. Wiederin, R. E. Smyczek, et R. S. Houk, « On-line standard additions with direct injection nebulization for inductively coupled plasma mass spectrometry », *Analytical Chemistry*, vol. 63, nº 15, p. 1626-1631, août 1991, doi: 10.1021/ac00015a024.

[131] J. A. McLean, H. Zhang, et A. Montaser, « A Direct Injection High-Efficiency Nebulizer for Inductively Coupled Plasma Mass Spectrometry », *Analytical Chemistry*, vol. 70, nº 5, p. 1012-1020, mars 1998, doi: 10.1021/ac9708553.

[132] K. Kahen, A. Strubinger, J. R. Chirinos, et A. Montaser, « Direct injection high efficiency nebulizer-inductively coupled plasma mass spectrometry for analysis of petroleum samples », *Spectrochimica Acta Part B: Atomic Spectroscopy*, vol. 58, nº 3, p. 397-413, mars 2003, doi: 10.1016/S0584-8547(02)00261-6.

[133] P. Giusti, Y. Nuevo Ordóñez, C. Philippe Lienemann, D. Schaumlöffel, B. Bouyssiere, et R. Łobiński, « μFlow-injection–ICP collision cell MS determination of molybdenum, nickel and vanadium in petroleum samples using a modified total consumption micronebulizer », *J. Anal. At. Spectrom.*, vol. 22, nº 1, p. 88-92, 2007, doi: 10.1039/B611542J.

[134] M. Grotti, F. Ardini, et J. L. Todolì, « Total introduction of microsamples in inductively coupled plasma mass spectrometry by high-temperature evaporation chamber with a sheathing gas stream », *Analytica Chimica Acta*, vol. 767, p. 14-20, mars 2013, doi: 10.1016/j.aca.2013.01.017.

[135] E. Paredes, M. Grotti, J. M. Mermet, et J. L. Todolí, « Heated-spray chamber-based low sample consumption system for inductively coupled plasma spectrometry », *Journal of Analytical Atomic Spectrometry*, vol. 24, nº 7, p. 903, 2009, doi: 10.1039/b904002a.

[136] R. Sánchez, C. Sánchez, J. L. Todolí, C.-P. Lienemann, et J.-M. Mermet, « Quantification of nickel, vanadium and manganese in petroleum products and biofuels through inductively coupled plasma mass spectrometry equipped with a high temperature single pass spray chamber », *J. Anal. At. Spectrom.*, vol. 29, nº 2, p. 242-248, 2014, doi: 10.1039/C3JA50146A.

[137] R. Sánchez, J. L. Todolí, C.-P. Lienemann, et J.-M. Mermet, « Effect of solvent dilution on the ICP-AES based silicon sensitivity, the aerosol characteristics and the resulting organic solution properties in the analysis of petroleum products », *Journal of Analytical Atomic Spectrometry*, vol. 25, nº 2, p. 178, 2010, doi: 10.1039/b918692a.

[138] G. Caumette, C.-P. Lienemann, I. Merdrignac, H. Paucot, B. Bouyssiere, et R. Lobinski, « Sensitivity improvement in ICP MS analysis of fuels and light petroleum matrices using a microflow nebulizer and heated spray chamber sample introduction », *Talanta*, vol. 80, nº 2, p. 1039-1043, déc. 2009, doi: 10.1016/j.talanta.2009.08.017.

[139] D. Günther, I. Horn, et B. Hattendorf, « Recent trends and developments in laser ablation-ICP-mass spectrometry », *Fresenius' Journal of Analytical Chemistry*, vol. 368, nº 1, p. 4-14, août 2000, doi: 10.1007/s002160000495.

[140] X. R. Liu et G. Horlick, « In situ laser ablation sampling for inductively coupled plasma atomic emission spectrometry », *Spectrochimica Acta Part B: Atomic Spectroscopy*, vol. 50, nº 4-7, p. 537-548, juin 1995, doi: 10.1016/0584-8547(94)00128-I.

[141] R. Russo, « Laser ablation in analytical chemistry—a review », *Talanta*, vol. 57, nº 3, p. 425-451, mai 2002, doi: 10.1016/S0039-9140(02)00053-X.

[142] N. Vorapalawut, P. Pohl, B. Bouyssiere, J. Shiowatana, et R. Lobinski, « Multielement analysis of petroleum samples by laser ablation double focusing sector field inductively coupled plasma mass spectrometry (LA-ICP MS) », *J. Anal. At. Spectrom.*, vol. 26, nº 3, p. 618-622, 2011, doi: 10.1039/C0JA00118J.

[143] N. H. Bings, « Direct determination of metals in lubricating oils by laser ablation coupled to inductively coupled plasma time-of-flight mass spectrometry », *J. Anal. At. Spectrom.*, vol. 17, nº 8, p. 759-767, 2002, doi: 10.1039/B202004A.

[144] E. Ricard, C. Pécheyran, G. Sanabria Ortega, A. Prinzhofer, et O. F. X. Donard, « Direct analysis of trace elements in crude oils by high-repetition-rate femtosecond laser ablation

coupled to ICPMS detection », *Analytical and Bioanalytical Chemistry*, vol. 399, nº 6, p. 2153-2165, févr. 2011, doi: 10.1007/s00216-010-4403-3.

[145] J. Heilmann, S. F. Boulyga, et K. G. Heumann, « Development of an isotope dilution laser ablation ICP-MS method for multi-element determination in crude and fuel oil samples », *Journal of Analytical Atomic Spectrometry*, vol. 24, nº 4, p. 385, 2009, doi: 10.1039/b819879a.

[146] M. Martínez, C. Arnaudguilhem, R. Lobinski, B. Bouyssiere, M. Caetano, et J. Chirinos, « Use of xerogels for the elemental analysis of crude oils by laser ablation inductively coupled plasma high resolution mass spectrometry », *Journal of Analytical Atomic Spectrometry*, vol. 27, nº 6, p. 1007, 2012, doi: 10.1039/c2ja00005a.

[147] M. L. Viger, J.-F. Y. Gravel, D. Brouard, D. Beauchemin, et D. Boudreau, « Use of Sol−Gels as Solid Matrixes for Trace Analysis by UV Laser Ablation and Laser-Enhanced Ionization Detection », *Analytical Chemistry*, vol. 77, nº 2, p. 706-710, janv. 2005, doi: 10.1021/ac048884i.

[148] T. Vogt, D. Bauer, M. Neuroth, et M. Otto, « Quantitative multi-element analysis of Argonne Premium Coal samples by ETV-ICP OES – A highly efficient direct analytical technique for inorganics in coal », *Fuel*, vol. 152, p. 96-102, juill. 2015, doi: 10.1016/j.fuel.2014.12.057.

[149] P. A. Mello, M. F. Pedrotti, S. M. Cruz, E. I. Muller, V. L. Dressler, et E. M. M. Flores, « Determination of rare earth elements in graphite by solid sampling electrothermal vaporization-inductively coupled plasma mass spectrometry », *Journal of Analytical Atomic Spectrometry*, vol. 30, nº 10, p. 2048-2055, 2015, doi: 10.1039/C5JA00136F.

[150] M. Bettinelli, S. Spezia, C. Terni, A. Ronchi, C. Balducci, et C. Minoia, « Determination of rare earth elements in urine by electrothermal vaporization inductively coupled plasma mass spectrometry », *Rapid Communications in Mass Spectrometry*, vol. 16, nº 6, p. 579-584, mars 2002, doi: 10.1002/rcm.609.

[151] M. Aramendía, M. Resano, et F. Vanhaecke, « Electrothermal vaporization–inductively coupled plasma-mass spectrometry: A versatile tool for tackling challenging samples », *Analytica Chimica Acta*, vol. 648, nº 1, p. 23-44, août 2009, doi: 10.1016/j.aca.2009.06.027.

[152] A. Limbeck, M. Bonta, et W. Nischkauer, « Improvements in the direct analysis of advanced materials using ICP-based measurement techniques », *Journal of Analytical Atomic Spectrometry*, vol. 32, nº 2, p. 212-232, 2017, doi: 10.1039/C6JA00335D.

[153] A. A. Gorbatenko et E. I. Revina, « A review of instrumental methods for determination of rare earth elements », *Inorganic Materials*, vol. 51, nº 14, p. 1375-1388, déc. 2015, doi: 10.1134/S0020168515140058.

[154] D. C. Gregoire et R. E. Sturgeon, « Analyte transport efficiency with electrothermal vaporization inductively coupled plasma mass spectrometry ☹ », *Atomic Spectroscopy*, p. 14, 1999.

[155] M. Resano, F. Vanhaecke, et M. T. C. de Loos-Vollebregt, « Electrothermal vaporization for sample introduction in atomic absorption, atomic emission and plasma mass spectrometry—a critical review with focus on solid sampling and slurry analysis », *Journal of Analytical Atomic Spectrometry*, vol. 23, nº 11, p. 1450, 2008, doi: 10.1039/b807756h.

[156] J. Hassler, R. Matschat, S. Richter, P. Barth, A. K. Detcheva, et H.-J. Waarlo, « Determination of 22 trace elements in high-purity copper including Se and Te by ETV-ICP OES using SF_6 , NF_3 , CF_4 and H_2 as chemical modifiers », *J. Anal. At. Spectrom.*, vol. 31, nº 3, p. 642-657, 2016, doi: 10.1039/C5JA00240K.

[157] R. E. Sturgeon et J. W. Lam, « The ETV as a thermochemical reactor for ICP-MS sample introduction », *Journal of Analytical Atomic Spectrometry*, vol. 14, nº 5, p. 785-791, 1999, doi: 10.1039/a809460h.

[158] S. Kaczala, A. B. Costa, E. L. Posselt, J. S. Barin, E. M. M. Flores, et V. L. Dressler, « Element Determination in Pharmaceuticals Using Direct Solid Analysis-Electrothermal Vaporization Inductively Coupled Plasma Optical Emission Spectrometry », *Journal of the Brazilian Chemical Society*, 2015, doi: 10.5935/0103-5053.20150300.

[159] E. S. Chaves, F. G. Lepri, J. S. A. Silva, D. P. C. de Quadros, T. D. Saint'Pierre, et A. J. Curtius, « Determination of Co, Cu, Fe, Mn, Ni and V in diesel and biodiesel samples by ETV-ICP-MS », *Journal of Environmental Monitoring*, vol. 10, nº 10, p. 1211, 2008, doi: 10.1039/b809501a.

[160] T. D. Saint'Pierre, L. F. Dias, D. Pozebon, R. Q. Aucélio, A. J. Curtius, et B. Welz, « Determination of Cu, Mn, Ni and Sn in gasoline by electrothermal vaporization inductively coupled plasma mass spectrometry, and emulsion sample introduction », *Spectrochimica Acta Part B: Atomic Spectroscopy*, vol. 57, nº 12, p. 1991-2001, déc. 2002, doi: 10.1016/S0584-8547(02)00202-1.

[161] J. S. Silva, A. Schneider Henn, V. L. Dressler, P. A. Mello, et E. M. M. Flores, « Feasibility of Rare Earth Element Determination in Low Concentration in Crude Oil: Direct Sampling Electrothermal Vaporization-Inductively Coupled Plasma Mass Spectrometry »,

Analytical Chemistry, vol. 90, nº 11, p. 7064-7071, juin 2018, doi: 10.1021/acs.analchem.8b01460.

[162] A. G. Marshall, C. L. Hendrickson, et G. S. Jackson, « Fourier transform ion cyclotron resonance mass spectrometry: A primer », *Mass Spectrometry Reviews*, vol. 17, nº 1, p. 1-35, 1998, doi: 10.1002/(SICI)1098-2787(1998)17:1<1::AID-MAS1>3.0.CO;2-K.

[163] M. B. Comisarow et A. G. Marshall, « The Early Development of Fourier Transform Ion Cyclotron Resonance (FT-ICR) Spectroscopy », *Journal of Mass Spectrometry*, vol. 31, nº 6, p. 581-585, juin 1996, doi: 10.1002/(SICI)1096-9888(199606)31:6<581::AID-JMS369>3.0.CO;2-1.

[164] M. Yamashita et J. B. Fenn, « Electrospray ion source. Another variation on the free-jet theme », *The Journal of Physical Chemistry*, vol. 88, nº 20, p. 4451-4459, sept. 1984, doi: 10.1021/j150664a002.

[165] M. Yamashita et J. B. Fenn, « Negative ion production with the electrospray ion source », *The Journal of Physical Chemistry*, vol. 88, nº 20, p. 4671-4675, sept. 1984, doi: 10.1021/j150664a046.

[166] D. B. Robb, T. R. Covey, et A. P. Bruins, « Atmospheric Pressure Photoionization: An Ionization Method for Liquid Chromatography−Mass Spectrometry », *Analytical Chemistry*, vol. 72, nº 15, p. 3653-3659, août 2000, doi: 10.1021/ac0001636.

[167] H. K. Park et R. F. Haglund Jr., « Laser ablation and desorption from calcite from ultraviolet to mid-infrared wavelengths », *Applied Physics A: Materials Science & Processing*, vol. 64, nº 5, p. 431-438, mai 1997, doi: 10.1007/s003390050501.

[168] D. Giraldo-Dávila, M. L. Chacón-Patiño, J. S. Ramirez-Pradilla, C. Blanco-Tirado, et M. Y. Combariza, « Selective ionization by electron-transfer MALDI-MS of vanadyl porphyrins from crude oils », *Fuel*, vol. 226, p. 103-111, août 2018, doi: 10.1016/j.fuel.2018.04.016.

[169] J. S. Ramírez-Pradilla, C. Blanco-Tirado, M. Hubert-Roux, P. Giusti, C. Afonso, et M. Y. Combariza, « Comprehensive Petroporphyrin Identification in Crude Oils Using Highly Selective Electron Transfer Reactions in MALDI-FTICR-MS », *Energy & Fuels*, avr. 2019, doi: 10.1021/acs.energyfuels.8b04325.

[170] Edward. Kendrick, « A Mass Scale Based on CH_2 = 14.0000 for High Resolution Mass Spectrometry of Organic Compounds. », *Analytical Chemistry*, vol. 35, nº 13, p. 2146-2154, déc. 1963, doi: 10.1021/ac60206a048.

[171] C. A. Hughey, C. L. Hendrickson, R. P. Rodgers, A. G. Marshall, et K. Qian, « Kendrick Mass Defect Spectrum: A Compact Visual Analysis for Ultrahigh-Resolution Broadband Mass Spectra », *Analytical Chemistry*, vol. 73, nº 19, p. 4676-4681, oct. 2001, doi: 10.1021/ac010560w.

[172] S. Kim, R. W. Kramer, et P. G. Hatcher, « Graphical Method for Analysis of Ultrahigh-Resolution Broadband Mass Spectra of Natural Organic Matter, the Van Krevelen Diagram », *Analytical Chemistry*, vol. 75, nº 20, p. 5336-5344, oct. 2003, doi: 10.1021/ac034415p.

[173] H. Korsten, « Characterization of hydrocarbon systems by DBE concept », *AIChE Journal*, vol. 43, nº 6, p. 1559-1568, juin 1997, doi: 10.1002/aic.690430619.

[174] G. C. Klein, S. Kim, R. P. Rodgers, A. G. Marshall, A. Yen, et S. Asomaning, « Mass Spectral Analysis of Asphaltenes. I. Compositional Differences between Pressure-Drop and Solvent-Drop Asphaltenes Determined by Electrospray Ionization Fourier Transform Ion Cyclotron Resonance Mass Spectrometry », *Energy & Fuels*, vol. 20, nº 5, p. 1965-1972, sept. 2006, doi: 10.1021/ef0600199.

[175] B. M. Ruddy *et al.*, « Targeted Petroleomics: Analytical Investigation of Macondo Well Oil Oxidation Products from Pensacola Beach », *Energy & Fuels*, vol. 28, nº 6, p. 4043-4050, juin 2014, doi: 10.1021/ef500427n.

[176] I. N. Evdokimov, A. A. Fesan, et A. P. Losev, « Occlusion of Foreign Molecules in Primary Asphaltene Aggregates from Near-UV–Visible Absorption Studies », *Energy & Fuels*, vol. 31, nº 2, p. 1370-1375, févr. 2017, doi: 10.1021/acs.energyfuels.6b02826.

[177] I. N. Evdokimov, N. Yu. Eliseev, et B. R. Akhmetov, « Assembly of asphaltene molecular aggregates as studied by near-UV/visible spectroscopy », *Journal of Petroleum Science and Engineering*, vol. 37, nº 3-4, p. 135-143, mars 2003, doi: 10.1016/S0920-4105(02)00350-9.

[178] T. Yokota, F. Scriven, D. S. Montgomery, et O. P. Strausz, « Absorption and emission spectra of Athabasca asphaltene in the visible and near ultraviolet regions », *Fuel*, vol. 65, nº 8, p. 1142-1149, août 1986, doi: 10.1016/0016-2361(86)90183-3.

[179] J. C. Putman, S. M. Rowland, D. C. Podgorski, W. K. Robbins, et R. P. Rodgers, « Dual-Column Aromatic Ring Class Separation with Improved Universal Detection across Mobile-Phase Gradients via Eluate Dilution », *Energy & Fuels*, vol. 31, nº 11, p. 12064-12071, nov. 2017, doi: 10.1021/acs.energyfuels.7b02589.

[180] A. H. Mehrkesh, S. Hajimirzaee, et M. S. Hatamipour, « A Generalized Correlation for Characterization of Lubricating Base-oils from Their Viscosities », *Chinese Journal of*

Chemical Engineering, vol. 18, nº 4, p. 642-647, août 2010, doi: 10.1016/S1004-9541(10)60269-8.

[181] V. V. Lobodin, P. Juyal, A. M. McKenna, R. P. Rodgers, et A. G. Marshall, « Silver Cationization for Rapid Speciation of Sulfur-Containing Species in Crude Oils by Positive Electrospray Ionization Fourier Transform Ion Cyclotron Resonance Mass Spectrometry », *Energy & Fuels*, vol. 28, nº 1, p. 447-452, janv. 2014, doi: 10.1021/ef401897p.